THÈSE de DOCTORAT DE L'ÉCOLE CENTRALE DE LYON
membre de l'Université de Lyon

École Doctorale N°162
Mécanique Énergétique Génie Civil Acoustique

Spécialité de doctorat : Acoustique

Soutenue publiquement le 07/07/2023, par
Arthur Guibard

Acoustic propagation in heterogeneous environments and communication networks in rock ptarmigan

Devant le jury composé de :

Pr.	DUTILLEUX, Guillaume	Norwegian University of Science and Technology	Rapporteur
Pr.	LARSEN, Ole Næsbye	University of Southern Denmark	Rapporteur
Dr.	GASC, Amandine	Aix Marseille Université	Examinatrice
Pr.	ROGER, Michel	École Centrale de Lyon	Président du jury
Pr.	GALLAND, Marie-Annick	École Centrale de Lyon	Directrice de thèse
Dr.	DRAGNA, Didier	École Centrale de Lyon	co-Directeur
Dr.	OLLIVIER, Sébastien	Université Lyon 1	co-Directeur
Dr.	SÈBE, Frédéric	Université de Saint-Étienne	co-Directeur

Two male ptarmigan fly off, the leading one is singing.

Remerciements

Je voudrais tout d'abord remercier chacun des membres du jury qui ont pris de leur temps pour évaluer mon travail de recherche. Merci aux professeurs Ole Larsen et Guillaume Dutilleux qui ont porté un grand intérêt à mon travail, ont accepté d'examiner en détail ce présent manuscrit, et sont venus de loin pour assister à ma soutenance.

Merci à Amandine Gasc de s'être intéressée de près à mon travail et d'avoir accepté évaluer mon apport à l'écoacoustique.

Merci à Michel Roger d'avoir pris à coeur le rôle de président du jury, et d'avoir eu la curiosité des applications bioacoustiques.

Je remercie Marie-Annick Galland, ma directrice de thèse, pour sa confiance et ses conseils avisés tout au long de ma thèse. Merci également pour l'organisation des cafés acoustiques, rendez-vous très prisés des doctorants.

A tous les membres du jury, merci pour leur implication lors de l'évaluation de ma thèse, et pour avoir encouragé la discussion entre les domaines souvent cloisonnés de la bioacoustique, l'écoacoustique et l'acoustique physique. Leurs remarques sont pour moi un encouragement à continuer dans cette voie.

Je voudrais dire ici toute ma gratitude à mes trois encadrants, qui ont eu la curiosité et la patience nécessaires pour me conseiller dans cette recherche, à la croisée des domaines physique et biologique. Merci à eux pour leur disponibilité et pour leur relecture exigeante de mes articles et de ce présent manuscrit. Mes recherches ne seraient pas allées bien loin sans leur détermination à me voir aboutir.

Frédéric Sèbe a proposé ce sujet de thèse passionnant et m'a fait confiance pour explorer ces questions autant sur le terrain que sur le papier. Il a permis les collaborations sur le site de Flaine, et m'a accompagné sur le terrain avec persévérance malgré les quelques déboires rencontrés et les conditions météo peu clémentes de la haute montagne.

Didier Dragna a été particulièrement présent et pédagogue pour m'aider à mettre en oeuvre des simulations et des analyses pertinentes. Il s'est beaucoup impliqué dans le développement et l'évaluation du code de calcul, mais également dans ses conseils pour mes communications scientifiques.

Sébastien Ollivier a mis un point d'honneur à faciliter mon dialogue entre les disciplines bioacoustique et acoustique, et entre les équipes. Il n'a pas hésité à monter à Flaine pour prendre la mesure des difficultés de terrain. Nos échanges souvent alimentés par une foule de questions m'ont permis de prendre de la hauteur sur mes sujets de recherche et mes méthodes.

Mon parcours a été ponctué par des échanges particulièrement encourageants avec Nicolas Mathevon et Jean-Christophe Béra. Je les remercie de m'avoir accompagné lors des comités de suivi.

Je souhaite remercier le LabEx CeLyA pour la bourse qui m'a permis de réaliser cette thèse dans de bonnes conditions, pour le financement du matériel nécessaire aux expérimentations, ainsi que pour le travail des chargées d'aide au pilotage : Carine Zambardi et Agnès Delebassée-Nabet.

Abstract

Acoustic propagation supports long-distance animal communication. However, attenuation processes also constrain the range of vocalizations. In this regard, the active space is a central bioacoustic concept to understand animal communication networks in the wild. In parallel, detection space determines the possibilities of recording biological data in ecoacoustic studies. Propagation of animal acoustic signals has mostly been studied by considering the natural environment as an homogeneous propagation medium. This resulted in an simplified circular active space representation that is still widely used. Only few studies have assessed the variations of the active space due to environment heterogeneities and transmitter position.

This thesis provides an integrative approach at the interface of bioacoustics and atmospheric propagation to robustly estimate active and detection spaces in rock ptarmigan, an emblematic species of the high mountains. For this purpose, we develop a stable and flexible tool to investigate the organization of communication networks as well as population densities and their dynamics. This tool is based on the numerical computation of the parabolic equation for acoustic propagation in the atmosphere, and takes into account topography, ground effects and weather conditions.

This thesis work consists of three parts: (i) a validation of the acoustic propagation code in a heterogeneous environment, (ii) an application of the model to the study of a communication network, and (iii) an application to the detection spaces for passive acoustic monitoring. First of all, comparisons of numerical simulations with measurements performed during an experimental campaign in the French Alps confirms the capacity of the code to accurately predict sound levels. We then use this model to show how mountain conditions affect surface and shape of active spaces, with topography being the most significant factor. The model is then applied to an ecological context using field data including a site of known topography, meteorological measurements, GPS tracking of birds and estimates of vocal activity. Our data reveals that singing during display flights is a good strategy for a transmitter to expand its active space in such an environment and reach conspecifics. It enables a quick defense of the territory, which would not otherwise be possible by the mere songs uttered from ground positions. Regarding detection spaces, application of the reciprocity principle to sound propagation allowed to use an indirect sound field computation from a receptor point to determine its sampling area for given conditions. We show from simulations that the variability of the detection spaces is crucial for the evaluation of the vocal activity of a given population. Overall, in both cases of active space and detection space, we show that the consideration of topography, meteorological conditions and background noise is required in long-distance communication studies but also in census campaigns using passive acoustic monitoring.

Keywords: acoustic communication, heterogeneous environment, outdoor sound propagation, active space, detection space, rock ptarmigan, bioacoustic, ecoacoustic.

Résumé

La propagation acoustique rend possible la communication animale à distance. Cependant, les processus d'atténuation limitent la portée des vocalisations. De ce point de vue, l'espace actif est un concept bioacoustique central pour comprendre les réseaux de communication des animaux en milieu naturel. En parallèle, l'espace de détection conditionne les possibilités d'enregistrement des données biologiques lors des études éco-acoustiques. La propagation des signaux acoustiques animaux a été principalement étudiée en considérant l'environnement naturel comme un milieu de propagation homogène. Cela a entraîné une représentation circulaire simplifiée des espaces actifs et de détection qui est encore largement utilisée. Seules quelques études ont évalué les variations de l'espace actif dues aux hétérogénéités de l'environnement et à la position de l'émetteur.

Cette thèse propose une une approche intégrative à l'interface entre la bioacoustique et la propagation atmosphérique pour estimer les espaces actifs et de détection de manière robuste chez le lagopède alpin, une espèce emblématique de la haute montagne. Pour cela, nous développons un outil stable et flexible pour étudier l'organisation des réseaux de communication ainsi que les densités de population et leur dynamique. Cet outil est basé sur la résolution numérique de l'équation parabolique pour calculer la propagation acoustique dans l'atmosphère, et prend en compte la topographie, les effets de sol et les conditions météorologiques.

Ce travail de thèse comporte trois parties : (i) une validation du code de propagation acoustique en environnement hétérogène, (ii) une application du modèle à l'étude d'un réseau de communication, et (iii) une application aux espaces de détection pour le monitoring passif. Tout d'abord, la comparaison des simulations numériques avec les mesures effectuées lors d'une campagne expérimentale dans les Alpes françaises confirme la capacité du code à prédire avec précision les niveaux sonores. Nous utilisons ensuite ce modèle pour montrer comment les conditions en montagne affectent la surface et la forme des espaces actifs. Une application est ensuite menée dans un contexte écologique à partir de données de terrain comprenant un site de topographie connue, des mesures météorologiques, un suivi GPS des oiseaux et une estimation de l'activité vocale. Nos données révèlent que le fait de chanter pendant les vols en cloche est une bonne stratégie pour un émetteur visant à étendre son espace actif dans un tel environnement, et ainsi atteindre ses congénères. Ce comportement permet une défense rapide du territoire, qui serait impossible avec les chants émis uniquement depuis le sol. Concernant les espaces de détection, l'application du principe de réciprocité permet d'utiliser un calcul indirect du champ de pression à partir d'un point récepteur pour déterminer sa zone d'échantillonnage dans des conditions données. Nous montrons à partir de calculs appliqués que la variabilité des espaces de détection est une donnée cruciale pour l'évaluation de l'activité vocale d'une population. Dans les deux cas de l'espace actif et de l'espace de détection, nous montrons que la prise en compte de la topographie, des conditions météorologiques et du bruit de fond est nécessaire lors des études sur la communication à longue distance, mais également lors des campagnes de recensement par acoustique passive.

Mots clés : communication acoustique, environnement hétérogène, propagation atmosphérique, espace actif, espace de détection, lagopède alpin, bioacoustique, éco-acoustique.

Contents

List of Figures

List of Tables

General introduction

Acoustic communication plays a major role in the interactions of social animals. In birds, these exchanges are particularly conspicuous, especially during the dawn chorus (McGregor, 1991; Gil & Llusia , 2020). The study of acoustic communication in birds was originally conducted mainly by naturalists in the field, and on captive subjects (Birkhead & Balen, 2008). Listening to songs and observing associated behaviors has led primarily to theories about male territoriality in passerine birds (Nice, 1941). Later, the development of recorders, microphones, and loudspeakers enabled the development of outdoor playback experiments and studies in controlled environments (in the laboratory), and thus to finely explore the functions of songs at different social scales (Hopp & Morton, 1998). Another advantage of audio techniques is the possibility to analyze the information content of songs. This now makes it possible to determine criteria for group discrimination, and individual recognition between conspecifics. It is now easier to identify the precise functions of different types of vocalizations in some species. Therefore, advances in recording techniques, audio analysis, detection and classification of animal sounds over the last decades have facilitated the rapid development of birdsong studies (Erbe & Thomas, 2022). Moreover, the analysis of social systems made possible by the introduction of the concept of network has opened the way to the research field of animal communication networks (McGregor, 2005; Whitehead, 2008).

However, while they qualitatively inform communications, these approaches do not address the spatial dimension of the acoustic communication networks. Yet, fine-grained analysis of acoustic signals in these communication networks not only refines our understanding of the informational content of the acoustic signals exchanged, but also provides information about the structure of the underlying social network (McGregor & Horn, 2014). We understand that the social network is conditioned by the effective possibilities of information transmission, sending and response. These are driven both by the spatial organization of the birds, and by the propagation of the sound in the surrounding environment. The propagation being dependent on the configuration of the environment, it may vary both spatially and temporally. Nevertheless, the variability of communication possibilities and its impact on the organization of networks is still largely unknown.

In parallel, the recent development of individual tracking by miniaturized GPS beacons enables the monitoring of spatial behaviors over long periods of time compared to simple field observations (Recio *et al.*, 2011). This provides valuable information to understand the spatial occupation of habitats, and daily or seasonal life habits. It is now possible to combine acoustic and spatial data collection to conduct integrative studies of

communication networks in many species, from both a spatial and functional perspective. A necessary criterion for the study of a communication network is to answer the question: "Who is talking to whom?" This requires a concrete assessment of "who hears what?" In the context of remote communication, answering this question is not trivial. Moreover, it seems that the statistical approach, commonly used in behavioral biology, is not sufficient to unravel this question. From an overall perspective, it is necessary to evaluate the propagation distances in order to infer the behaviors actually at stake in given situations, based on the quantity of information received.

Two complementary approaches are emerging to evaluate sound propagation distances: an experimental approach, which requires extensive resources and provides reliable but very localized indications (in time and space) (Wiley & Richards, 1978; Michelsen & Larsen, 1983; Hardt *et al.*, 2021); and a simulation-based approach, which can provide indications for a large number of cases, given a minimum of field data (Embleton, 1996). This second approach can provide representative metrics, within the limits of validity of the physical model used and uncertainties on the input data. Attempts to computationally estimate effective communication distance are fairly scarce to date (Henwood & Fabrick, 1979). In addition, the integration of these estimates in larger behavioral studies remains rare to date (Larom *et al.*, 1997). However, the integration of the complexity of the acoustic propagation phenomenon seems to be essential for those who want to realistically describe an acoustic network. Using the current knowledge on outdoor sound propagation and a dedicated code applied to a bioacoustic study framework, we aim to set the basis of an integrative approach for the communication network studies. The modeling of acoustic signal propagation can provide valuable information at different scales of study and enhance analysis capabilities in bioacoustic and eco-acoustic studies. In bioacoustics, at the scale of individuals, this modeling brings new knowledge on the modality of propagation in communication networks. It makes it possible to quantify the information transmitted between the coding by an emitter and the decoding by receivers. In eco-acoustics, at the scale of populations and ecosystems, this modeling reveals the active space of communication, but also the detection space. The latter is a decisive tool to quantify the areas sampled by a network of autonomous recorders. Indeed, to get the best out of the field data, it is crucial to evaluate the sampling area associated with each audio data collected. For this, we used the same propagation code with a few modifications to apply it to audio recording situations.

This thesis focuses on the fluctuating nature of propagation in a heterogeneous environment, and on its consequences for acoustic communication networks and for the application of acoustics-based censusing. We consider the case of alpine mountains, an open and heterogeneous habitat, spatially and temporally. Furthermore, we have taken as a study model an emblematic bird of this environment: the rock ptarmigan.

This manuscript is structured in seven chapters, and organized as follows:

– Chapter 1 sets the framework of the thesis and the background for the study of communication networks.

– Chapters 2 and 3 respectively introduce the experimental and numerical methods used in the whole thesis.

– Chapter 4 focuses on the experimental validation of the propagation code in a heterogeneous environment, together with the investigation of the variability in spatial limits of communication in birds.

– Chapter 5 focuses on the study of a communication network in rock ptarmigan using the propagation code developed earlier. It explicitly examines communication modalities from a temporal and spatial point of view.

– Chapter 6 details the application of the acoustic reciprocity principle for the evaluation of sampling areas associated with audio recordings in the field. It also brings together our investigations on the consideration of sampling area in the monitoring of a rock ptarmigan population.

– Chapter 7 discusses the limits of the methods and the answers to the questions raised in this introduction. It also discusses the contribution of recent knowledge in physical acoustics to bioacoustic and ecoacoustic study protocols, as well as perspectives for further studies.

Chapter 1

Background to the study of bird communication and thesis framework

Abstract

This chapter presents the context of the study within the field of acoustic communication in birds. First the behavioral significance of communication in animals, the concept of network and the framework of the information transmission chain are reminded. Second, the bird species used as an example throughout the thesis and its characteristics are introduced. Third, the physical phenomena involved in outdoor acoustic propagation and the state of the art on numerical methods are briefly reviewed. These prerequisites are then used to define the concepts of active space and detection space. Finally, the approach adopted in this thesis is presented, as well as the three research axes investigated.

Contents

1.1 Acoustic communication in birds

In different biological contexts such as courtship and mating, parent-offspring recognition, and dissuasive alarm call, the communication signals involved have several components: visual, auditory or olfactory (Bradbury & Vehrencamp , 2011). In birds, the acoustic modality of communication is predominant in the majority of conspecific interactions (Catchpole & Slater, 2008). Whether in passerines or non-oscines, singing enables information to be spread over long distances through the environment, regardless of whether the receivers are in direct view or not (e.g. in dense forests (Barker *et al.*, 2009)). Moreover, this diffusion is limited in time, with a duration or a rhythm controlled by the signaler[1], contrary to the olfactory marks which persist. The emission can be adjusted very finely in time, but also in amplitude and frequency according to the needs of the signaler. These particularities and the versatile character of vocalizations explain why acoustic communication is largely privileged in birds. We only focus on acoustic communication in this thesis, to study its particularities and associated behaviors in birds.

1.1.1 Functions of the acoustic communication

Acoustic communication is used in many contexts, whether between known conspecifics, neighbors or offspring, or with unknowns like distant neighbors, or even individuals of other species (Kroodsma, 1982; Marler, 2004; Malavasi *et al.*, 2013). It is thus decisive in the life of the bird, and its effectiveness determines the progress of the relations between associated or competing individuals. For a brief overview of the different contexts, we can list the stages of a typical bird's social life. In the early stages of the bird's life, recognition between parents and offspring is essential to ensure sufficient feeding and

---

[1]The terms "signaler", "emitter", and "sender" refer to the individual that is vocalizing, and are used as synonyms thereafter.

good development (Beecher*et al.*, 1985). For example, distress calls and contact calls provide protection for youth (Gill & Bierema, 2013). Later, collaboration in the search for food is ensured though contact calls. In addition, alarm calls and mobbing calls enable the collective avoidance of predators. Once sexual maturity is reached, the songs are a major criterion in the selection of a partner through courtship, and enable mating and maintenance of the couple for the rearing of the offspring (Searcy & Andersson, 1986). The defense of a territory by deterrent calls ensures the reproduction and the defense of the offspring. Many of these behaviors are driven by the signaling of a motivational state to conspecifics, and enabled by the possibility of individual recognition.

These interactions can be mediated by different types of vocalizations like songs, calls or contact calls. They are intended to have an attractive, repulsive, or alarming effect (positive or negative phonotaxi), and the observed behavioral responses lead us to infer their functions. Although observations have led to conclusions about the precise meaning of certain songs in some species (Templeton *et al.*, 2005), the finer meanings are still largely unknown for many. The vocal repertoire associated with each individual is a function of the species and the habitat area, given the existence of regional dialects (in passerines in particular (Kroodsma, 2004; Podos & Warren, 2007)). Nevertheless, the vocalizations are also likely to evolve during the life of the bird depending on the season, or according to its age, its fitness level, or its hormonal condition (Warren, 2003; Gil & Gahr , 2002; Catchpole & Slater, 2008). This provides clues to the receivers about the behavioral and physiological traits of the emitter (Vehrencamp, 2000). In addition, in some contexts, signaling behavior may not honestly reflect the condition of the emitter (although these effects remain uncommon) (Searcy & Nowicki, 2005, 2008). These examples show the variety of situations and the complexity of communication challenges. All these exchanges of information take place in the context of a particular habitat, and are governed by a determined social organization. Thus each individual necessarily deals with a communication network for its survival and reproduction (Templeton & Carlson, 2019).

1.1.2   Acoustic communication networks

Generally speaking, the term communication network refers to a set of signalers and receivers engaged in the exchange of information. Studies of animal communication were traditionally focused on interactions between single pairs of signalers and receivers, but communication is now considered to occur within networks involving multiple emitters and receivers (McGregor, 2005). Networks can be studied at several spatial and social scales: close exchanges between parents, or parents and offspring (Boucaud *et al.*, 2017; Mathevon *et al.*, 2003), group interactions in social birds (Adrian *et al.*, 2022), longer range interactions between residents and neighbors or intruders of the same species (Szymkowiak, 2022), or broader interspecific relationships in acoustic communities

([Templeton & Greene, 2007](#); [Tobias *et al.*, 2014](#); [Farina & James, 2016](#)). These networks can be effectively separated in their uses and rules ([Fernandez *et al.*, 2016](#)). Here we are particularly interested in the relationships between conspecific adults, and more specifically between males at the crucial moment of territory establishment and reproduction. Note that the term "territory" is used to designate any defended area, as defined by [Nice](#) ([1941](#)).

We now introduce three interaction modalities involved in bird communication networks (see Fig. 1.1): (a) The most basic form of communication within a network is the diffusion of information by an individual. This can be an alarm call in a context of imminent danger, or a signalling that claims the status of the singer. All listeners are then concerned, and no response is required as shown Fig. 1.1 (a).
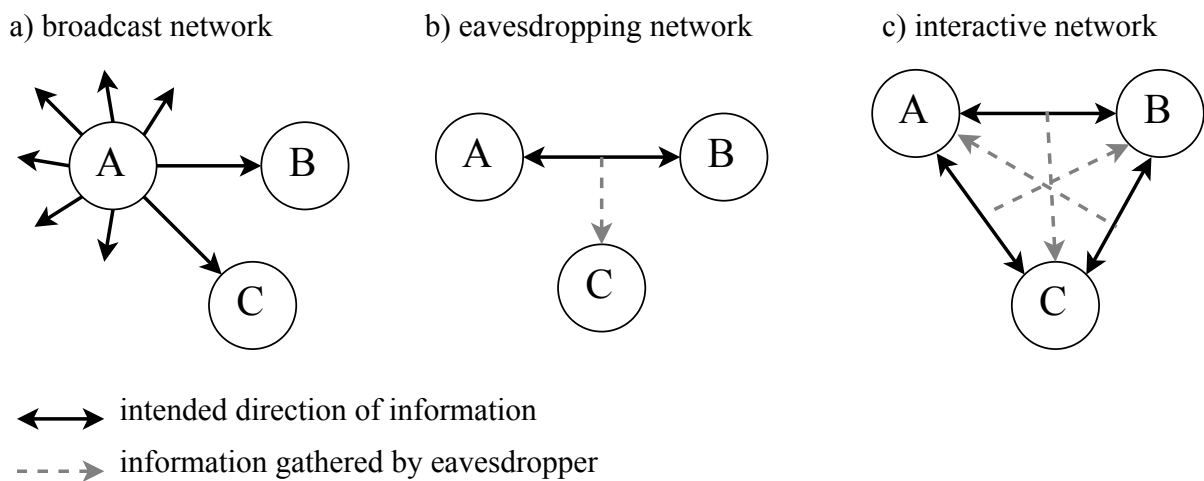
Figure 1.1 − Schematic representation of different communication modalities that can occur in an acoustic communication network. A network can be either: a) in a broadcasting configuration from one individual to the whole audience, b) in a case of eavesdropping on exchanges between two individuals, or c) in a case of interactive exchanges between more than two individuals who signal and retrieve the information emitted by each of them. Adapted from [Burt & Vehrencamp](#) ([2005](#)).

(b) In the context of breeding season, interactions between conspecifics are driven by interests in sexual selection and territory defense. This is why every information recovered from the local population is precious, for the females and also for the competing males. Thus, eavesdropping of acoustic communications is a good way to evaluate potential mates or the quality of competitors. A bird chooses not to signal its presence, and waits for the result of interactions between two or more of the nearby conspecifics. Eavesdropping is one of the modalities of the communication network, as detailed Fig. 1.1 (b).

(c) Finally, when individuals are aware of each other's presence, and all communicate and receive the information transmitted, it is an interactive network (see Fig. 1.1 (c)).

It should be noted that these representations of the network correspond to particular situations of the communication between protagonists. A communication network is actually dynamic, and its temporal evolution in a given area can be described by a succession

of these different situations. The network as a social interaction depends on the status and motivational state of the participating individuals. In addition, social awareness in birds is highlighted by the audience effect, i.e. the tuning of the acoustic properties of the song according to the attending listeners (Marler *et al.*, 1986; Baltz & Clark, 1997; Striedter *et al.*, 2003). In addition, the social status of group-mates is considered to modulate vocal behavior (Vignal *et al.*, 2004). Communications are thus codified and constrained by the social network as a whole. They are thus based on the transmission of information between protagonists, and on the content of the transmitted information.

1.1.3 Information transmission

The calls and songs in birds are generated through the respiratory system by the vocal organ, namely the syrinx (Brackenbury, 1982). When expiratory muscles compress the air sacs in the thorax, the air flows out through the syrinx and trachea. This flow causes the membranes of the syrinx to vibrate, thus producing a pressure oscillation at a fundamental frequency f_0. The constitution and the shape of the vocal tract induce the amplification or the attenuation of the f_0 harmonics. In addition, the control on the respiratory and syringeal muscles, and the movements of the entire vocal tract, can modulate the signal in amplitude and frequency (Larsen & Goller, 2002; Suthers, 2004; Kazemi *et al.*, 2023).

We leave aside the broad meaning of the term information, which includes everything that reduces an individual's uncertainty about the state of his environment (Little *et al.*, 2022), including all of the bird's perceptions. In the following we use the term "information" to refer only to those elements of a song that can be meaningful from a receiving bird's perspective. This information can be either "static", and not vary according to the context, or "labile", and vary according to the emitter's current activity and motivational state (Perez *et al.*, 2012). A song produced by a bird could carry information on location, species, sex, identity, motivational state, communication context, and explicit messages (Larsen, 2020). This information is either contained in the signal itself, or through the simple act of singing (or possibly not singing). The latter includes presence, location and motivation cues.

The so-called information theory introduced by Shannon & Weaver provides a foundation for describing the information transmission between emitter and receiver (Weaver, 1949). This process applied to outdoor acoustic communication – including the successive steps of coding, propagation and decoding – is described Fig. 1.2. Thanks to the vocal production, information contained in a signal can be coded according to the three dimensions of time, frequency and amplitude. The volume of equivalent information produced during a song propagates in the atmosphere, and may be reduced by various effects related to the geometry, the boundaries (ground, obstacles) and the atmosphere itself (Brenowitz, 1982a). The instant of the singing but also the respective positions of the singer and the

receiver determine the effects of the boundaries and the atmosphere on the acosutic propagation. Thus, we name the "environmental constraints" the set of environmental factors inducing the conditions of information degradation during its transmission to the singer's neighborhood.
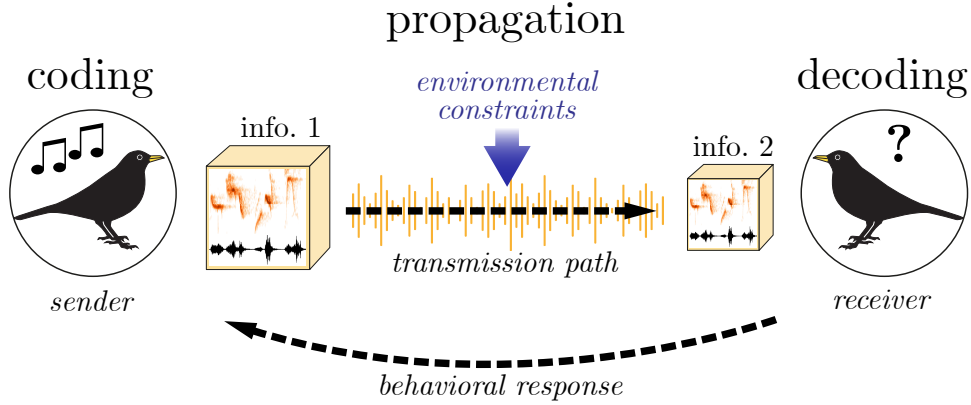
Figure 1.2 − Schematic representation of the information transmission in bird communication. The sender codes a volume of information in its song (info.1). This signal propagates in atmosphere and the environmental constraints determine the received volume of information (info.2). The receiver then decodes the signal, which elicits its behavioral response.

One of the major issues for the study of communication networks is the identification of the emitter. To do this, we can distinguish between specific information (Becker, 1982), group information (Briefer *et al.*, 2009), and individual information (Aubin *et al.*, 2004). This information is extracted by the receivers and enables them to identify the emitter; thus it indicates the social link. The recognition of conspecifics is essential to the establishment of mutualistic behaviors. At the local level, the group information enables, among other things, the discrimination between neighbors and strangers. Finally, between known birds, individual recognition facilitates more active relationships such as the parent-offspring relationship.

During the propagation of a song between singers, the signal is degraded, in the sense that the volume of recoverable information is reduced (Brenowitz, 1982a). Along the transmission path, the amplitude decreases, the frequency content degrades in a non-uniform way, and the initial rhythm may suffer from reflections (Embleton, 1996). This degradation is inherent to the remote communication mode (Larsen, 2020), and must be considered when studying acoustic communication networks in birds. Phenomena specific to outdoor propagation are described below in Sec. 1.3. In the next section, we present the biological model studied in this thesis.

Acoustic communication in birds ———————————— **Summary**

Vocal plasticity in birds ensures the specific and individual variability of calls and songs, with a diverse repertoire across species. The identity information contained in these songs is crucial for mutualistic or competitive relationships. Complex social networks are thus maintained through the use of acoustic communication. This network is subject to the effective constraints of the environment on propagation. This is why it is crucial to consider the physical phenomenon of acoustic propagation if one wants to understand the influence of environmental conditions on a communication network.

1.2 The rock ptarmigan

1.2.1 Biological model

The rock ptarmigan is chosen as biological model for several reasons. Remote vocal communication is crucial in this species during the breeding season. In its irregular habitat, and because of its mimetic plumage, visual communication is very limited. The long distance communication is thus preferentially acoustic. Moreover, the heterogeneity of the environmental conditions of the mountain exerts a particular pressure on the vocal exchanges, by constraining the acoustic propagation. We are particularly interested in the adaptation of behavior to this environmental pressure. In addition, ptarmigan males show a very marked behavior of territory defense, which is conducive to interpretations of remote vocal interactions. Finally, ptarmigan is a non-oscine bird with a simple stereotyped song whose propagation can be easily simulated considering the main frequencies of its spectrum.

Studying the rock ptarmigan is also interesting as it is considered to be a sentinel species in the French Alps and Pyrenees. So it is an indicator of the conservation status of protected biomes of natural parks and biodiversity reserves. This species has already been monitored for many years on different mountain sites in France, including the Flaine site in the Alps (Novoa *et al.*, 2011; Canonne *et al.*, 2020). These data are essential for the realization of bioacoustic and eco-acoustic applications of our propagation code, and thus to answer the behavioral and methodological questions raised in Sec. 1.5.

1.2.2 Species description

The rock ptarmigan (*Lagopus muta*, Montin 1776) is a galliform of the phasianidae family, and tetraoninae subfamily more commonly called grouses, which lives in cold environments of the northern hemisphere such as the tundra, and alpine or subalpine ranges (Potapov & Sale, 2014). Its genus comes from the contraction of the two ancient Greek

words *lagos* meaning "hare", and *pous* which we translate as "foot". The ptarmigan's feathered feet and legs are reminiscent of those of the hare. Yet the name of the species comes from the New Latin *muta*, which means "mute". It refers to the gutural aspect of the male's song which sounds like a croak, very different from a passerine song, and the fact that it sings little (Jobling, 1991).

This medium size grouse has a length of 33–38 cm and a wingspan of 54–60 cm, and weighs 470 to 740 g for the male and 430 to 700 g for the female (at high-latitudes), mainly depending on time of the year (del Hoyo *et al.*, 1994). Ptarmigans show a sexual dimorphism, mainly visible during the mating season, as can be seen in Fig. 1.3 (a) and (b). The male is slightly heavier than the female, and has a very different feather pattern in spring and summer. Males also have a red comb that develops above the eye during the mating season that is a visual cue for sexual selection (Holder & Montgomerie, 1993). Ptarmigans have three different molts during the year. They wear a cryptic feather pattern adapted to the seasons, which limit their exposure to predators. The essentially white winter plumage of both sexes is gradually replaced in the spring by brown and black feathers on the back of the male and by light brown feathers with black stripes on the female (see Fig. 1.3 (a) and (b). The chicks as well as the eggs also have this mimetic aspect which makes them almost invisible to predators in the mixed zones of moors, bushes and rocks (see Fig. 1.3 (c) and (d).
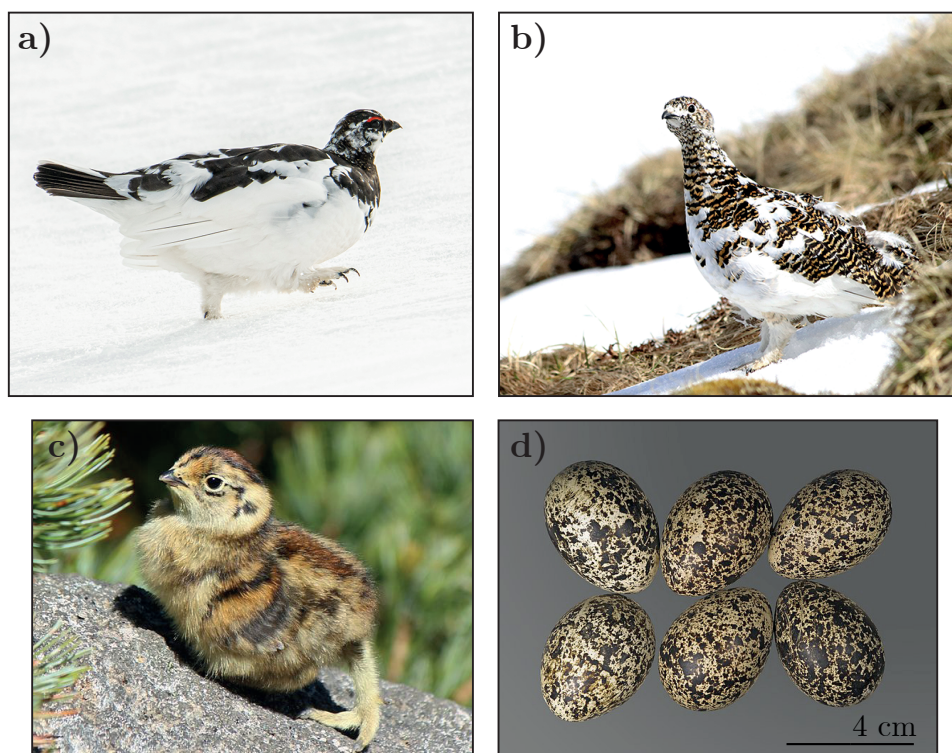
Figure 1.3 – Pictures of the rock ptarmigan: a) male, and b) female with spring feathers molt, c) few days old chick, d) eggs with scale. (Sources: (a) Clément Cornec, (b) Clément Sabatier, (c) and (d) Wikipedia Commons [2])

There are three different species that belong to the ptarmigan (*lagopus*) genus: rock ptarmigan (*Lagopus muta*), willow ptarmigan (*Lagopus lagopus*), and white-tailed ptarmigan (*Lagopus leucura*). Thirty subspecies have been described to date. They have small differences, and live in various regions and habitats (del Hoyo *et al.*, 1994). Only the rock ptarmigan is present in the French mountains, so our study focuses on this particular species.

1.2.3 Habitat and ecology

Distribution

The rock ptarmigan distribution area is limited to the northern hemisphere, and mainly in North America and Eurasia. It extends from the lowlands of the subarctic and arctic regions (e.g. Greenland coast) to high mountains such as the Alps and the Himalayas, which maintain remnant glaciers from the last ice age, the Pleistocene (Mourer-Chauvire, 1975). The southernmost known populations are located in the Japanese Alps. This range is shown Fig. 1.4. It can be seen that most of the populations are year-round residents, with seasonal movements remaining within a regional range, except for the central part of Canada.
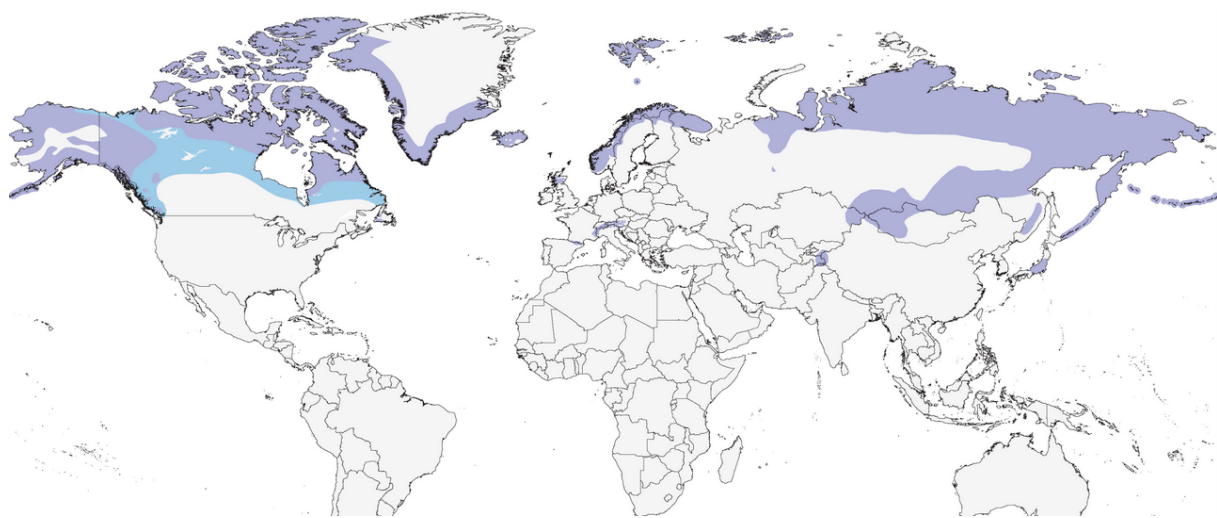
Figure 1.4 – Rock Ptarmigan (Lagopus muta) distribution map according to BirdLife International data: ▇ year-round, ▇ non-breeding.

Ecology

In mountain ranges such as the Alps and Pyrenees, ptarmigan lives above the tree line in the alpine and subalpine levels, with a low altitude limit around 1800 m. This habitat is mostly composed of rocky outcrops, low bushes, and alpine heath (Potapov & Sale,

---

[2]https://en.wikipedia.org/wiki/Rock_ptarmigan, consulted in January 2023.

2014). The ptarmigan is considered as a sedentary species. However, regional movements of about 10 km can be observed between certain wintering and breeding areas.

The weather conditions are harsh with very low temperatures, thick snow cover in winter, and potentially snowfall even in spring with high interannual variability (López-Moreno & Vicente-Serrano, 2007). Ptarmigan are well adapted to this climate, having a very downy plumage that protect them from cold. It has a diverse diet that provides them access to food resources regardless of snow cover. It feeds on soft bushes, leaves, buds, mosses, lichens, twigs, berries and insects. In addition, they roam the northern slopes in winter to feed where the snow is blown by the wind, and where grasses and lichens are accessible.

The rock ptarmigan is a prey for carnivorous mammals and raptors. In the Alps, attacks by red foxes, golden eagles or goshawk are common. However, its discreet behavior during the day and its cryptic plumage limit these attacks.

1.2.4 Populations and conservation issues

Annual counts of ptarmigan are conducted at a few known breeding sites, mainly located in the large mountain ranges. These local estimates can be used to derive indicators at the national level. The population in France is considered to be in decline and is classified as near threatened (UICN France, 2016). The rock ptarmigan population is currently estimated at 6,000 to 10,000 individuals in the Pyrenees (Observatoire français des galliformes de montagne, unpublished data), and at about 100,000 individuals in the Alps (Storch, 2000). Despite the great uncertainty about the total population and about its past and future evolution, hunting this species is still authorized in France for part of the year. In Spain and Italy, the rock ptarmigan is classified as threatened in the red list (Storch, 2000).

Ptarmigan populations are subject to several pressures, both anthropogenic and climatic. These pressures modify the living environment and can impact behavior and survival rates. Infrastructure developments in mountain ranges are the cause of significant bird mortality due to frequent collisions with power lines and ski lift cables (Bevanger & Brøseth, 2004; Bech et al., 2012; Buffet & Dumont-Dayot, 2013). It has been shown that anthropogenic structures have a negative effect on grouse survival (Hovick et al., 2014). Moreover, facilities increase the probability of direct disturbance on the wintering areas. It is likely that the expansion of touristic activities and infrastructures in the French mountains, associated with the habitat fragmentation and the continuation of traditional hunting have contributed to a reduction in the range of the rock ptarmigan in the last decades. Indeed, climate change, habitat fragmentation and anthropic pressures could lead to local extinctions (Furrer et al., 2016; Martinoli et al., 2017).

Global warming affects numerous bird species including rock ptarmigan. According

to the predictions of global warming in the alps, this species will suffer a contraction and a fragmentation of its suitable habitat in the next decades, accompanied by a shift of its living areas towards "climatic refuges" at higher altitudes (Brambilla *et al.*, 2022; Revermann *et al.*, 2012). This habitat restriction to mountain islets fragments the living areas and leads to isolation by distance in sedentary species like ptarmigan, which results in genetic impoverishment (Voskamp *et al.*, 2022). The reduction in regional movements thus implies a reduction in genetic diversity and weakens ptarmigan populations especially in the mountains of southern Europe (Caizergues *et al.*, 2003). This last point being crucial for the survival of a species, it is likely that the populations of rock ptarmigan will undergo a drastic decline if the warming trend continues. Moreover, it is known that species living in extreme environments show particular adaptations to their habitat, and are therefore less able to cope with rapid changes (Chevin & Hoffmann, 2017). While the sensitivity of ptarmigan to global warming and human disturbance is well documented (Imperio *et al.*, 2013), the effectiveness of conservation efforts is also recognized (Scridel *et al.*, 2021).

The example of bird populations in the temperate mountains of North and South America shows the interest of this type of habitat in maintaining the biodiversity richness at regional scales, as well as the conservation challenges associated with mountain species (Martin *et al.*, 2021). From this point of view, the study of non-invasive counting techniques, as well as the adaptation of monitoring protocols through the use of eco-acoustics, could eventually lead to an improvement in conservation measures for mountain bird species and for rock ptarmigan in particular.

1.2.5   Social interactions and communication behavior

Ptarmigans are ground dwellers, which walk in search of food. They are not much inclined to fly, except to perform courtship display, to defend their territory, or to escape from predators. Flight-related behaviors involve a significant expenditure of energy in grouses (Vehrencamp *et al.*, 1989). After pairing, the female and male follow each other most of the time at a few meters distance, and fly away when a danger approaches. Contact calls can be exchanged between paired males and females, and between female and chicks after hatching. They participate in maintaining contact when moving, as well as helping each other in the search for food. They are however very discreet and difficult to hear or record.

Conspecific attraction in habitat selection is well acknowledged in birds (Buxton *et al.*, 2020). It results in a grouping of territories during the breeding season, and this leads to the need for borders to be negotiated between males in ptarmigan. At an advanced stage of the breeding season, territories of paired ptarmigans are settled and other potential territories are not occupied. The effect of territorial signaling is therefore rather repel-

lent to neighbors or floaters than attractive (Stamps, 1994). The ability of the male to defend a quality territory is strongly linked to its reproductive success in rock ptarmigan (Bart & Earnst, 1999). The more vigilant the male is, the more the female increases her feeding time, thus improving reproductive conditions (Artiss & Martin, 1995). Besides, the "mate guarding" behavior is pronounced in grouse. It aims to prevent the occurrence of mating of other males with the female (Brodsky, 1988).

As a result, remote vocal interactions are of major importance in resolving neighborhood conflicts. The deterrent vocalizations of the males make it possible to remotely assess the competitors' value without necessarily engaging in a pursuit or a physical conflict. Brodsky & Montgomerie (1987) have shown that resident-neighbor contests are of low intensity and brief, while resident-floater contests are higher intensity, can last, and can escalate to fighting. This behavior is consistent with observations of "dear enemy effect" in many species (Ydenberg et al., 1988; Briefer et al., 2008). Paired neighbors have become familiar, and territorial boundaries are usually observed. The morning chorus then has the function of reminding their presence, and deterring newcomers. In this context, the display flight behavior is a crucial component of territorial defense (MacDonald, 1970). It is discussed in the next paragraph.

Display flights

The mating behavior in grouse involve different ground courtship displays (Guan et al., 2022). Males ptarmigans perform frontal display addressed to the female, and this participate to the sexual selection. Another display is very present in ptarmigans, that of the bell-shaped flights (see Fig. 1.5). Note that aerial displays are also observed in many passerine species in a breeding context (Mikula et al., 2022). In ptarmigan, only the male performs these demonstrations, and a song is systematically uttered during the flight. This is most often done during the dawn chorus. This visual and vocal demonstration is addressed to the females but also to the competing males. This behavior is therefore used both to attract and seduce a female, and to repel surrounding males. After the pairing, the same behavior is used to defend the territory from potential intrusions. It ensures the male to avoid unwanted mating of the female with other males, and to create a safe area for her to incubate the eggs. The term "display flight" is then used to refer to the bell shape flight and the song behavior as a whole.

Display flight is the ptarmigan's most conspicuous communication behavior, and the main one for repelling intruders, whether neighboring males or floater males. That is why its importance in the communication network is studied in detail in this work.

Figure 1.5 – Drawing of a Ptarmigan display flight from a sequence of photographs (from left to right). Adapted from del Hoyo *et al.* (1994).

Vocalizations

The rock ptarmigan is a non-oscine bird and as such does not learn its song (Kroodsma *et al.*, 1982). Inter-individual disparities in acoustic signatures between males are therefore mainly due to genetic and morphological characteristics. Thus males have a very reduced acoustic plasticity compared to oscines. Their vocalizations have a very stereotyped pulsatile character, and a complete song consists of series of pulses, with a pulse rate of 21 ± 3 ms (see Fig. 1.6). Songs of different subspecies can be listened on the Xeno-canto
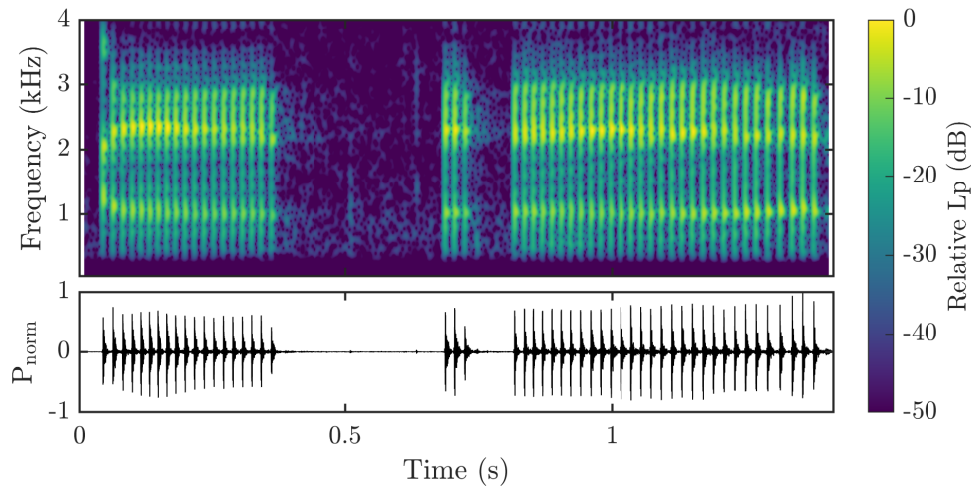
Figure 1.6 – Spectrogram (relative pressure level) and waveform (pressure normalized by the maximum amplitude) of a ptarmigan recording at a distance of 6 m, at the time of its take-off. Spectrogram settings: sampling frequency= 44.1 kHz, 900 points hanning window with 99 % overlap, filtering outside [400 − 4000] Hz frequency range.

website[3]. These vocalizations are produced by the syrinx and amplified by the trachea (MacDonald, 1970). The song's energy is mostly situated in the frequency range [800 - 3000] Hz.

---

[3]https://xeno-canto.org/species/Lagopus-muta

Individual identity information is present in these songs, and the information criteria have been identified by Marin-Cudraz *et al.* (2019). These criteria are essentially temporal: number of pulses per sequence, duration of the sequences and silences, pulse rate and acceleration. Two other parameters are frequency-based, that are the median frequency of the first two formants, visible at 1050 Hz and 2200 Hz in Fig. 1.6. For territorial birds, the information content of the signal enables them to address the functional constraints of the network organization: partner recognition and location, neighbor recognition and location, location and discrimination of strangers. In ptarmigan, the songs uttered during male-to-male confrontations are used to discriminate between neighbors and floaters, which is necessary for the territorial behavior of the species.

The rock ptarmigan ———————————————— **Summary**

The rock ptarmigan is a bird adapted to cold environments that lives in tundra or high mountain habitats. This species is concerned by the conservation issues of the alpine wildlife due to anthropic pressure and global warming which reduce its living range and will impact it in the coming decades. Ptarmigan lives in loose networks during the breeding season. The males defend both a territory and a female by performing display flights during the dawn chorus and in contests. The song performed during these display flights is a stereotyped communication behavior that has been little studied. As a non-oscine bird, the rock ptarmigan has a simple song composed of series of pulses carried by two main frequencies, used for long distance communication. This species is considered as a biological model to study communications in heterogeneous environments.

1.3   Outdoor acoustic propagation

This section is dedicated to a brief description of the different phenomena observed in outdoor acoustic propagation, as well as an overview of the state of the art on computational models. Several phenomena constrain the propagation of an acoustic wave, both in the heterogeneous medium that is the atmospheric surface layer (ASL), and also at the boundaries (Embleton, 1996). These boundaries are essentially the natural ground which often has an irregular geometry and a mixed structure. A summary of the characteristics of the propagation environment is presented Fig. 1.7. A distinction is made between effects related to the state of the atmosphere and effects related to the geometry and natural or artificial boundaries. The physical state of the ASL is determined by humidity, heat flux exchanged with the ground, mean wind speed, and the turbulence. The boundaries are defined by topography profile, soil type, and obstacles. The local nature of the soil determines its impedance, i.e. its behavior under the acoustic wave incidence.

The above-mentioned conditions are likely to change at different scales in both space and time. Therefore, outdoor acoustic propagation essentially takes place in heterogeneous environments. The study of acoustic propagation by field experiments is complex to implement, costly in time and investment, requires specific equipment, and gives access only to partial information at the time of the measurements, and in few measurement points. Numerical methods have the advantage of allowing the study of propagation under different conditions and over a wide area. As the different effects are well described by wave physics, a numerical method is used in this thesis to simulate many cases pertaining to communication in ptarmigan.

In the context of linear acoustics, the pressure level at a receiver position can be expressed by,

$$L_p(f, \mathbf{r}) = \text{SL}(f) + \text{PL}(f, \mathbf{r}), \tag{1.1}$$

with f the frequency in Hz, $\mathbf{r} = (r, \theta, z)$ the receiver position in cylindrical coordinates, SL the source level related to the sound power level L_w according to $L_w = \text{SL} + 10 \log_{10}(4\pi)$, $L_p = 20 \log_{10} p(f, \mathbf{r})/p_{\text{ref}}$ the pressure level (also called SPL thereafter, with $p_{\text{ref}} = 2.10^{-5}$ Pa), and PL the propagation loss. This PL accounts for the pressure attenuation outdoors and is due to the following effects: geometric decay, atmospheric absorption, refraction of the atmosphere, scattering by turbulent structures, ground effects, and diffraction by barriers. The PL is a negative value, which corresponds to the transmission loss that is positive.
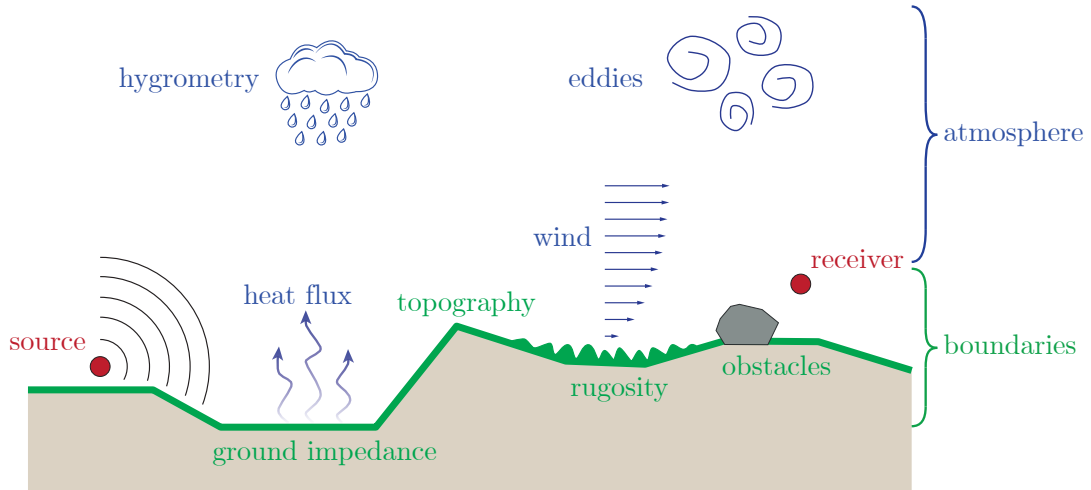
Figure 1.7 – Schematic representation of the different phenomena involved in outdoor acoustic propagation, relative to atmosphere and boundaries.

The geometric decay induces a wide range of pressure levels between near field and far field. It is therefore difficult to compare a model with measurements, or different models between them. To make the comparisons clearer, and to look in detail at the other effects, the geometric decay is usually removed. To make the comparisons clearer, the other effects are examined in detail, without the geometric decay. The term "free

field" refers to pressure levels calculated using geometric decay only, sometimes adding atmospheric attenuation. The mention "relative to free field" thus refers to the sum of the other contributions to the pressure field. The level relative to free field is ΔL, also called excess attenuation (EA).

In a complex environment as described Fig. 1.7, some of the atmospheric and boundary effects actually combine. For example, the atmospheric refraction induced by the wind and temperature profiles modifies the shape of the wavefront reaching the ground and therefore combines with the ground effects. These combined effects mean that a sum of attenuation coefficients can only give very rough estimates of the sound levels received under given conditions. If a more realistic estimate of the received sound level is to be calculated, it is necessary to model the propagation of the actual acoustic wave. In the following we detail the different physical effects, and then we briefly present the models currently used to study acoustic propagation.

1.3.1 Geometrical decay

The geometric decay is inherent to the propagation of a non-planar wave, it is the result of the expansion of the wavefront in three dimensions. The pressure perturbation of a spherical wavefront emitted by an omnidirectional point source decreases with the propagation distance. This is due to the distribution of a given amount of energy over an increasingly larger spherical surface. The complex pressure amplitude p_c propagating through an unbounded homogeneous atmosphere from an omnidirectional point source can be expressed by:

$$p_c(\mathbf{r}) = S\frac{\exp(ik_0R)}{R}, \tag{1.2}$$

where S is the source amplitude, k_0 stands for the wave number, and R is the distance to the source. This leads to a pressure decay according to $1/R$, which is very fast in near the source, while it slows down as the distance increases. At long distances, the wavefront can be considered locally as plane.

1.3.2 Atmospheric effects

The atmospheric effects related to acoustic propagation are cumulative, so they are more pronounced the longer the distance compared to the wavelength. This must be kept in mind when comparing the different atmospheric and boundary effects. Hereafter we describe atmospheric absorption, refraction, and turbulence.

Atmospheric absorption

The air composition in the ASL (atmospheric surface layer) induces energy losses that increase with the frequency. This attenuation in dB is proportional to the distance and can

be calculated via the absorption coefficient $\overline{\alpha}$ that depends on the atmospheric pressure, the temperature, the relative humidity and the frequency. Two phenomena generate the dissipation of the energy of the acoustic wave. A first type of absorption, called classical, is due to the viscosity of the air. Mechanical losses, as well as thermal losses in the medium induce energy decay (Bass *et al.*, 1995). In addition, the vibratory relaxation of the nitrogen and oxygen molecules, which represent 99 % of dry air, as well as the rotational relaxation, dissipate the energy at the micro scale. This is called molecular absorption.

The vibratory relaxation frequencies of the nitrogen and oxygen molecules are first described respectively in Eq. (1.3) and Eq. (1.4) according to the international standards (ISO, 1993):

$$fr_O = \frac{P_0}{P_{\text{ref}}}\left(24 + 4.04 \times 10^4 h \frac{0.02 + h}{0.391 + h}\right) \tag{1.3}$$

$$fr_N = \frac{P_0}{P_{\text{ref}}}\left(\frac{T_{20}}{T}\right)^{1/2}\left[9 + 280h \times \exp\left(-4.17\left[\left(\frac{T_{20}}{T}\right)^{1/3} - 1\right]\right)\right] \tag{1.4}$$

where P_0 stands for the ambient atmospheric pressure, and P_{ref} the reference value of atmospheric pressure (1 atm), T is the temperature of the atmosphere in Kelvin, and $T_{20} = 293.15$ K the reference value at 20°C. In addition, h is the molar fraction of water vapor, which can be calculated from RH (the relative humidity, in %) with $h = \rho_{\text{sat}}\text{RH}P_{\text{ref}}/P_0$, $\rho_{\text{sat}} = 10^{C_{\text{sat}}}$, $C_{\text{sat}} = -6.8346(T_0/T_{01})^{1.261} + 4.6151$, and $T_{01} = 273.15$ K the triple-point temperature of water. For conditions such as $P_0 = 760$ hPa, $T = 4$ °C, and RH $= 60$ %, the vibrational relaxation frequencies are such that $fr_O = 1249$ Hz and $fr_N = 135$ Hz. Given the ptarmigan frequency band [800 - 3000] Hz, we observe that both fr_N and fr_O influence the α values in our application.

The resulting $\overline{\alpha}$ coefficient is obtained in dB/m, depending on the frequency f with Eq. (1.5):

$$\begin{aligned} \overline{\alpha} = {} & 8.686f^2\left(\left[1.84 \times 10^{-11}\left(\frac{P_0}{P_{\text{ref}}}\right)^{-1}\left(\frac{T}{T_{20}}\right)^{1/2}\right]\right. \\ & + \left(\frac{T}{T_0}\right)^{-5/2} \times \left(0.01275\left[\exp\left(\frac{-2239.1}{T}\right)\right]\left[fr_O + \frac{f^2}{fr_O}\right]^{-1}\right. \\ & \left.\left. + 0.1068\exp\left(\frac{-3352}{T}\right)\left[fr_N + \frac{f^2}{fr_N}\right]^{-1}\right)\right). \end{aligned} \tag{1.5}$$

The absorption coefficient calculated with these expressions presents an uncertainty estimated to be ± 10 % within the intervals: 0.05 % $< h <$ 5 %, $253 < T < 323$ K, $P_0 < 200$ kPa, and $4 \times 10^{-4} < f/P_0 < 10$ Hz/Pa (Salomons, 2001). Thereafter we use the α in nerpers.m^{-1} given by (Bass *et al.*, 1995, 1996) Eq.(3), to directly apply

the atmospheric attenuation to the pressure values through the factor $\exp(-\alpha R)$, as in Eq. (3.32).

Atmospheric absorption varies throughout the day and year depending on the climate (Harris, 1966; Larsson, 1997). Fig. 1.8 shows the attenuation coefficient according to temperature variation (with fixed RH) and to RH (with fixed T), for the frequency band [0 - 4000] Hz. It is observed that atmospheric absorption and its variability, in relation to temperature and humidity, increase with frequency.
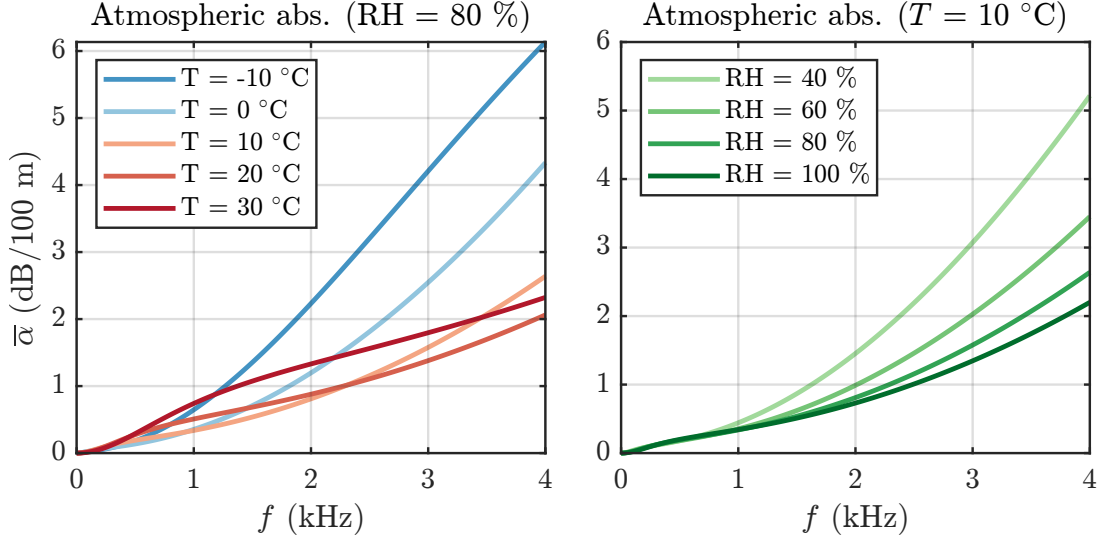
Figure 1.8 − Atmospheric absorption coefficient in dB/100 m for various temperature and relative humidity values. Left: temperature from −10 °C to 30 °C with fixed RH = 80 %. Right: relative humidity from 40 % to 100 % with fixed temperature T = 10 °C.

In free field and for a homogeneous atmosphere at rest, the total attenuation at a receiver point can be expressed by summing the geometrical decay and the absorption effect following,

$$L_p(f, \mathbf{r}) = \mathrm{SL}(f) - 20 \log_{10}(R) - \overline{\alpha}(f) R. \tag{1.6}$$

From Eq. (1.1), the free field propagation loss considering atmospheric absorption is equal to:

$$\mathrm{PL}(f, \mathbf{r}) = -20 \log_{10}(R) - \overline{\alpha}(f) R. \tag{1.7}$$

The PL is thus always negative.

Atmospheric refraction

Refraction due to atmospheric conditions has been noticed and experimentally studied for centuries (Gabrielson, 2006). It corresponds to the bending of the wavefront induced by a vertical sound speed gradient or wind speed gradient in the atmosphere, compared to a homogeneous case where the wavefront is perfectly spherical (Wilson, 2003). For convenience we can approximate a moving atmosphere by an atmosphere at rest with an effective sound speed $c_{\mathrm{eff}} = c + V$, with c the adiabatic sound speed, and V the component

of the wind speed in the propagation direction. This parameter is used hereafter for propagation computations in a vertical plane (see Sec. 2.5.1). The effective sound speed gradient $\partial c/\partial z$ depends on the temperature profile and wind profile in the considered direction of propagation. The refraction index n is defined as $n = c_0^2/c_{\text{eff}}^2(z)$, where $c_0 = c_{\text{eff}}(z = 0)$ is the reference sound speed at ground level. We refer to a "downward" condition when the wavefront is bent towards the ground, and to an "upward" condition when it is bent towards the sky.

The acoustic rays depict the trajectory of acoustic energy at several points of the wavefront (see Fig. 1.9), and describe the geometrical expansion of the wavefront as well as the specular reflections on the ground. For a homogeneous case, with $\partial c/\partial z = 0$, the acoustic rays are rectilinear. Each ray reaching the ground is reflected only once and there is no refraction. In the upward case, with $\partial c/\partial z < 0$, the rays are bent upwards, which implies the formation of a zone with no rays. In this zone, the acoustic energy is zero in the ray-tracing approach. This zone is called the acoustic shadow zone. For the downward case, with $\partial c/\partial z > 0$, the rays are bent towards the ground. The curvature of the rays implies multiple reflections and thus an increase in the acoustic energy density near the ground compared to the homogeneous case. Note that a linear sound speed gradient implies rays with constant curvature, i.e. corresponding to arcs of a circle.
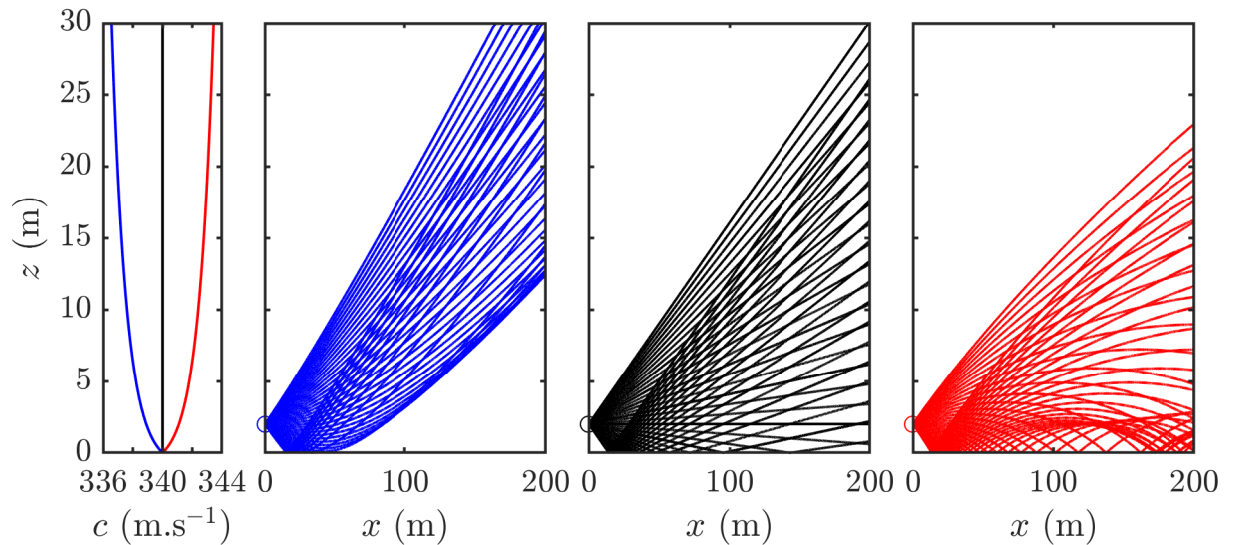
Figure 1.9 – Acoustic rays under upward (——), homogeneous (——), and downward (——) conditions, and corresponding effective sound speed profile c_{eff}. The point source is depicted by a circle at $x = 0$ m, $z = 2$ m.

Atmospheric scattering

The term atmospheric turbulence refers to different spatial scales of fluctuation of the meteorological quantities temperature and wind. The meso scale, at which organized turbulence is observed, is of the order of a hundred meters to a kilometer. This turbulence

can typically be described by large eddy simulation (LES) models (Cheinet & Siebesma, 2009; Cheinet & Cumin, 2011). Wind and temperature fluctuations on medium scales are distributed down to millimeter scales. The local turbulence can be seen as a stochastic quantity, characterized by a variance and a length scale. Different theoretical models describe the turbulent scalar field produced by temperature fluctuations in the atmosphere (Hinze, 1975; Ostashev & Wilson , 2016). These can be implemented under certain conditions in advanced numerical methods like FDTD or PE (see Sec. 1.3.4). In comparison, the scale of global weather forecasts is typically of the order of ten or a hundred kilometers.

This turbulence induces local fluctuations of the refraction index in the atmosphere, and diffusion of acoustic waves is observed. It leads to a decorrelation of the acoustic pressure in the wavefront. The interference patterns observed for still air are partly smoothed out by the spatial dispersion of the energy.

The intermittent character of the local turbulence makes it difficult to predict instantaneous levels (Wilson *et al.*, 1989). To address this problem some models consist of averaging the pressure field for a large number of realizations of temperature or wind speed fluctuations (Chevret *et al.*, 1996). An example using this method is shown Fig. 1.10. The two results without (a) and with (b) turbulence show the smoothing of the interference that can be induced at 4000 Hz by strong turbulence.
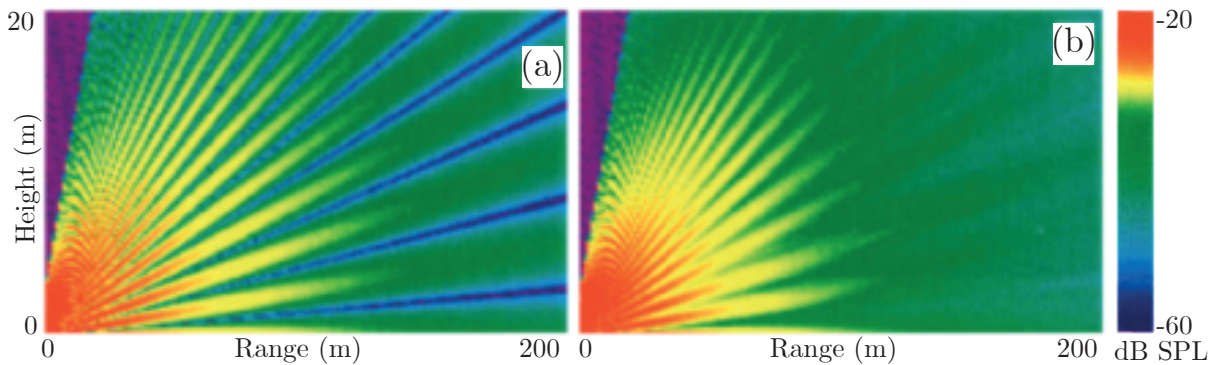
Figure 1.10 – Sound-pressure level near a rigid boundary, for a non-turbulent (a) and a turbulent (b) atmosphere (f = 4000 Hz, z_S = 1.2 m), with 50 realizations of the computation using a Gaussian turbulence. Figure adapted from (Chevret *et al.*, 1996).

Turbulent atmosphere near the ground and in upward refracting condition can significantly insonify the shadow zone, especially at high frequency (Gilbert *et al.*, 1990; Chevret *et al.*, 1996). Indeed, the scattering is all the stronger as the wavelength is small compared to the characteristic length of the refractive index fluctuations. We do not consider this phenomenon in the remainder of the thesis, due to the computational costs required to account for it and other considerations for the habitat studied (see Sec. 3.4). In addition, to integrate turbulence into our model, it would be necessary to have access to measurement data of rapid sub-second fluctuations in the atmosphere. This type of data can however be obtained using a three-dimensional anemometer, or a LIDAR technique for example.

1.3.3 Boundary effects

Ground effects

The ground is usually characterized by its acoustic surface impedance, that determines the attenuation and the phase shift of the wave reflected on the ground. In the case of a perfectly reflecting ground, the ground surface impedance is infinite, which implies that all the energy of incident waves is reflected. Conversely, natural soils such as lawns, decomposing leaves, sandy soils or snow cover are porous. The incident acoustic wave penetrates the micro-cavities of the soil, and undergoes viscous friction effects on a small scale that induce energy losses by heat exchange (Bérengier *et al.*, 2003; Attenborough, 2007). The attenuation of the reflected wave is frequency dependent. The description of the ground impedance is thus crucial for the estimation of the reflected wave (see Sec. 2.4).

The ground effect is the result of the interference between the sound reflected by the surface and the sound propagating directly from the source to the receiver. The pressure field can locally be amplified or attenuated, depending on the phase shift between the two contributions. We refer to this as destructive or constructive interference. This results in a reinforcement of the low frequencies in the vicinity of the ground, because the reflected wave adds to the direct wave. This implies that amplification can reach a maximum of +6 dB above a perfectly reflective ground for a homogeneous atmosphere. As shown Fig. 1.10 (a), a spatial interference pattern is induced by the presence of a rigid ground, and determined by the height of the source and by the frequency. Moreover, destructive and constructive interferences are all the more marked, i.e. entail a great excess attenuation (EA), if the the ground is hard. Note that the ground effect is all the less significant as the source is at a great height compared to the receiver distance. The ground effect is also less marked under upward propagation conditions because there is then a limited number of reflections on the ground. On the contrary, the ground effect is significant in the case of a source close to the ground, which implies a grazing incidence, and a fortiori in downward conditions because the wave is reflected many times (see Sec. 1.3.2).

Reflection and diffraction by edges

In the simple case of propagation in still air over a rigid plane ground, there is only one reflection. This can be clearly observed by the temporal calculation of a pulse emitted by an omnidirectional source point in Fig. 1.11. The expansion of the wavefront at regular time intervals enables one to see its spherical shape. When the wavefront reaches the rigid surface there is then a specular reflection, and a second wavefront appears. The latter propagates with a delay induced by the relative distance between the image-source and the source.

The presence of an obstacle in the propagation medium, like a wall in Fig. 1.12, generates multiple reflections. The first reflection on the ground creates a second wavefront
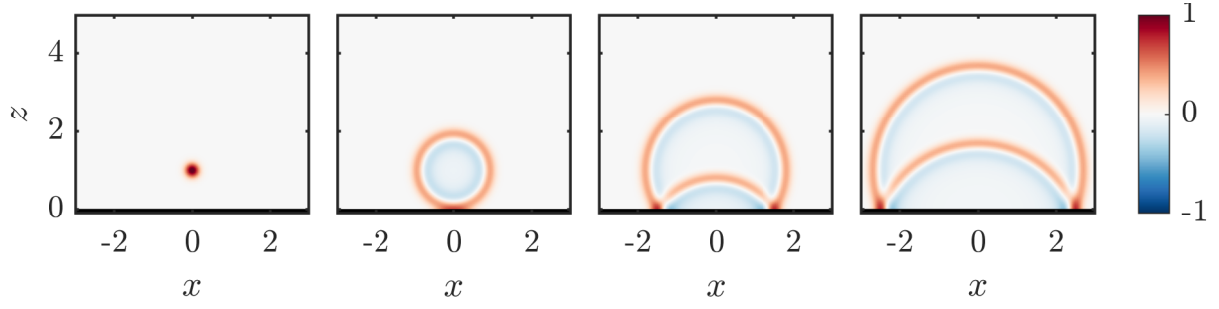
Figure 1.11 − Normalized pressure contour map of a Gaussian pulse propagating over a rigid plane surface, with dimensions normalized by the source position equal to $x = 0, z = 1$ (sketches for regular time intervals).

as before. These two fronts are then reflected on the wall and propagates towards $x < 0$. In addition, some of the energy is diffracted by the edge at the top of the wall. In the geometrical shadow zone, i.e. outside the line of sight of the source, at the right of the wall two wavefronts propagate in a distorted manner, and with a lower amplitude. The edge of the wall behaves as a secondary point source.
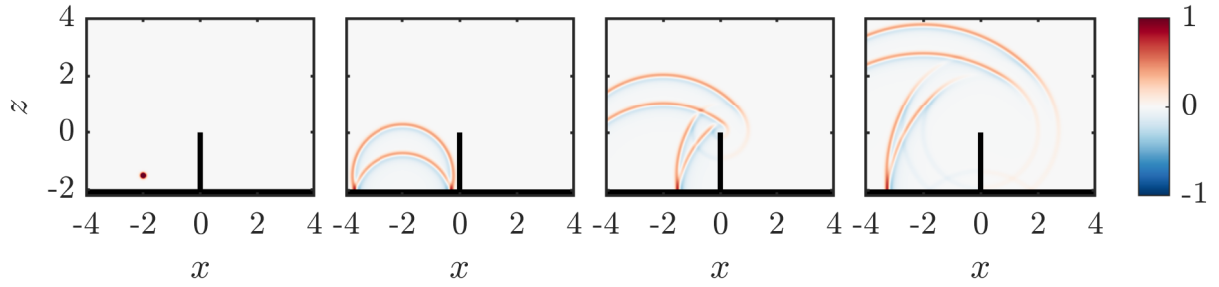
Figure 1.12 − Normalized pressure contour map of a Gaussian pulse propagating around a rigid wall, with x, z dimensions relative to the top of the wall (sketches for regular time intervals).

This effect is particularly noticeable for rigid obstacles such as the wall in Fig. 1.12; an absorbing wall would reflect and diffract the wavefront to a lesser extent. Similarly, in natural environments, the edges of rugged terrains induce multiple diffractions. These are likely to result in the propagation of a part of the wave in the geometric shadow zones, and also to produce back-scattering directed towards the source. As for specular reflections on the ground, the diffracted energy depends on the impedance of the ground.

1.3.4   Solving methods

Analytic solutions remain limited to simple configurations (flat ground and homogeneous atmosphere). When considering topography, meteorological effects or inhomogeneous grounds, numerical approaches are required. Calculation of signal propagation between source and receivers can be done using different models. Given a natural, and therefore complex, outdoor propagation medium, the accuracy of sound pressure estimations increases with both physical complexity and computational cost of the method used. One

method may consist in the calculation of the overall pressure levels by adding attenuations approximated using semi-empirical equations. This type of method includes the so-called "engineering models", and some recent statistical approaches. Advanced approaches are used to explain more finely the physical phenomena, that enable to describe the pressure field associated to a source. We outline these different approaches in the following.

Semi-empirical approaches

Semi-empirical approaches as proposed by Henwood & Fabrick (1979) are based on a sum of effects defined by wave physics or set empirically. It can be designated as an engineering model insofar as it is a simplified and efficient solution that provides a rough estimate of sound levels in a given area. The PL (propagation loss) is thus defined as a sum of attenuations due to the following effects: geometric decay (A_{div}), atmospheric absorption (A_{abs}), refraction of the atmosphere (A_{ref}), scattering by turbulent structures (A_{scatt}), attenuations due to ground effects (A_{ground}), and diffraction by obstacles (A_{diff}). We can possibly add attenuation vegetation. At a receiving point, the overall pressure level can be expressed as:

$$L_p = L_w + A_{div} + \underbrace{A_{abs} + A_{ref} + A_{scatt}}_{\text{ATMOSPHERE}} + \underbrace{A_{ground} + A_{diff}}_{\text{BOUNDARIES}}, \tag{1.8}$$

with L_p the pressure level at the receiver position (sometimes named RL for "receiver level"), and $A_{...}$ the above-mentioned attenuations. The attenuations taken into account are considered as decays in dB per meter. In this model, refraction by temperature and wind velocity gradients are considered by calculating the distance to the shadow zone.

This type of approach that gives an overall idea of the received sound levels as a function of frequency is largely used in bioacoustic research field. However, their use is limited to flat terrain, without taking into account the ground effect or obstacles. In the past decade, sound level mapping tools have been developed. The SPreAD-GIS toolbox for example has been created to be implemented in the open-source Sound Mapping Tools of the ArcGIS platform, to enable computation of noise map by frequency band (Reed *et al.*, 2009, 2012). This toolbox uses the same principle of attenuation summation by adding a topography effect and the possibility to set a background noise map. It has been notably used to study the propagation of bird signals (Raynor *et al.*, 2017). In a conception of the habitat as a homogeneous and isotropic propagation medium (Dabelsteen *et al.*, 1993), and given the difficulty of modeling the forest environment (Fang *et al.*, 2003), some studies have considered an overall habitat attenuation criterion (Haupert *et al.*, 2022). Other authors have considered statistical approaches that also involve environment-specific attenuation coefficients (Royle, 2018). These methods do not capture the fine interactions between the physical phenomena. Moreover, they do not provide a time signal after

propagation.

Ray tracing method

The ray tracing method consists in calculating the evolution of the amplitude and the direction of propagation of the wave fronts over time using rays trajectories. This method is based on a high frequency approximation, based on the assumption that the medium properties vary little at the scale of a wavelength (Candel, 1977; Pierce, 2019). It enables one to consider the range-dependent variations of both the boundaries and the atmosphere in three dimensions and at a low computational cost. It can thus take into account irregular terrain, as well as refraction by wind and temperature gradients (Lamancusa & Daroux, 1998) (as seen Fig. 1.9). Its low computational cost makes it particularly interesting in the context of very long propagation distances. However, the evaluation of pressure levels is impossible in shadow zones, because this method does not consider the sound field diffraction. Another limitation concerns the case of logarithmic wind profiles, since a strong gradient in the vicinity of the ground can lead to numerical errors (Li *et al.*, 1998a). Also, the calculation of levels through a receiving volume implies an ambiguity on the number of contributing rays. Other methods have been developed on the basis of geometric acoustics, such as Gaussian beams (Gabillet *et al.*, 1993) and sound particle (Heimann & Gross, 1999) and have attempted to address the limitations of this approach.

Boundary Element Method (BEM)

The BEM method is based on the solution of the integral formulation of the Helmholtz equation and on Green's theorem (Chandler-Wilde & Hothersall, 1985; Kirkup, 2019). It requires the discretization of the boundaries of the computational domain. The resolution requires the inversion of matrices involving the values of the acoustic potentials of all these points, and this can lead to a high computational cost if the domain is large. However, it is very efficient in the case of small complex geometries and mixed surfaces (Duhamel, 1996; Boulanger *et al.*, 1997). This method is therefore mainly used for compact problems, given the size of the domain and the wavelength. Initially, it cannot handle acoustic propagation in heterogeneous atmosphere. However, more recent works have included atmospheric refraction (Premat *et al.*, 2000).

Parabolic equation methods (PE)

The parabolic equation enables to describe the propagation in heterogeneous atmosphere with uneven ground and variable impedance (Candel, 1979; Gilbert & White, 1989; Salomons, 1998). Multiple solving methods are derived from this equation. They are all based on a step by step resolution of the complex pressure field generated by a harmonic source (as seen Fig. 1.10). PE methods are based on a paraxial approximation which considers that

the wave has a main direction of propagation. This neglects backscattering, and limits the solution validity to a propagation angle around the privileged direction (Ostashev *et al.*, 2019). The WAPE (wide angle parabolic equation) is a widely used method for outdoor acoustics. Its validity angle is about 40°. PE methods are usually solved in a 2D configuration, neglecting propagation in the transverse direction (assuming an axisymmetric approximation which postulates that the medium is constant with respect to the angle around the source). The 2D resolution induces a relatively low computational cost, which is well adapted to large scale problems (i.e. long distance and high frequency, which means a large number of wavelengths). These models can deal with uneven heterogeneous ground by a rotating domain method or a coordinate transformation, and account for refraction through the use of an effective sound speed gradient (Sack & West, 1995; Blairon *et al.*, 2002; Lihoreau *et al.*, 2006). It can also include a turbulent field and calculate by successive iterations the resulting average levels (Chevret *et al.*, 1996; Blanc-Benon *et al.*, 2002). In addition, 3D approaches make it possible to consider the complex effects related to the interactions between atmosphere and topography (Khodr *et al.*, 2020). Note also that non-linear effects can be accounted for (Yuldashev *et al.*, 2021).

Transmission Line Matrix (TLM)

A temporal approach called Transmission Line Matrix (TLM) was initiated by Johns & Beurle (1971) for electromagnetic applications and was taken up by Saleh & Blanchfield (1990) for acoustic wave propagation. It is based on the Huygens principle, which describes the wavefront as a coherent set of secondary point sources (Kagawa *et al.*, 1998). The pressure information is transmitted from point to point by successive iterations on adjacent spatial steps (Hofmann & Heutschi, 2007; Guillaume *et al.*, 2011). It can account for all the phenomena affecting acoustic propagation in the time domain as does the FDTD (see next section), with the advantage of a low computational cost (Faure, 2014; Chobeau, 2014). The refraction effects must however be approximated by an effective sound speed profile. Moreover, problems of computational stability and dispersion due to numeric scheme may arise for long distance propagation, and errors may appears depending on the spectral distribution of the source (Goestchel *et al.*, 2022). Nevertheless, this method is promising for temporal computation in heterogeneous environments because of its lower computation cost than FDTD.

Linearized Euler Equations - FDTD

Acoustic propagation can also be simulated using equations derived from fluid mechanics such as the Linearized Euler Equations (LEE). These equations involve few physical approximations and are therefore very general and applicable to many complex problems. The increase in computational capabilities in the last decades made their use possible.

Finite-Difference Time-Domain methods (FDTD) are commonly used to solve the LEE (Yee, 1966). The need to use fine meshes implies high computation costs, which is even more critical for large scale and three dimensional problems. This formulation consists in solving the propagation equations in an iterative way, thanks to a discretization in time and in space. It can provide a temporal description of the wavefront progression for any given source (see Figs. 1.11 and 1.12 for examples). This type of resolution is very accurate for describing acoustic propagation in stratified media and through turbulence, and currently used to resolve complex problems in outdoor acoustics (Bailly & Juvé, 2000; Ostashev *et al.*, 2005; Van Renterghem, 2014). Moreover, time-domain solvers were developed in curvilinear coordinates for sound propagation over complex terrain (Dragna *et al.*, 2013). In addition, the low-dispersion numerical schemes enable simulation for large-scale problems without artificial signal distortion (Tam, 2012; Cotté *et al.*, 2009).

Note that non-Cartesian meshes could be used with other methods such as finite volume schemes (Jameson & Baker, 1983), discontinuous Galerkin methods (Wang *et al.*, 2021), or the finite element method (Mattiussi, 2000). Yet, they are less used in the context of outdoor propagation.

1.3.5 Choice of a solving method

We have seen the different methods used to predict outdoor sound levels. For our application, the choice is based on several criteria: the balance between the efficiency to account for complex phenomena and the overall computational cost, the necessary input data, and the possibilities in terms of output data. It is necessary to have an efficient and versatile tool to simulate the propagation in various situations. We summarize in Tab. 1.1 the ability of the numerical models described in the previous sections to account for the physical effects involved in acoustic propagation, and the comparative computational cost. Note that these comparisons are indicative, as the various possible implementations each model is not necessarily considered here.

For the study of communication in ptarmigans, constraints on habitat and behavior must be considered. The mountain environment requires consideration of topography as well as meteorology and ground heterogeneity. In addition, since ptarmigan can communicate over long distances, it is estimated that computations over distances of about one kilometer, and at frequencies of 1000 to 2000 Hz, are required.

We discard semi-empirical and analytical approaches because they are only valid for simple cases. Moreover, we have not considered the use of BEM and TLM solutions because of their limitation to handle large scale problems. Also FDTD code requires too much resources for the domain sizes involved. Finally, after several test calculations on real mountain topographies, it appeared that edge diffraction is a key phenomenon to be taken into account in this context. The active space estimate requires to evaluate

Table 1.1 – Comparison of solving methods for outdoor acoustic propagation, adapted from (Blairon, 2002). The ability to account for propagation effects is indicated by the symbols: $\emptyset$ null, $*$ partial, $**$, full. The reader can find in the above mentioned references for each model the information used in the table.

Parameter	Methods	Rays	BEM	WAPE	TLM	LEE
Impedance	$**$	$**$	$**$	$**$	$**$
Temperature profile	$**$	$*$	$**$	$**$	$**$
Wind profile	$**$	$\emptyset$	$*$	$*$	$**$
Topography (reflection)	$**$	$**$	$**$	$**$	$**$
Topography (diffraction)	$\emptyset$	$**$	$*$	$**$	$**$
Turbulence	$**$	$\emptyset$	$*$	$?$	$**$
Time signal computation	$**$	$*$	$*$	$**$	$**$
Computational cost	low	medium	low	medium	high

received levels outside the line of sight of the sources. Since the ray tracing method does not explicitly deal with diffraction, it is not used in this thesis. We therefore chose to base our propagation code on a rotating WAPE method introduced by Blairon *et al.* (2002).

The signal energy of the ptarmigan is essentially distributed between two main frequencies that are f_1 and f_2 formants (see Sec. 1.2), which can be handled simply by the frequency computation of WAPE. In addition, the study of acoustic communications requires the ability to evaluate not only the received levels but also to simulate the signal at the receiver. To do this, a code based on the wave equation in time or frequency domain is mandatory. In this perspective, the WAPE code propagates the amplitude and phase information that are necessary for the reconstruction of the signal. It is therefore possible to obtain the levels received as a function of the frequency, but also the temporal signal, by means of a sufficient number of narrow band computations and a Fourier synthesis.

Regarding the input data, the WAPE code requires the terrain DEM (Digital Elevation Model), the sound speed profile, and the ground impedance. The DEM can be provided by mapping services, and the other two parameters can be determined by field measurement (see Sections 2.4 and 2.5). For all these reasons, a WAPE code is a good compromise to study long-distance acoustic communication through physical simulations.

Outdoor acoustic propagation ——————————————————— **Summary**

The outdoor sound propagation is governed by many phenomena related to the atmosphere and the ground. In heterogeneous environments these effects combine, which makes their modeling complex. In order to estimate and map sound levels in the alpine environment, the use of a numerical model is required. In a compromise between the consideration of physical effects, the computational cost, and the possibility to integrate field data informing the propagation environment, we choose to base our computation code on the rotated WAPE method.

1.4 Active space & detection space

The active space (AS) is a central bioacoustic concept to understand animal communication networks. It corresponds to the area within which a bird can detect the song of a conspecific and extract information. This area can be divided into subspaces according to the quality of communication defined by the signal to noise ratio (SNR). The following interactions are thus ordered by their increasing SNR requirement: detection, discrimination, recognition, comfortable conversation (Larsen, 2020). An example of these subspaces is shown Fig. 1.13. The active space related to these interactions is depicted by areas with concentric distribution according to the RL (received level): the smaller the zone around the emitter, the better the communication quality. An information transmission ratio of 100% ensures comfortable communication, whereas a ratio of 0% prevents detection. Hence the active space defines which surrounding birds receive information from a singer, and the ratio of transmitted information to that contained in the emitted signal. The group of potential receivers associated with this area is called the "audience".
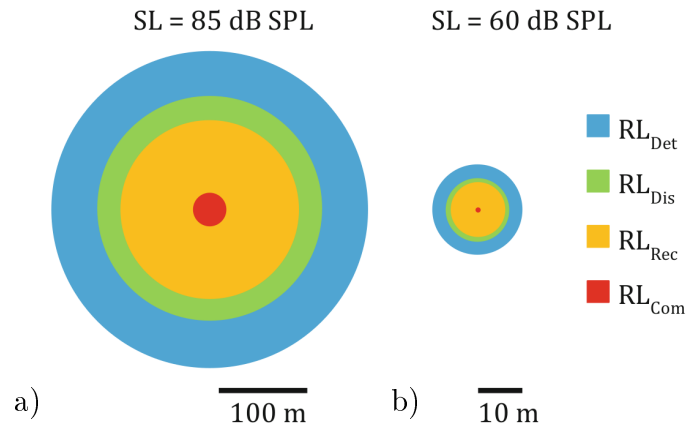
Figure 1.13 – Active spaces under homogeneous conditions calculated only with geometric decay, for SL = 85 dB a), and SL = 60 dB b), for a detection threshold set to 40 dBSPL. Examples of four AS limits defined according to the minimum RL (received level) required in any species for: detection (RL_{Det} = 40 dB), discrimination (RL_{Dis} = 43 dB), recognition (RL_{Rec} = 45 dB), and comfortable communication (RL_{Com} = 60 dB). Figure adapted from (Larsen, 2020)

In parallel of the active space, the detection space determines the possibilities of recording biological data in ecoacoustic studies. The detection space is considered hereafter as the sampling area when recording a soundscape. These two quantities are crucial for the study of communication behavior and for the population census by acoustic methods. This section is dedicated to the definition of these spaces, according to the four determining parameters that are the source level (SL), the background noise (BN), the propagation loss (PL), and the signal to noise ratio (SNR) that enables signal detection in noise. These are the key parameters for spatial limits of outdoor acoustic interactions.

To fix the limit of the AS, a threshold on the PL decay is defined according to the

other three parameters following:

$$PL \geqslant BN + SNR - SL. \tag{1.9}$$

The intersection between PL decay obtained from Eq. (1.7) and the PL threshold, as shown Fig. 1.14, leads to a maximum distance $r_{\max}$ up to which the signal can be detected for an ideal case in free-field and homogeneous atmosphere. This threshold must be distinguished from the absolute detection threshold (DT) at the receiver position, that is a positive value defined by: DT = BN + SNR.
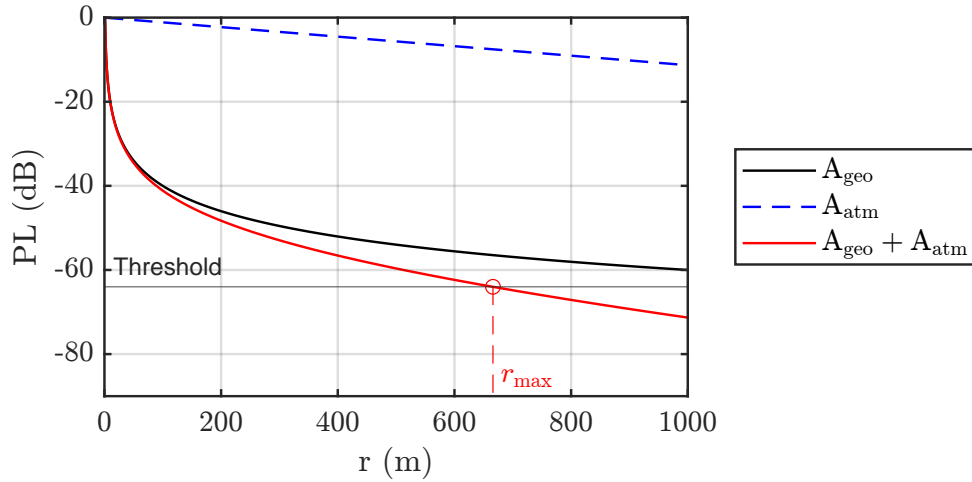
Figure 1.14 − Example of PL according to the radius r, considering only geometric decay and atmospheric absorption. Detail of geometric and atmospheric attenuations, and determination of maximum distance $r_{\max}$ according to a PL threshold. In this example, the threshold depends on: SL = 90 dB, BN = 23 dB, SNR = 3 dB. The physical settings are: frequency f = 2000 Hz, temperature T = 5 °C, pressure P_0 = 760 hPa, relative humidity RH = 70 %.

The following sections detail the three parameters affecting the active space, excluding PL driven by the propagation phenomena.

1.4.1 Source level (SL)

The source level (SL) is the first parameter to be estimated to evaluate remote acoustic communications. It is defined as the pressure level received at 1 m in the axis of the singing bird in free field. The ideal conditions for measuring SL are rarely found in wild birds. Therefore, a measurement further away from the source is usually made. The geometric decay can be calculated by knowing the precise distance between the microphone and the bird at the time of singing according to Eq. (1.2). The SL can be estimated from the RL at a microphone by subtracting the geometric decay occurring between the source and the receiver.

It has been shown that oscine and non-oscine birds could adapt their SL in response to a variation in background noise level (Brumm, 2004; Brumm *et al.*, 2009;

Brumm & Zollinger, 2013). This phenomenon is called the Lombard effect. In practice, this effect only partially compensates for the increase in background noise, with an increase ratio of less than 1:1. The additional energy expended must be justified by the context that makes this increase necessary (Zollinger *et al.*, 2011). A more conservative alternative for birds is to wait and communicate when the background noise has decreased. On the other hand, the physiological limitations of the bird's vocal organ limits the ability to increase in SL. Therefore, this effect should be viewed with caution. It is not necessarily present in all contexts and may vary depending on the ecology and the type of communication network to which the bird belongs.

1.4.2   Background noise - soundscape

Background noise (BN) is defined as the noise that exists in a given location without the contribution of the source of interest, i.e. the bird song being studied. It depends on three potential contributions: *geophony*, which is the set of abiotic sources such as wind, rain or mountain stream; *biophony*, which is the set of sounds produced by the species sharing the environment; and *anthropophony*, consisting of the sounds induced by human activities. Thus BN is intimately linked with the soundscape notion, which gathers all sound produced in a landscape, including biophony, geophony, and anthropophony (Pijanowski *et al.*, 2011). The soundscape contains unique acoustic compositions in the frequential, spatial and temporal dimensions. As a result, the BN varies in space and time. In practice, it is very expensive to finely map the BN because it requires a large number of autonomous recording units (ARU). Nevertheless, eco-acoustic studies can use ARU to estimate the area sampled at the time of recording from the BN level (Haupert *et al.*, 2022).

To determine the BN, it is necessary to use a representative indicator over the time period. It is therefore preferable to use an indicator that is not sensitive to pressure peaks caused by isolated sound events. This is why the statistical index L_{90} is used. It is defined as the pressure level exceeded 90 % of the time, and is calculated from the increasing cumulative curve of short-term L_{eq} levels measured with a sound level meter.

Variations of BN can be observed in amplitude and frequency, showing temporal patterns at different time scales. In particular, circadian behaviors cause daily patterns of biophony and anthropophony that can be noted at many high density sites (Pijanowski *et al.*, 2011). The soundscape is thus highly dependent of the habitat, and it is influenced by many intricate biotic and abiotic factors (Grinfeder *et al.*, 2022).

Because it partly defines the received level at a given location, the BN is one of the determining characteristics of the active space. Moreover, the active space (AS) is all the more sensitive to the BN parameter as the latter is low. Indeed, the received level decreases according to the logarithm of the distance r. At large distances, and considering a fixed

SNR for the detection, a small variation of BN implies a large variation of the spatial limit of the AS (as seen Fig. 1.14). Therefore, the BN must be carefully determined. Note that the spatial distribution of BN is not known. Therefore, caution is required when using BN estimates in AS applications.

1.4.3 Signal detection & detection in noise

The hearing threshold has not been measured in grouse to our knowledge. However, an order of magnitude can be obtained from experiments on other Galliforms. Audiograms are similar in Japanese quail (*Coturnix japonica*) and domestic chicken (*Gallus gallus domesticus*), with minima in the $[1000 - 6000]$ Hz and $[500 - 4000]$ Hz frequency bands, respectively (Strawn & Hill, 2020; Hill *et al.*, 2014). The hearing threshold at 1000 Hz is 16 dBSPL (sound pressure level in dB relative to 20 µPa) for Japanese quail, and 10 dBSPL for chicken. We can thus consider that the ptarmigan is able to detect very low levels of its first formant, around 10 to 16 dBSPL, which is a great advantage for long distance communication.

The hearing threshold is an important parameter to consider the lowest levels detectable by the species studied. However, in a natural environment background noise is omnipresent, and it is most often above this threshold. This is why it is necessary to consider the possibilities of communication in noise. The determining criterion is then the hearing threshold in noise. To our knowledge, there is no measurement of detection or discrimination in noise in Galliformes. Alternatively, we can consider thresholds measured in a passerine bird, in the wild, the Red-winged Blackbird (Brenowitz, 1982b). The signal-to-noise ratios during playback responses of other males lead to identify a threshold at 3 dB above the ambient noise that elicits a strong response (song octave band $[2830 - 5660]$ Hz, ambient noise levels in this band: 15 to 36 dBSPL). The same SNR has been obtained for response of females in Brown-headed Cowbirds (*Molothrus ater ater*) which supports this finding (King *et al.*, 1981). On the other hand, the detection threshold in frequency-modulated noise was measured in the waved parakeet, a non-oscine bird (50 % chance of detection). This threshold varies from 2 to 5 dB depending on the number of modulations per octave (Amagai *et al.*, 1999). These data appear to be relevant to estimate the hearing threshold in noise for rock ptarmigan at SNR = 3 dB.

The SNR value obtained by Brenowitz (1982b) in the wild is preferred to those derived from laboratory studies measuring critical ratios (CRs) (Saunders *et al.*, 1978), for several reasons. First, laboratory studies condition birds to a different motivated response behavior than typical bird-to-bird communication behavior. Second, the masking noises used are limited to specific frequency bands, which do not correspond to a typical outdoor noise spectrum (Saunders *et al.*, 1978; Okanoya & Dooling, 1987; Dooling & Blumenrath, 2013). Finally, for our application, we rather consider a threshold that makes at least pos-

sible species discrimination, not only sound detection. Only this discrimination can result in an informed response behavior in the context of a communication network. This is why SNRs corresponding to CRs obtained in the laboratory do not seem to be appropriate for our application, which must be representative of a realistic network.

Active space & detection space ─────────────────── **Summary**

The active space is the area within which a bird can detect the song of a conspecific and extract information. It represents the area of influence of the singing bird. Conversely, the detection space is the sampling zone from which a bird (or recorder) can extract information from any conspecific. It represents the listening area of a bird. These two spaces vary depending on the position of the bird (singing or listening), the source level of the emitter, the propagation conditions, the background noise, and the receiver's ability to detect sound in noise. In ecoacoustic studies, the detection space is determined by the detection performance of the sound processing algorithm used.

In this thesis, the parameters of the active and detection spaces are partly set by thresholds, and their probability distribution has not been considered. The determination of each parameter is detailed in Chap. 2. This configuration is used for the study of communication by focusing on the physical aspects of propagation.

1.5   Questions, hypothesis and scientific approach

We have seen how acoustic communication between birds occurs largely within a network that is spatially spread out. Based on this observation, interactions between individuals, and in the first place the reporting and listening behaviors, are impacted by the effective transmission of information through their habitat. In other words, the conditions of propagation exert a pressure on the modalities of communication used. In response to these constraints, individuals can modify their behavior at different levels: spatially, by adapting their movements and their singing positions (Wilczynski *et al.*, 1989; Mathevon *et al.*, 1996; Dabelsteen *et al.*, 1993; Mathevon *et al.*, 2005); temporally, by changing their daily signaling habits (Henwood & Fabrick, 1979; Staicer *et al.*, 1996; Dabelsteen & Mathevon, 2002); or in the coding of the information, by modifying their songs (Ey & Fischer, 2009; Hardt *et al.*, 2021). Many hypotheses related to this potential adaptation of species to the acoustic context of the habitat have been formulated in the last decades. They are grouped under the name of acoustic adaptation hypothesis (AAH).

To fully grasp the scope of the issues raised here, we schematize the habitat-network system in Fig. 1.15. Environmental conditions constrain propagation, and thus the active and detection spaces. In response, individual behaviors can deal with these two physical

limits of information transmission in different ways; through organization in time and space, and through coding of information. Finally, each individual behavior determines the nature of the communication network over time. And as a corollary, the network from the individual's point of view, i.e. the set of conspecifics within earshot, constitutes the framework for decisions to communicate or not and in what manner.
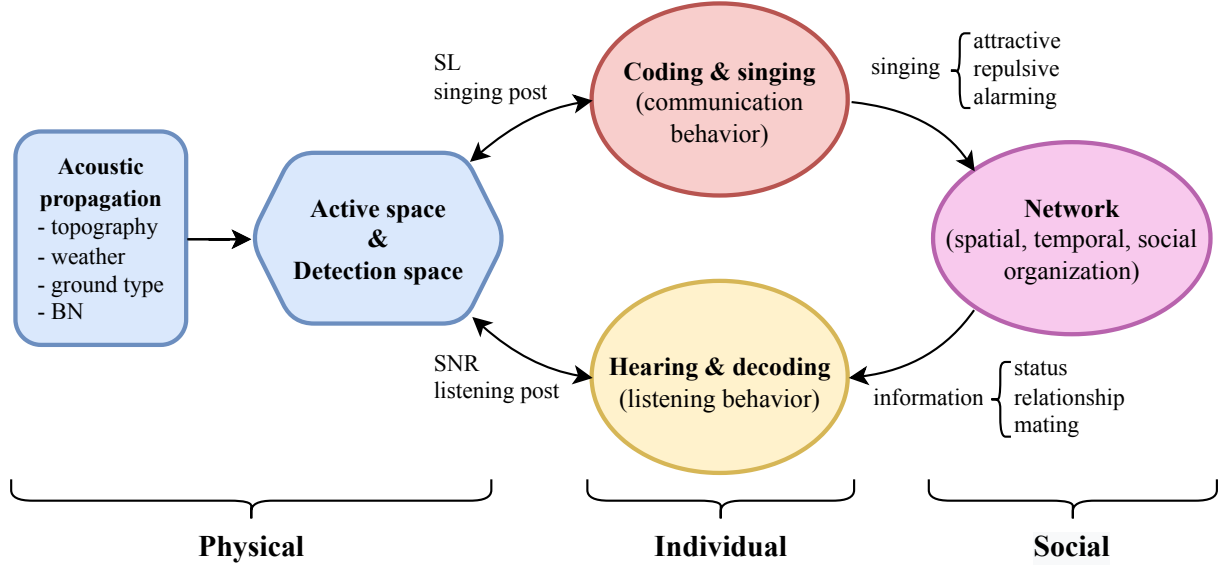
Figure 1.15 – Diagram of the relations between the communication spaces (active space and detection space) and the network, via the singing and listening behaviors at the individual level ($\rightarrow$ cause and effect relationship).

Therefore, the remote acoustic communication network is likely to change at three distinct levels: according to the physical propagation of the sound, by individual behavior, and by social interactions as a whole. Studies dealing with communication networks usually focus on one of these aspects, as the subject is complex by definition and concerns distinct research areas: neuro-ethology, behavioral studies, bioacoustics, ecology, and acoustics. In this context, we choose to deal with three research axes presented in the remainder of this section as Q1, Q2 and Q3. The three chapters 4, 5 and 6 written as independant studies. provide some answers to these three research axes. These are limited to the physical dimensions of the propagation, as well as to the spatial and temporal organization of the network. Thus we deliberately leave the social dimension and the contribution of vocal plasticity for the coding of information aside. In addition, we do not address the developmental dimension of the innate or acquired communication behavior. We are interested in the effective communication possibilities of adult individuals located in a given habitat and at a given moment. To this end, and for the sake of consistency, we choose as biological model a non-oscine bird that lives in a loose network, and that presents a very stereotyped song with little variation. The rock ptarmigan, which presents these particularities, is taken as an example throughout this thesis.

Q1: How do environmental conditions affect active space?

The first questions regarding the active spaces of communication are those of variability: how do environmental conditions affect the active space, and to what extent? We therefore seek to answer to these questions both qualitatively and quantitatively, in order to understand the impact that may exist on communication networks. Prior to this considerations, this line of research should provide insights into that complex question: can we reliably estimate the sound propagation in a heterogeneous environment for high mountain birds, using a relatively limited set of environmental data, and with a low computational cost? To tackle this methodological questions we carried out acoustic propagation measurements with two objectives: (1) It should constitute a relevant data set in the context of acoustic propagation in a mountain environment. It serves as a basis for comparison with numerical simulations, and thus enables to validate the propagation code later used in concrete applications. (2) These experiments should inform the required physical measurements to accurately describe the environment. Indeed, we use meteorological and ground impedance measurements to determine the input data of the propagation code. These data must therefore be sufficient both quantitatively and qualitatively to enable realistic estimation of long-range sound levels by the numerical simulation. The development of a tool adapted and validated for propagation in mountain environment gives the possibility to answer our first two questions concerning the variability of active spaces.

This work, which was published in 2022, is reported in Chapter 4. The related article (Guibard *et al.*, 2022) is available at the following link: https://doi.org/10.1121/10.0011545.

Q2: How does a remote acoustic communication network cope with propagation constraints?

It is assumed that the spatial and temporal organization of the communication network is affected by environmental conditions. We expect the influence of weather, singing post, and habitat characteristics on communication. We therefore question the ability of the network to adapt to propagation conditions. To date, the consequences of AS variability on the organization of communication networks remain largely unexplored. However, to take into account the complexity of the environment and be able to model a communication network it is necessary to use the previously developed computational tool. We therefore propose a physical study of propagation constraints in the heterogeneous environment of the high mountains, and an analysis of its effect on a communication network in birds. To do so, we use field data from a population of rock ptarmigan, an emblematic species of the high mountains that is adapted to its extreme conditions. We base the study on dawn chorus recordings, GPS tracking of the birds, and meteorological data collected on site. The active spaces are estimated using numerical simulations performed with the

previously developed code. The question is separated into two distinct issues, concerning adaptation to weather on the one hand, and adaptation to topography on the other: (1) Do weather conditions influence the temporal organization of communication? (2) How is the spatial organization of communication driven by the emitter position? This study is detailed in Chapter 5.

Q3: How can evaluation of detection spaces improve acoustic monitoring of bird populations?

During biodiversity monitoring campaigns carried out using ARUs, the sampling area, i.e. the detection space (DS) of the recorder, is likely to vary as the active space (AS). Based on this observation, and considering that few ecoacoustic studies take this aspect into account for acoustic monitoring, we introduce a method to physically estimate the detection space. This estimation provides a quantification of the sampling pressure applied at each time interval. In addition, it enables to calculate proxi estimates of the occupancy per unit area as well as the pseudo-replication rate contained in the data. To do this, we test a method based on the acoustical reciprocity principle, by adapting the computational code previously developed. Then, we apply this method to an instrumented mountain site dedicated to the monitoring of a ptarmigan population. The problematic is thus divided into two questions: (1) Can we reasonably use the reciprocity principle to estimate detection areas? (2) How does the variability of the sampled area impact the assessment of activity or presence metrics on a monitored site over space and time? These investigations are presented in Chapter 6.

Chapter 2

Experimental methods

Abstract

To carry out our three research axes presented in Sec. 1.5, it is necessary to conduct both field experiments and numerical simulations, the former providing valuable inputs to the latter. This chapter is dedicated to the description of the various methods used on site for the physical measurements, and for the evaluation of the ptarmigan behavior. The physical measurements conducted include acoustic propagation experiments, determination of ground impedance parameters, and measurement of wind and temperature profiles for effective sound speed estimation. Besides, the measurements concerning ptarmigan include spatial tracking by GPS, evaluation of song characteristics, and estimation of vocal activity from automated passive recorders. These methods are employed throughout the thesis chapters. Slight adjustments are then specified where necessary in the respective chapters.

Contents

2.1 Introduction

The study of acoustic communication in birds requires knowledge of the habitat, ecology and behavior of the species. As we have seen, birds can respond to habitat constraints and also to peer pressure. On the other hand, effective communication is constrained by environmental conditions. In order to identify the parameters influencing both propagation and behavior, we decided to collect both physical data from the study sites and biological data from a rock ptarmigan population.

In one hand, we have to measure meteorological conditions, ground impedance, and to consider the topography data to be able to inform our propagation code and conduct realistic estimations of the propagation in alpine environment. In addition, a protocol of acoustic measurement is set up on the Col du Lac Blanc to acquire long range propagation data, together with meteorological data, in a heterogeneous environment. This measurement campaign then makes it possible to reliably compare the propagation code with field data, and thus to evaluate the relevance of the use of our method (comparisons detailed in Chap. 4).

On the other hand, several types of biological data concerning the rock ptarmigan must be measured in order to study the acoustic communication within a population monitored at the Flaine ski resort. A GPS monitoring protocol has been applied since 2017 on the site during the breeding season, and it provides information on the birds' movements and their territories. In addition, manual recordings of ptarmigan songs are made in order to measure their SL, and to know precisely their spectrum. These data are then used to precisely define the active space in our behavioral study (see Chap. 5).

Finally, an acoustic monitoring protocol is also conducted in Flaine using autonomous recorders throughout the breeding season. These data are used to assess the vocal activity of ptarmigan on the site using an in-house detection algorithm. It is then possible to question the relevance of acoustic monitoring in heterogeneous environments, and the benefit of estimating detection spaces by a propagation code (see Chap. 6).

This chapter is thus dedicated to the description of the study sites, as well as the materials and experimental methods used throughout the thesis.

2.2   Experimentation sites

The two experimental sites of this thesis work are located in the French Alps (see Fig. 2.1). They both have the characteristics of the typical rock ptarmigan habitat with an altitude above 1800 m, large rocky areas and alpine meadows in summer, and a thick snow cover in winter. Site 1 at Col du Lac Blanc is dedicated to propagation experiments with meteorological measurements. Site 2 at Flaine ski resort is dedicated to the study of bird behavior and passive acoustic monitoring (PAM) techniques. These two sites are presented in more detail hereafter.
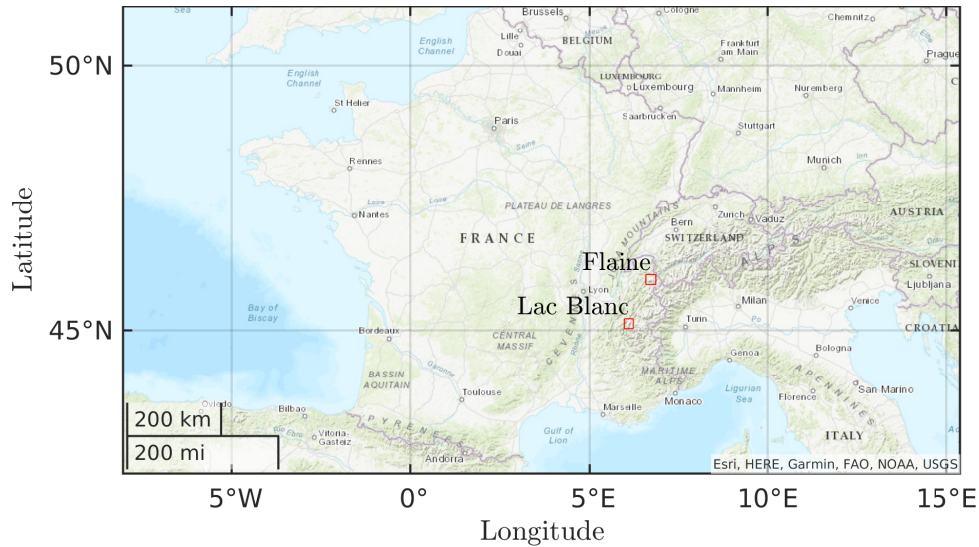
Figure 2.1 – Location map of the two study sites in the French Alps: Col du Lac Blanc and Flaine.

2.2.1   Site 1: Col du Lac Blanc (CLB)

A mountain site was chosen to conduct long range acoustic measurements, and to characterize snow impedance. These measurements are then used as reference for comparison with numerical simulations (propagation code). Several constraints are considered for the choice of the site. First, the topography must be precisely known. Second, the site must be far enough from human infrastructure so that background noise level is sufficiently low.

Third, the site must be located at a sufficiently high elevation so that there is a snow cover in the mid-season, when the weather conditions are suitable for the experiments. It must also be adapted to the fine measurement of local meteorological conditions in cold environment. For all these reasons, the site of the Col du Lac Blanc (Isère, France, see Fig. 2.1) was chosen with the agreement of the CEN (Centre d'Etudes de la Neige), which maintains an experimental station there. A photograph shows the site from above with the weather stations and the shelters positioning in Fig. 2.2. A Digital Elevation Model (DEM) of the entire pass with bare ground was previously determined by Guyomarc'h *et al.* (2019), using a laser scanning technique (see Fig. 2.3). The horizontal resolution of 1 m and vertical resolution of 0.1 m is sufficient to finely describe the topography. This made possible to observe the phenomena appearing at medium frequencies of about 500 Hz to 2000 Hz in acoustic propagation simulations.

Figure 2.2 – Overview of the Col du Lac Blanc experimentation site in June 2021 from the Dôme de Petites Rousses (altitude 2720 m, Grandes Rousses massif, France). The viewpoint of the photo is located on Fig. 2.3. Note that the snowpack is thicker than during measurements in October 2020, and the topography smoothed out at the pass, along the north-south axis.

The meteorological instrumentation of the site is detailed in Sec. 2.5. Meteorological data along with the digital elevation model (DEM) enable relevant comparisons of the acoustic measurements and the simulation results. Two automated weather stations (AWS) are used to measure separately wind speed and direction (AWS INRAE), and temperature and humidity profiles (AWS CEN). The experiments of propagation and snow impedance measurements were conducted on this site between the 19th and 30th of October 2020. Propagation experiments were performed on 200 m transects arranged along the north-south axis at the pass crossing. The studies conducted on this site are presented in Chap. 4.
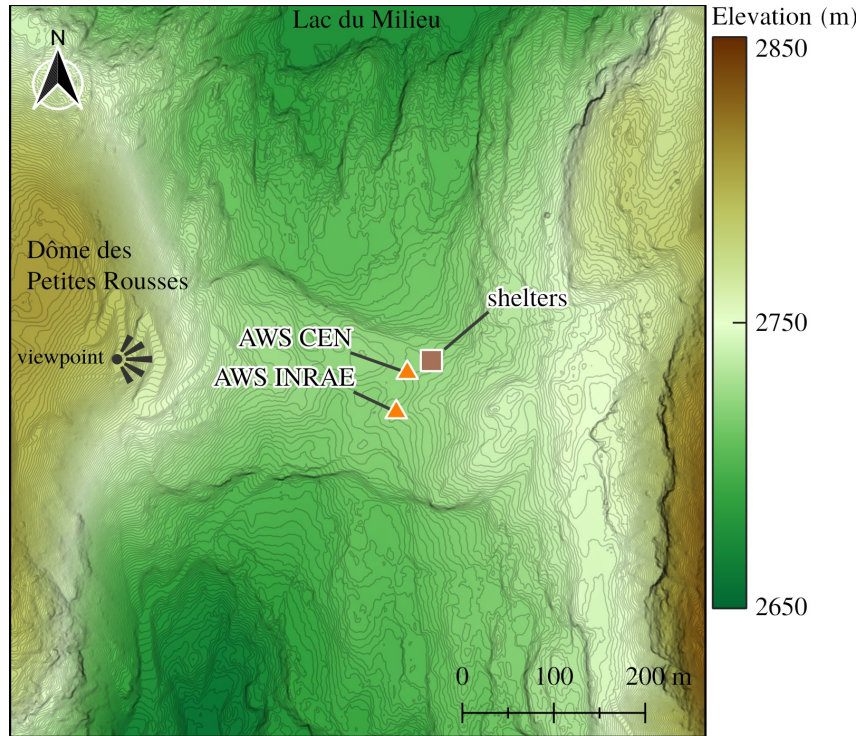
Figure 2.3 – Map of the Col du Lac Blanc experimentation site (massif des Grandes-Rousses, France), with 1 m elevation contour lines. The DEM with bare ground was reused from Guyomarc'h *et al.* (2019). The viewpoint (on the left) corresponds to the photograph in Fig. 2.2.

2.2.2 Site 2: Flaine ski resort (Flaine)

Another mountain site was chosen to conduct the studies applied to rock ptarmigan and PAM (passive acoustic monitoring) techniques, the Flaine ski resort (Savoie, France, see Fig. 2.1). It hosts a known population of rock ptarmigan that are annually counted since 2016, and are GPS tracked since 2017 (see Fig. 2.4). The monitored population is on the border of the Sixt-Fer-à-Cheval/Passy National Nature Reserve[1], which extends east of the line between the peaks Grandes Platières and Tête Pelouse. Three automated record units (ARU) are installed during breeding season to monitor vocal activity and study the detection of rock ptarmigan songs. They have already been used to study specific and individual signatures in ptarmigan, as well as the automatic detection of individuals (Marin-Cudraz, 2019). For the present research, they are used to quantify the vocal activity.

From one to five ptarmigan have been equipped with GPS tags every spring season since 2017 by Frédéric Sèbe's team (ENES, Saint-Étienne) in partnership with the OFB (Office Français de la Biodiversité). These data are used to study reproduction, and in particular territorial behavior, through the analysis of site occupation, presence hot spots, and display flights. All occupied territories of birds monitored between 2017 and 2021 are shown in Fig. 2.4. We observe that birds equipped for several years (same colored

---

[1]website: https://www.reserves-naturelles.org/sixt-fer-a-cheval-passy
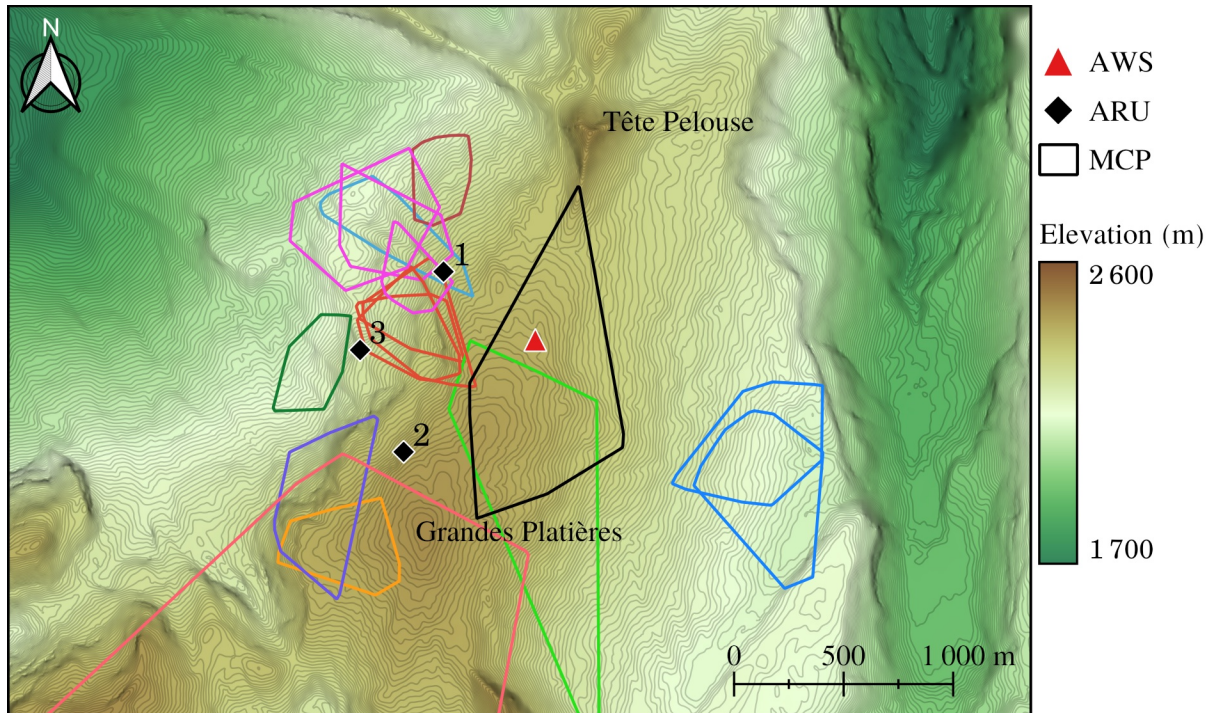
Figure 2.4 – Territories of monitored birds of Flaine site during springtime from 2017 to 2021 determined as minimum convex polygons (MCP) from GPS points, depicted with one color per bird. Elevation contour lines are 5 m apart. Several birds have returned to their territories in consecutive years.

polygons) returned to the same areas to establish their territories.

For the purpose of the thesis, a stand-alone weather station (AWS) was designed and installed in the center of the site, in an open area far from the cliffs. This AWS collected data during the spring of 2021 (sensor details in Sec. 2.5). The studies associated with this site are presented in Chap. 5 and Chap. 6.

2.3 Acoustic measurement on field

We present here the principle of the propagation measurements carried out at the Col du Lac Blanc in October 2021. This section specifies the sound source, the emitted signal, the recording technique, the calibration, and the audio processing. The October 2020 measurement campaign was conducted over two weeks and included long-range propagation measurements in different configurations and weather conditions. Propagation measurements were conducted in absence of snowfall and when the wind speed was below 5 m/s on two days: October 24 and 28.

2.3.1 Acoustic source

The study of the propagation of acoustic waves over long distances requires a powerful sound source to ensure that the pressure level remains higher than the background noise despite the pressure decay. It is noteworthy that bird vocalizations can extend over a

wide frequency range. It is therefore important to ensure that the source is sufficiently powerful and has a sufficiently wide frequency response. In addition, the loudspeaker must be battery-powered and operate in cold environmental conditions. For all these reasons, we designed and built an autonomous loudspeaker adapted to outdoor propagation experiments (see Fig. 2.5).
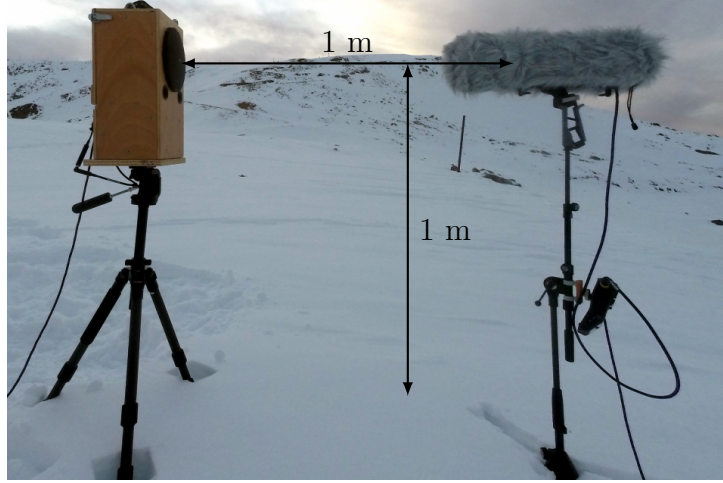
Figure 2.5 – Set-up of the source and microphone linked to a Zoom H6 on the Col du lac Blanc experimentation site.

The design and characterization of the source (measurements of frequency response, directivity, and harmonic distortion) are detailed in Appendix. A. The loudspeaker frequency response is shown in Fig. 2.6. We set a frequency band of interest for impedance and propagation measurements within $[90 - 3150]$ Hz. The frequency response is within 5 dB over this frequency band. In addition, it can produce pressure levels up to 110 dB-SPL (sound pressure level in dB, ref. 20 µPa) at 1 m, which makes it possible to carry out propagation experiments over hundreds of meters.
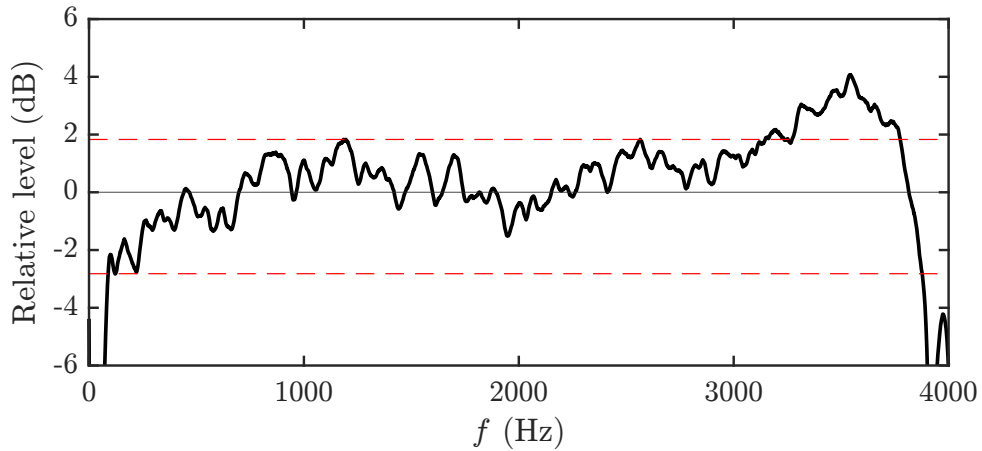
Figure 2.6 – Frequency response measured in the axis of the loudspeaker designed for the propagation study. Dashed lines indicate the minimum and maximum levels in the frequency band $[90 - 3150]$ Hz.

2.3.2 Emitted signal

The signal used for propagation experiments must allow the comparison of broadband spectra. Moreover, it must be limited in time to avoid unwanted distant echoes. This is why we use a frequency sweep of 1 s duration consisting of a sine whose frequency increases exponentially, called sweep or chirp hereafter. The instantaneous frequency f_i of the upsweep is defined by:

$$f_i(t) = f_0 \times \beta^t, \tag{2.1}$$

where

$$\beta = \left(\frac{f_1}{f_0}\right)^{(1/t_1)}, \tag{2.2}$$

with the following settings: $f_0 = 50$ Hz, $f_1 = 4800$ Hz, $t_1 = 1$ s. This signal is shown in Fig. 2.7. The obtained upsweep of one second duration is then windowed by a Tuckey window to avoid clipping when playing on the speaker, and to avoid pronounced loudspeaker resonance at 4000 Hz (see full frequency response Appendix. A), resulting in a usable source signal in the $[100 - 3800]$ Hz frequency band.
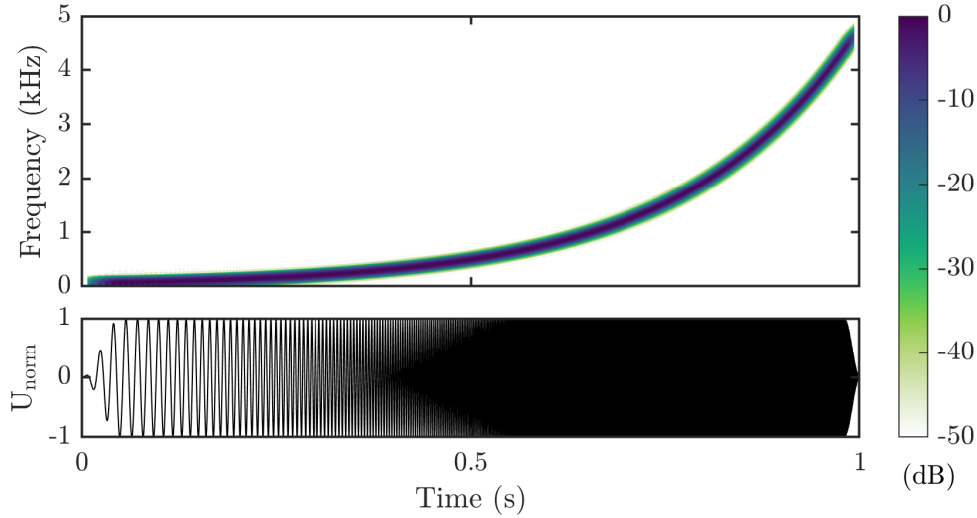
Figure 2.7 – Spectrogram of the relative level (top) and normalized value (bottom) of the upsweep signal sent to the speaker. It is windowed temporally (fade in, fade out) to avoid clipping when playing.

The sound pressure level (SPL) measured at 1 m in the axis of the speaker, and at 1 m above the snow is shown in Fig. 2.8. The 60 repetitions of the chirp in 10 minutes show slight differences in level above 1500 Hz, but they do not exceed 1.5 dB. These differences may be due to a slight shift of the source or microphone mount, resulting in a misalignment of the source-receiver geometry.
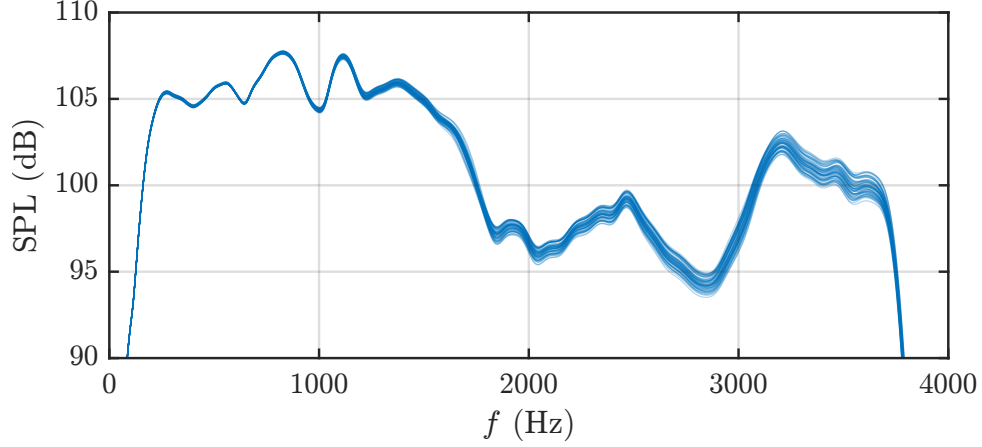
Figure 2.8 – Sound pressure level measured at 1 m in the axis of the speaker, and at 1 m above the snow (60 repetitions of the chirp in 10 minutes, in upwind condition).

2.3.3 Microphones and recordings

To perform measurements in mountainous environment, a flexible configuration is required to ensure a quick set-up. For this reason, stand-alone H6 audio recorders (Zoom, San Jose, CA) are used, each one connected to a microphone Beyerdynamic (Heilbronn, Germany) MM1. The source is placed at 1 m above the ground level, i.e. the snow surface, using a tape measure. The microphones are placed at a height of 1 m with respect to the ground and at the targeted distances from the source of 50, 100 and 200 m. A Bushnell (Lenexa, Kansas USA) G-Force 1300 ARC 6x laser rangefinder is used, as well as a reflective photographic screen to place the microphones at chosen distances from the source. One operator stands at the source with the rangefinder and another places the microphones in the axis of propagation and at the right distance following the indications of the former. The positioning error with respect to the source is estimated to be ±1 m. To limit the effect of wind noise on the microphone membranes, each microphone is covered by a simple windscreen, then suspended in a RØDE (Sydney, Australia) Blimp MkII windscreen covered with a synthetic RØDE DeadWombat fur (see Fig. 2.5).

Calibration of the acoustic measurement chain

Due to the limited dynamic range of the recorders (less than 60 dB), it is required to limit the contribution of numerical noise on recordings (due to low levels) and to avoid saturation. Thus we adjust the gain of each recorder according to its distance from the source. This is why a calibration of the different acquisition chains is necessary. First a calibration is performed on the microphone acquisition chain at 1 m from the source (reference receiver) using a Class 1 calibrator (Cirrus CR517) at 94 dBSPL and 1000 Hz. The second calibration step is done with respect to the reference microphone, and performed at an average pressure level so that none of the four recorders saturates. This procedure is performed out of the wind. The 4 microphones, each with their own

fixed gain, are aligned on a dedicated stand in the axis of the loudspeaker at a distance of 1.2 m (see Fig. 2.9). All microphones receive a signal of 50 dBSPL at 1000 Hz for 20 seconds. The obtained calibration files make possible in post-processing to retrieve the

Figure 2.9 – 3D view of the calibration setup for the three microphones, with a reference microphone, in the source axis (distance scale not respected).

real recorded pressure levels. In order to compare the narrow-band PSD (power spectral density) around the source signal at 1000 Hz, each recording is filtered between 970 Hz and 1030 Hz by an FIR (finite impulse response) filter. The PSD calculation of each recording allows us to determine the sensitivity of each acquisition chain, and thus to retrieve the absolute pressure level of each measurement recording.

Frequency response determination at the receiver positions

The audio files are processed to determine the spectra at the receiving points. The recording tapes are first synchronized using the impulse signal recorded just before propagation, and produced at the source point by a balloon bursting. Then the autocorrelation of the electrical signal of the sweeps is used to identify each period of interest in the receiver tapes. Audio recordings are filtered in the [100 − 3800] Hz frequency band. Then the calculation of the spectra is carried out from the 60 sweeps of each measurement series of 10 minutes duration. A spectrogram is computed for each sweep, using Matlab's *pspectrum* function, and the sweep spectrum is derived from the maxima of the spectrogram at each frequency step. An example of a chirp recorded at 50 m is shown in Fig. 2.10. The spectrogram has a frequency resolution of 5 Hz and a time resolution of 3.75×10^{-4} s. Above the main chirp, harmonics of higher frequency and lower amplitude are observed. They are caused by distortions of the loudspeaker at high level.

This method eliminates the contribution of possible echoes, as well as harmonics produced by the loudspeaker at high level. We consider that for each receiver no external noise source is stronger than the wave produced by the source and coming from the most
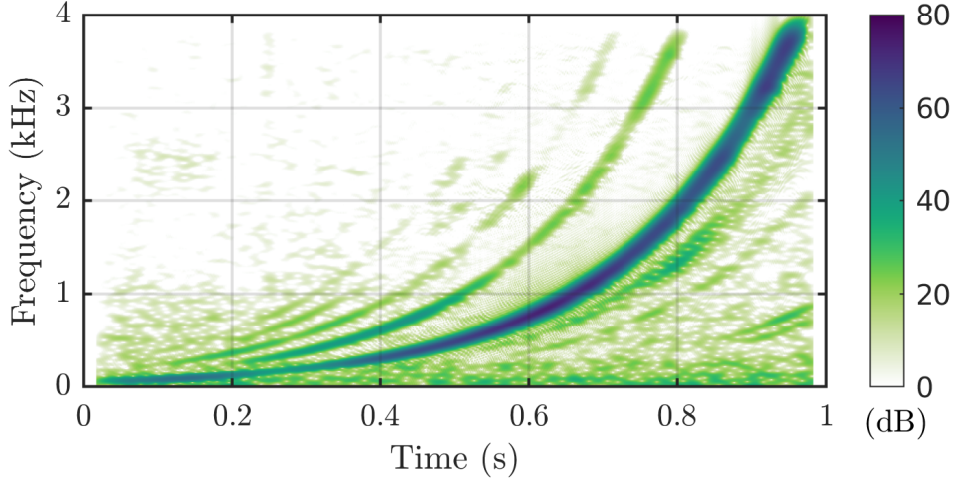
Figure 2.10 – Spectrogram of a recorded chirp over the snow and 50 m from the source (dBSPL).

direct path. The background noise is calculated in the same way on the silences between the sweeps, then averaged over the 60 repetitions. All measurements showed a signal-to-noise ratio greater than 10 dB in the frequency band $[300 - 3000]$ Hz.

2.4 Impedance determination of natural grounds

This section details the ground impedance model, the measurement protocol, and the numerical processing implemented to experimentally evaluate the impedance of the snow. Ground impedance is a critical parameter of the ground effect during wave propagation. Therefore measurement of the ground impedance is of major importance in order to be able to compare, all things being equal, the sound levels measured during the propagation experiments and the results provided by the simulation. For this purpose, the snow impedance measurement sessions are conducted at the Col du Lac Blanc site at the same time as the propagation experiments.

2.4.1 Analytic pressure calculation over a finite impedance ground

The geometry used in these impedance measurements is detailed Fig. 2.11. We consider a point source producing a harmonic sound, and positioned at a given distance from the receiver. The acoustic field can be described by the direct and reflected contributions, traveling respectively the distances r_d and r_r. According to the usual conventions, the angle of incidence θ is defined with respect to the normal to the ground and ψ represents the grazing angle of incidence.

The pressure field at a receiver position R above a plane ground of finite impedance, excited by a given source is calculated analytically. It can be formulated according to the modified Weyl-Van der Pol equation (Chien & Soroka, 1975). Using the temporal

51
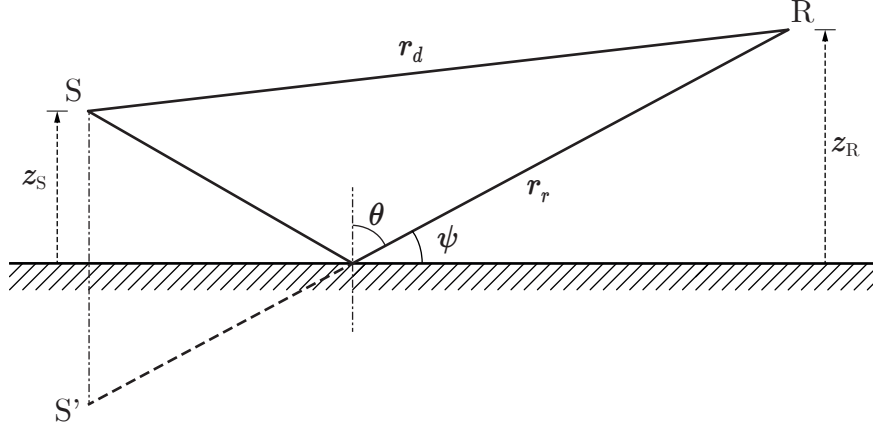
Figure 2.11 – Propagation geometry between a source S and a receiver R in still air over a flat ground. θ and ψ are respectively the incidence angle and the grazing angle. z_S is the source height and z_R the receiver height. r_d is the direct path length and r_r is the reflected path length.

convention $\exp(-i\omega t)$, is is written:

$$p(\mathbf{r}) = \frac{S_d}{r_d}\exp(ik_0 r_d) + Q\frac{S_r}{r_r}\exp(ik_0 r_r), \tag{2.3}$$

with $\mathbf{r} = (r, \theta, z)$ the receiver position in cylindrical coordinates, r_d the direct source-receiver distance, r_r the image-source-receiver distance, S_d and S_r the source amplitudes of the direct and reflected waves. Note that $S_d = S_r$ for an omnidirectional source. Q represents the reflection coefficient on the ground for a spherical wave. It can be directly deduced from the plane wave reflection coefficient R_p according to Bérengier *et al.* (2003), and is given by:

$$Q = R_p + (1 - R_p)F(w), \tag{2.4}$$

where R_p is calculated from the normalized surface impedance Z and the angle of incidence θ with the relation:

$$R_p = \frac{Z\cos\theta - 1}{Z\cos\theta + 1}. \tag{2.5}$$

Note that $R_p = 1$ in the case of a rigid ground of infinite impedance. In addition, $F(w)$ is the boundary loss factor expressed like:

$$F(w) = 1 + i\sqrt{\pi}w\ \exp(-w^2)\mathrm{erfc}(-iw), \tag{2.6}$$

where w is called the numerical distance and depends on the ground model. It can be approximated following Salomons (2001) in the case of a local ground reaction by:

$$w = \sqrt{\frac{ik_0 r_r}{2}}\left(\frac{1}{Z} + \cos\theta\right), \tag{2.7}$$

with $k_0 = \omega/c_0$ the wave number in air, Z the normalized surface impedance, θ the angle of incidence with respect to the normal to the ground, and r_r the distance traveled by

the reflected ray. The term $(\exp(-w^2)\text{erfc}(-iw))$ in Eq. (2.6), where erfc stands for the complementary error function, is called the Faddeeva function, and is obtained according to Abrarov & Quine (2011).

This expression of Q enables a valid pressure field calculation for grazing incidence with $r_d \gg z + z_S$ and $\theta \to \pi/2$, but it appears to be sufficiently accurate even for $r_d \gg z + z_S$, as described in Salomons (2001) Appendix D.

The function $F(w)$ enable to consider the wave reaction for a ground of finite impedance as well as the surface wave. It is worth mentioning that surface waves could be observed at the vicinity of a very porous ground. Surface waves have been shed to light above snow in the measurements reported by Albert (2003). However, these waves are propagative mainly for low frequencies, below 100 Hz. Given the frequencies considered later in our study, it is expected that surface waves will not be involved.

Local reaction

In the case of a locally reacting ground, the surface impedance Z_s of a rigidly backed layer of porous materials is given by:

$$Z_s = Z_c \coth\left(-ik_c e\right). \tag{2.8}$$

with the finite thickness e, the wavenumber in the porous material k_c, and the characteristic impedance Z_c. The characteristic impedance Z_c is equal to the ratio of the acoustic pressure and the particle velocity in the porous medium seen as a rigid frame filled with air.

The surface impedance can be normalized by the air impedance $Z_0 = \rho_0 c_0$ as:

$$Z = \frac{Z_s}{\rho_0 c_0}. \tag{2.9}$$

The term $\coth\left(-ik_c e\right)$ in Eq. (2.8) accounts for the thickness effect, i.e. the incident wave makes a round trip inside the porous layer, as illustrated on Fig. 2.12.
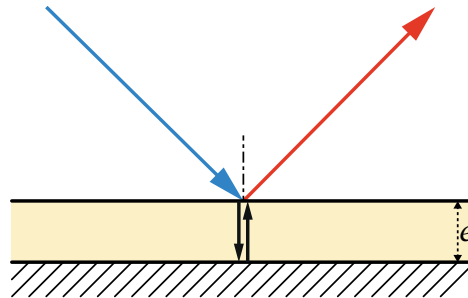
Figure 2.12 – Principle of the local reaction of a porous layer of finite thickness on a rigid bottom layer

The local reaction impedance model will not be used for impedance determination.

We prefer the extended reaction model detailed below, given the low air flow resistivity of snow (Li *et al.*, 1998b).

Extended reaction with thickness effect

In real conditions, the snow layer thickness is not infinite. If it does not exceed a few tens of centimeters, or if several layers of snow of varying density are superimposed, which is often the case after several snowfalls interspersed with frost, the incident wave passes through a porous layer of finite thickness, laid on a perfectly reflective layer. The wave is then reflected several times in the porous layer, as shown in Fig. 2.13. We then use the
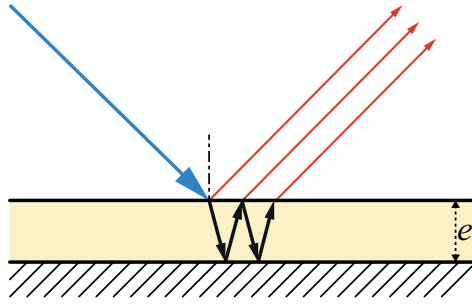
Figure 2.13 – Principle of the extended reaction with thickness effect of the porous layer

formulation proposed by Li *et al.* (1998b), which calculates the admittance of a porous layer of finite thickness over a rigid surface. Note that the impedance and admittance are related by $\beta = 1/Z$. The surface admittance β is normalized, and a function of the incidence angle θ like:

$$\beta = -im_1\sqrt{n_1^2 - \sin^2\theta} \, \tan\left(k_0 e\sqrt{n_1^2 - \sin^2\theta}\right),\tag{2.10}$$

where $n_1 = k_c/k_0$ and $m_1 = \rho_0/\rho_c$. Since the porous medium is treated as an equivalent fluid, the parameter ρ_c corresponds to its density and k_c is the wave number in the fluid. Their relation is defined by:

$$\rho_c = \frac{k_c Z_c}{\omega}.\tag{2.11}$$

2.4.2 Impedance model

The complexity and diversity of the soil layers can make it difficult to determine the impedance by measurement. Indeed, many models are designed to provide an impedance approximation for natural ground according to the frequency (Attenborough *et al.*, 2011). Here we consider the application of an impedance model to the determination of snow impedance from in-situ measurements.

The snow impedance is calculated according to the phenomenological model of Hamet and Bérengier (Bérengier *et al.*, 1997). This model enables to obtain a physically admissi-

ble surface impedance Z_s, since its real part is always positive. The impedance input parameters are: R_s the resistivity to air flow in Pa.s.m^{-2} (or cgs with 1 cgs = 1 kPa.s.m^{-2}), Ω the porosity (dimensionless, $\in [0, 1]$), q^2 the tortuosity (dimensionless, otherwise called form factor), and e the effective thickness of the porous layer (in meters). The thickness is used for the case of a local or extended reaction calculation, which takes into account a rigid bottom layer. For the case of an extended reaction calculation, with a semi-infinite thickness layer, the model has only three parameters (R_s, Ω, q^2).

The fluid parameters are:

- f the frequency of the wave given by the source signal in Hz,
- T_0 the temperature in Kelvin degrees,
- P_0 the ambient atmospheric pressure in Pa,
- $\gamma = 1.4$ the air specific heat ratio (dimensionless),
- $\mathrm{Pr} = 0.7$ the Prandtl number in air (dimensionless),
- $R_{\mathrm{GP}} = 287$ JK^{-1}.mol^{-1} the perfect gas constant,
- $\rho_0 = P_0/(R_{\mathrm{GP}} \, T_0)$ the air density in kg.m^{-3},
- $c_0 = \sqrt{\gamma \, R_{\mathrm{GP}} \, T_0}$ the sound speed in the air in m.s^{-1}.

The characteristic impedance Z_c of the ground and its complex wave number k_c are functions of the dynamic complex density ρ_g and the bulk modulus K_g according to the pulsation $\omega = 2\pi f$, following:

$$k_c = \omega[\rho_g(\omega)/K_g(\omega)]^{1/2}, \tag{2.12}$$

$$Z_c = [\rho_g(\omega)K_g(\omega)]^{1/2}/\Omega. \tag{2.13}$$

The dynamic complex density ρ_g and the bulk modulus K_g respectively describe the viscous and thermal effects occurring when wave passes through the micro cavities of the ground. They are obtained according to the phenomenological model of Hamet and Bérengier with:

$$\rho_g(\omega) = \rho_0 q^2(1 + i\omega_\mu/\omega), \tag{2.14}$$

$$K_g(\omega) = \gamma P_0[1 + (\gamma - 1)/(1 - i\omega/\omega_\theta)]^{-1}, \tag{2.15}$$

where ω_μ and ω_θ are two characteristic pulsations as:

$$\omega_\mu = \Omega R_s/(\rho_0 q^2), \tag{2.16}$$

$$\omega_\theta = R_s/(\rho_0 \mathrm{Pr}). \tag{2.17}$$

Numerous studies detail the impedance parameters according to the model used and the ground type. We summarize in Tab. 2.1 the limiting values for the phenomenological

model, deduced from several measurements in literature (Moore *et al.*, 1991; Attenborough *et al.*, 2011; Maysenhölder *et al.*, 2012; Datt *et al.*, 2016).

The number of parameters to be fitted can be reduced from 4 to 3 by applying an approximation proposed by Attenborough *et al.* (2011), such that the tortuosity q^2 is equal to $1/\Omega$. However Attenborough (1992) does not present tortuosity values equal to $1/\Omega$ for snow, but values between 2 and 5. This approximation seems therefore not valid for snow. Thus tortuosity has to be adjusted independently of the porosity. It has been shown by Moore *et al.* (1991) that tortuosity and porosity are positively correlated in the case of a recently fallen snowpack. In the case of a metamorphosed and compacted snowpack with higher density and lower porosity, tortuosity can be very high.

Ground type	R_s (kPa.s.m^{-2})	Ω	q^2
Snow	$2-32$	$0,4-0.95$	$1-35$
Meadow	$36-340$	$0.5-0.86$	...
Pine forest	$7-650$	$0.3-1$	...
Beech wood	$10-75$	$0.35-0.52$	...
Rock	∞	...	...

Table 2.1 − Limit values of impedance parameters from the literature for several natural grounds, determined from on-site measurements by fitting models. (Moore *et al.*, 1991; Attenborough *et al.*, 2011; Maysenhölder *et al.*, 2012; Datt *et al.*, 2016)

The impedance parameters of a given ground can dramatically fluctuate over time, and according to the weather conditions preceding the measurement. In a porous soil, rain infiltrates the pores and significantly reduces the porosity and increases the air flow resistivity. Temperature can also play an important role, especially during freezing periods. Indeed, because of the thermal inertia of the soil, the ground can remain frozen even when the air temperature is positive. If this occurs, measuring the soil temperature can provide information on the state of the water it contains, and therefore on its structure. To determine its structure, it is also appropriate to take a soil sample or to make a vertical cross-section. In the case of a snowpack, it preserves the layers of accumulated snowfall that have metamorphosed over time. The snowpack can therefore be a complex layered structure with many strata of very different densities. The liquid water content determines the shape of the pores and thus the parameters of tortuosity, air resistivity and porosity of the wet snow.

During this thesis, measurements were mainly conducted on dry snow, with few accumulated layers, which allowed determination of the impedance parameters. It should be noted that the snowpack melts rapidly at high altitudes in late spring; the snow then contains a large proportion of liquid water, and presents a complex structure due to the superposition of layers with various densities. The progressive melting of the snow also modifies its surface aspect. The surface presents ripples which deepen from day to day

due to the sun's radiation and the deposited dust. Thus, ripples are the main difficulty in determining the impedance of snow at the end of the season. Indeed, the measurement protocol used hereafter is not suitable to treat these configurations where the characteristic length of the ripples are close to the considered wavelengths. However, this problem has not been addressed in the thesis.

2.4.3 Impedance determination method

The method used for the measurement of ground impedance is based on Guillaume *et al.* (2015). It consists of performing a propagation experiment between a point source emitting a swept sine and two omnidirectional microphones placed at two different heights (see Fig. 2.14). The transfer function between both signals received at the two microphones are then calculated from measurements (called the experimental transfer function). Besides an analytic transfer function is calculated for an extended reacting ground layer of finite thickness using the Weyl-Van der Pol equation (Li *et al.*, 1998b). A curve fitting procedure is then used to match the two transfer functions at the first ground dip or the first constructive interference. The parameters of the equivalent impedance are then determined, and the characteristic impedance is obtained.

The sketch in Fig. 2.14 details the geometry of the experimental setup with $d = 4$ m the horizontal distance between the source S and the microphones R_1 and R_2. The heights above the ground are $z_S = z_{R_2} = 0.6$ m and $z_{R_1} = 0.05$ m. For accurate measurements, the ground surface must be flat and smooth, without any diffracting obstacle in the vicinity. In addition, the wind speed must be lower than 3 m/s at the height of the microphones to ensure a sufficient SNR (signal-to-noise ratio) on the frequency band of interest. We consider that SNR must be above 10 dB.
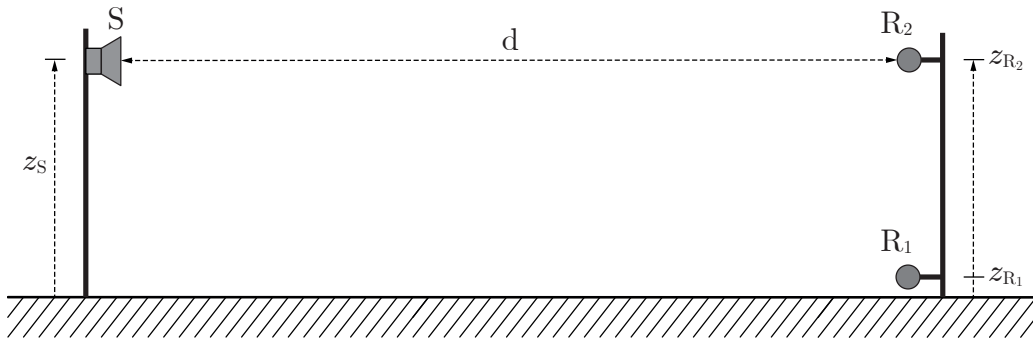
Figure 2.14 – Experimental set-up for the determination of ground impedance, with $d = 4$ m the horizontal distance between the source S and the microphones R_1 and R_2, and the heights above the ground are $z_S = z_{R_2} = 0.6$ m and $z_{R_1} = 0.05$ m (scale not observed).

The source used is the same as for the propagation experiment (see Sec. 2.3.1). It emits a frequency sweep of 2 seconds duration as detailed in Sec. 2.3.2. This signal is followed by a silence of 1 s. This sequence is repeated 50 times to ensure a temporal averaging of

the measurements during the analysis. Measurements are made with two Beyerdynamic MM1 omnidirectional microphones equipped with windscreens. The recorder is a Zoom H6. Two acquisition channels are calibrated with a Class 1 calibrator (Cirrus CR517) at 94 dBSPL and 1000 Hz. In addition, the source signal sent with a cell phone is recorded in a third channel of the Zoom H6 to simplify the audio processing.

Measurement processing and fitting procedure

The data analysis procedure is illustrated with the preliminary measurements carried out on a meadow on March 6, 2020 in Saint-Etienne. The autocorrelation of the source signal is used to locate the recorded sweeps in time. Then an averaging is performed on the temporal signals, including all the repetitions of the sweep on each recording. This procedure enables us to get rid of spurious noise. We obtain the average recorded sweep for each receiver as seen in Fig. 2.15.
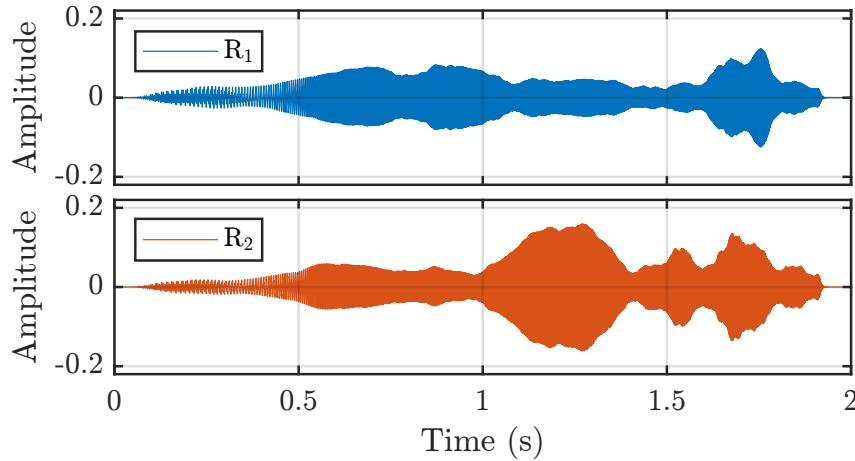
Figure 2.15 – Time signals received at microphones R_1 and R_2 averaged over 50 bursts.

The power spectral density (PSD) is estimated by a Welch periodogram method, using *pwelch* function on Matlab[2] (see Fig. 2.16). This makes it possible to compare the background noise and the measured signal, and thus to check whether the required SNR is reached.

We calculate the Fast Fourier Transforms (FFT) H_{R_1} and H_{R_2} of the average sweep received at R_1 and R_2 respectively. Then the corresponding energy ratio of these two transfer functions is calculated in decibels as follows:

$$\Delta L_{\text{exp}} = 20 \log_{10} \left(\frac{|H_{R_2}|}{|H_{R_1}|} \right). \tag{2.18}$$

The curve fitting is manually performed between the experimental and analytical ΔL, starting from the parameters of the literature based on the ground type (see Tab. 2.1). The

---

[2]For details on the *pwelch* function: https://fr.mathworks.com/help/signal/ref/pwelch.html
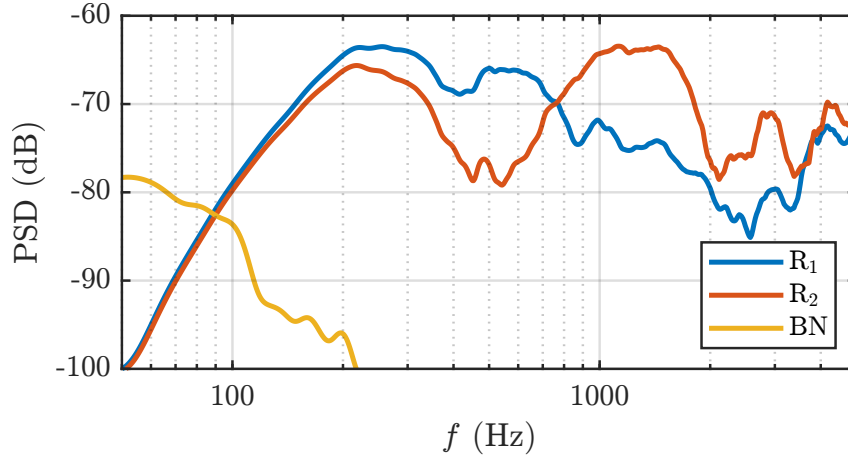
Figure 2.16 – PSD estimation of the average burst at R_1 and R_2, and background noise (BN).

best fit presented Fig. 2.17 corresponds to the impedance parameters: $R_s = 90 \, \text{kPa.s.m}^{-2}$, $\Omega = 0.7$, $q^2 = 1/\Omega$, and $e = 0.022$ m. Many modulations are observed on the experimental transfer function above 400 Hz. This may be due to the non-perfectly flat aspect of the meadow, with small bumps, and to the presence of small stones in the porous layer. Nevertheless, this measurement confirmed the applicability of this method. We therefore decided to apply this protocol afterwards. Note that the determination of snow impedance is discussed for measurement/model comparisons in Sec. 4.3.
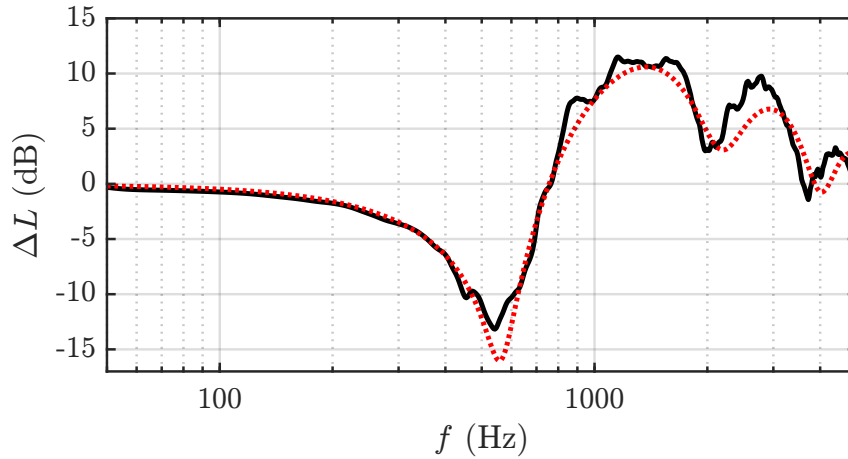
Figure 2.17 – Transfer functions ΔL for the determination of the surface impedance of a meadow: measured (———) and analytical fit (⋯⋯⋯⋯).

Surface impedance of natural grounds

Several ground impedance measurements were performed during the experiments at the CLB site over snow, and at Flaine on alpine moor. The impedance spectra as well as the absorption coefficient deduced from these measurements are briefly presented here. The parameters of the considered ground types are detailed in Tab. 2.2.

The real and imaginary parts of the normalized impedance are respectively defined

Table 2.2 – Impedance parameters of several ground types obtained on the CLB and Flaine sites: effective thickness e, airflow resistivity R_s, porosity Ω, and tortuosity q^2.

Ground type	e (m)	R_s (kPa.s.m^{-2})	Ω	q^2
powder snow	0.15	7	0.6	1.3
packed snow	0.15	30	0.6	1.3
meadow	0.022	90	0.7	$1/\Omega$
alpine moor	0.006	400	0.8	$1/\Omega$

as $\mathrm{Re}(Z) = \mathrm{Re}(1/\beta)$, and $\mathrm{Im}(Z) = \mathrm{Im}(1/\beta)$. Their plot on Fig. 2.18 reveal different frequency behavior. However, for these four ground types, the real part remains relatively constant, and the imaginary part decreases with frequency.
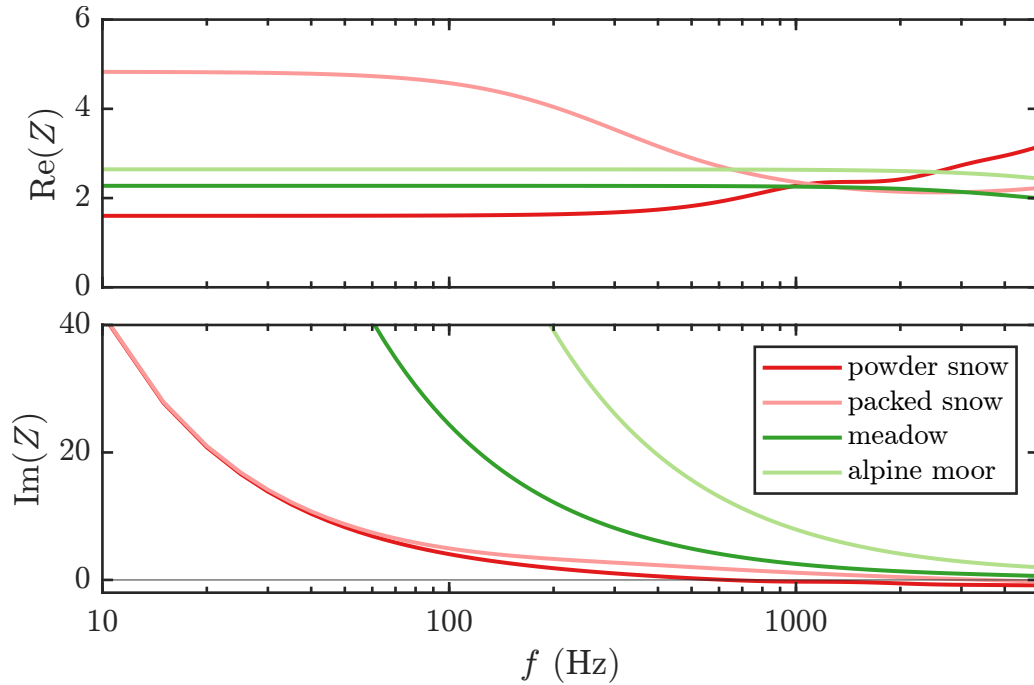
Figure 2.18 – Impedance functions of several natural grounds (real (Re) and imaginary (Im) parts).

To give an idea of the effective absorption which exists when a wave is reflected on a flat ground, we calculate the absorption coefficient α_r from the plane wave reflection coefficient R_p such as:

$$\alpha_r(\theta) = 1 - |R_p^2|, \tag{2.19}$$

where R_p depends on the incidence angle θ of the reflected ray (see Eq. (2.5) and Fig. 2.11). The α_r coefficients are plotted in Fig. 2.19 for the two source-receiver distances $d = 5$ m and $d = 50$ m, with $z_\mathrm{S} = z_\mathrm{R} = 1$ m. Absorption for short-range reflection (5 m) is essentially at high frequencies. It is greater than 0.5 above 100 Hz for snow, above 500 Hz for grassland and above 1500 Hz for alpine moor. At greater distances (50 m), grazing incidence implies a different absorption behavior: compacted snow is absorbing at low

frequencies ($\alpha_r = 0.51$ at 80 Hz); snow powder, meadow and alpine moor have a similar absorption behavior at this distance, slowly increasing with a value of $\alpha_r = 0.3$ at 1000 Hz.
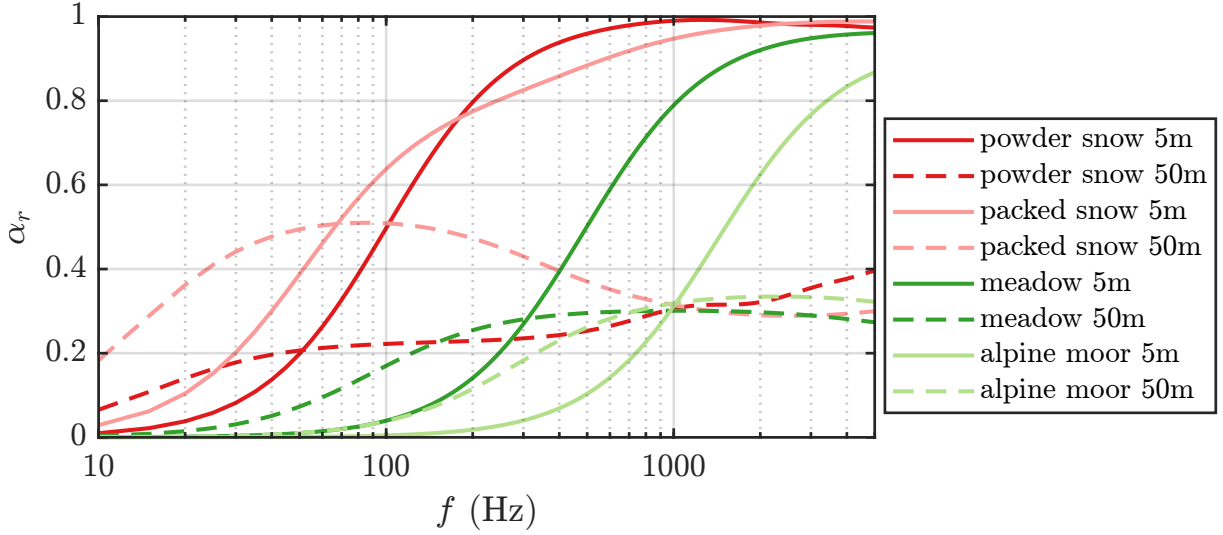
Figure 2.19 – Ground absorption coefficient α_r of natural grounds calculated with parameters of Tab. 2.2, for two propagation distances: $d = 5$ m and $d = 50$ m, with fixed source and receiver heights $z_\mathrm{S} = z_\mathrm{R} = 1$ m.

2.5 Meteorological measurements

In order to make comparisons between the sound propagation experiments and simulations, it is necessary to measure atmospheric parameters during the acoustic measurements. Meteorological data are acquired at specific points with the CLB weather stations (see location in Sec. 2.2.1). These data must then be extrapolated to obtain local wind and temperature profiles. This extrapolation is carried out in accordance with the similarity theory described in Sec. 2.5.2. These profiles are then used to determine a vertical effective sound speed gradient for numerical computations.

Another use of long-term weather stations is to obtain statistics on seasonal conditions in a given habitat. This is why a weather station is designed and installed on the Flaine site. The data acquired during the spring season of 2021 provide useful information on the conditions that ptarmigan encounter at this altitude. It is thus possible to make propagation computations applied to ptarmigan with realistic parameters for the atmosphere. The measurements of the local atmospheric conditions together with the determination procedure of the sound speed profile are detailed in this section.

2.5.1 Measurements and automated weather stations

Automated weather stations on CLB

Weather stations in CLB are maintained all year round to provide data to Meteo France. We had access to the data but we could not modify the acquisition protocol. Two automated weather stations (AWS) are used to measure separately wind speed and direction (AWS INRAE), and temperature and humidity profiles (AWS CEN). They are located on the center of the pass (see Fig. 2.3). The sensors are listed in Tab. 2.3. An atmospheric pressure sensor (PTB110, Vaisala, Vantaa, Finland) is installed in the acquisition box. The sensors are connected to a data acquisition system (CR10X, Campbell Scientific, Montrouge, France). The latter records the average, minimum and maximum values of temperature and humidity and the average values and standard deviation of wind speed and wind direction. Data are recorded every 10 minutes. The sound propagation measurements were performed following the same time sequence.

Table 2.3 – Automated Weather Station (AWS) installed and maintained by INRAE and CEN, and sensors used in October 2020 at Col du Lac Blanc, France. Sensors heights are relative to bare soil.

AWS	Measure	Sensor model	Manufacturer	Heights (m)
CEN	temperature, humidity	HMP155A	Vasaila	0.8, 1.3, 3.2, 5, 7
INRAE	wind speed	A100LK	Vector Instr.	1.76, 3.25, 4.1, 7.25, 9.42
	wind direction	W200P-01	Vector Instr.	11.08

The anemometers and wind vane are equipped with heating resistors to protect them from snow accumulation and freezing. The snow height is measured by an ultrasonic distance sensor (SR50, Campbell Scientific) attached to the CEN mast. Since the snow height was close to zero at the mast during the propagation measurements, no height correction was required for the weather profiles. Nevertheless, the site was covered with an average snow depth of 20 cm except for the southern and northern slopes which had snow accumulations (see Sec. 4.3.2 for details).

Automated weather stations on Flaine

A weather station has been designed and installed in Flaine in early spring 2021 for the purpose of this thesis. It was configured with the same types of sensors as the CLB stations (see Fig. 2.20). The power supply by solar panel ensures the autonomy of the station and therefore permits its installation in the center of the ptarmigan study area (see Fig. 2.4). Nevertheless, this type of power supply does not provide sufficient energy to include anemometer heating.
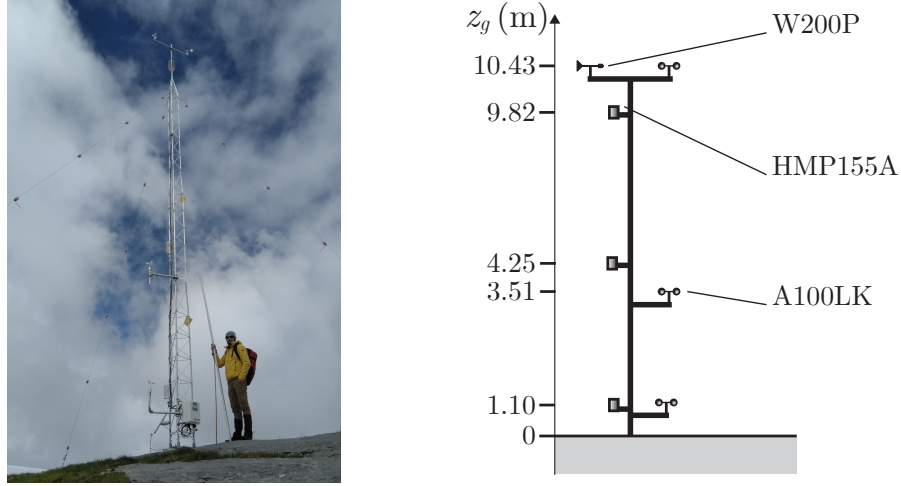
Figure 2.20 − Picture of the AWS Flaine in July 2021 before dismantling (man for scale), and sketch of the same AWS functioning in spring 2021 with detailed sensor types and fixed heights (see Fig. 2.4 for location). The height z_g is relative to the snowpack surface, regardless of the snow depth.

An atmospheric pressure sensor (PTB110, Vaisala) was installed in the acquisition box. All the sensors were connected to the data acquisition system (CR1000X, Campbell Scientific, Montrouge, France), which logged the minimum and maximum values, the standard deviations, and the averages of all quantities over 10-minute periods.

These data are processed in a similar way for both sites. The wind and temperature profiles are estimated based on the similarity theory presented below.

2.5.2 Elements of the similarity theory

The similarity theory was first developed by Monin & Obukhov (1954) and then enhanced by various authors as Stull (1988). It is used to describe the behavior of the air mass in the atmospheric surface layer (ASL), usually defined as the portion of the atmospheric boundary layer contained in the first 100 m above the ground that is affected on a short time scale by ground radiation and surface roughness conditions. The similarity relations, obtained empirically, describe the coupled thermal and convective effects in the ASL. They are used to deduce from meteorological measurements the vertical wind and temperature profiles that satisfy the predicted behavior of the ASL. These profiles can then be used as input data for acoustic propagation modeling (Salomons, 2001; Wilson, 2003).

It should be noted that the similarity relations are adapted to flat terrain. They are not valid in the case of hills or valleys, nor on heterogeneous terrain (Tayor & Lee, 1984; Heimann & Gross, 1999). However, there are several reasons why we choose this option. On the one hand, we consider a spatial scale smaller than 1 km, and therefore prefer to use real meteorological data measured locally instead of a mesoscale forecast model. On the other hand, since snow covers most of the studied areas, we consider that the ground reacts uniformly to heat exchange with the atmosphere. Moreover, the smoothness of the snow surface strongly reduces the irregularities of the bare ground. The meteorologic profiles

determined on the basis of the similarity theory are thus expected to be representative, even in the mountainous environment. This section describes the elements of similarity theory used in the following. We largely adopt the notations presented in Salomons (2001) Appendix N.

Notations

The wind speed is described by three components: V_x, V_y and V_z. Each component is split into an average value and a turbulent part, that is written as follows:

$$V_x = \overline{V_x} + V_x', \tag{2.20a}$$

$$V_y = \overline{V_y} + V_y', \tag{2.20b}$$

$$V_z = \overline{V_z} + V_z'. \tag{2.20c}$$

Considering that the horizontal mean components $\overline{V_x}$ and $\overline{V_y}$ prevail, the vertical mean component $\overline{V_z}$ is neglected in the following. Since the wind direction is known, it is possible to set the coordinate system such that $\overline{V_y} = 0$.

For a perfect gas in adiabatic conditions, the Laplace law relates the pressure and temperature are related with:

$$\frac{T_0}{P_0^{(\gamma-1)/\gamma}} = \text{constant}, \tag{2.21}$$

with P_0 the atmospheric pressure, T_0 the temperature and γ the ratio of specific heats.

The atmospheric static pressure decreases with altitude in the surface layer due to gravity. It yields a decrease in temperature with height (see Eq. (2.21)). To account for this, we define the dry adiabatic lapse rate α_0 by:

$$\alpha_0 \equiv \frac{dT}{dz} = -\frac{\gamma-1}{\gamma}\frac{\rho_0 T}{P_0}g, \tag{2.22}$$

where ρ_0 is the air density and $g = 9.8$ m.s^{-2} is the gravitational acceleration. Consequently, the dry adiabatic lapse rate can be approximated by substituting the mean values at ground level $\rho_0 = 1.2$ kg.m^{-3}, $P_0 = 10^5$ Pa, et $T = 300$ K, which leads to $\alpha_0 \approx -0.01$ K.m^{-1}. This gives the commonly assumed temperature gradient of -1 degree every 100 m.

As a substitute for the absolute temperature, the potential temperature θ is defined according to:

$$\theta = T\left(\frac{P_{\text{ref}}}{P_0}\right)^{(\gamma-1)/\gamma}, \tag{2.23}$$

where $P_{\text{ref}} = 10^5$ Pa is the reference pressure. At first order approximation $P_0 \approx P_{\text{ref}} +$

$(\mathrm{d}P/\mathrm{d}z)z$ one has,

$$\theta \approx T - \alpha_0 z. \tag{2.24}$$

From this definition, we note that for an adiabatic atmosphere, the potential temperature remains constant with altitude leading to $\mathrm{d}\theta/\mathrm{d}z = 0$. As previously done with the wind, we split the potential temperature into an average part $\overline{\theta}$ and a turbulent part θ' with:

$$\theta = \overline{\theta} + \theta'. \tag{2.25}$$

In order to capture the atmospheric state, the coupled convective effects due to wind and air heating must be considered. To this end, the kinematic turbulent heat flux $\overline{V_z'\theta'}$ is used as an indicator of atmospheric stability. It represents the vertical transport of the turbulent part of the potential temperature θ' by the turbulent component of the vertical wind V_z'. If $\overline{V_z'\theta'} > 0$, the atmosphere is said to be **unstable**, which implies that a volume of air tends to warm up and move upwards, while another volume of air tends to cool down and move downwards. This condition, which is the source of thermal currents, commonly occurs during the day when a sufficient amount of solar radiation warms the ground surface. On the contrary, if $\overline{V_z'\theta'} < 0$, the atmosphere is said to be **stable**. This usually occurs during the night, when the ground radiates the stored thermal energy towards the atmosphere and the air temperature increases with altitude. Finally, the atmosphere is said to be **neutral** when $\overline{V_z'\theta'} \approx 0$.

Similarity relations

The vertical profiles of the mean potential temperature $\overline{\theta}$ and the mean wind speed $\overline{V_x}$ in the atmospheric surface layer are derived from empirical relations linking dimensionless numbers. These relations are called similarity relations. To detail them, we first introduce the friction speed and the temperature scale.

The friction velocity is equivalent to the square root of the sum of the turbulent momentum fluxes such that:

$$u_*^2 = \left[\overline{(V_x'V_z')_s}^2 + \overline{(V_y'V_z')_s}^2 \right]^{1/2}. \tag{2.26}$$

Besides, the temperature scale θ_* of the atmospheric surface layer is written as:

$$\theta_* = \frac{-\overline{(V_z'\theta')_s}}{u_*}. \tag{2.27}$$

The "s" index in Eq. (2.26) and Eq. (2.27) means that the turbulent fluxes are evaluated near the surface. We define two quantities, such as the dimensionless derivative of the mean wind speed:

$$\phi_v = \frac{\kappa z}{u_*} \frac{d\overline{V_x}}{dz}, \tag{2.28}$$

and the dimensionless derivative of the potential temperature

$$\phi_t = \frac{\kappa z}{\theta_*} \frac{d\bar{\theta}}{dz}, \tag{2.29}$$

with $\kappa = 0,41$ the Von Kármán constant. Finally, the Monin–Obukhov length is obtained according to:

$$L_{\mathrm{MO}} = -\frac{\bar{\theta} u_*^3}{\kappa g \overline{(V_z' \theta')_s}}. \tag{2.30}$$

Based on Eq. (2.27) and Eq. (2.30), we deduce a simplified formulation:

$$L_{\mathrm{MO}} = -\frac{\bar{\theta} u_*^2}{\kappa g \theta_*}. \tag{2.31}$$

The Monin–Obukhov length is an indicator of the atmospheric stability since the sign of $1/L_{\mathrm{MO}}$ is opposite to that of the kinematic turbulent heat flux $\overline{(V_z' \theta')}$. The atmosphere is therefore **unstable** if $1/L_{\mathrm{MO}} < 0$, **stable** if $1/L_{\mathrm{MO}} > 0$, and **neutral** if $1/L_{\mathrm{MO}} \approx 0$.

Similarity relations link the dimensionless variables ϕ_v , ϕ_t , and z/L_{MO}. The formulations used here are called Businger–Dyer relations. For an **unstable** atmosphere with $1/L_{\mathrm{MO}} < 0$, it yields:

$$\phi_v = (1 - 16z/L_{\mathrm{MO}})^{-1/4}, \tag{2.32a}$$

$$\phi_t = (1 - 16z/L_{\mathrm{MO}})^{-1/2}. \tag{2.32b}$$

For a **stable** atmosphere with $1/L_{\mathrm{MO}} > 0$, these relations become:

$$\phi_v = \phi_t = 1 + 5z/L_{\mathrm{MO}}. \tag{2.33}$$

The variables $\overline{V_x}(z)$ and $\bar{\theta}(z)$ are obtained by integrating the dimensionless derivatives of Eq. (2.28) and Eq. (2.29) between the ground ($z = 0$) and the height z such as:

$$\overline{V_x}(z) = \frac{u_*}{\kappa} \left[\ln\left(\frac{z + z_0}{z_0}\right) - \psi_v \right], \tag{2.34a}$$

$$\bar{\theta}(z) = \theta_0 + \frac{\theta_*}{\kappa} \left[\ln\left(\frac{z + z_0}{z_0}\right) - \psi_t \right]. \tag{2.34b}$$

At ground level, the wind speed is assumed to be zero, hence $\overline{V_x}(z = 0) = 0$ in Eq. (2.34a). Moreover, in Eq. (2.34b), θ_0 correspond to the potential temperature at ground level, and from Eq. (2.24) we have $\theta_0 = \theta(z = 0) = T(z = 0)$. The height z_0 above the ground is called the aerodynamic roughness length. It corresponds to the average of the ground roughness over a relatively large area compared to the considered lengths. The term z/z_0 in ln functions used for the profiles presented for example in Stull (1988) is approximated as $(z + z_0)/z_0$ in Eq. (2.34a) and (2.34b) to extend the integration to the

ground level. We observe that this approximation is valid for a sufficiently small value of z_0. This enables us to obtain continuous profiles up to $z = 0$, which is required to define a sound speed profile in acoustic propagation codes. This leads to $\overline{V_x}(z = 0) = 0$ and $\overline{\theta}(z = 0) = \theta_0$.

Indicative values of z_0 are available in Foken (2017) p.51., adapted from Reithmaier *et al.* (2006). They range from 10^{-5} m for smooth ice, to 2 m for forests or buildings. The value of z_0 on irregular snow-covered topography is considered hereafter equal to 0.01 m or 0.1 m depending on the situation.

The ψ_i functions result from the ϕ_i functions as per:

$$\psi_i = \int_0^{z/L_{\mathrm{MO}}} \frac{1 - \phi_i(\xi)}{\xi} d\xi, \tag{2.35}$$

with the subscript i denoting v or t. The substitution of similarity relations Eq. (2.32) and (2.33) in Eq. (2.35) leads to the following results:

- For **unstable** atmosphere ($1/L_{\mathrm{MO}} < 0$),

$$\psi_v = 2\ln\left(\frac{1+x}{2}\right) + \ln\left(\frac{1+x^2}{2}\right) - 2\arctan(x) + \frac{\pi}{2}, \tag{2.36a}$$

$$\psi_t = 2\ln\left(\frac{1+x^2}{2}\right) \tag{2.36b}$$

where $x = (1 - 16z/L_{\mathrm{MO}})^{1/4}$.

- For **stable** atmosphere ($1/L_{\mathrm{MO}} > 0$),

$$\psi_v = \psi_t = -5z/L_{\mathrm{MO}}. \tag{2.37}$$

- In case of neutral atmosphere ($1/L_{\mathrm{MO}} \approx 0$), $\psi_v = \psi_t = 0$. It induces that $\overline{V_x}(z)$ and $\overline{\theta}(z)$ profiles, given by Eq. (2.34a) and Eq. (2.34b) are log functions.

The similarity relations detailed here are only valid for a height scale $z \in [-2L_{\mathrm{MO}}, L_{\mathrm{MO}}]$. This range of validity always depends on the given situation. It is therefore very variable since the Monin–Obukhov length can span from a few meters to several hundred meters depending on the conditions. Note that the Alpine environment implies complex wind profiles due to Venturi effects induced by unevenness of the topography. Moreover, at low wind speeds, the kinematic and heat fluxes can be of equivalent intensity, which implies small L_{MO} lengths. However, without more precise description of the atmosphere on the study sites, the sound speed profiles approximated on the basis of similarity relations will be used in spite of their reduced range of validity.

2.5.3 Determination of effective sound speed profiles (c_{eff})

The modeling of sound propagation in the atmosphere requires vertical profiles of temperature and wind speed.Concerning the wind direction in the surface layer, a constant value is assumed over the 10-minute period considered, using the average value.

The aerodynamic roughness length z_0 is fixed according to the type of terrain. Typical values range from 10^{-5} m to 2 m depending on the average size of the roughness that impedes the wind. Given the smoothness of the snow and the slightly uneven terrain at the Col du Lac Blanc site, an intermediate value of $z_0 = 0.01$ m was chosen. It is assumed to be constant over the time scales considered, since no snowfall occurred during the measurement campaign. For the Flaine site, which has more pronounced roughness throughout the site, a value of $z_0 = 0.1$ m is used.

The parameters L_{MO}, u_*, θ_*, θ_0 and z_0 of the Businger–Dyer profiles can be considered as adjustable. These parameters are determined by fitting the profiles to measured values of wind speed and temperature. We use an iterative optimization algorithm on the variables u_*, θ_*, θ_0. An optimization is performed at each iteration by the function *fminsearch* integrated in Matlab®, and the parameter L_{MO} is reevaluated each time. The routine stops when the optimization has resulted in a deviation of less than 1 % on two successive L_{MO} estimates. Moreover, the adiabatic lapse rate is assumed to be constant, and fixed at $\alpha_0 = -0.01$ K.m^{-1}.

The routine, based on the work of Cotté (2008), performs the following successive steps:

- The atmosphere is assumed to be neutral for the first iteration, with $\psi_v = \psi_t = 0$ for the calculation of $\overline{V_x}(z)$ and $\overline{\theta}(z)$ (see Eq. (2.34a) and Eq. (2.34b)).

- Depending on the sign of L_{MO}, the following iterations are performed according to Eqs. (2.36) in the unstable case and according to Eq. (2.37) in the stable case. The function *fminsearch* is used to minimize errors (sum of the errors squared) between the estimated profiles and the measurements, from random values.

- The algorithm stops when a difference lower than 1% is obtained between two successive estimates of L_{MO}.

During the sound speed profile computation procedure, we considered a logarithmic wind profile and not a lin-log one in the stable cases, in order to better match the weather measurements. In the stable case ($1/L_{\text{MO}} > 0$), the linear part was considered null with $\psi_v = 0$, and $\overline{V_x}(z) = u_*/\kappa \ln((z + z_0)/z_0)$. Considering this approximation, the algorithm quickly converges and a few tens of iterations are enough to obtain the parameters u_*, θ_*,

θ_0. Wind and temperature profiles are obtain according to:

$$U_{\text{fit}}(z) = \frac{u_*}{\kappa} \left[\ln\left(\frac{z + z_0}{z_0}\right) - \psi_w\left(\frac{z}{L_{\text{MO}}}\right) \right], \tag{2.38}$$

$$T_{\text{fit}}(z) = T_0 + \frac{\theta_*}{\kappa} \left[\ln\left(\frac{z + z_0}{z_0}\right) - \psi_t\left(\frac{z}{L_{\text{MO}}}\right) \right] + \alpha_0 z, \tag{2.39}$$

with T_0 the air temperature near the ground.

From the temperature and wind profiles, and the relative directions of the wind with respect to the direction of propagation, it is possible to deduce the effective sound speed profile. The effective sound speed is defined as the sum of the sound speed and the horizontal component of the wind speed in the propagation direction according to:

$$c_{\text{eff}}(z) = c(z) + U_{\text{fit}}(z)\cos\psi, \tag{2.40}$$

where ψ is the angle between the mean wind direction and the direction of the acoustic propagation plane. The sound speed is then approximated by:

$$c(z) = \sqrt{\gamma R_{\text{GP}} T_{\text{fit}}(z)}, \tag{2.41}$$

This procedure for estimating the effective sound speed profile is used in Chapters 4, 5, and 6. Fig. 2.21 illustrates the fitting procedure by measurements carried out on the Flaine site, and effective sound speed profiles associated.
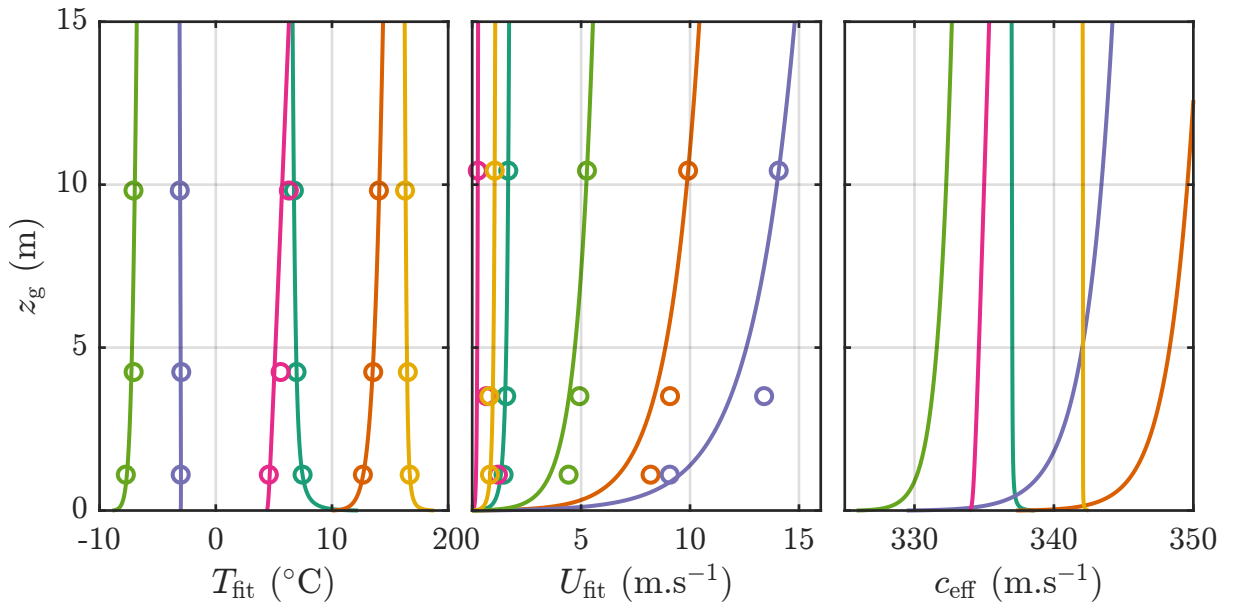
Figure 2.21 − Fitted temperature T_{fit} and wind U_{fit} profiles, deduced from several measurements carried out in Flaine. Corresponding measured data $U(z_{\text{g}})$, $T(z_{\text{g}})$ are depicted by markers (O). Effective sound speed profile c_{eff} calculated in wind direction ($\cos\psi = 1$).

2.5.4   Determination of c_{eff} from the sensible heat flux

The study of meteorological constraints on active spaces requires propagation simulations in specific test cases. The sound speed profiles must be related to physical quantities typically encountered in alpine climates. This is why we use here the sensible heat flux Q_{H}, and the friction velocity u_* as input data to manually set representative atmospheric conditions that may exist in Flaine for example. According to Ostashev & Wilson (2016), the temperature scale θ_*, as well as the Monin–Obukhov length L_{MO} can be deduced following:

$$\theta_* = -Q_{\text{H}}/(\rho_0 C_P u_*), \tag{2.42}$$

$$L_{\text{MO}} = -u_*^3 T_0 \rho_0 C_P/(g\kappa Q_{\text{H}}), \tag{2.43}$$

where $\rho_0 = P_0/(RT_0)$ is the air density, T_0 is the air temperature at ground level, $C_P \approx 1000$ J.K^{-1}.kg^{-1} is the heat capacity of the air at constant pressure, $g = 9.8$ m.s^{-1} the gravity, and $\kappa = 0,41$ the von Kármán constant.

	clear sky			cloudy sky	
	day	night (low wind)	night (moderate to strong wind)	day	night
Q_{H} (W.m^{-2})	200	-4	-20	0	0
u_* (m.s^{-1})	$0.1 - 0.6$	0.1	$0.3 - 0.6$	$0.1 - 0.6$	$0.1 - 0.6$

Table 2.4 – Typical values of Q_{H} and u_* over a grassy ground according to Ostashev & Wilson (2016).

Typical values of Q_{H} and u_* are given in Tab. 2.4. These values are valid over a grassy ground. Over snow, however, the sensible heat flux behaves differently. It rarely takes positive values during the day, and can drop at night to -100 W.m^{-2} or less, especially if there is wind (Sterk *et al.*, 2013; Mott *et al.*, 2017; Schlögl *et al.*, 2018). From sunset onwards, the temperature of the snow on the ground becomes very cold because of its high emissivity in the infrared spectrum. This radiative cooling implies a very marked temperature inversion in the atmospheric surface layer, and therefore a very stable atmosphere. This inversion persists during the day when the thermal radiation from the atmosphere is low, on a clear day, and when the solar radiation is also low, in winter. During the day, the soil is much less heated because of the insulating nature of the porous snow layer. On the other hand, the smoothing of the topography by the snow cover implies smaller roughness lengths than for grass. This reduces the absolute value of the fluxes exchanged between the ground and the atmospheric surface layer.

The determination of wind and temperature profiles as a function of sensible heat flux is used in Chap. 4 to set reference cases for propagation over snow.

2.6   Monitoring of birds with GPS tags

To study the territorial behavior of ptarmigan, it is necessary to obtain position and movement data. Given the difficulty of conducting long-term observations in this habitat, the solution of equipping some males with GPS-tags (Global Positioning System Bird solar tag, e-obs GmbH, Gruenwald, Germany) was chosen. The GPS-tag is shown on the equipped rock ptarmigan in Fig. 2.22. The ptarmigan's positions are recorded at fixed time intervals of one minute, with ±3 m uncertainty on the horizontal plane. Thus, it is possible to analyze the territories occupied over different periods of time, the hot spots, and the flights. Due to the difficulty of capturing birds, only a few birds are equipped each year on the Flaine site. Consequently, a maximum of 5 birds were equipped, during the year 2017. Moreover, some failures or lack of battery can occur on the tags, which was the case in 2021. Therefore, the study of the communication behavior related to the territory defense is carried out with these previous data (see Chap. 5).

Figure 2.22 − A rock ptarmigan equipped with a GPS tag on back, just before the release.

The captures are carried out with the help of Bertrand Muffat-Joly, technician at the OFB (Office Français de la Biodiversité). Birds are captured one at a time, by leading them to a net previously installed above the ground (Brenot *et al.*, 2002). To attract a male, it may be necessary to install a caller. A stuffed hen is placed under the net with a remotely controlled speaker (Fusion, FoxPro). Playback of female or male calls will attract nearby males. Once captured, a cover is placed over the bird's head to limit its stress and prevent mortality. Biometric data (weight, size, feather sample) are rapidly acquired, and then a GPS-tag is adjusted on the back of the bird with elastics making a harnesses. This equipment weights 10 grams and does not exceed 2.5 % of the bird's weight, which is considered non-damaging to the bird. This way of equipping ensures that the bird is not injured and that it can keep the tag for several years. These GPS-tags are set to provide one location per minute during the dawn period in spring: 2h40 to 4h15 UTC. The data are then downloaded by UHF (ultra-high frequency) transmission

at the end of the recording period.

Data processing was mainly done with R (2021) software by Charlotte Albert (ENES team). It consists in deleting the spurious data and determining the position of the display flights. Outliers including altitude error greater than 150 m above the ground or excessive speed greater than 54 km/h (900 m/min) and creating a round trip with an angle of less than 1° between three consecutive points were discarded. This method of trajectory correction is adapted from Bjørneraas *et al.* (2010). Display flights are determined as the displacement greater than 50 m in one minute. This threshold was set after years of observations, based on the fact that ptarmigan typically move by walking slowly, which is also observed in other grouse. Since the elevation data (on the z axis) measured by GPS-tags are less accurate, we subsequently refer to the underlying topography to infer flight heights.

2.7 Ptarmigan song measurements

To conduct active space simulations applied to rock ptarmigan, it is necessary to know the source level of this bird. Field measurements enable us to determine the spectrum of its songs and their variations. Since there are no captive ptarmigans bred in France, the measurements have been conducted on the Flaine site. This section details the ptarmigan records and their analysis.

2.7.1 Source level determination

Ptarmigan sing little at ground level, and it does not seem feasible to measure their song when captured. Therefore, we opted for measurement at the time of disturbance. Male ptarmigan systematically sing at takeoff when fleeing from danger, and this behavior is used to perform relevant measurements. The source level (SL, in dB ref. 20 µPa) of ptarmigan song is deduced from on site measurements in Flaine during June 2021. Birds were recorded at takeoff, using a hand-held sound level meter (NL52 Class 1, Rion, Tokyo, Japan) calibrated on site prior to measurements. At the same time, the distance between the sound level meter and the take-off point is measured with a laser telemeter with an accuracy of ±1 m. The measured distances are between 6 and 20 m. Audio files are calibrated according to the sensitivity of the sound level meter and then filtered with a band-pass filter $400 - 4000$ Hz. Since the ptarmigan song is a pulsed signal, the RMS (root mean square) level is very dependent on the pulse rate, and does not seem to be relevant to predict the signal detection. We therefore prefer to consider the peak level of the pulses to calculate the SNR thereafter. The maximum instantaneous level is then picked up from the first pulses sequence (see for example Fig. 2.23).

The SL is then deduced by subtracting the spatial decay in free field from the recorded
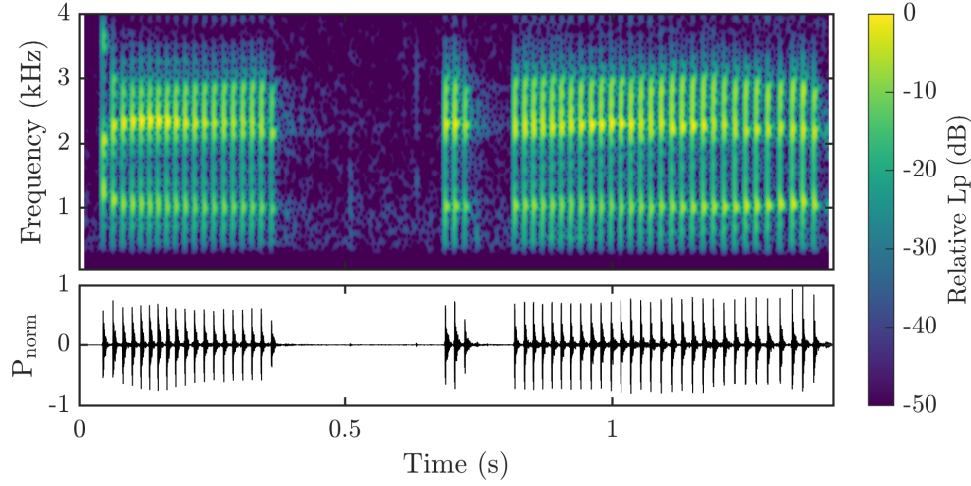
Figure 2.23 – Spectrogram (relative pressure level) and waveform (pressure normalized by the maximum amplitude) of ptarmigan recordings. Spectrogram settings: sampling frequency= 44.1 kHz, 900 points hanning window with 99 % overlap, filtering outside $[400 - 4000]$ Hz frequency range.

level (RL, in dB ref. 20 μPa). Only the geometric decay is considered here, assuming free field propagation. Thus we use the relation $\mathrm{SL} = \mathrm{RL} + 20\log_{10}(r/r_{\mathrm{ref}})$ with $r_{\mathrm{ref}} = 1$ m to obtain an estimate of the mean source level. The four birds whose songs were recorded showed the following result: $\mathrm{SL} = 85 \pm 2$ dB. These SL values should be interpreted with caution, as they are derived from few measurements with poor control on the directivity and distance parameters. Nevertheless, this average value is then used for the active space determinations in Chap. 5 and Chap. 6. Note that SL measurements were not yet carried out at the beginning of the thesis, hence Chap. 4 refers to a default value. A tracking method using a microphone array could give a more direct result for SL, eliminating the need to measure the bird's distance separately (Dutilleux *et al.*, 2023). However, this type of method has not been tested, as such equipment is fragile and complicated to implement in difficult alpine conditions.

2.7.2 Spectrum determination

The average spectrum of the ptarmigan song is obtained by taking the harmonic mean of the pressures measured on the first series of pulses of the 4 short songs recorded (see Fig. 2.24). The harmonic mean method is chosen as it maximizes the peaked shape of the spectrum. It is defined as:

$$p_{\mathrm{mean}}(f) = \frac{n}{\sum_{i=1}^{n} 1/p_i(f)}, \tag{2.44}$$

with n the number of spectra, and p_i the spectrum of each recording. This average spectrum is used later for propagation calculation tests with two formants or the overall spectrum (see Sec. 3).

The four spectra, normalized according to the amplitude of the first formant, are

shown in Fig. 2.24. They show inter-individual variations in frequency and amplitude. Thus, formant 1 ranges from 960 to 1140 Hz, and formant 2 ranges from 2160 to 2280 Hz. A third formant could be detected around 2800 Hz, but its presence is not clear for all the birds. The pressure level of the second formant is between -10 dB and +6.5 dB compared to formant 1. This variation is probably due to the high frequency directivity of the bird as well as the measurement conditions. Indeed, the birds were recorded from behind, from the side or from below. Further measurements or modelling of the ptarmigan's sound production would provide more information on its directivity. In the absence of this, we consider the bird as an omnidirectional source in the following.
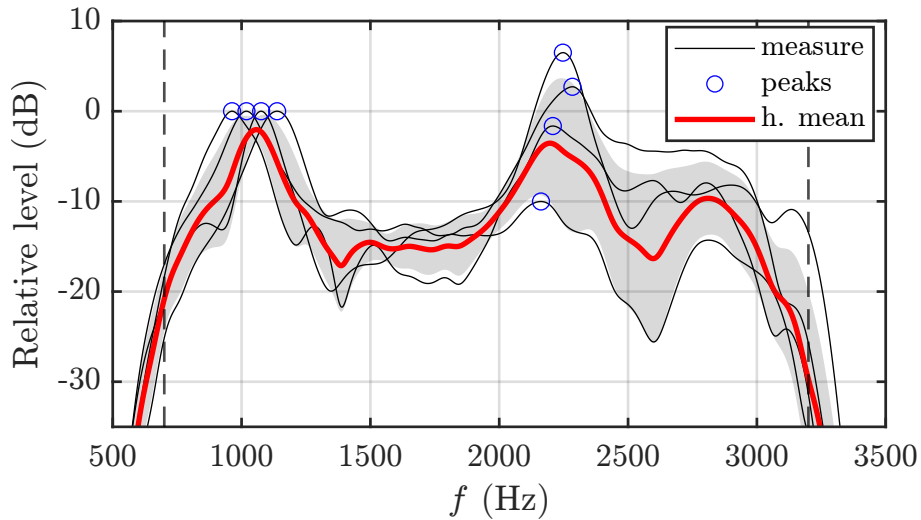
Figure 2.24 – Measured male rock ptarmigan spectra filtered on $[700-3200]$ Hz and normalized according to the 1st formant (———), harmonic mean of the spectra (———), standard deviation of levels in dB (shaded area), and peaks of measured formants ($\circ$).

The width of the peaks found on the spectra is directly related to the frequency shift of the formants during the song. Indeed, the songs present slight articulations especially at its beginning. This is probably due to the bending of the vocal tract during the flight of the bird. This frequency variation of the formants can be seen on the song spectrograms.

In order to use this spectral information in the calculation of broadband active space, the normalized pressure p_{norm} is deduced from the average spectrum as shown in Fig. 2.25. Then, discrete values are interpolated every 50 Hz to be used in frequency based computations.

2.7.3   Evaluation of ptarmigan far-field directivity using BEM

We want to study the directivity of ptarmigan song to discuss its importance in determining active space. As it is very difficult to measure it on a living bird, we perform an acoustic modeling with a numerical model based on BEM (boundary element method). The Akabak software (Akabak , 3.1.7), initially developed for the simulation of loudspeakers, is used to map the radiated sound around the bird and to trace the directivity
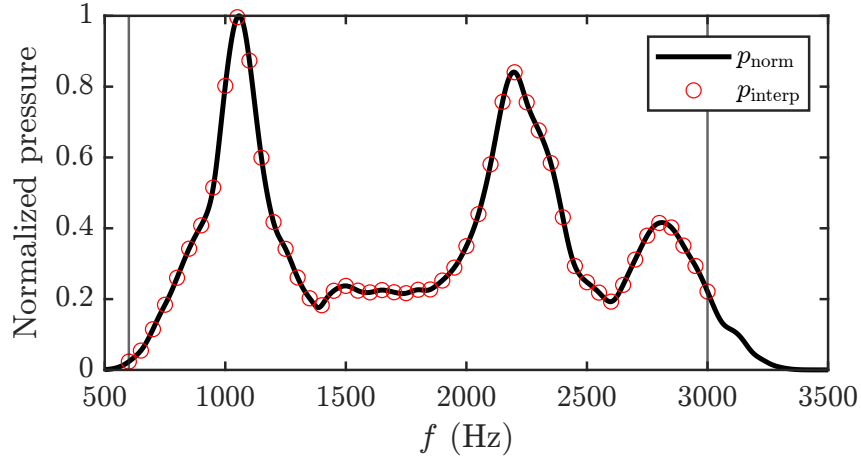
Figure 2.25 – Relative pressure of the harmonic mean of the recorded ptarmigan spectra filtered on [700 − 3200] Hz, and interpolated discrete values for active space computations.

patterns.

A 3D model of a ptarmigan is drawn from a stuffed male bird (see Fig. 2.26). The bird mesh shown in Fig. 2.26 ensures a minimum of 6 points per wavelength for the computation. The source is simulated by an oscillating plane piston of diameter 0.8 cm at the beak location. This dimension corresponds to the width of the beak at its half. The surface of the bird is considered as reflective. The BEM computation is performed in free field for different pure frequencies fixed with respect to the third octaves from 400 to 4000 Hz.
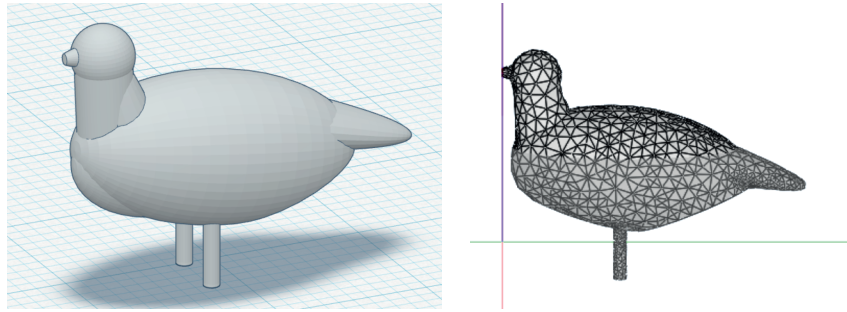
Figure 2.26 – Ptarmigan 3D model and mesh for directivity computation.

The results shown in Fig. 2.27 detail the directivity patterns in the far field (10 m distance to the source). The axis of the bird's beak (in front) is fixed at the angle 0 degrees, and the radial axis indicates the deviation, i.e. the difference in pressure level in dB from the pressure level in front. On the horizontal plane the radiation is omnidirectional in low frequencies [400-1000] Hz. At 1000 Hz the largest deviation is -1.7 dB. From 1250 Hz on, the directivity pattern is no longer circular and a back lobe is visible. For higher frequencies up to 4000 Hz, different back and side lobes are present. We note that at 2000 Hz the largest deviation is -3.6 dB. In the vertical plane the radiaton is also omnidirectional at low frequencies. At 1600 Hz and above, the directivity diagram shows lobes that intensify and sharpen with increasing frequency. Note that for the

frequencies 1000 Hz and 2000 Hz the largest deviation is -2 dB and -5.2 dB respectively.
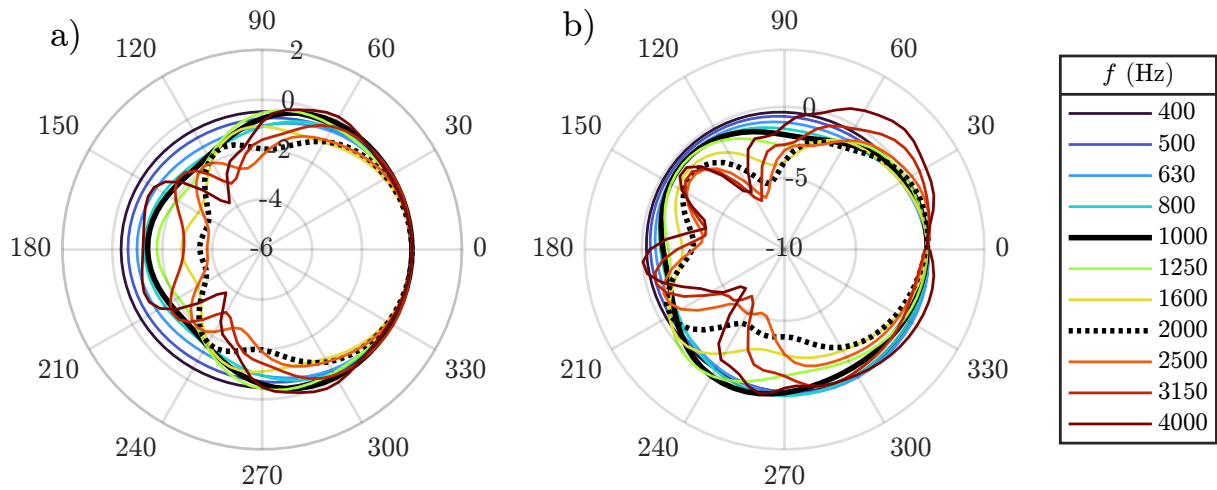
Figure 2.27 – Directivity computed in far field (10 m distance) by BEM modeling from a 3D ptarmigan model, in horizontal plan (a), and vertical plan (b). The bird's head is located at 0 degrees, and the radial axis represents the relative pressure level.

The omnidirectional behavior at low frequencies is due to the small size of the source (the piston) in relation to the wavelengths. Moreover the size of the bird which is 10 cm wide and 23 cm long in its standing position, makes that diffraction is observable above 1000 Hz (wavelength of about 34 cm). We observe important deviations at high frequencies with directivity lobes, but not significant at 1000 Hz, the main frequency of the ptarmigan. These results must be put into perspective according to the approximations of the modeling. First, we simulated the wave front coming out of the vocal tract with a plane piston. The vocal production of the bird can induce a different wavefront at the exit of the beak given the complexity of the vocal tract and the impedance discontinuity at its exit. Secondly, the reflective boundary condition at the surface of the 3D model accentuates the diffraction effect, and we expect a more omnidirectional pattern for a real bird with thick feathers and down, due to absorption.

Despite the inherent simplifications of this modeling, it provides a fairly good idea of the far-field directivity patterns that a bird of this size might have. Moreover, these patterns are consistent with the actual measurements reported in the literature (Larsen & Dabelsteen, 1990). However, we do not use these results later in the propagation code for several reasons. First, it is reasonable for us not to add a source of uncertainty to the computation of the acoustic propagation. Indeed these results are preliminary and must be consolidated by other simulations in more realistic configurations, and eventually by measurements. Second, our applications do not give a precise knowledge of the direction of the bird and in particular when it is on the ground. Therefore, we consider the ptarmigan as an omnidirectional point source in the following. Note that it is possible to include a source directivity in many different models including the parabolic equation method (Vecherin *et al.*, 2011).

2.8   Monitoring of vocal activity & background noise

Recordings of the sound landscape of Flaine are made every spring in an automated way with the help of SM4 dual-channel recorders (Wildlife Acoustics, Massachusetts, United States), called automated record unit (ARU) thereafter (see Fig. 2.28). Their locations are visible on Fig. 2.4. Twelve audio samples of 10-minutes long are recorded daily. Recording times are scheduled as follows: eight samples from 1h10 before sunrise to 20 minutes after, three samples at fixed hours 7h10, 12h10 and 15h10 UTC, and one sample at sunset time. Most samples are recorded before sunrise to focus on the period of maximum ptarmigan communication activity. A determination of the vocal activity on the entire site is estimated from these audio samples.

Figure 2.28 – Example of the type of audio recorder deployed on Flaine site (SM4, Wildlife Acoustics).

Audio analyses are performed with a Python code developed by Jérémy Rouch (ENES team) called LagoNet. To ensure the best signal-to-noise ratio for the detection algorithm, only the least noisy channel of the ARUs (left or right) is considered. To analyze recordings in the ptarmigan frequency band, the signal is first filtered with a bandpass finite impulse response filter (FIR) on the $400 - 4000$ Hz frequency band.

The SM4 microphone sensitivity is previously determined by calibration in the anechoic chamber of the ENES lab. This permits to determine the short time sound pressure level (SPL, in dB, ref. 20 µPa) recorded on site. The levels are calculated according to non-overlapping 0.5 s windows, which leads to $L_{eq,0.5s}$. Then the statistical level L_{90} defined as the pressure level exceeded 90 % of the time is computed from the $L_{eq,0.5s}$

on each 10 minutes audio file. This sound pressure metric is chosen to characterize the background noise because it is not affected by short duration sound events. Unwanted noise such as the songs of passerines near the recorders or passing aircraft will not affect these levels. This calculation of L_{90} is performed from samples excluding detected singing periods.

The song detection is performed using a convolutional neural network (CNN) algorithm in Python language (Python, 3.9), with an architecture inspired by previous work on automated identification of animal sounds (Ruff et $al.$, 2021). It is based on PyTorch Python library (Paszke et $al.$, 2012). This CNN is trained to classified spectrogram samples with 40 mel frequency bands and 139 time steps. It is composed of 4 convolution layers, 1 fully connected layer and 1 decision layer as shown on the block diagram in Fig. 2.29.
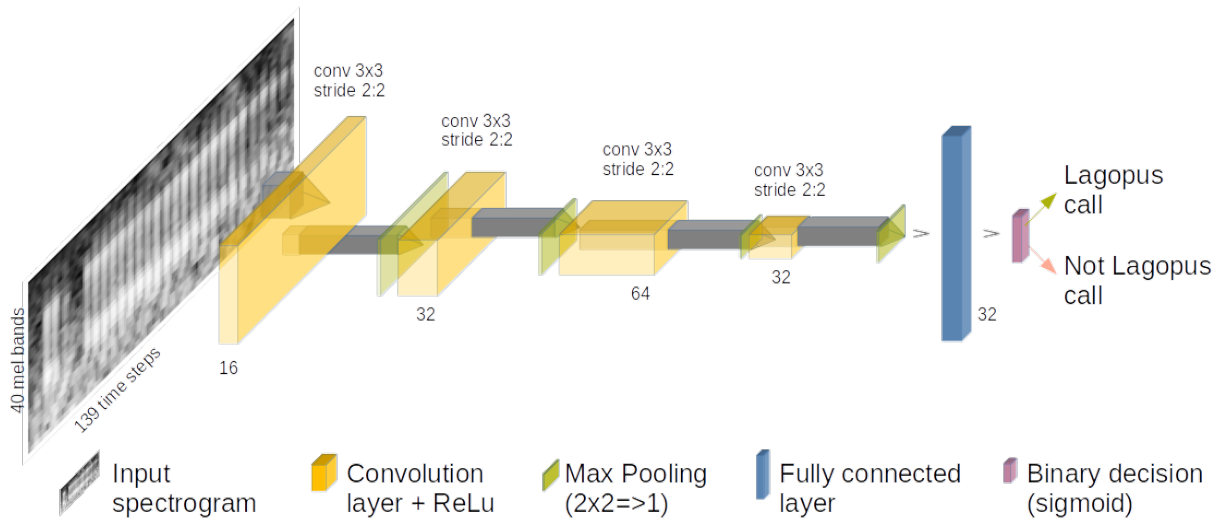
Figure 2.29 – Block diagram of the detection CNN (provided with the agreement of Jeremy Rouch).

LagoNet has been previously trained on manually annotated rock ptarmigan song data taken from field recordings in Norway, French Alps, and Pyrenees. All these training data represent 20630 original song samples of 0.66 s each, with an overlap of 80 %. It corresponds to a total of 47 min of ptarmigan song. Besides, 336270 negatives (non-sung) samples are collected from the same field recordings. Data augmentation and external data sets have been used for a 1200 epochs training process. The validity of the CNN is assessed on the basis of the detection rates: True Positives (TP), False Positives (FP), True Negatives (TN), and False Negatives (FN). With the validation data set processed, the retained model performances are excellent as confirmed by the CNN detection rates shown in Tab. 2.5.

The algorithm estimates the probability of a ptarmigan song presence according to windows of 0.66 s with a 33 % time overlap. Each time step of 0.22 s is considered as a song period if the average probability over the 3 enclosing windows is greater than 50 %. The vocal activity rate is defined as the time percentage of song detected in the ARU

Table 2.5 – Performance parameters of the CNN detection algorithm LagoNet.

LagoNet	Perf.	Formula	Definition
Precision	97.4 %	$TP/(TP + FP)$	proportion of apparent "hits" that are real detections
Recall	94.6 %	$TP/(TP + FN)$	proportion of real examples that are detected and correctly labeled
Balanced accuracy	94.3 %	$\left(\dfrac{TP}{(TP + FN)} + \dfrac{TN}{(TN + FP)} \right)/2$	proportion of samples correctly labeled
F1 score	96 %	$\dfrac{(2 \times \text{Precision} \times \text{Recall})}{(\text{Precision} + \text{Recall})}$	overall performance: balanced combination of precision and recall

recording. In Chap. 6, the VA (vocal activity) is defined as the total time sung over the dawn chorus period.

The performance in terms of detection in noise is evaluated with a new set of recording data by adding random noise with a given SNR. LagoNet is tested with 100 different samples for each SNR value between -30 dB and 10 dB. The result of these tests is shown Fig. 2.30. It shows a sigmoid detection curve. Thus LagoNet detects 50 % of the songs for an SNR equal to -11.4 dB, and 95 % of the songs for an SNR equal to 0.9 dB. This latter SNR value is used in the following Chap. 6 to determine the calculation of the detection spaces.
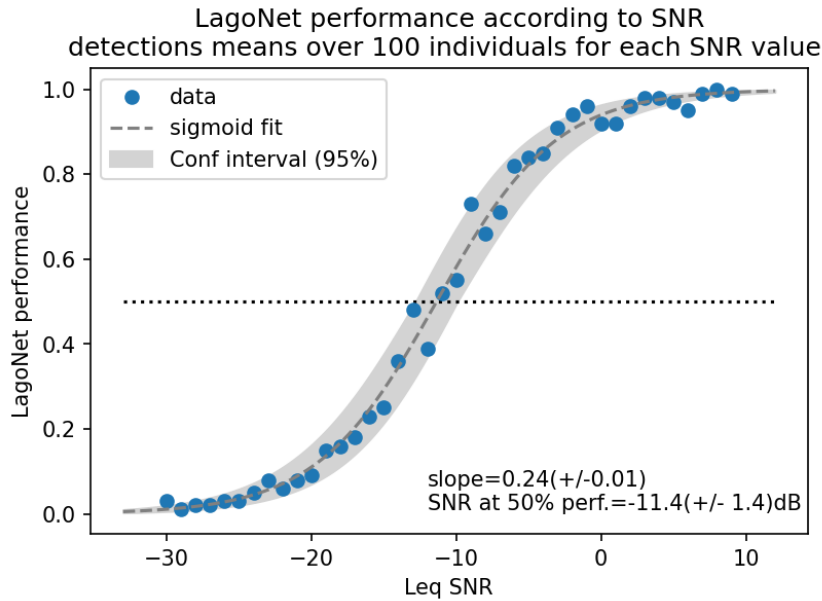
Figure 2.30 – Performance of the LagoNet detection algoritm (provided with the agreement of Jeremy Rouch).

Experimental methods ———————————————————————————— **Summary**

We have seen the different experimental methods implemented in this thesis. They are used to inform both the acoustic propagation in heterogeneous environment and the physical conditions encountered in alpine environment, as well as the communication network studied in ptarmigan using GPS, SL, spectrum, and vocal activity data. These elements make it possible to carry out our three research axes presented in Sec. 1.5.

• First, propagation experiments at the CLB are used to validate the propagation code developed for bioacoustic applications in heterogeneous environments (see Chap. 4). The variability of active spaces is also studied through the example of the Flaine site.

• Then, the physical and biological data enable parametric studies and realistic comparisons of different communication situations within the studied network (see Chap. 5). The temporal and spatial dimensions of the network can be investigated, and a particular attention is paid to the interest of display flights for remote communications in alpine environment.

• Finally, the meteorological data measured in Flaine as well as the audio data recorded by three ARUs are used to study the possibilities of acoustic monitoring in heterogeneous habitats (see Chap. 6). Moreover, the computation of the active spaces associated with these ARUs brings new elements to discuss the interest of these simulations for large scale acoustic census.

In the next chapter, the development of the propagation code is detailed. This one requires the use of the topography, ground impedance and sound velocity profile data that have been presented in this chapter.

Chapter 3

Numerical methods for the computation of active spaces in heterogeneous environments

Abstract

In this chapter, we present the theoretical formulation of the WAPE, as well as the development of the computational code adapted to acoustic propagation in open heterogeneous environments. The formulation is presented for a 2D geometry, and its numerical implementation is detailed. Then, the method is generalized to an N×2D computation, detailing the particularities of this type of approach. Finally, the application framework is reviewed by detailing the limitations of the method.

Contents

3.1   Introduction

To answer the three main questions of this thesis (see Sec. (1.5)), acoustic communication is considered from a propagation perspective. Thus we developed a sound propagation model adapted to bioacoustic studies in heterogeneous environments. This propagation code must provide accurate estimates of long-range noise levels for a particular topography and for realistic sound speed profiles encountered in alpine environments. The outputs should include not only sound levels, in order to map the signal-to-noise ratio obtained from a source in a given habitat, but also the temporal signals after propagation. The latter make it possible to obtain the transmitted information. A trade-off has to be made to have a sufficiently accurate propagation model while keeping a reasonable computational cost. For these reasons, and for other technical considerations discussed in Sec. 1.3.5, the WAPE (wide angle parabolic equation) approach was chosen as a basis to develop the computation code.

3.2   WAPE method in 2D

The PE (parabolic equation) methods were originally developed in the electromagnetic research field (Fok, 1965), and rapidly adopted to resolve sound propagation problems in ocean acoustics (Tappert, 1977). In the 80's, the method was adapted by Gilbert & White (1989) to perform the first outdoor applications on flat ground. Extensions have been also proposed for uneven ground (Sack & West, 1995; Blairon *et al.*, 2002; Lihoreau *et al.*, 2006), so it is well suited for long range sound propagation with a slowly varying slope (Lee *et al.*, 2000).

3.2.1   Theoretical formulation

The parabolic equation (PE) is formulated based on the classical linear wave equation describing the propagation of acoustic pressure fluctuations in an inhomogeneous propagation medium as:

$$\left(\frac{1}{c^2(r,z)}\frac{\partial^2}{\partial t^2} - \Delta\right)p(\mathbf{r},t) = 0, \tag{3.1}$$

where $c(r,z)$ (m/s) is the sound speed, Δ the Laplace operator, t (s) the time, and $\mathbf{r} = (r,\theta,z)$ the considered position in a cylindrical coordinate system. Note that $c(z) = \sqrt{\gamma R_{\mathrm{GP}} T(z)}$ for an ideal gas, and the atmosphere is considered as such, with γ the specific heat ratio, $R_{\mathrm{GP}} = 287$ (J/kg/K) the ideal gas constant, and T (K) the temperature. A point source term could be added on the right side of Eq. (3.1) as $-\hat{S}\delta(\mathbf{r})$, with a finite amplitude $\hat{S}$.

For a harmonic excitation at frequency f (Hz), the acoustic pressure can be sought

as:

$$p(\mathbf{r}, t) = \mathrm{Re}[p_c(\mathbf{r}) \exp(-i\omega t)], \tag{3.2}$$

with the complex pressure amplitude p_c, the angular frequency $\omega = 2\pi f$, and the imaginary unit i such that $i^2 = -1$. It can be shown that p_c satisfies the frequency-domain wave equation, or Helmholtz equation:

$$\left(\nabla^2 + k^2(z)\right) p_c(\mathbf{r}) = 0, \tag{3.3}$$

with $k(z) = \omega/c(z)$ is the wave number.

In cylindrical coordinates, we have:

$$\left\{\frac{1}{r}\frac{\partial}{\partial r}\left(r\frac{\partial}{\partial r}\right) + \frac{1}{r^2}\frac{\partial^2}{\partial\theta^2} + \frac{\partial^2}{\partial z^2} + k^2(z)\right\} p_c(\mathbf{r}) = 0. \tag{3.4}$$

The equation (3.4) refers to the acoustic pressure field in a three dimensional space (3D). To simplify it and reduce the problem to a two dimensional space (2D), the physical properties are assumed to be invariant with respect to the azimuth θ. This allows to write it in a (r, z) plane and yields:

$$\left\{\frac{\partial^2}{\partial r^2} + \frac{\partial^2}{\partial z^2} + k^2(z) + \frac{1}{4r^2}\right\} q_c(r, z) = 0, \tag{3.5}$$

where the complex pressure p_c is now replaced by the axisymmetric complex pressure q_c like $p_c = q_c/\sqrt{R}$. The distance from the source is expressed as $R = \sqrt{(x - x_s)^2 + (z - z_s)^2}$, where (x_s, z_s) is the source position. Considering the far-field approximation (with $|kr| \gg 1$), we can neglect the term $1/4r^2$ compared to k^2 in Eq. (3.5). In the following, the r dimension is then replaced by x to represent the 2D plane.

In the considered plane, two wave contributions propagating along two opposite directions appear: one qualified as progressive according to $+x$ direction, and one qualified as regressive in the opposite $-x$ direction. By making this separation, Eq. (3.5) becomes:

$$\left\{\frac{\partial}{\partial x} - ik(z)\mathcal{Q}\right\}\left\{\frac{\partial}{\partial x} + ik(z)\mathcal{Q}\right\} q_c(x, z) = 0. \tag{3.6}$$

with $\mathcal{Q} = \sqrt{1 + \mathcal{L}}$. The operator $\mathcal{L}$ is given by

$$\mathcal{L} = \epsilon + \frac{1}{k_0^2}\frac{\partial^2}{\partial_z^2} \tag{3.7}$$

with $\epsilon(z) = n^2 - 1$, with n the refraction index given by $n = c_0^2/c^2(z)$. Note that $c(z)$ has to be replaced by c_{eff} (see Eq. 2.40) for a moving atmosphere in the effective sound speed approximation.

If the operators $\mathcal{Q}$ and $\partial/\partial x$ permute, then the equation (3.6) can be decoupled into

two parabolic equations for q_c^+ and q_c^-, with $q_c = q_c^+ + q_c^-$. This permutation is valid in the case of a stratified atmosphere, with $\mathcal{Q}$ invariant along x, and yields:

$$\left\{\frac{\partial}{\partial x} - ik(z)\mathcal{Q}\right\} q_c^+(x,z) = 0, \tag{3.8a}$$

$$\left\{\frac{\partial}{\partial x} + ik(z)\mathcal{Q}\right\} q_c^-(x,z) = 0. \tag{3.8b}$$

The parabolic equation is now obtained from the one-way approximation by neglecting the back-scattering contribution of q_c^-. This approximation holds as long as the ground variations along z are small compared to the propagation distance.

The complex pressure q_c^+ is now named q_{PE}, and the PE can be written for the variable $\psi(x,z)$ defined as the slowly varying envelope of q_{PE} according to:

$$q_{\mathrm{PE}} = \psi(x,z)\exp(ik_0 x), \tag{3.9}$$

with the factor $\exp(ik_0 x)$ which accounts for the fast oscillations along x, and $k_0 = \omega/c_0$, with c_0 the reference sound speed at ground level. This variable change leads to a PE for which the solution $\psi(r,z)$ is free of fast variations according to the x direction.

$$\frac{\partial\psi(x,z)}{\partial x} = ik_0(\mathcal{Q}-1)\psi(x,z). \tag{3.10}$$

The pseudo-differential operator $\mathcal{Q}$ could be written as a Padé (1,1) approximation according to Collins (1998),

$$\mathcal{Q} \approx \frac{1 + p_1\mathcal{L}}{1 + q_1\mathcal{L}}, \tag{3.11}$$

with $p_1 = 3/4$ and $q_1 = 1/4$. This approximation fixes the validity of the calculated pressure field to an aperture of $\pm 40°$ around the direction x (Ostashev *et al.*, 1997). It leads to the wide angle parabolic equation (WAPE) expressed as:

$$(1 + q_1\mathcal{L})\frac{\partial\psi(x,z)}{\partial x} = ik_0(p_1 - q_1)\mathcal{L}\psi(x,z). \tag{3.12}$$

Ground boundary conditions

The ground boundary condition is implemented according to the normalized admittance value β previously determined in Sec. 2.4. We define the boundary condition for the variable ψ as,

$$\left.\frac{\partial\psi(x,z)}{\partial z}\right|_{z=0} + ik_0\beta\psi(x,z=0) = 0. \tag{3.13}$$

Perfectly matched layer

A boundary condition at the top of the computation domain must be applied to avoid any reflections. We use for that a dedicated computational layer located on the upper part of the domain, named PML (perfectly matched layer). This technique, introduced for the electromagnetic propagation (Berenger, 1994), simulates the evanescence of acoustic waves (Collino, 1997). It consists in the modification of the partial derivative along the vertical direction according to:

$$\frac{\partial}{\partial z} \rightarrow \frac{1}{1 + i\sigma(z)/\omega} \frac{\partial}{\partial z}, \tag{3.14}$$

where $\sigma(z)$ is a strictly positive function in the PML.

The size of the PML required to attenuate the waves is about the order of one wavelength. We define the $\sigma(z)$ function over two intervals, under the PML ($z < z_\delta$) and inside it ($z > z_\delta$), which gives:

$$\sigma(z) = \begin{cases} \sigma_0[(z - z_\delta)/(N_{\mathrm{PML}}\Delta z)]^n & \text{if } z \geq z_\delta \\ 0 & \text{if } z < z_\delta. \end{cases} \tag{3.15}$$

where $N_{\mathrm{PML}} = 100$ is the number of points allocated to the PML, and Δz the vertical spatial step. We fix the parameters σ_0 and n in order to have a minimal reflection both at the interface and at the top of the domain. They are set to $\sigma_0 = 250/\mathrm{d}z$ and $n = 2.5$, which ensure a high attenuation in a wide frequency range $[100 - 3000]$ Hz.

Besides, the $\mathcal{L}$ operator is now expressed, according to the PML condition, in the form:

$$\mathcal{L} = \epsilon + \frac{1}{(k_0 + i\sigma(z)/c_0)^2} \left[\frac{\partial^2}{\partial z^2} - i\frac{\sigma'(z)}{\omega + i\sigma(z)} \frac{\partial}{\partial z} \right], \tag{3.16}$$

where σ' stands for the z derivative of σ.

3.2.2 Numerical computation

Definition of computational domains

The parabolic equation is solved in 2D (two dimensions). We define the x, z axes for the computation plane, which correspond to the r, z axes of the 3D cylindrical coordinates. The numerical calculation must handle arbitrary ground geometries. This is why we choose to compute the pressure solution in successive rectangular domains as shown in Fig. 3.1. The terrain profile is then a piecewise affine function defined by a set of points $(x_c^{(i)}, z_c^{(i)})$. We associate on each portion of the terrain a computation domain with a reference axis (x_i, z_i) whose origin is the point $(x_c^{(i)}, z_c^{(i)})$. Thus, each domain is rotated by an angle a_i with respect to the absolute reference frame x, z. It is possible to switch from the local coordinate system of the domain i to the global coordinate system with

the formulas:

$$x = x_c^{(i)} + x_i \cos a_i - z_i \sin a_i, \tag{3.17}$$

$$z = z_c^{(i)} + x_i \sin a_i + z_i \cos a_i. \tag{3.18}$$

This method using domain rotation has been previously validated by Blairon (2002). The length of each domain is set to 5 m, which is sufficient to properly fit most real topographies.
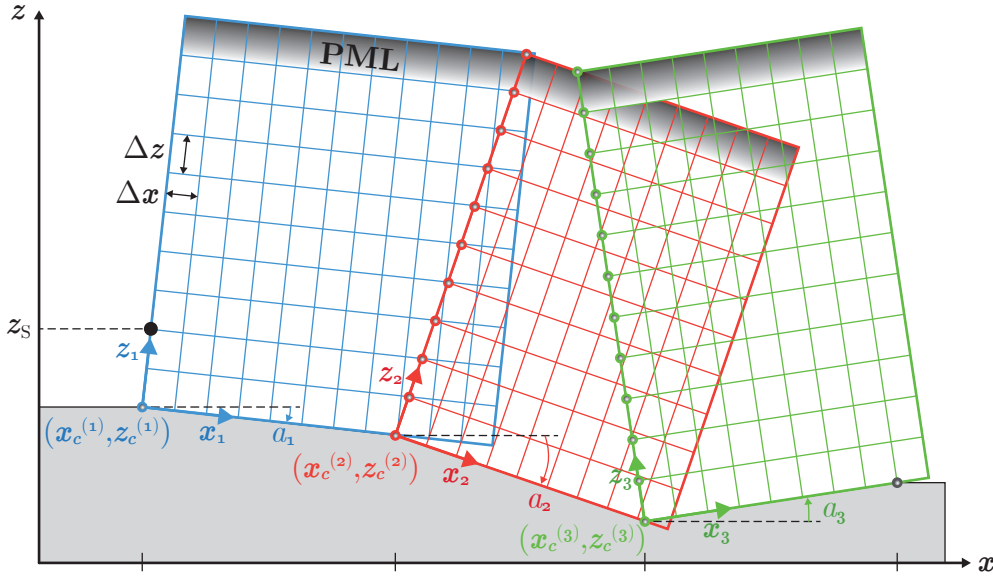
Figure 3.1 − Sketch of the rotated PE method: grids in the (x_n, z_n) planes, with fixed tangent grid spacing Δx and orthogonal grid spacing Δz. A Perfectly Matched Layer (PML) is set at the top of each domain to ensure a reflectionless condition.

The width of domain i is $L_i = (x_c^{(i+1)} - x_c^{(i)})/\cos a_i$. If $a_{i+1} < a_i$, it is necessary to increase the domain size to ensure interpolation of ψ. In this case, we extend the domain i with a size $L_i' = L_i + \tan(a_i - a_{i+1})H_i$. This adjustment is presented Fig. 3.2 a). On the contrary if the next domain is like $a_{i+1} > a_i$ the width adjustment is not necessary. For the height of the domain, we initialize the value of H_1 to a desired height. The heights of the following domains must then be defined in relation to H_1 and the terrain profile. The case $a_{i+1} < a_i$ yields: $H_{i+1} = H_i/\cos(a_i - a_{i+1})$. The case $a_{i+1} > a_i$ brings to two situations. If the deviation remains small ($\tan(a_{i+1} - a_i) < L_i'/H_i$), we can define the height of the domain $i + 1$ with the same formula $H_{i+1} = H_i/\cos(a_{i+1} - a_i)$, as it is shown in Fig. 3.2 b). If the deviation is more important ($\tan(a_{i+1} - a_i) > L_i'/H_i$), it is necessary to define the height of the domain $i + 1$ from the previous domains. To do so, we determine the new height by comparing the position of the upper corners of the $i + 1$ domain to those of the previous domains intersected by the $i + 1$ starter half-line originating at $(x_c^{(i+1)}, z_c^{(i+1)})$. We thus use two distinct conditions in x and in z. These geometrical calculations are not detailed here. Generally, the size of the domain increases

with the number of domains, especially when the topography is rough.
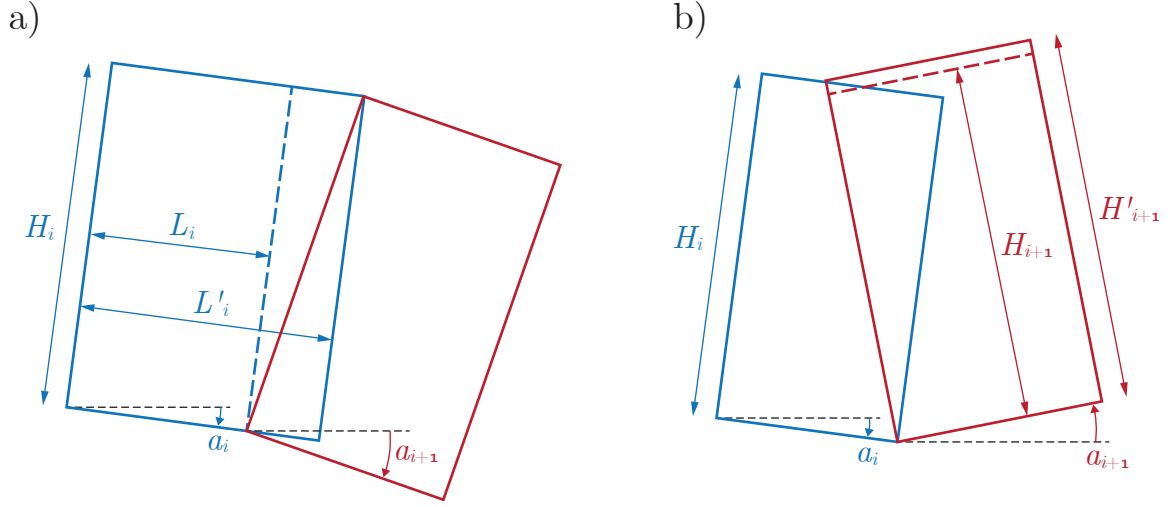
Figure 3.2 − Sketch of the domain size determination for the rotated PE method.

An example of domain definition above a real topography can be seen Fig. 3.3 where both the source and the receiver are shown, with the PML area at the top of each domain. The calculation of the domains' size in relation to the previous ones is crucial to ensure their matching and thus a continuity in the PML. We can see Fig. 3.4 that the PML does not reflect energy back to the ground, and the PL is quickly attenuated in the layer. Moreover, the layer does not have any discontinuities that could constitute new unwanted sources.
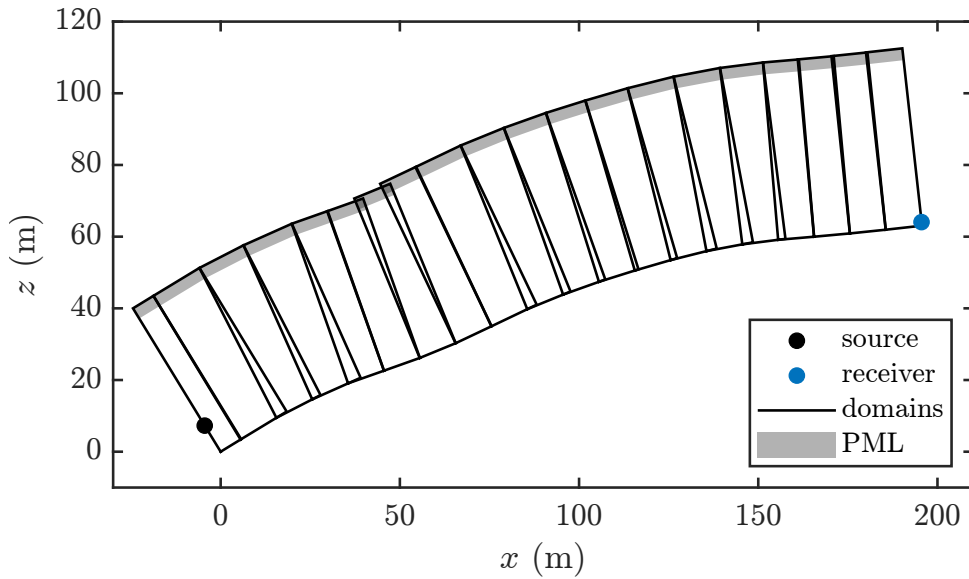
Figure 3.3 − Example of a 2D computational domains on a real topography defined between the source and the receiver, and the associated PML area: $z_S = 10$ m, $z_R = 1$ m
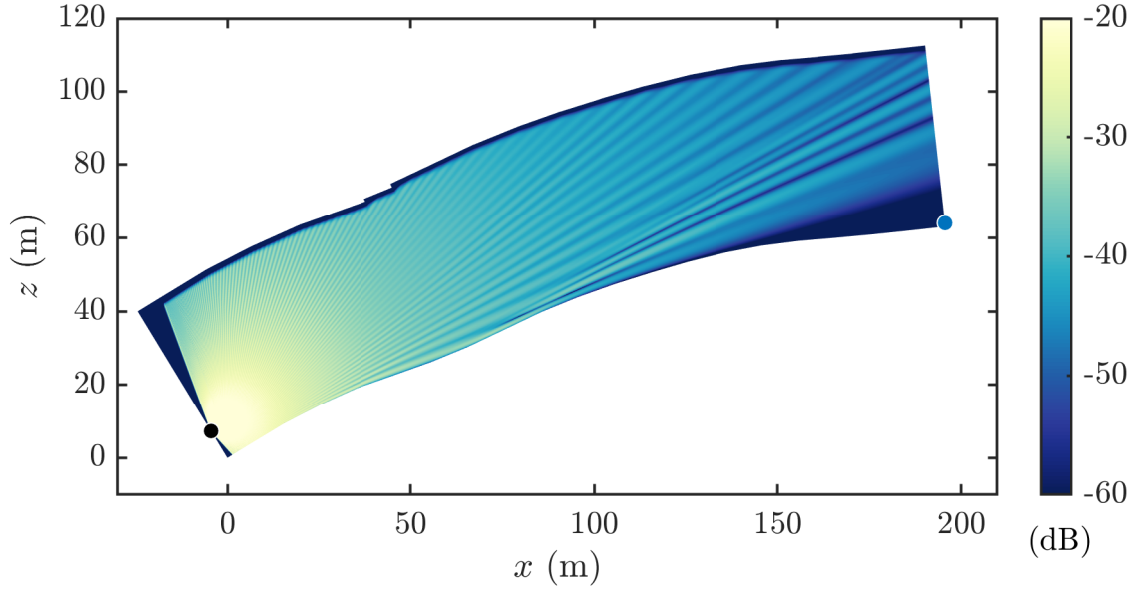
Figure 3.4 – Example of a 2D computation of the PL (propagation loss) over a real topography: $z_S = 10$ m, $z_R = 1$ m, $f = 1000$ Hz, $u_* = 0.05$ m/s, $\theta_* = 0.3$ K, snow cover ($e = 0.15$ m, $R_s = 20$ kPa.s.m^{-2}, $\Omega = 0.6$, and $q^2 = 1/\Omega$).

Discretization and resolution

To resolve Eq. (3.10), we discretize the computational domain in space following a Δx step along x and Δz along z as shows Fig.3.1. The discretization steps are fixed to $\Delta x = \Delta z = \lambda/10$, with the wavelength $\lambda = c_0/f$, to ensure sufficient consistency. The Crank-Nicolson method is used to proceed the solution along the x-direction, and centered finite difference schemes are used to compute the z derivatives. These schemes are highly stable for this application (Dallois, 2000).

We present hereafter the step by step resolution of numerical scheme for the equation. We introduce the following notation: $\psi_m^n = \psi(m\Delta x, n\Delta z)$. The Crank-Nicolson method applied to Eq. (3.12) leads to:

$$(1 + q_1 \mathcal{L})\frac{\psi_{m+1} - \psi_m}{\Delta x} = ik_0(p_1 - q_1)\mathcal{L}\frac{\psi_{m+1} + \psi_m}{2}, \tag{3.19}$$

that can be written as:

$$(1 + \nu_1 \mathcal{L})\psi_{m+1} = (1 + \mu_1 \mathcal{L})\psi_m, \tag{3.20}$$

with coefficients μ_1 and ν_1 given by:

$$\mu_1 = \frac{1 + ik_0\Delta x}{4}, \text{ and } \nu_1 = \frac{1 - ik_0\Delta x}{4}.$$

The discretization of the partial derivatives along the vertical direction ($\partial/\partial z$, $\partial^2/\partial z^2$)

is written as second-order centered finite differences:

$$\frac{\partial \psi^n}{\partial z} = \frac{\psi^{n+1} - \psi^{n-1}}{2\Delta z}, \tag{3.21}$$

$$\frac{\partial^2 \psi^n}{\partial z^2} = \frac{\psi^{n+1} - 2\psi^n + \psi^{n-1}}{\Delta z^2}. \tag{3.22}$$

The resolution itself consists in treating a linear system at each m step forward, which is expressed as:

$$\mathcal{A}\psi_{m+1} = \mathcal{B}\psi_m, \tag{3.23}$$

where the two matrices $\mathcal{A}$ and $\mathcal{B}$ are tridiagonal. They consist of six coefficients according to:

$$\mathcal{A} = \begin{bmatrix} B_1 & C_1 & & \\ A_1 & & \ddots & \\ & \ddots & & C_{N-1} \\ & & A_{N-1} & B_N \end{bmatrix} \text{ where } \begin{cases} A_n = \dfrac{\nu_1}{(k_0 + i\sigma/c_0)^2}\left[\dfrac{1}{\Delta z^2} + i\dfrac{\sigma'}{\omega + i\sigma}\dfrac{1}{2\Delta z}\right], \\ B_n = 1 + \nu_1\epsilon - 2\dfrac{\nu_1}{(k_0 + i\sigma/c_0)^2}\dfrac{1}{\Delta z^2}, \\ C_n = \dfrac{\nu_1}{(k_0 + i\sigma/c_0)^2}\left[\dfrac{1}{\Delta z^2} - i\dfrac{\sigma'}{\omega + i\sigma}\dfrac{1}{2\Delta z}\right], \end{cases} \tag{3.24}$$

$$\mathcal{B} = \begin{bmatrix} E_1 & F_1 & & \\ D_1 & & \ddots & \\ & \ddots & & F_{N-1} \\ & & D_{N-1} & E_N \end{bmatrix} \text{ where } \begin{cases} D_n = \dfrac{\mu_1}{(k_0 + i\sigma/c_0)^2}\left[\dfrac{1}{\Delta z^2} + i\dfrac{\sigma'}{\omega + i\sigma}\dfrac{1}{2\Delta z}\right], \\ E_n = 1 + \mu_1\epsilon - 2\dfrac{\mu_1}{(k_0 + i\sigma/c_0)^2}\dfrac{1}{\Delta z^2}, \\ F_n = \dfrac{\mu_1}{(k_0 + i\sigma/c_0)^2}\left[\dfrac{1}{\Delta z^2} - i\dfrac{\sigma}{\omega + i\sigma}\dfrac{1}{2\Delta z}\right]. \end{cases} \tag{3.25}$$

The impedance boundary condition implementation is done by modifying the first row in the two resolution matrices:

$$B_1 = 1 + \nu_1\epsilon - 2\frac{\nu_1}{(k_0 + i\sigma/c_0)^2}\frac{1}{\Delta z^2} + 2ik_0\beta\frac{\nu_1}{(k_0 + i\sigma/c_0)^2}\left[\frac{1}{\Delta z} + i\frac{\sigma'}{\omega + i\sigma}\frac{1}{2}\right], \tag{3.26}$$

$$C_1 = \frac{\nu_1}{(k_0 + i\sigma/c_0)^2}\frac{2}{\Delta z^2}, \tag{3.27}$$

$$E_1 = 1 + \mu_1\epsilon - 2\frac{\mu_1}{(k_0 + i\sigma/c_0)^2}\frac{1}{\Delta z^2} + 2ik_0\beta\frac{\mu_1}{(k_0 + i\sigma/c_0)^2}\left[\frac{1}{\Delta z} + i\frac{\sigma'}{\omega + i\sigma}\frac{1}{2}\right], \tag{3.28}$$

$$F_1 = \frac{\mu_1}{(k_0 + i\sigma/c_0)^2}\frac{2}{\Delta z^2}. \tag{3.29}$$

We remind that outside the PML, the variable σ is equal to 0. If we apply $\sigma = 0$, we find the CNPE (Crank–Nicolson Parabolic Equation) resolution used for example by Dallois (2000). The description of the computation method is now complete, except for the pressure field at the first step m. We describe below the starter used in the following.

Starter and domain initialization

For the first domain, the calculation is initialized by a wide-angle starter given in Salomons (2001), that accounts for the source image weighted with a complex reflection coefficient. This starter, detailed by Eq. (3.30) and (3.31) is set to reproduces a monochromatic omnidirectional point source in the acoustic far field (with $k_0 R \gg 1$):

$$q_{PE}(0, z) = q_0(z - z_S) + \left(\frac{1 - \beta}{1 + \beta} \right) q_0(z + z_S), \tag{3.30}$$

where $q_0(z)$ is the starting field at position $(x, z) = (0, 0)$ if no ground exist, and $R_p = (1 - \beta)/(1 + \beta)$ is the plane wave reflection coefficient at normal incidence. The starting field $q_0(z)$ is expressed as:

$$q_0(z) = \sqrt{ik_0}(X_1 + X_2 k_0^2 z^2) \exp \left(\frac{-k_0^2 z^2}{X_3} \right), \tag{3.31}$$

where the factors are $X_1 = 1.3717$, $X_2 = -0.3701$ and $X_3 = 3$. Note that the propagation code does not allow a precise prediction of the near field. The amplitude of the source is set so that the SPL in free field at 1 m is equal to SL.

The starters of the following domains are obtained by interpolating the complex field ψ. In practice, at the end of each computation of a domain n, the interpolated information is stored in all the starters of the following domains which intersect the domain n. The starters are thus "filled" from top to bottom to ensure that they are complete and that the recovered information comes from the last domain involved. These intersections between consecutive domains can be observed in Fig. 3.3. They enable the computation of a continuous ψ field in a given plane above the ground as seen with the PL map in Fig. 3.4.

3.2.3   Definition of input parameters

Ground finite impedance

Our computations are performed considering a constant snow cover on the sites. Indeed, during the period of ptarmigan courtship display, territory fixation and breeding, more than three quarters of the habitat is covered with snow on average (observations in Flaine; annual variations are significant for a given date). Moreover, the few outcropping rocks are smaller than the spatial scale of the DEM, so it is not possible to take into account these small reflective surfaces in a simple way. One possibility could be to take an aerial photo of the site, and deduce the ground type for each pixel, from its color. This type of measurement was not be performed during the thesis. The impedance data used are from on-site measurements, and the determination procedure is described in Sec. 2.4.

Sound speed profile

Effects of the wind on sound propagation are approximated with an effective sound speed approach. This one accounts for the temperature profile and the horizontal component of the wind speed projected on the propagation plane in the ASL (atmospheric surface layer). The calculation of this effective sound speed profile c_{eff} is detailed in Sec.2.5. The sound speed profile is computed for each domain. The temperature is then considered as varying only vertically (in z_g), while the wind profile follows the slope variations of the topography (in z_{n}).

3.2.4 Definition of the outputs

Propagation computations are performed to estimate the pressure level decay at the frequencies of interest, taking into account the above-mentioned effects: reflections depending on the ground impedance, diffraction by the topography, and refraction due to temperature and wind profiles of the atmosphere.

From the WAPE method described above, it is possible to compute a complex impulse response between a source and a receiver over a wide frequency band, i.e. the Green's function. This makes it possible to convolve the desired source signals with the Green's function and to obtain an estimate of the propagated signal.

We did not explore temporal signal propagation in the following, instead we focused on level mapping to determine the active spaces of the communication.

Calculation of pressure levels relative to free field

The output required to perform a mapping is the pressure loss (PL), and it is calculated as follows. First, the 2D axisymmetric WAPE is solved on a slice (x, z) with the source located at (x_s, z_s), which gives a q_{PE} field. We remind that $p_{\text{PE}} = q_{\text{PE}} \sqrt{R}$, with $R = \sqrt{(x - x_s)^2 + (z - z_s)^2}$ the distance from the source. Since the WAPE solution does not account for atmospheric absorption, a correction is applied to the pressure like,

$$p(f, x, z) = p_{\text{PE}}(f, x, z) \ \exp[-\alpha(f)R(x, z)], \tag{3.32}$$

where α is the atmospheric absorption factor calculated according to Eq. (1.5), based on the ISO9613-1 standard (ISO, 1993). The sound pressure level L_p at the receiver is related to the PL by the following relationship:

$$\text{PL}(f) = Lp(f) - \text{SL}(f). \tag{3.33}$$

Since the starter used for the computation reproduces a pressure of $p_{1m} = 1$ Pa at $R_{1m} = 1$ m in free field, corresponding to SL=94 dBSPL, it is possible to express the PL with:

$$\text{PL}(x, z) = 10 \log_{10} \left(\frac{|p(x, z)|^2}{p_{1m}} \right). \tag{3.34}$$

The pressure level relative to free field ΔL, also called excess attenuation (EA), is used later for the comparison of the pressure fields in Chap 4. It is defined as a pressure level difference in dB, considering a 2D decay (calculation according to PE) and the theoretical 2D free field decay (2DFF) according to:

$$\Delta L = Lp_{2D} - Lp_{2D(FF)}. \tag{3.35}$$

We present how to obtain the calculation of ΔL from ψ. First the 2D free field pressure level is defined as,

$$Lp_{2D(FF)} = 20 \log_{10} \left(\frac{|p_{2D(FF)}|}{p_{ref}} \right), \tag{3.36}$$

where $p_{ref} = 2 \times 10^{-5}$ Pa. The free field 2D pressure is equal to,

$$|p_{2D(FF)}| = p_{1m} \sqrt{\frac{R_{1m}}{R}}. \tag{3.37}$$

We then calculate the pressure level,

$$Lp_{2D(FF)} = 20 \log_{10} \left(\frac{p_{1m}}{p_{ref}} \sqrt{\frac{R_{1m}}{R}} \right). \tag{3.38}$$

Besides, we remind that $q_{PE} = \psi(x, z) \exp(ik_0 x)$ is the 2D pressure field. Its level is thus equal to:

$$Lp_{2D} = 20 \log_{10} \left(\frac{|\psi|}{p_{ref}} \right). \tag{3.39}$$

From these two expressions of $Lp_{2D(FF)}$ and Lp_{2D}, its possible to write ΔL as:

$$\Delta L = 20 \log_{10} \left(\frac{|\psi|}{p_{ref}} \right) - 20 \log_{10} \left(\frac{p_{1m}}{p_{ref}} \sqrt{\frac{R_{1m}}{R}} \right). \tag{3.40}$$

Simplifying both members leads to the expression of ΔL according to ψ:

$$\Delta L = 20 \log_{10} \left(\frac{|\psi|}{p_{1m}} \sqrt{\frac{R}{R_{1m}}} \right). \tag{3.41}$$

Excess attenuation makes it possible to compare pressure fields while ignoring the geometric decay that is always involved. This makes it easier to observe propagation effects

due to the presence of the ground and the atmosphere.

Calculation with ptarmigan pressure levels

Since sound propagates differently depending on frequency, the mapping of sound levels may vary depending on whether we assume a pure frequency source or a broadband source. In addition, the sources considered in our study are of biological origin, and may involve a spectral variation as seen previously in Sec. 2.7. Therefore, it is essential to be able to estimate the overall pressure level decay from a given source spectrum.

To calculate a global pressure loss PL_g from a source spectrum, it is necessary to integrate the levels between two cut-off frequencies f_1 and f_n according to:

$$\mathrm{PL_g} = 10 \log_{10} \left[\int_{f_1}^{f_n} 10^{\left(\frac{\mathrm{SL+PL}}{10} \right)} \, \mathrm{d}f \right] - \mathrm{SL_g}, \tag{3.42}$$

where $\mathrm{SL_g}$ is the global source level integrated over the same frequency band as $\mathrm{PL_g}$.

In practice, the pressure at a receiver position (x, z) is weighted according to p_{interp} (see Fig. 2.25) which is the normalized pressure of the ptarmigan average spectrum. This leads to an energetic ratio between the squared weighted sound pressure at receiver, and the squared normalized source level:

$$\mathrm{PL_g}(x, z) = 10 \log_{10} \left[\left(\int_{f_1}^{f_n} (p_{\mathrm{interp}}(f) \times |p(f, x, z)|)^2 \, \mathrm{d}f \right) \Big/ \left(\int_{f_1}^{f_n} p_{\mathrm{interp}}^2(f) \, \mathrm{d}f \right) \right]. \tag{3.43}$$

This global pressure loss is then used to compare the active space maps according to the source frequencies taken into account.

3.3 Acoustic field computation in 3D

The computation of 3D (three-dimensional) maps of the propagation loss is necessary to obtain a realistic picture of the active spaces in a heterogeneous environment. This is why we implement a code for N×2D computation in the following. This N*times*2D method has already been implemented in underwater acoustics (Lin *et al.*, 2019), but not applied to terrestrial bioacoustics to our knowledge.

3.3.1 Extension to the N×2D Rotating WAPE

The N×2D computation is performed in a cylindrical coordinate system (r, θ, z) as shown in Fig. 3.5 that depicts one propagation plane. Vertical propagation planes are defined for every $\mathrm{d}\theta$ step. The receiver points are placed at a fixed height z_R above the ground, and at every dr step.
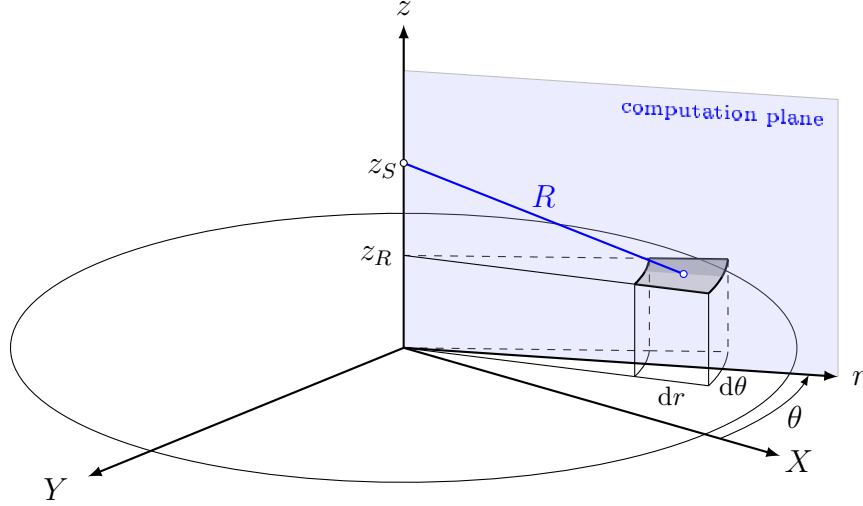
Figure 3.5 – Definition of the coordinate system used for the N×2D computation, with (X, Y) the horizontal plane, (z, r) the vertical computational plane, θ the azimuthal propagation angle, R the source-receiver distance, and $(\mathrm{d}r, \mathrm{d}\theta)$ the elementary horizontal surface around a receiver point.

For each computation plane, the ground profile is interpolated from the DEM starting from the ground reference point below the source to the required distance $r_{\max}$. To obtain a computation with a fixed source regardless of the computation angle, a correction of the interpolated ground profile is performed to fix the starter of the first domain so that it intersects the source point. Moreover, the first domain must be long enough to contain the entire second domain's starter. To ensure a feasible interpolation for the second domain starter on the first domain whatever the source height z_S, we arbitrary set the first domain length $l_{\mathrm{d}1}$ according to z_S and an angle of 45° like,

$$l_{\mathrm{d}1} = \frac{z_S}{2 \tan(45°)}. \tag{3.44}$$

This precaution ensures accurate results with WAPE method. Note that this lengthening modifies very little the result of the computation at long distance. Given the errors that can occur in the PE computation below the angle of validity, we set the r distance between the source and the first receptors as,

$$r_{\min} = \frac{z_S}{\tan(45°)}. \tag{3.45}$$

Consequently the area contained in the circle of radius $r_{\min}$ is considered as part of the active space. Fig 3.6 illustrates these two definitions.

In order to evaluate the active space dimensions, we calculate its surface projected on the horizontal plane (X, Y), which allows us to compare the areas obtained whatever the topography. The term active space will be used hereafter to refer to this area. This is calculated by summing the elementary surfaces $s_i = r \mathrm{d}r \mathrm{d}\theta$ relative to all the receivers which receive a level higher than the decay threshold defined previously according to the
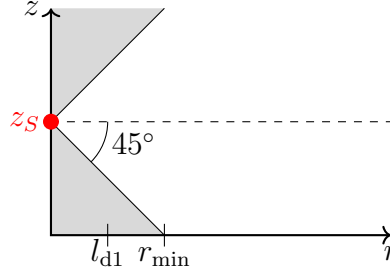
Figure 3.6 − Definition of the minimum distance $r_{\min}$ from the source to the receivers.

SNR.

The radial step $\mathrm{d}\theta$ implies that the spatial sampling depends on the distance to the source. The elementary surfaces s_i are much larger at the limits of the computation plane than near the source. Indeed, the arc length $\eta = r\mathrm{d}\theta$ increases linearly with the radial distance. The estimation of the active space area converges when the arc length $\eta(r_{\max})$ tends towards the spatial resolution of the DEM used. In the context of a natural environment application, it is considered that the uncertainty on the sound level increases with the propagation distance. In this respect, the spatial resolution accuracy becomes less crucial as the distance increases. Hereafter, the $\mathrm{d}\theta$ step is fixed to 2°, which implies 180 computation plans for a 3D application.

Application to an active space calculation

A computation is performed over a uneven topography, with a azimuthal step $\mathrm{d}\theta = 2°$ in the case of a homogeneous atmosphere, at a frequency of 1000 Hz (see Fig. 3.7). One can see on this map of the PL the decay of the sound levels from the source in the center, and superimposed the contour lines of the terrain. No interpolation is done between the receivers for this map, which makes the elementary surfaces s_i visible. The ripples in the color gradient indicate interference or shadow zones. An arbitrary threshold is set at PL $= -70$ dB, which enables one to see a first view of the particular shapes that the active space can take on a non-flat terrain. Areas not affected by the sound are for example found overhanging the source (see the right side of Fig. 3.7). From this pressure level mapping method, it is possible to elaborate parametric studies in relation to the environment or to the behavior of the source. This will be examined in Chap. 5.

3.3.2 Computational cost

Extensive long-distance, high-frequency, and/or broadband computations requires sufficient numerical resources. Before proceeding to parametric studies for example, it is interesting to evaluate the order of magnitude of the computation times. An indication about the required computation time is available in Tab. 3.1. Computations are performed
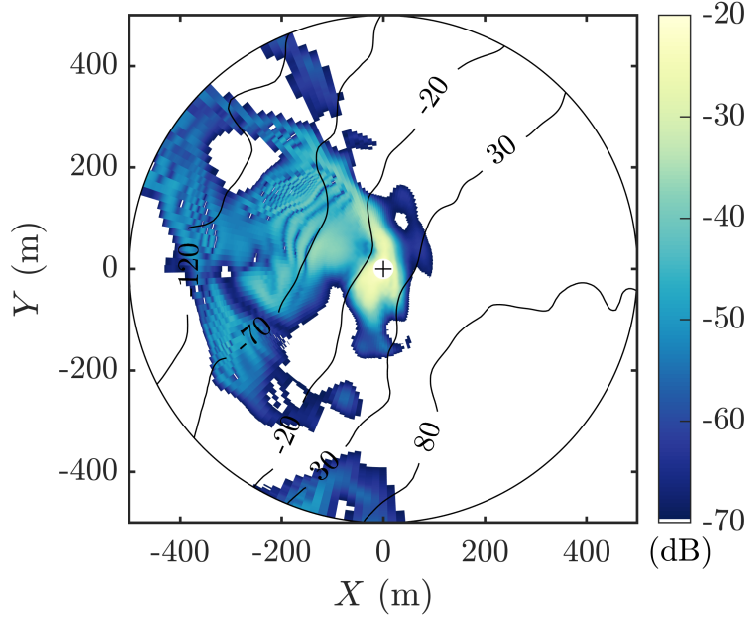
Figure 3.7 – Example of a 3D computation of the PL over a real topography: $z_S = 1$ m, $z_R = 1$ m, $f = 1000$ Hz, homogeneous atmosphere, snow cover($e = 0.15$ m, $R_s = 20$ kPa.s.m^{-2}, $\Omega = 0.6$, and $q^2 = 1/\Omega$).

for the same position as Fig. 3.7, and for several bandwidth settings, and maximum computation distance $r_{\max}$.

Table 3.1 – Computation time tests for a 3D active space: parallelized computations on 30 cores (type Xeon Gold 6130 and Xeon Gold 6226R) based on θ angles

$r_{\max}$(m)	dθ(°)	f_{min}	f_{max}	df(Hz)	CPU time(h)
500	2	200	3000	50	15
500	2	200	3000	100	8
500	6	200	3000	100	3.7
500	6	400	2600	100	2.6
800	6	1000	–	–	0.075 (4'30")

We notice that the calculation times are very dependent on the frequency band considered. We will therefore try to limit the number of frequencies in order to quickly calculate many active spaces.

We then plot the computation time versus frequency for an active space at the same source position, but for $z_S = 25$ m and a distance of $r_{\max} = 1000$ m. By tracing the computation time, we see that it increases as a quadratic function of the frequency. This result is expected, since the spatial resolution steps (Δx, Δz) are determined in two dimensions according to the considered wavelength, as $\Delta x = \Delta z = \lambda/10$. Multiplying by a factor τ the computation frequency results in multiplying by τ^2 the number of points where the pressure computation must be performed. The polynomial resulting from the quadratic adjustment makes it possible to anticipate the computation time required for

further studies.
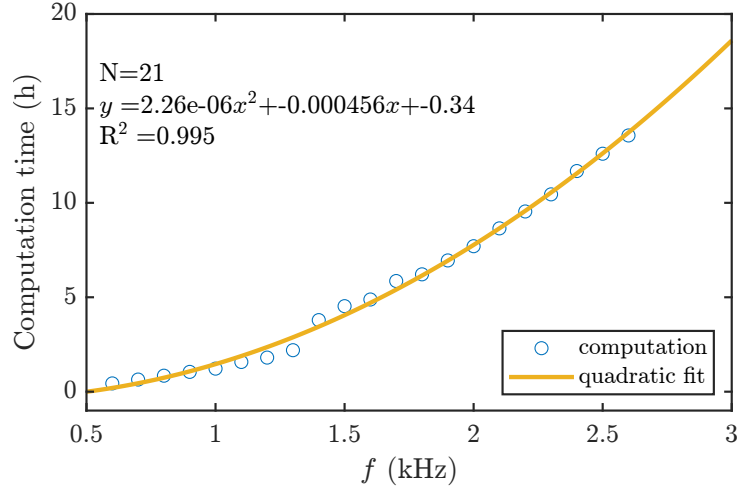
Figure 3.8 – Computation time for a position on Flaine site according to frequency: $r_{\max} = 1000$ m, $\mathrm{d}\theta = 2°$.

3.3.3 Consideration of a ptarmigan signal

In the context of biological signal propagation, it is essential to consider the representativeness of the computations from a frequency point of view. To adress this issue, a comparison of active space is made by considering different frequency contents of the source in Fig. (3.9). A wide band computation $[600 - 3000]$ Hz every 50 Hz is used for this, with a typical configuration: on the Flaine site in moderate wind speed, with a source located at 10 m height. For this same WAPE computation, we plot the PL according to different frequency contents: pure tone at 1000 Hz, 2 formants (1100 Hz and 2200 Hz), normalized ptarmigan spectrum (see Fig. (2.25), p_{interp}), and broadband unweighted spectrum (global, with $p_{\mathrm{interp}} = 1$). The PL calculation is performed according to Eq. (3.43) for a source located 10 m above the ground, with a moderate wind ($u_* = 0.3$ m/s) depicted by the red arrow, with a homogeneous temperature ($\theta_* = 0$ K).

We notice that the interference and shadow zones that streak the active space are more numerous for a pure frequency than for the other spectra. Moreover, since the energy is contained in a single frequency (1000 Hz), the extreme limits of the active space are slightly wider. The PL map of the active space is smoother for a whole ptarmigan spectrum, as the interference pattern of each frequency is blended with that of the other frequencies as a result of the integration (see Eq. (3.43)). Finally, the unweighted global spectrum does not allow to observe the interference. These results were obtained for a fixed limit of the PL. However, for a concrete application, it would be interesting to consider a measured background noise spectrum. Since the pressure level of the background noise typically decreases with frequency, this could potentially modify the AS computed from broadband spectra. Thereafter, and unless otherwise specified, we perform most PL computations at

97
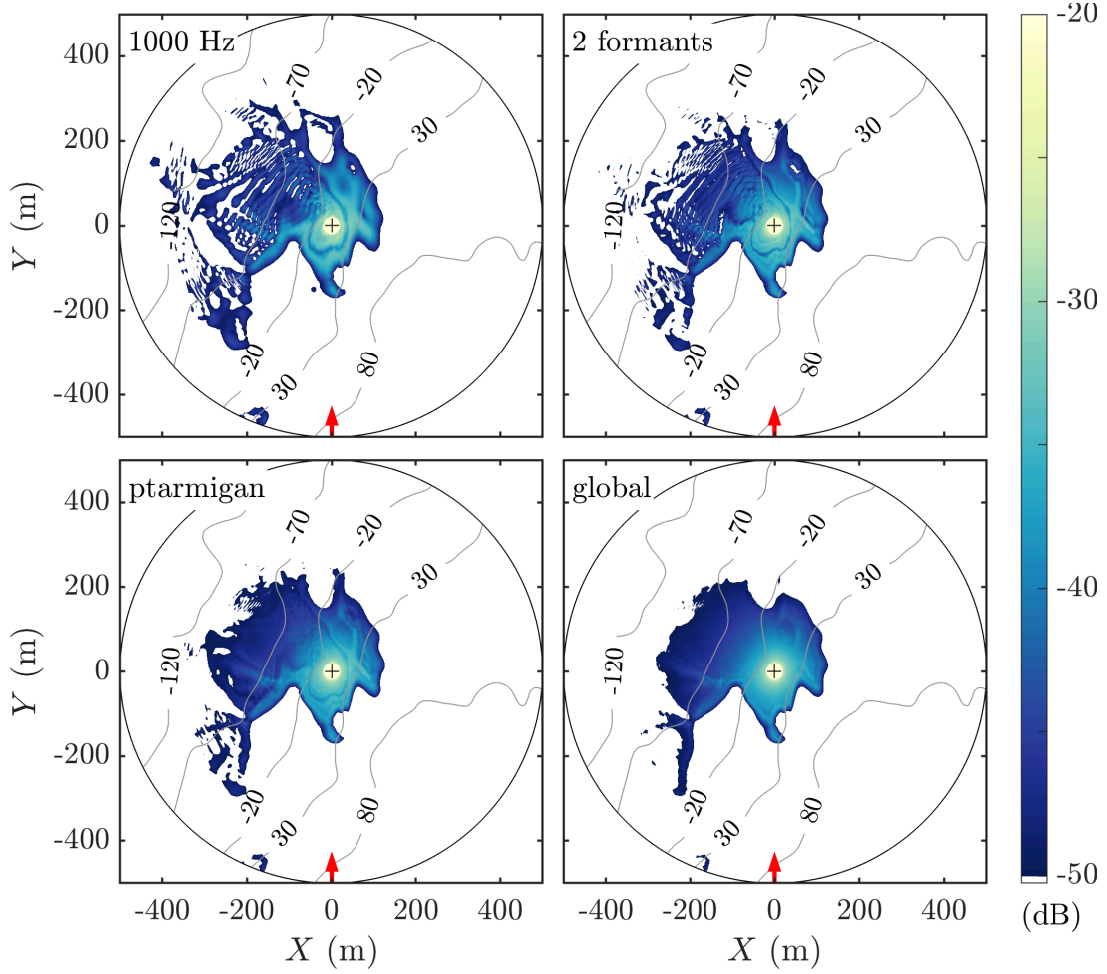
Figure 3.9 – PL map for various source spectra: 1000 Hz pure tone, 2 formants of the ptarmigan (1100 Hz and 2200 Hz), ptarmigan spectrum, and broadband unweighted spectrum (global). Settings are: $z_S = 10$ m, $z_R = 1$ m, $f = 1000$ Hz, $u_* = 0.3$ m/s, $\theta_* = 0$ K, snow cover($e = 0.15$ m, $R_s = 20$ kPa.s.m^{-2}, $\Omega = 0.6$, and $q^2 = 1/\Omega$).

the frequency of 1000 Hz in order to limit the computing time.

3.3.4 Adjusting the source and receiver heights for the ground positions of the birds

The choice of source and receiver heights on the ground is delicate insofar as the geometric shadow zones are very present on uneven topography. The line of sight of the emitter is particularly sensitive to its height relative to the topography. In addition, no spatial averaging of pressure is performed around the receivers to compute the PL. This implies that the levels are sensitive to small differences in receiver height. Fig. 3.10 shows a comparison of the AS computed for different source and receiver heights near the ground. We consider a reference height at 1 m and a representative ptarmigan height at 0.3 m. It is observed that the AS is reduced when the height of the receivers is 0.3 m instead of 1 m. Moreover, the source height plays an important role in the near shadow zones.

Indeed, these are clearly enlarged if the source height is set to 0.3 m instead of 1 m. We see that the AS is sensitive to source and receiver positions close to the ground. It is therefore necessary to make an informed choice about the source and receiver heights for our application in order to achieve spatial consistency between the particularities of the propagation code and the biology of the considered species.
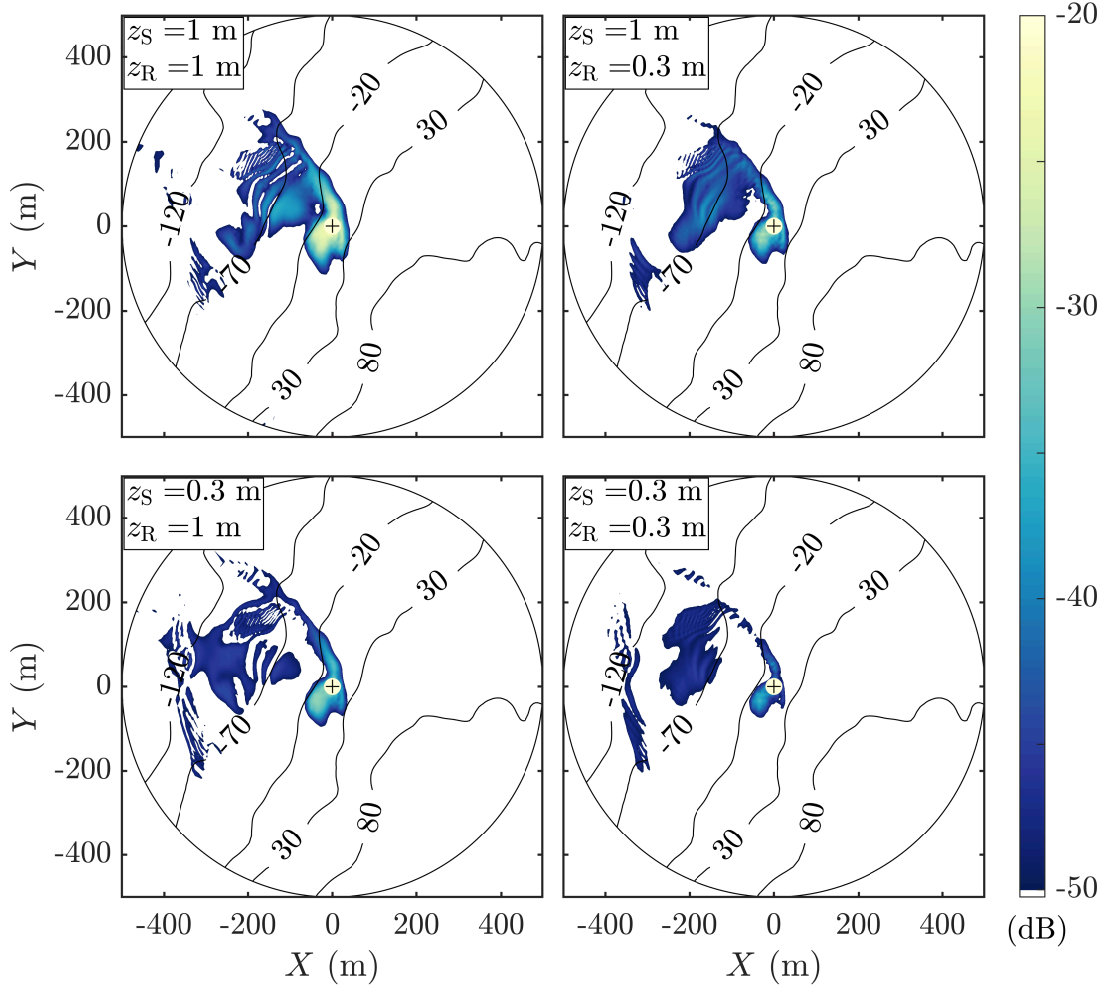
Figure 3.10 − PL map for various source and receiver heights near the ground. Same settings as in Fig. 3.9 except for z_S and z_R.

There are several reasons for choosing one or the other of the heights z_S and z_R. First, the receivers are usually fixed at a reference height, 1 m or 2 m (at human height), to simplify the comparison with other studies of noise propagation in the environment. However, our application being different and concerning sources likely to vary in height, this point is not retained. From a computational standpoint, the discretization of the topography to 5 m may be coarse compared to the small differences in bird positions. In addition, birds often post on high spots during dawn choruses. However, the accuracy of the GPS data is in the order of ± 3 m, so it is not possible to infer the precise position of the birds with respect to fine irregularities in the topography. Finally, we observed in test computations that the initial Gaussian solution for the WAPE computation can cause

numerical problems if the source height z_S is much smaller than the wavelength λ. We therefore do not fix z_S below 0.3 m given the ptarmigan spectrum and its main frequency around 1000 Hz (wavelength around 0.34 m).

For the sake of consistency, we have fixed $z_S = z_R = 0.3$ m in our ground communication applications (see Chap. 5), and the source height has been modified where necessary to simulate the songs in flight.

3.4   Limits and approximations of the WAPE method

Several approximations limit the range of application of the PE method in some cases. Only the progressive wave is calculated in the preferred direction of propagation. The energy potentially reflected backwards by reflections on walls is therefore neglected by the formulation. This can lead to errors when a sound source propagates towards a section of the topography whose angle with the previous one is positive (upward slope). The noise levels calculated in front of this slope may therefore be underestimated by the model. However, Blairon (2002) has shown (Tab 3.1) the part of the diffracted energy that is not considered in the computation by successive domains. It remains limited to less than 1 % in the case of a rising slope with an angle $a = 40°$ between two domains and a frequency of 500 Hz. Moreover it decreases for smaller angles and when the frequency increases. The solution obtained by this rotating domain method is therefore acceptable above a slope for angles less than 40 degrees and frequencies greater than a few hundred Hertz.

The model propagates the waves in 2 dimensions, and therefore neglects the 3D effects. During propagation in a real configuration, a microphone could record echoes due to the presence of cliffs or outcropping rocks that lead to additional reflections. Besides, it has been previously shown that 3D diffraction could lead to modify the shadow zone limit and sound levels behind a hill (Khodr *et al.*, 2020; Ochi & Swearingen, 2022). Here, these echoes and 3D diffraction are not be taken into account, only reflections on the ground in the computation plane.

Another cause of 3D effects is the convection of the propagation medium. In mountainous areas, the movement of the air is highly related to topography in the ASL (Fernando *et al.*, 2019). The model only takes into account a horizontal wind speed profile, projected in the computation plane. The vertical wind speed is therefore neglected, as well as the transverse component, and the same wind profile is considered for the whole study area. A transverse wind is likely to bring back to the receivers part of the energy of the source. The integration of 3D convection effects require a code such as 3D PE or ray tracing for example, which have not been implemented in this study. The 3D PE method requires more computational resources than the WAPE, and the ray tracing does not take into account the diffraction by the corners. These solutions were therefore not retained.

In addition, these 3D effects are closely related to the directionality of the source. In

our case the source is considered omnidirectional because we do not have precise information on the directionality of the song in ptarmigan. The approximation by a source point seems reasonable given the far-field calculation necessary for the estimation of the active space. Nevertheless, it is possible to take into account the effect of directionality in a WAPE calculation when defining the sound pressure field starter. These adjustments were not considered in the following.

Atmospheric turbulence is not taken into account in our implementation of the WAPE method while it could modify the dispersion of the acoustic energy and have a smoothing effect on the interference patterns. In addition, they can also induce an energy contribution in the shadow zones. Their processing is possible with the WAPE method by using Fourier modes and performing ensemble-averaging of pressure fields for several turbulent fields (Chevret *et al.*, 1996; Blanc-Benon *et al.*, 2002). This option has not been considered here for two reasons. On the one hand, these iterative calculations make the estimation of noise levels very demanding in terms of computation time. Indeed, it is necessary to multiply the number of calculations by an order of 10 or 20 to converge. On the other hand, the characteristic lengths of turbulence are difficult to measure or estimate in a mountainous environment. In addition (and we will see later Chap. 5) the occurrences of weather conditions with positive sensible heat flux are very minor in the habitat considered above the snow. Vertical convection due to ground heating, which is the source of much of the turbulence in the outdoor environment, remains very limited in our case.

We observe the appearance of a roughness on the snow cover in Flaine during its progressive melting in late spring. This roughness forms ripples by the daily melting, which are accentuated by the dust that accumulates in the depressions and accelerates this melting. However, this roughness is not taken into account in our propagation code. It has been shown that the effect of the ground roughness can be described through an effective admittance in simulations, as long as the sound wavelength is significantly larger than the mean height and spacing of the roughness (Attenborough & Waters-Fuller, 2000; Attenborough, 1992). However, the order of magnitude of the ripple width (dip to dip) is 30 to 50 cm. This must be compared to the wavelengths related to the ptarmigan formants, that is 30 and 15 cm (for 1100 and 2200 Hz). Given the similarity of the lengths, the description by effective admittance is not adapted to our case. It would be interesting to consider a new method to take into account this ripples along with a finer resolution of the topography (Faure, 2014). Nevertheless, as this ripples appears only late in the breeding season, after territory fixation and mating, we will neglect them thereafter.

N×2D Rotating WAPE ———————————————————————— **Summary**

• The propagation models currently used in bioacoustics studies are essentially based on a semi-empirical approach such as the one proposed by Henwood & Fabrick (1979), and the SPreAD-GIS package for example (Reed *et al.*, 2012). These apply a simplified calculation of the pressure levels obtained after propagation by considering a sum of attenuations related to the various physical effects. In contrast, our code adopts an explicit resolution of the propagation of acoustic waves based on the wave equation. It considers in the same formulation the ground effects and the atmospheric effects, and thus includes their interaction for the pressure computation. Note that this has been done in the past using the Fast Field Program (FFP) method, but for a study on flat terrain (Larom *et al.*, 1997). By developing the N×2D rotating WAPE method, we now generalize the computation to 3D and uneven terrain applications. Moreover it is possible to take into account the heterogeneity of the ground type. Finally, as the code computes the complex pressure, modulus and phase information are available to determine the Green's function between a source point and a receiver point. This can then be convolved to any source signal to obtain the propagated time signal.

• The input data required for the code can be fixed by default, or determined from field measurements. Thus, it is possible to take into account a digital elevation model, wind and temperature profiles, and ground impedance. For the estimation of the active and detection spaces, the parameters of background noise, source level and detection threshold can be modified later, after the PL computation.

• This deterministic computation method can thus be used for many study cases in terrestrial bioacoustics for open and semi-open habitats. It is therefore interesting to conduct parametric studies according to environmental conditions or animal behavior. This code is used in the rest of this thesis to numerically simulate the active spaces of rock ptarmigan. This provides a tool to study a communication network in a controlled way as presented in Chap. 5, which is a difficult challenge when using simple field measurements. Another perspective is the computation of the detection space. We see in Chap. 6 that a reciprocal computation from a receiver point is possible, and that the estimation of the detection space of a recorder opens an opportunity to improve passive acoustic survey methods.

• Prior to these applications, in chapter 4, we examine the validity of this code in the context of an alpine habitat, thanks to on on-site measurements.

Influence of meteorological conditions and topography on the active space of mountain birds

Abstract

The active space is a central bioacoustic concept to understand communication networks and animal behavior. Propagation of biological acoustic signals has often been studied in homogeneous environments using an idealized circular active space representation. Few studies have assessed the variations of the active space due to environment heterogeneities and transmitter position. To study these variations for mountain birds like the rock ptarmigan, we developed a sound propagation model based on the parabolic equation method that accounts for the topography, the ground effects, and the meteorological conditions. The comparison of numerical simulations with measurements performed during an experimental campaign in the French Alps confirms the capacity of the model to accurately predict sound levels. We then use this model to show how mountain conditions affect surface and shape of active spaces, with topography being the most significant factor. Our data reveals that singing during display flights is a good strategy to adopt for a transmitter to expand its active space in such an environment. Overall, our study brings new perspectives to investigate the spatio-temporal dynamics of communication networks.

The content of this chapter has been published and the article is available in open access in the Journal of the Acoustical Society of America (Guibard *et al.*, 2022).

Contents

4.1 Introduction

In acoustic communication systems, the transmission of sound through the environment is a major source of signal degradation, caused by attenuation, absorption and reflections. In bioacoustics and more particularly in the analysis of communication networks (Reichert *et al.*, 2021), one of the biggest challenges is the modeling of acoustic propagation to study the impact of the transmission channel on information exchange (Forrest, 1994).

Long-distance acoustic communication is used by many species of birds. Moreover, outdoor sound propagation is ruled by the influence of the habitat and environmental parameters (Embleton, 1996; Dabelsteen *et al.*, 1993). To study communication in birds, the bioacoustic notion of active space (AS) was introduced by Marten & Marler (1977) as being the "effective distance" of a signal, the distance from the source over which signal amplitude remains above the detection threshold of potential listeners. This definition was later extended to the "effective space" by McGregor and Dabelsteen, to describe communication networks (McGregor & Dabelsteen, 1996; McGregor, 2005). Considering an acoustic signal, the associated AS is determined by four factors: (1) amplitude of the signal at the source; (2) the rate at which signal energy attenuates by transmission through the environment; (3) amplitude of ambient noise in the environment; and (4) masked auditory threshold of receivers since the signal is embedded in a background noise (Brenowitz, 1982b).

To the authors' knowledge, previous studies on long-distance acoustic communication have mostly considered homogeneous propagation environments, and the maximum

distance at which a transmitter could be heard as a criterion of AS. They were usually focused on the estimation of global excess attenuation (EA), signal-to-noise ratio (SNR), tail-to-signal ratio (TSR), or blur ratio (BR) over some frequency bands depending on the distance to a transmitter, to estimate a radius of audibility. Many of these earlier works are based on field propagation experiments and playback experiments (Lohr *et al.*, 2003; Darden *et al.*, 2008; Loning *et al.*, 2021). The effect of transmitter and receiver heights on propagation has been investigated as well as environmental parameters (temperature, wind, humidity) (Dabelsteen *et al.*, 1993; Holland *et al.*, 1998; Mathevon *et al.*, 2005; Jensen *et al.*, 2008). The impact of diurnal variations was investigated through a similar methodology (Henwood & Fabrick, 1979; Dabelsteen & Mathevon, 2002), as was the constraint of the rain on communication (Lengagne & Slater, 2002). Although these previous works provide answers about the effects of the environment on communication, they are not as suitable as a dedicated model could be.

Modeling acoustic propagation is crucial for studying animal communication, since recordings and playback experiments require a lot of time and material, and can hardly be carried out on large areas. Therefore, propagation models have been proposed in the literature to estimate ASs of communication and information degradation. Most of them are based on simplified semi-empirical approaches as proposed by Henwood & Fabrick (1979) and Parris (2002), or more recently Raynor *et al.* (2017), in which the engineering-based SPreAD-GIS model was used. These models are computationally efficient, but they do not account for all the physics, and their outputs are often restricted to global indicators. Wave-based models, i.e. models that describe the wave propagation in time or in frequency domain, are more accurate, but due to their computational cost, they have been barely used in bioacoustics. A rare example is the study of Larom *et al.* (1997) that used a Fast Field Program (FFP) model to show that the ASs of African savanna elephants depend on wind and temperature profiles.

Actually, topography and meteorological conditions depend on the habitat. These conditions obviously have a strong effect on AS, especially in mountainous areas, which represent a noticeably heterogeneous environment as stated by Reiners & Driese (2001). Moreover, it is essential to take these parameters into account to understand the impact of habitat on communication in both space and time. The study of these effects could provide interesting clues about the features of signal propagation in communication networks and their potential adaptation to the species' habitat (Mathevon *et al.*, 2008; Wiley & Richards, 1978).

To highlight the impact of the habitat on AS, we chose to work on an iconic species of high mountains: the rock ptarmigan (*Lagopus muta*). It is a species living in the northern hemisphere, in arctic or alpine habitat. Considering the period of intense vocal activity that is the breeding season in spring between April and June, environmental conditions and species behavior are known (Bossert, 1977; Watson, 1972). During this period, male

ptarmigans sing at dawn to defend their territory and indicate their location. Their songs are often made during flights, which is the main territorial demonstration (Johnsgard, 2008; MacDonald, 1970).

At altitudes above 1800 m, alpine mountain ranges are usually still largely covered with snow. The propagation distance of this type of vocalization is about a few hundred meters. The vocalizing birds may be placed either on the ground or at a height of a several dozen meters. The characteristic frequencies of ptarmigan vocalizations are in the kilohertz range. These particularities imply a large-scale problem, which must be taken up by a computational method fast enough to be applicable.

The study of ASs is carried out using numerical simulations, allowing us to test a large number of propagation conditions. With this approach, we are trying to answer two questions: How do environmental constraints affect the vocal communication of mountain birds? And how do ptarmigans adapt and optimize their communication behavior?

The objectives of this study are (1) to develop a method to estimate ASs of a bird in heterogeneous environment; (2) to compare numerical results with *in situ* measurements to evaluate the model for the intended application; (3) to assess the influence of topography, temperature and wind on the AS; and (4) to study the potential benefit of singing during display flight for the rock ptarmigan.

This article is organized as follows. Section 4.2 describes the model used in this study and the different assumptions made. The on-site measurement campaign and the comparisons between measurements and model estimations are detailed in Sec. 4.3. Then Sec. 4.4 presents an application of the previously tested model on a typical mountain site where a population of ptarmigan lives. Here, we investigate the variability of the AS in such a context. Concluding remarks are given in Sec. 4.5.

4.2 Active space and propagation model

4.2.1 Definition of the active space

Determination of AS is based on the propagation loss (PL), defined as the sound pressure level (SPL) relative to source level (SL). It represents the attenuation of the signal energy during propagation over an area. Following Brenowitz (1982b), to set the PL threshold that defines the limits of the AS, several parameters must be considered: the source level (SL), the auditory threshold in masking noise, and the background noise.

Active spaces are investigated for the rock ptarmigan (*Lagopus muta helvetica*), which is considered as a model of mountain bird. The rock ptarmigan uses acoustic vocalizations to communicate, especially during display flights, when it significantly increases its altitude up to 75 m from the ground (Johnsgard, 2008). Its vocalizations are sequences of pulse trains, with a pulse rate of 21 ± 3 ms, and an energy distributed in the fre-

quency range of 900–3700 Hz (Marin-Cudraz *et al.*, 2019), the maximum amplitude being around 1000 Hz. Neither the directivity nor the nearfield sound pressure level (SPL, in dB relative to 20 µPa) of ptarmigan vocalizations is yet well characterized. For simplicity, in the present study, the directivity is assumed to be omnidirectional. To estimate the SPL, we assume that it is comparable to that of the corncrake (*Crex crex*), which is a non-passerine bird of similar size that also produces a broadcast call with pulsed signal. Its SL has been measured in the range of 80–101 dBSPL (Ręk & Osiejuk, 2011; Aubin & Mathevon, 2020). Therefore, the SL of rock ptarmigan vocalizations, defined as the SPL at 1 m from the source, is set at a median value of 90 dBSPL in the present study. [Note that SL measurements of ptarmigan had not yet been carried out at this early stage of the thesis.]

In this species, there is not much competition for vocal communication or selection pressure for encoding information, because the density of birds is low with a relatively simple communication network (two to three neighbors maximum for each bird). In addition, they are the only birds that vocalize in a relatively low frequency range in this environment compared to other birds, and the latter are also scarce at this altitude. Thus, the situation is one of energetic masking due to background noise alone. For the purpose of this study, we arbitrarily set a detection threshold of 10 dB, regarded as the SNR required for comfortable communication in the sense of Dooling & Leek (2018). This value is sufficient to achieve the objectives of this article, but for a detailed study concerning the effect of ambient noise, it will be necessary to perform an estimation of the detection threshold of ptarmigan in noise. Background noise levels around 30 dBSPL or less were measured during clear daytime on the site considered in Sec. 4.4, where a population of ptarmigan lives. This value is kept in this chapter. From the last two elements, it is assumed that above a pressure level of 40 dBSPL, a receiver is able to detect and decode the information and is thus within the limits of the AS. Below this 40 dBSPL threshold, the probability of detection decreases, and a receiver is no longer considered to be in the active space. In other words, considering a SL = 90 dBSPL and a detection threshold of 40 dBSPL, the AS is the area such that the propagation loss from the source does not exceed -50 dB. This PL threshold set to -50 dB could be corrected when the ptarmigan SL and detection threshold in noise are measured and could be different if considering other bird species.

4.2.2 Propagation model

In the context of atmospheric propagation, the choice of a model is a compromise between the computational cost, the complexity of environmental effects to be considered, and the type of results desired. For application to bird communication in mountains, the model must be able to compute vocalizations after propagation at long distances and

high frequencies and include a stratified atmosphere with irregular topography.

The propagation model used here is based on the wide-angle parabolic equation (WAPE), described e.g. by Salomons (2001), which is an efficient computational method for long-range sound propagation within the ASL. It is obtained from the Helmholtz equation, by considering forward propagating waves only. An N×2D (two dimensions) approach is followed: the problem is not considered on a full three-dimensional (3D) geometry but on vertical slices, as illustrated in Fig. 4.1.
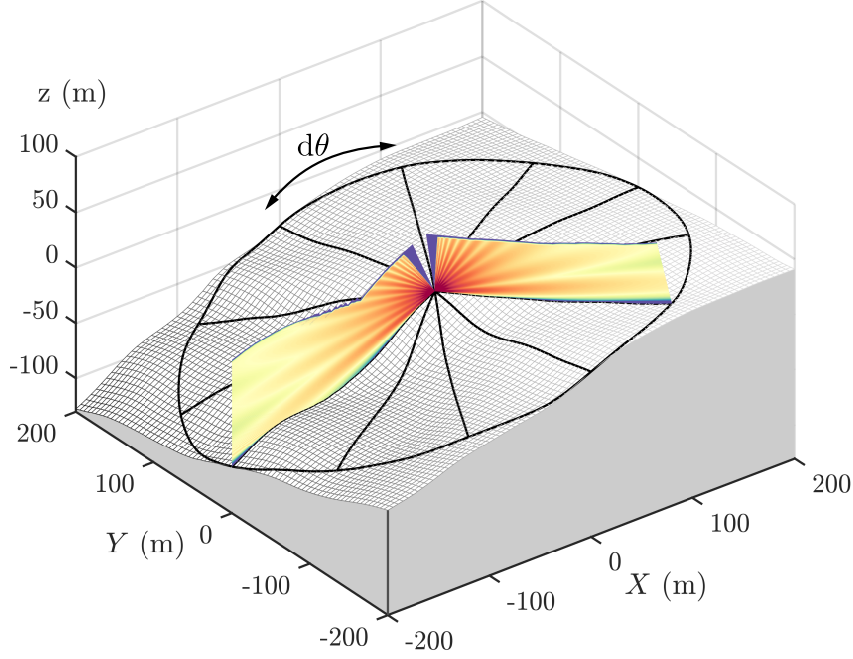
Figure 4.1 − Principle of the N×2D approach. Propagation loss PL plotted on 2D domains.

On each slice (x, z), the 2D axisymmetric WAPE is solved. The source is located at (x_s, z_s). Denoting by p_{PE} the pressure and introducing $q_{PE} = \sqrt{R}\, p_{PE}$, with $R = \sqrt{(x - x_s)^2 + (z - z_s)^2}$ the distance from the source, the WAPE equation can be written as,

$$\left\{ \frac{\partial}{\partial x} - ik_0 \mathcal{Q} \right\} q_{PE}(x, z) = 0, \tag{4.1}$$

where $k_0 = \omega/c_0$ is the reference wave number, c_0 is the reference sound speed chosen at the ground level, and $\omega = 2\pi f$, with f the frequency. The pseudo-differential operator $\mathcal{Q}$ is written as a Padé (1,1) approximation,

$$\mathcal{Q} = \frac{1 + \eta_1 \mathcal{L}}{1 + \eta_2 \mathcal{L}}, \tag{4.2}$$

with $\eta_1 = 3/4$ and $\eta_2 = 1/4$. The operator $\mathcal{L}$ is given by:

$$\mathcal{L} = \epsilon_{\text{eff}} + \frac{1}{k_0^2} \frac{\partial^2}{\partial_z^2}, \tag{4.3}$$

with $\epsilon_{\text{eff}} = c_0^2/c_{\text{eff}}^2 - 1$. The parameter c_{eff} is the effective sound speed, which accounts for temperature and wind variations. Its calculation is detailed in Sec. 4.3.1. The effective sound speed approach is a reasonable approximation in the lower ASL for low wind speed. Note that Ostashev *et al.* (2020) recently proposed a parabolic equation (PE) formulation that improves the inclusion of wind profiles. In addition, full 3D PE formulations (Khodr *et al.*, 2020) have been already proposed in the literature for atmospheric sound propagation. Although they describe 3D propagation effects, they induce a large increase in the computational cost. For application to bioacoustics, a 2D approach was deemed to be sufficient.
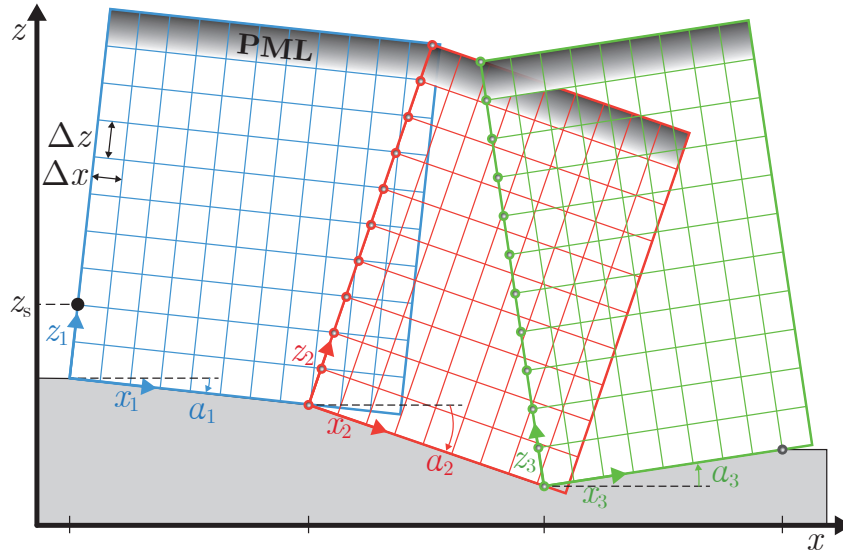
Figure 4.2 – Sketch of the rotated PE method: grids in the (x_n, z_n) planes, with fixed tangent grid spacing Δx and orthogonal grid spacing Δz. A Perfectly Matched Layer (PML) is set at the top of each domain to ensure a reflectionless condition.

The topography is described by a succession of flat domains of fixed length, defined by an angle a with respect to the horizontal x axis, as suggested by Blairon *et al.* (2002) and Lihoreau *et al.* (2006). In each domain, the (x_n, z_n) coordinate system is rotated to keep the x_n axis parallel to the ground, as shown in Fig. 4.2. The length of each domain is set to 5 m, which is sufficient to properly fit most real topographies. For the first domain, the calculation is initialized by the wide-angle starter, which accounts for the source image weighted with a complex reflection coefficient, derived in Salomons (2001). This reproduces a monochromatic omnidirectional point source in the acoustic far field ($k_0 R \gg 1$). Note that the propagation model does not allow a precise prediction of the near field. The amplitude of the source is set so that the SPL in free field at 1 m is equal to SL. For the other domains, the starter is obtained by interpolating the pressure field of the previous domains.

In each domain, the problem is discretized using the Crank–Nicolson marching scheme in the propagating direction x_n and second-order finite-differences in the transverse direction z_n. The discretization steps are fixed to $\Delta x = \Delta z = \lambda/10$, with the wavelength

$\lambda = c_0/f$. The WAPE method ensures accurate results within a propagation angle of $40°$ above and below the x direction (Ostashev *et al.*, 1997). This implies that the angle between two consecutive domains must remain between these limits.

At the top of each domain, a Perfectly Matched Layer (PML), based on the work of Collino (1997), is implemented as a non-reflecting boundary condition. At the ground, a surface admittance boundary condition is applied. This assumes that the ground is locally reacting. Because of its small flow resistivity, snow is, however, usually considered as an extended-reacting ground. To mimic the effect of extended reaction at long distance, the normalized surface admittance β_s is evaluated from that of an extended-reacting hard-backed porous layer of constant effective thickness e (Li *et al.*, 1998b) at grazing incidence (angle of incidence equal to $\pi/2$). This yields:

$$\beta_s = \beta_c \frac{\sqrt{n^2 - 1}}{n} \tanh(-\mathrm{i}k_0 e \sqrt{n^2 - 1}), \tag{4.4}$$

with $n = k_c/k_0$ and β_c and k_c the characteristic admittance and the wavenumber of the snow layer. The acoustic properties of the snow (β_c, k_c) are defined according to the phenomenological model proposed by Bérengier *et al.* (1997),

$$\beta_c = \frac{\Omega}{q} \left[1 - \frac{\omega_1}{\mathrm{i}\omega}\right]^{-1/2} \left[1 - \frac{\omega_2}{\mathrm{i}\omega}\right]^{-1/2} \left[1 - \frac{\omega_3}{\mathrm{i}\omega}\right]^{1/2} \tag{4.5}$$

$$k_c = k_0 q \left[1 - \frac{\omega_1}{\mathrm{i}\omega}\right]^{1/2} \left[1 - \frac{\omega_2}{\mathrm{i}\omega}\right]^{-1/2} \left[1 - \frac{\omega_3}{\mathrm{i}\omega}\right]^{1/2}, \tag{4.6}$$

with $\omega_1 = R_s\Omega/(\rho_0 q^2)$, $\omega_2 = R_s/(\rho_0\mathrm{Pr})$, $\omega_3 = \gamma R_s/(\rho_0\mathrm{Pr})$, ρ_0 the air density at the ground, $\gamma = 1.4$ the specific heat ratio, and $\mathrm{Pr} = 0.7$ the Prandtl number. This model uses three parameters: the airflow resistivity of the porous structure R_s, the porosity of air-filled connected pores Ω, and the tortuosity q^2. Note that other impedance models can also be used such as the relaxation model (Wilson, 1993) or the slit-pore model (Attenborough & van Renterghem, 2021).

The PE method is a frequency-domain approach. For broadband signals, the calculation must be repeated for all frequencies of interest. In addition, it can be noted that the time signal after propagation can be determined from a broadband spectrum using an inverse Fourier transform. Several remarks can be made with regard to the limits of application of this model in mountainous areas. First, back-scattering is neglected, and thereby the possible echoes are not considered. Second, three-dimensional effects relative to wind and topography are neglected by the N×2D approach.

4.2.3   3D pressure calculation and active space

The determination of the AS from the PE solution is detailed. Since the PE solution does not account for atmospheric absorption, a correction is then applied to the pressure,

$$p(f, x, z) = p_{\mathrm{PE}}(f, x, z) \ \exp[-\alpha(f)R(x, z)], \tag{4.7}$$

where the atmospheric absorption factor α is based on the ISO9613-1 standard (ISO, 1993). From this, the SPL $L_p(x, z)$ is calculated with:

$$L_p(x, z) = 10 \log_{10} \left(\frac{|p(x, z)|^2}{p_{\mathrm{ref}}^2} \right), \tag{4.8}$$

with $p_{\mathrm{ref}} = 2 \times 10^{-5}$ Pa. Finally, the propagation loss is determined in each slice with $\mathrm{PL}(x, z) = L_p(x, z) - \mathrm{SL}$.

To obtain the acoustic field on the whole 3D geometry, PE calculations are repeated for each vertical slice by varying the angle θ around the z-axis, with a step $\mathrm{d}\theta$, as shown in Fig. 4.1. The 2D topography profiles are obtained by interpolation of the 3D topography. We further consider an angular step of $\mathrm{d}\theta = 2°$. A map of the PL around the source at a given height above the ground, chosen as 1 m, is deduced as illustrated in Fig. 4.3.
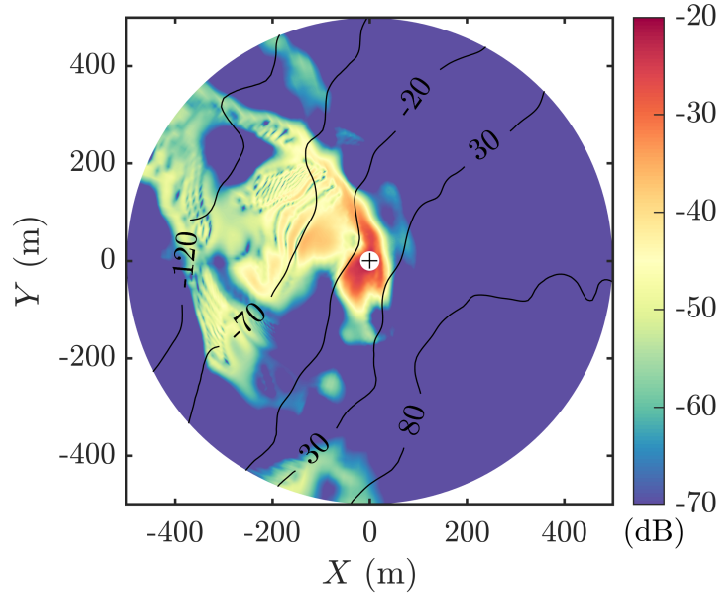
Figure 4.3 – Example map of the propagation loss (PL) at 1 m height for a frequency of 1000 Hz. Contour lines are drawn every 50 m in thin line. Conditions: topography 1 in Fig. 4.13, homogeneous atmosphere, and $z_{\mathrm{s}} = 1$ m.

The area of the AS, denoted by A, is then computed from the PL map. For that, the PL is determined at receivers placed at 1 m height from the ground, with a step $\mathrm{d}x = 1$ m. The receivers for which the propagation loss is above the threshold are identified. The AS area is thus the sum of elementary surface areas $x \, \mathrm{d}x \, \mathrm{d}\theta$. Because of the limitation in

the propagation angle associated with the PE method, receivers placed under this angle near the source are not considered in the PE calculation, and are assumed to belong to the AS.

4.3 Comparison of WAPE model with on-site measurements

To validate the prediction capacity of the model, measurements were performed in a mountain environment. This section details how the environmental parameters were measured, and presents the comparisons between the results of the acoustical field measurements and the corresponding numerical simulations.

4.3.1 Experiments

Measurement site

The measurements were conducted in October 2020 in the French Alps on the site of Col du Lac Blanc in the Massif des Grandes Rousses [45.13 N, 6.11 E, 2720 m above sea level (a.s.l.)]. This site was chosen because two research institutes [Centre d'Études de la Neige (CEN) and the Institut National de Recherche pour l'Agriculture, l'Alimentation et l'Environnement (INRAE)] maintain two complementary Automated Weather Stations (AWSs) at this location. This allows us to obtain the meteorological data during the experiments. Despite the site not being dedicated to the monitoring of rock ptarmigan population, it is typical of mountain environments where the rock ptarmigan lives.

The site is a mountain pass that presents a hill shape of 15 m height in its longitudinal section (north-south direction), called hereafter the "hill". The wind is naturally channeled in this north-south direction. The weather instrumentation is installed at the top of the small hill. A Digital Elevation Model (DEM) of the site with bare ground was determined by Guyomarc'h *et al.* (2019), using a laser scanning technique (Fig. 4.4). The DEM has an horizontal resolution of 1 m and a vertical resolution of 0.1 m. The chosen propagation zone is such that echoes are absent or manageable in post-processing thanks to the short duration of the source signal.

Three transects, depicted in Fig. 4.4, were chosen on either side of the mountain pass. Transects t1 and t2 are directed to the south, uphill and downhill, respectively. Transect t3 is reversed with respect to t1, and thus faces north downhill. Several measurements were carried out on these different transects in various weather conditions. Among the available data, results for four representative configurations, denoted by A, B, C and D, are presented in this paper, and summarized in Tab. 4.1. The configurations A and B are for similar meteorological conditions but for two different topographies, transects t1 and
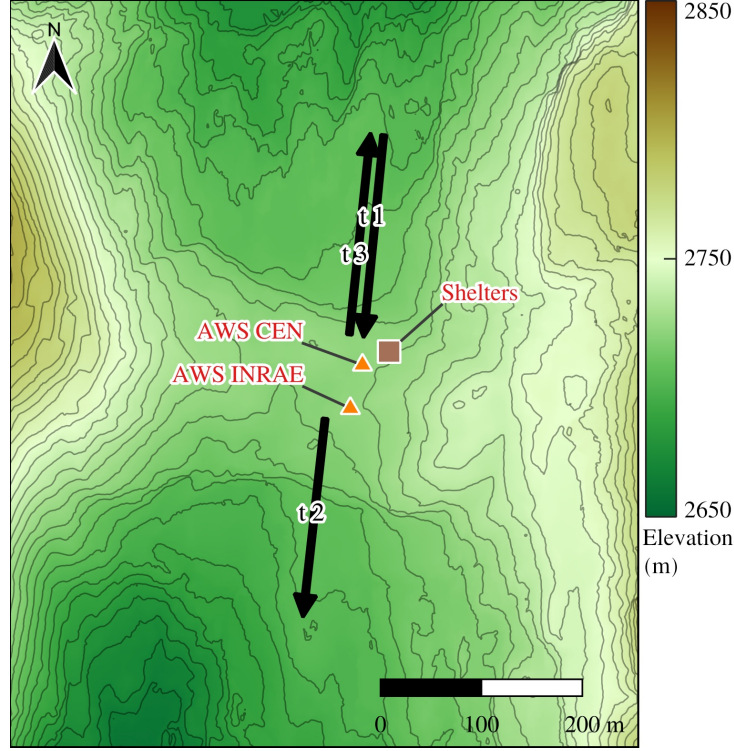
Figure 4.4 – Map of the measurement field at Col du Lac Blanc (massif des Grandes-Rousses, France), with 5 m contour lines. Propagation transects (t1, t2, t3) and their direction are drawn with black arrows. Automated Weather Stations (AWS CEN) and (AWS INRAE) are depicted by triangles.

Table 4.1 – Detailed measurement configurations (A, B, C, D) with the transect concerned (t1, t2, t3), the propagation condition, and the gradient of effective sound speed near the ground $\Delta c_{\mathrm{eff}}(\mathrm{m.s}^{-1})$.

Config.	Transect	Condition	Δc_{eff} $(\mathrm{m.s}^{-1})$
A	t1	strong downward	4.3
B	t2	strong downward	6.4
C	t3	slight upward	-0.3
D	t3	moderate upward	-1.8

t2. The configurations C and D are both for the same topography, transect t3, but with different meteorological conditions.

Meteorological data

Atmospheric conditions during the propagation experiments, were available from two AWSs, named "AWS CEN" and "AWS INRAE", which are located close to the acoustic source (Figs. 4.5 and 4.6). Temperature and humidity were measured by five sensors (HMP155A, Vaisala, Vantaa, Finland) mounted on the AWS CEN at heights of 0.8, 1.3, 3.2, 5, and 7 m above the snow surface. Wind direction and velocity were obtained from the AWS INRAE. The wind vane (W200P-01, Vector Instruments, Saint Asaph, UK) was mounted at a height of 11.08 m, and five anemometers (A100LK, Vector Instruments) were
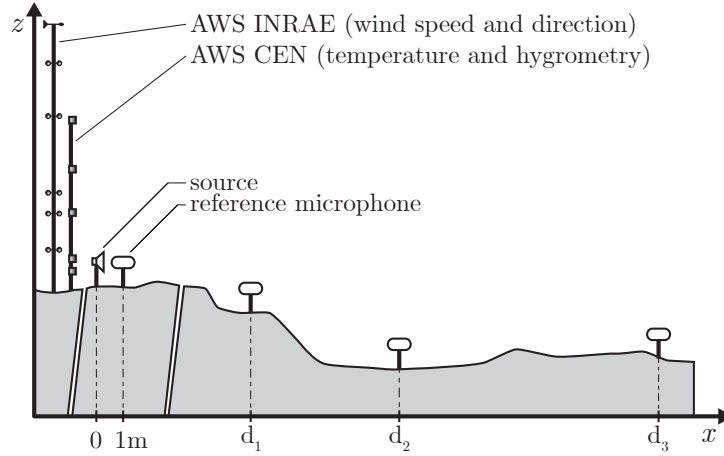
Figure 4.5 − Sketch of the measurement setup used on a transect. Source-microphone distances are: $d_1 = 50$ m, $d_2 = 100$ m, and $d_3 = 200$ m.
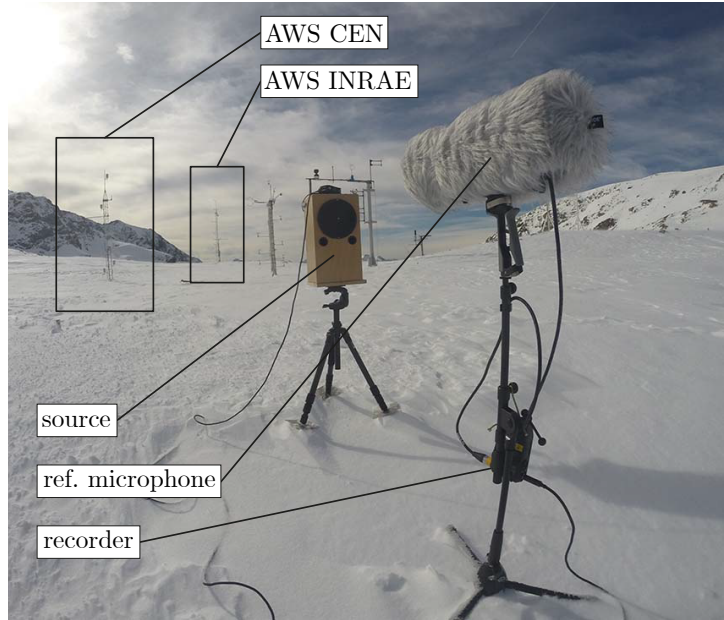
Figure 4.6 − Picture of the measurement setup used for acoustic propagation: source, reference microphone and automated weather stations AWS CEN and AWS INRAE (set up of transect 3).

mounted at heights of 1.76, 3.25, 4.1, 7.25, and 9.42 m. The atmospheric pressure P_0 was around 750 hPa during the two days of measurement. Data discussed in the following paragraphs are the average temperature, and the average and standard deviation of the wind velocity, both integrated over periods of 10 min, and measured during the sound propagation experiments.

The raw data of temperature and wind speed measured with the two AWS are plotted with markers in Fig. 4.7 as functions of the height above the snow cover z_g. The wind speed profile presents a significant acceleration in the first 4 m above the ground. This is due to a localized Venturi effect induced by the hill in the middle of the pass.

Meteorological data were extrapolated by means of an iterative fitting procedure based on the Monin & Obukhov (1954) similarity theory (MOST). One of the assumptions of

114

MOST is that the ground is flat and homogeneous, which is clearly not the case here. However, with no better description of the atmosphere, MOST is used as it provides representative wind and temperature profiles encountered in the ASL. Wind and temperature profiles are given by:

$$U_{\text{fit}}(z_g) = \frac{u_*}{\kappa} \left[\ln\left(\frac{z_g + z_0}{z_0}\right) - \psi_w\left(\frac{z_g}{L_{\text{MO}}}\right) \right], \tag{4.9}$$

$$T_{\text{fit}}(z_g) = T_0 + \frac{\theta_*}{\kappa} \left[\ln\left(\frac{z_g + z_0}{z_0}\right) - \psi_t\left(\frac{z_g}{L_{\text{MO}}}\right) \right] + \alpha_0 z_g, \tag{4.10}$$

with $\kappa = 0.41$ the von Kármán constant, u_* the friction velocity, T_0 the air temperature near the ground, θ_* the temperature scale, L_{MO} the Monin–Obukhov length, $\alpha_0 = -0.01$ K.m^{-1} the dry adiabatic lapse rate, and z_0 the roughness length of the ground surface set to 0.01 m. The functions ψ_w and ψ_t are derived from the Businger–Dyer relations, as detailed in Salomons (2001). To get rid of the local acceleration discussed above, the fitting procedure takes into account the five measured temperature values but only the three wind speeds at the upper positions. The fitted profiles are plotted in Fig. 4.7 according to the four configurations. The fit with the measurements appears appropriate for the temperature $T(z_g)$. For the wind speed $U(z_g)$, noticeable discrepancies are observed: they are related to the local acceleration near the ground. The corresponding MOST parameters obtained are listed in Tab. 4.2.

Typical values for u_* are indicated in Ostashev & Wilson (2016): 0.1, 0.3, and 0.6 m/s correspond to a light, moderate and strong wind condition respectively. Therefore, all four configurations are under light or moderate wind conditions as u_* is between 0.13 and 0.19 m/s. The angle ψ between measured wind direction and each transect remains relatively constant during each measurement period as shown by the values of its standard deviation σ_ψ, given in Tab. 4.2.

Table 4.2 − Parameters of the fitted temperature and wind profiles for (A, B, C, D) configurations: Monin-Obukhov length L_{MO}, air temperature near the ground T_0, temperature scale θ_*, friction velocity u_*, angle between wind direction and the transect $\psi \pm \sigma_\psi$ (σ as the standard deviation), and relative humidity RH.

Config.	L_{MO} (m)	T_0 (°C)	θ_* (K)	u_* (m.s^{-1})	$\psi \pm \sigma_\psi$ (°)	RH (%)
A	8.4	-6.57	0.09	0.10	22 ± 12	98
B	6.4	-4.04	0.13	0.11	6 ± 13	40
C	9	-0.76	0.01	0.03	314 ± 30	90
D	205	-1.06	0.00	0.09	20 ± 19	96

The extrapolated profiles of wind speed and temperature are used to determine the

effective sound speed. It is defined as the sum of the sound speed and the horizontal
component of the wind speed in the direction of propagation:

$$c_{\text{eff}}(z_{\text{g}}) = \sqrt{\gamma R_{\text{GP}} T_{\text{fit}}(z_g)} + U_{\text{fit}}(z_g) \cos \psi, \tag{4.11}$$

with ψ the angle between the mean wind direction and the transect direction from the
source, and $R_{\text{GP}} = 287$ J.kg^{-1}.K^{-1} the specific gas constant for dry air. The effective
sound speed profiles are plotted in Fig. 4.7. It appears that configurations A and B
present a predominant effect of the temperature gradient, while configurations D show
a predominant effect of the wind speed gradient. Finally, configuration C is a nearly
homogeneous case.
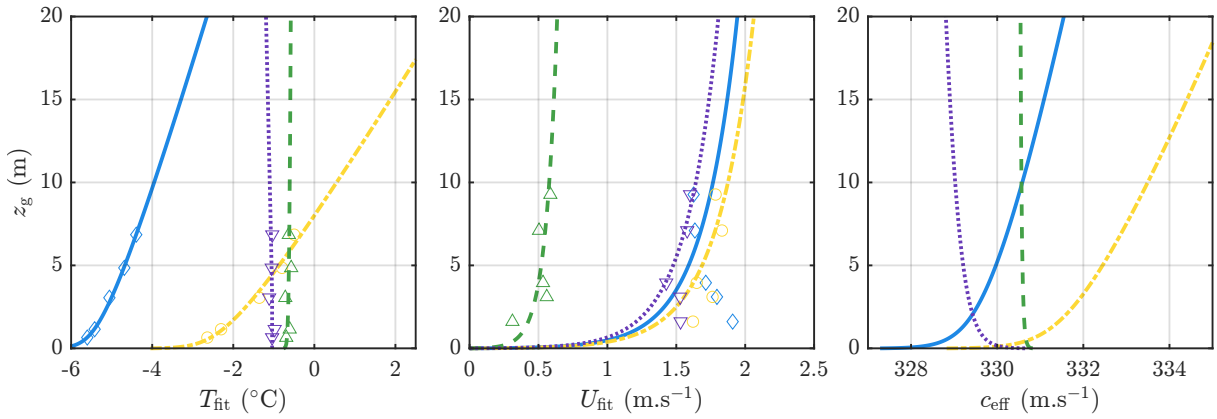
Figure 4.7 – Fitted temperature T_{fit} and wind U_{fit} profiles, and c_{eff} from the 4 measurements carried out:
A (——), B (—·—·—), C (— — —), D (········). Corresponding measured data $U(z_{\text{g}})$, $T(z_{\text{g}})$ are depicted
by markers: A ($\diamond$), B ($\circ$), C ($\triangle$), D ($\triangledown$).

To characterize the sound speed gradient near the ground, the parameter $\Delta c_{\text{eff}} = c_{\text{eff}}(z_g = 20 \text{ m}) - c_0$ is introduced. It determines the atmospheric refraction: upward for
$\Delta c_{\text{eff}} < 0$, downward for $\Delta c_{\text{eff}} > 0$ or homogeneous for $\Delta c_{\text{eff}} \approx 0$. Downward condition is
induced by a temperature inversion and/or a downwind condition. It leads to refraction
of sound waves toward the ground, and to an increase in sound level at the vicinity of the
ground. Conversely, upward conditions occurs for negative temperature gradients and/or
for headwind. Now sound waves are refracted toward the sky, inducing shadow zones at
long range. The values of Δc_{eff} for the four configurations are given in Tab. 4.1: A and B
correspond to strong downward refracting conditions, and C and D correspond to slight
and moderate upward refracting conditions, respectively.

In addition to average meteorological profiles, two other conditions are defined considering each configuration to investigate the influence of meteorological variability on sound
propagation. For that, it is assumed that the temperature evolves more slowly with time
than the wind speed and, as a consequence, that the meteorological variability is only
due to that of the wind speed. Two other set of temperature and wind speed profiles are
thus obtained using MOST from $T(z)$ and from the reduced values $U(z) - 2\sigma_U(z)$ and

increased values $U(z) + 2\sigma_U(z)$, where $\sigma_U(z)$ is the standard deviation of the wind speed given by the AWS. They are then used to determine the corresponding effective sound speed profiles.

Finally, RH (the relative humidity) (Tab. 4.2), used to calculate the atmospheric absorption factor α, is determined as the time average of the values measured by the five humidity sensors.

Acoustic propagation measurements

The sound source was a high power portable loudspeaker, designed and built for the experiment. Its directivity was measured in an anechoic chamber. Microphones used were four Beyerdynamic (Heilbronn, Germany) MM1 audio microphones covered with a RØDE (Sydney, Australia) Blimp MkII windscreen (Fig. 4.6). Four H6 audio recorders (Zoom, San Jose, CA) were used. The source and the microphones were placed at 1 m above the snow cover surface. A reference microphone was first calibrated at 94 dBSPL at the frequency of 1000 Hz with a Class 1 calibrator (Cirrus CR517). A relative calibration of the microphone with their recorder was performed at the same time for all microphones in front of the source with a 50 dBSPL, 1000 Hz signal. The reference microphone was then positioned at 1 m from the loudspeaker as seen in Fig 4.5, and the three other microphones were moved 50, 100 and 200 m away from the source using a GPS receiver. The relative distances were measured using a laser telemeter with an accuracy on the order of ± 1 m.

The source signal was a 1 second chirp made of a sinus sweep with frequency increasing exponentially from 100 to 3600 Hz. To ensure that the level measured at 200 m from the source is significantly higher than the background noise, the SL is set to 110 dBSPL at 1 m from the loudspeaker, which is higher than the estimated level of the vocalizations of the ptarmigan. This allows for relevant comparisons with our model in the following. The chirp was repeated every 10 s during 10 min. This led to a series of 60 measured waveforms per 10 min period that can be related to corresponding meteorological data since the weather stations provide the mean wind and temperature profiles averaged over 10 min periods.

The background noise SPL was always at least 10 dB lower than the levels measured at the microphones over the frequency band $[300 - 3000 \text{ Hz}]$. It is therefore reasonable to consider that the background noise had no influence on the measured pressure levels.

Snow impedance

Several techniques can be used to measure ground impedance (NORDTEST, 1999; ANSI, 2010; Moore *et al.*, 1991; Albert, 2001; Datt *et al.*, 2016; Guillaume *et al.*, 2015). In the present study the snow impedance was measured *in situ* using the method proposed by
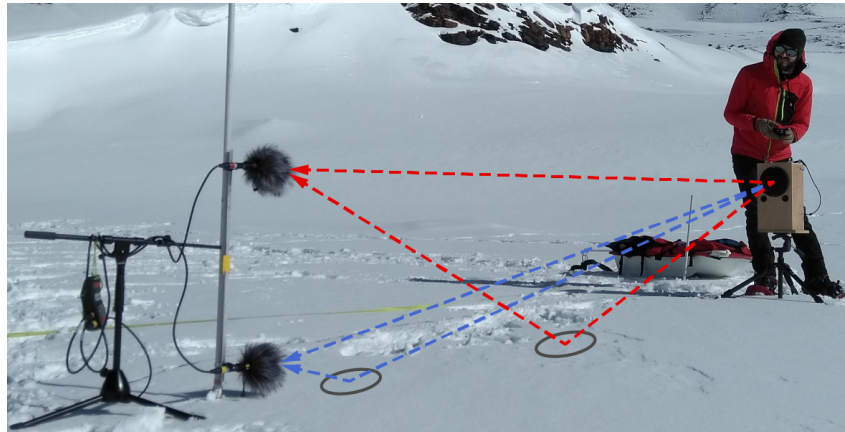
Figure 4.8 – Picture of the measurement setup for snow impedance. The different wave path are represented by dotted lines. The loudspeaker is on the right and two microphones on the left.

Guillaume *et al.* (2015), which is suited for grazing angles and has been shown to provide reliable data for long-range propagation computation (Dragna *et al.*, 2014a). These measurements were made just before or after the propagation experiments, at a single location representative of the snow cover along the propagation path. The method consists in carrying out a propagation experiment between a source placed at 0.7 m from the ground and two microphones 4 m apart and placed at 0.1 and 0.7 m from the ground, as shown in Fig. 4.8. The source signal was a 1 s exponential frequency chirp from 100 to 3000 Hz, repeated 50 times at 4 s intervals. From the measured signals, the transfer function between the two microphones is calculated, and then compared to the analytical transfer function whose impedance parameters are adjusted to adapt to the measured data. Assuming that the ground is flat and the snow cover is uniform with a constant thickness, the transfer function can be calculated analytically using the Weyl–Van der Pol equation (see, e.g. (Attenborough & van Renterghem, 2021)). Note that extended reaction has been taken into account in the analytical formulation. The four parameters of the surface admittance model (see Eq. (4)-(6)) are then manually fitted to match the analytical transfer function with the measured one. The corresponding analytical and measured transfer functions are represented in Fig. 4.9 for the 2 days concerned. Tab. 4.3 indicates the resulting parameters of the impedance model. These results are consistent with those in Moore *et al.* (1991), Albert (2001) and Datt *et al.* (2016) for the same type of snow (powder snow).

It should be noted that the method is based on assumptions that are not always valid for this type of *in situ* measurement of snow impedance. First, in the model, the snow depth is assumed to be constant, while in reality it is not uniform over the entire propagation domain. However, specific tests carried out during the present measurement campaign in different parts of the domain showed that the surface impedance in the frequency band of interest was only slightly modified by the thickness of the snow layer, as soon as it exceeds 15 cm. This thickness value is comparable to the computed values
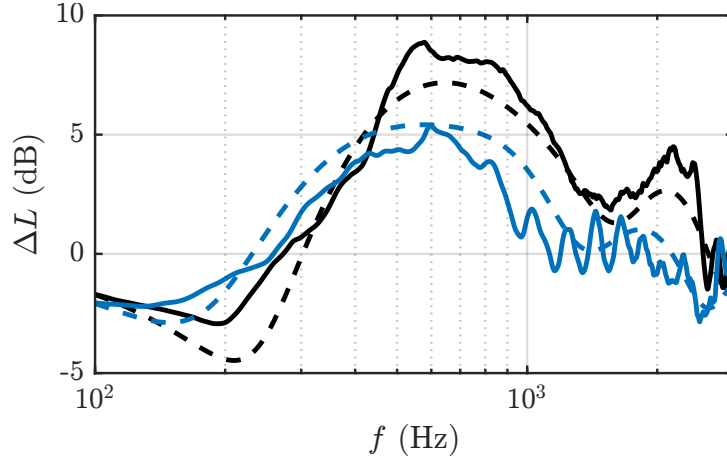
Figure 4.9 – Transfer functions ΔL for the determination of snow impedance in configurations A and B (———) and configurations C and D (———): measure (solid) and analytical fit (dashed).

of the effective thickness e. Second, the ground is assumed to be flat. This assumption is reasonable for the measurements presented here because the layer of fresh snow present on the site had a homogeneous structure and a smooth surface, but this may not always be the case, especially when the wind generates a wavy surface and when the surface layer is made of frozen wet snow. This could induce a rough surface, which is outside the scope of this method.

Table 4.3 – Impedance parameters obtained during the two days of measurement on the site of Lac du Col Blanc: the effective thickness e, the airflow resistivity R_s, the porosity Ω, and the tortuosity q^2. The corresponding configurations (A, B, C, D) are indicated.

Config.	e (m)	R_s (Pa.s.m^{-2})	Ω	q^2
A, B	0.13	10000	0.6	1.3
C, D	0.2	7000	0.6	1.3

4.3.2 Comparisons with the propagation model

Description

To fairly compare the results of the propagation model to the measurements, the measured data were processed as explained in Sec. 4.3.1 for the meteorological conditions and Sec. 4.3.1 for the snow impedance, to obtain input data of the numerical simulations. The four configurations (A, B, C, D) are described in Tab. 4.1, with corresponding MOST parameters in Tab. 4.2 and snow impedance parameters in Tab. 4.3. The position of each transect is shown in Fig. 4.4, and their corresponding topographic profiles are shown in Fig. 4.10. As the DEM of the site is given for a bare ground, it does not account for the snow cover. The DEM is then corrected by adding a snow cover estimated at 20 cm on the entire site, based on our observations.

119

In addition, a significant snow accumulation was noticed along the slopes of the hill: the snow cover was measured using a probe in the middle of the slopes, yielding a depth of 1 m on the north slope and of 1.4 m on the south slope. An additional correction is thus applied to the DEM along the hill slopes to account for this accumulation.

With this corrected DEM, the microphones at $x = 100$ m for configuration B and at $x = 50$ m for configurations C and D are in geometrical shadow zones, where the source has no direct view of the receivers assuming a homogeneous atmosphere with no refraction effect. Low SPLs are expected in these areas.

Computations are performed for the effective sound speed profile obtained from the average wind speed and temperature (T, U) reported in Sec. 4.3.1, as well as for the profiles accounting for wind speed variability $(T, U \pm 2\sigma_U)$.

Results

The 2D maps of the SPL relative to the free-field solution $\Delta L = \text{PL} + 20 \log_{10}(R)$ computed for $f = 1000$ Hz are plotted in Fig. 4.10 for the four configurations. The quantity ΔL represents the deviation from SPL in free field due to atmospheric refraction and diffraction effects. The 2D maps show a strong decrease in the acoustic pressure at the vicinity of the ground caused by the snow cover. The pressure level is equivalent to or lower than that in free field in the first centimeters above the ground due to its unevenness. In all four cases, ΔL has a variability of ± 10 dB for the majority of microphone positions except in the shadow zones. Shadow zones are noticed at $x = 100$ m for configuration B and at $x = 50$ m for configurations C and D. They are visible in Fig. 4.10, where ΔL approaches -10 dB or less (in dark blue).

The influence of the sound speed gradient Δc_{eff} is visible on the distribution of the acoustic field across the domain. In particular, in case B, the acoustic energy is directed to the ground beyond 150 m due to downward conditions. This refraction reduces the size of the shadow zone compared to the homogeneous case. Conversely, case D shows an upward refraction due to upwind condition.
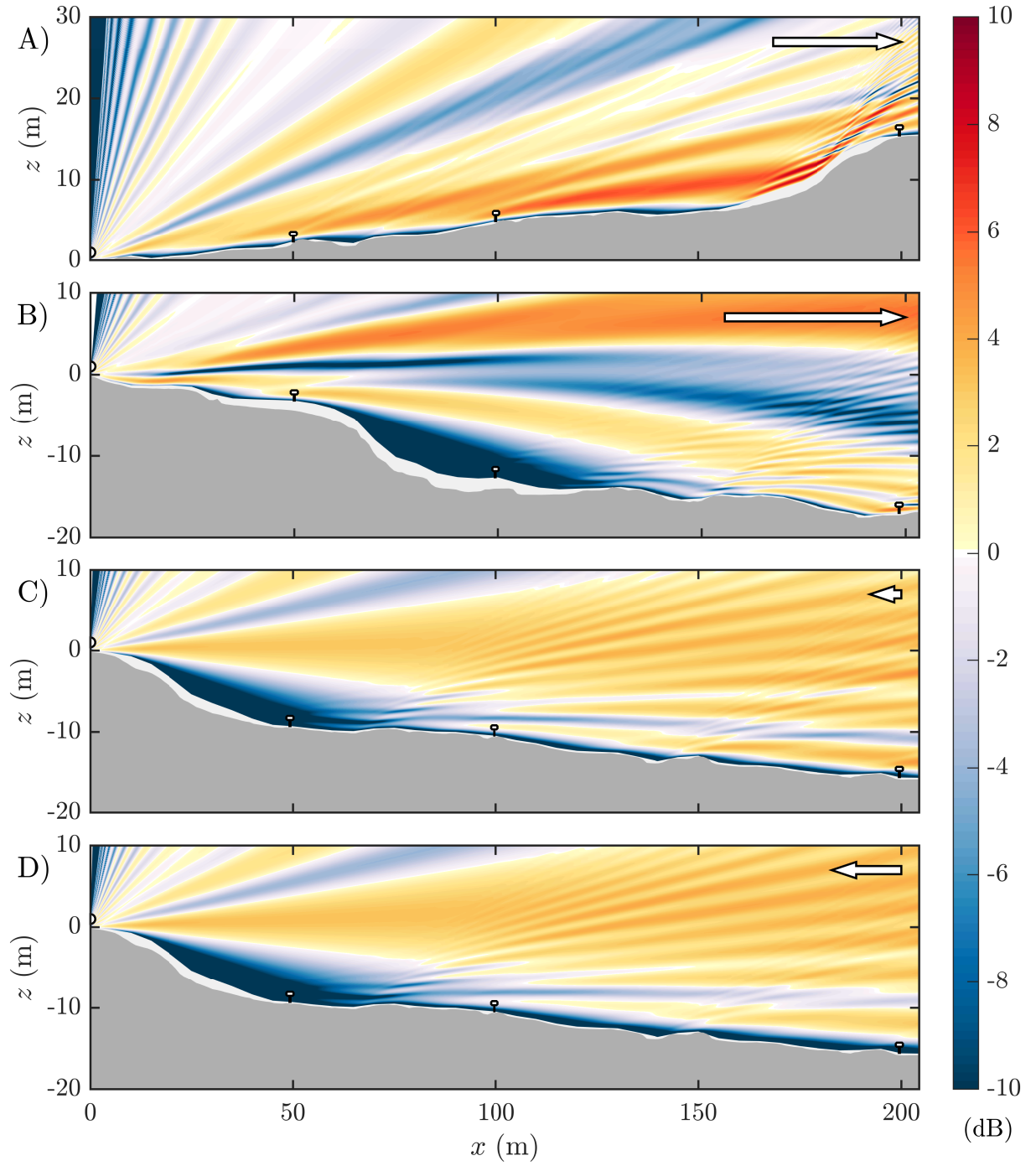
Figure 4.10 – Pressure levels relative to free field ΔL simulated at 1000 Hz, for 4 configurations (A B C D): actual terrain profile relative to source position $x_S = 0$, $z_S = 1$ m (gray surface), snow cover depth considered over the bare ground and smoothed every 5 m (white surface), microphone positions $x = 50, 100, 200$ m (dots), and arrows of length proportional to Δc_{eff}. Scale $z/x = 1/2$.

The results of the simulations are compared to the measurements using the relative SPL ΔL_p defined as $\Delta L_p(x, z) = L_p(x, z) - L_p(x_{\text{ref}}, z_{\text{ref}})$, with the reference point located at 1 m in front of the source. The pressure obtained with the WAPE method is not accurate in the nearfield. Then the reference level $L_p(x_{\text{ref}}, z_{\text{ref}})$ is obtained from the analytical solution of the Weyl-Van der Pol equation over a flat ground of the same impedance (Attenborough & van Renterghem, 2021). To match experimental conditions, the reflected wave amplitude is corrected by the source directivity of the loudspeaker.

For each configuration, the frequency spectrum at the receivers is deduced from computations carried out on 200 frequencies logarithmically distributed over the $200 - 3000$ Hz band. The relative pressure levels ΔL_p obtained at each receiver ($x = 50,\ 100,\ 200$ m) are plotted in Fig. 4.11, along with the 60 measured spectra. In this figure we can see for all configurations, that the SPL computed by the propagation model closely matches the measurements both in downward and upward condition over the frequency band $200 - 3000$ Hz, except for some pronounced interferences. Moreover, the variability in the frequency of the destructive interference pattern is fairly well reproduced by taking into account the variability of the wind speed. The discrepancy on the absolute position of the interference patterns can be explained by the piecewise linear approximation of the topography used in the propagation model, by the uncertainty on the wind speed along the propagation path, and by the uncertainty on the position of microphones. Note that small uncertainties influence the spectra calculated by the model, and in particular above a certain frequency whose wavelength approaches the size of the error on the geometry. This could also be due to the single value approximation of the snow impedance boundary condition. The level estimations in shadow zone for configuration B at 100 m show a relative agreement in variability due to wind speed. For configurations C and D in upward conditions, the measured pressure levels are also in good agreement with the propagation model in the geometrical shadow zone of transect 3 at 50 m and in the shadow zone at 200 m induced by upward refraction.

An additional comparison between measurements and numerical results is shown in Fig. 4.12. It presents the boxplots of ΔL_p integrated on the 1000 Hz octave band for the 60 measured waveforms at the three microphones and for the four cases. The 1 kHz octave band is chosen because the amplitude of ptarmigan vocalization is maximal in this band. For readability, the boxplots are centered on the median of the measured data. The four configurations are sorted according to the sound speed gradient Δc_{eff}. The boxplots indicate the variability of the measured SPL. The SPL calculated with the propagation model for the profiles of average temperature and wind speed (T, U) and for the profiles accounting for wind speed variability $(T, U \pm 2\sigma_U)$ are also plotted in Fig. 4.12.

The correspondence between the median of the measured SPL and the SPL predicted with the propagation model for the average meteorological conditions is first analyzed. For all conditions the model provides an accurate estimation of the levels measured in
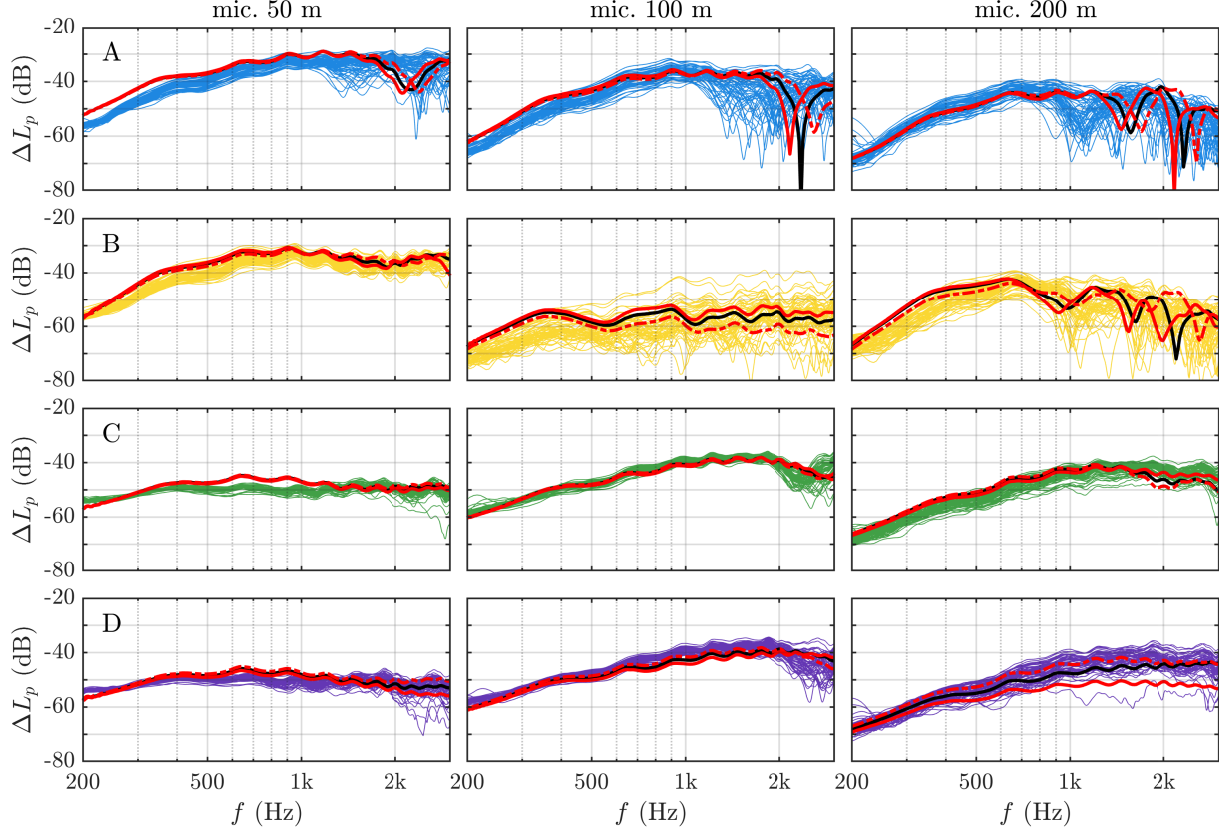
Figure 4.11 − ΔL_p determined from the measurements (in thin color line) and simulated for $c_{\text{eff}}(T, U)$ (———), $c_{\text{eff}}(T, U - 2\sigma_U)$ (–·–·–) and $c_{\text{eff}}(T, U + 2\sigma_U)$ (———)). These results are for the four cases (A, B, C, D from top to bottom) and for the three microphone locations ($x = 50, 100, 200$ m from left to right). Same colors as in Fig. 4.7.

the 1000 Hz band for receivers placed at 50, 100, and 200 m. The differences are between −3.1 and +2.9 dB, including estimated levels in geometrical shadow zones (case B at 100 m and C and at 50 m) and also in refraction-induced shadow zone (case D at 200 m). At a distance of 50 m, meteorological effects have little influence and overestimates are more likely due to topography approximation and uncertainty in snowpack depth, which define the line of sight and therefore the geometric shadow areas. The propagation model also allows analysis of the variability of the SPL due to sound speed profiles. For that, the dispersion between the first and third quartiles in the boxplots is compared with the difference in the SPL calculated for the profiles $(T, U - 2\sigma_U)$ and $(T, U + 2\sigma_U)$. A fair agreement is obtained overall. However, in case A the simulated variability is not accurately reproduced at 50 and 100 m. This is due to inaccurate prediction of the destructive interference frequency on the 1000 Hz octave band. In case B, the level variability matches well the measurements, except at 50 m. Cases C and D also show a good agreement for the three microphone positions. This implies in particular that the variability of the measured SPL is partly explained by the variability of the wind speed. However, we only consider the variability of wind speed at the weather station, while pressure levels may depend on local wind speed and direction fluctuations along the
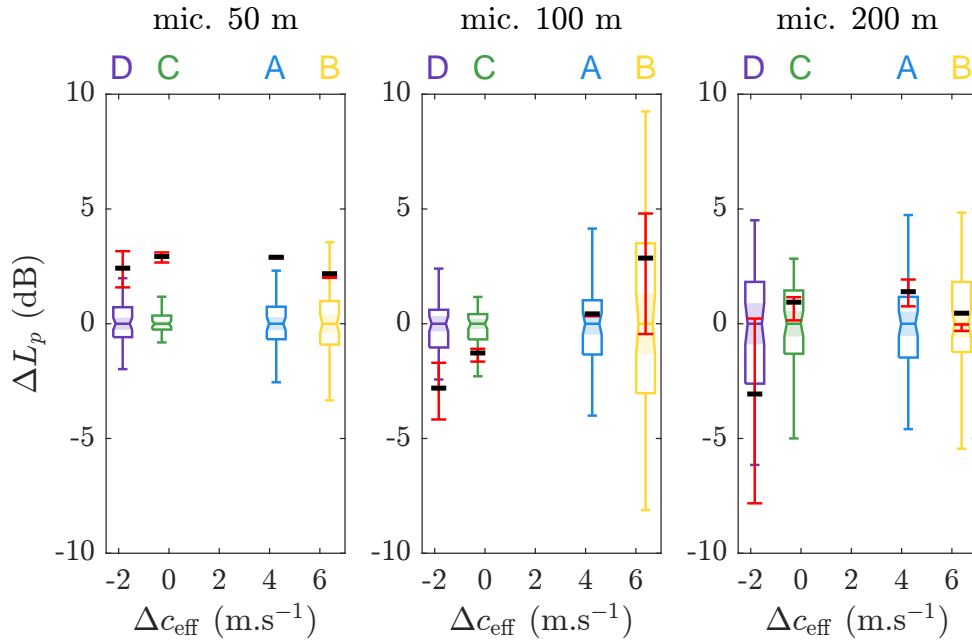
Figure 4.12 – Comparison of ΔL_p of the measurements and simulations on the octave band 1000 Hz (global levels) ploted around the median of the measurements for the four configurations (A, B, C, D) and according to the three microphones distances (50, 100, 200 m). Measurements depicted by boxplots (without outliers), and simulations depicted by linked dashes, with same colors as in Fig. 4.11.

propagation path, as well as local changes in the temperature profile.

In summary, these results show that predictions of SPLs using a wave propagation model are consistent with field measurement. Levels are correctly estimated in shadow zones, whether geometric or headwind induced, allowing the model to be used to study the AS of birds in a mountainous habitat. However, we note that partial knowledge of input parameters and approximations may induce errors in the prediction of levels. We mentioned that the approximation of terrain profiles and snowpack thickness can shift the location of geometric shadows zones. Atmospheric parameters can hardly be characterized over the entire area of interest, and must be extrapolated from weather stations. In addition, the model does not account for rapid temporal nor spatial variations in wind direction, nor for turbulence. The impedance value determined for one location was applied to the entire propagation path because the snow parameters in the chosen measurement site were nearly constant. However, in more complex area the composition of the snowpack, the surface shape, and the presence of rocks may require more complex ground impedance modeling. If more complete and more complex propagation models are possible in the future, it is to the detriment of the computational cost, which is a parameter to be taken into account for parametric studies. The expected gain in terms of accuracy is also not guaranteed if one is not able to characterize the medium in more detail.

4.4 Variability of the active space of communication

The propagation model is now applied to investigate the influence of the topography, the meteorological conditions, and the source altitude on the AS of rock ptarmigans. Here, the source is considered static with a height above the ground defined as the typical flight altitude of the bird.

4.4.1 Description

The study is done for another site in the French Alps, which is chosen because a population of rock ptarmigans lives on this site all year round, especially during the breeding season (Marin-Cudraz *et al.*, 2019; Canonne *et al.*, 2020; Novoa *et al.*, 2011). This site is the Flaine ski resort (45.99N, 6.73E, 2400m a.s.l.), and is referred to as "Flaine" in the remainder of this section. Its topography is presented in Fig. 4.13. DEM data of the bare ground with 5 m resolution were provided by the French National Geographic Institute (IGN: Institut national de l'information géographique et forestière). To avoid any sharp slopes, a low-pass filter has been applied to the topography. This smoothing procedure is reasonable since the actual snow layer naturally fills the depressions in the ground. The acoustic properties of the snow cover are identical in all configurations. They are chosen as: $e = 0.15$ m, $R_s = 20000$ Pa.s.m^{-2}, $\Omega = 0.6$, $q^2 = 1.66$, to be representative of a moderately compacted snow as measured by Datt *et al.* (2016). The meteorological conditions are imposed using wind speed and temperature profiles from MOST (see Sec. 4.3.1), and a wind direction from south to north. The pressure field calculation is done within a 500 m radius around the point source. All the following maps are oriented with north at the top in the present section.
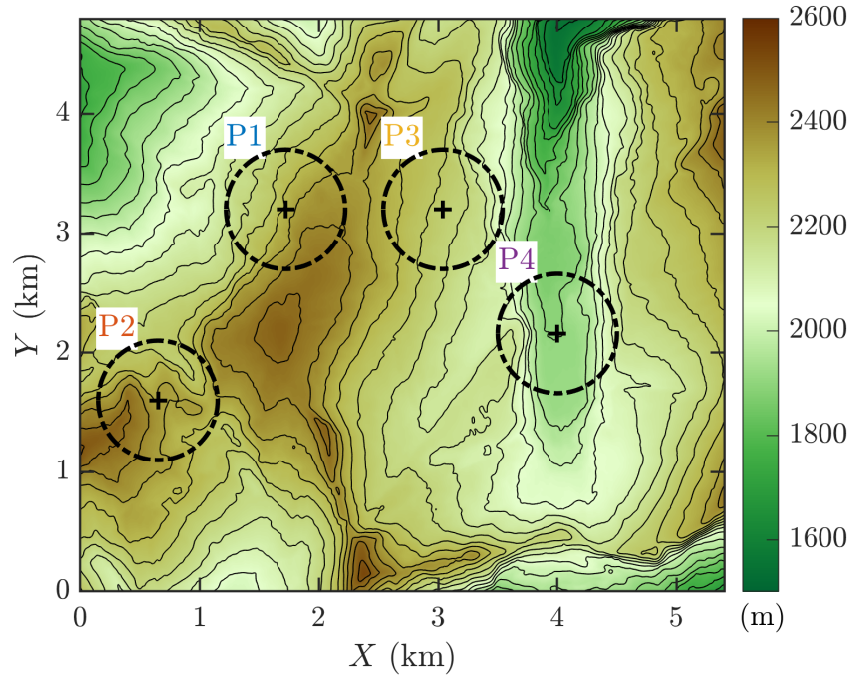
Figure 4.13 − Topography of the Flaine ski resort, X,Y positions of sources (1, 2, 3, 4) marked with crosses and circular computation domains for active space estimation in thick dotted lines. The map is oriented north up, and 50 m contour lines are drawn in thin black lines.

4.4.2 Results

Influence of topography

The ASs are computed for the four positions on the Flaine site presented in Fig. 4.13. These positions illustrate typical situations encountered in mountain environments: terrain with a steep slope (P1), gentle slope (P3), a promontory (P2), and a valley (P4). To isolate topographic effects, nearly homogeneous conditions are considered, with $u_* = 0.05$ m.s^{-1}, and $\theta_* = 0$ K.

Maps of the propagation loss are plotted in Fig. 4.14 for the four positions indicated in Fig. 4.13 on the Flaine site. They show that the shape of the AS depends significantly on the topography. Even in homogeneous atmospheric conditions AS is therefore neither circular nor symmetrical over uneven landforms. In details, for P1, sound propagates preferentially towards the west, down the slope. For P2, the AS has a comparably small area and is essentially limited to the top of the promontory. For P3, the AS is discontinuous: it is made of a disk with a radius of about 200 m centered at the source and of small spots that can be seen at a large distance from the source (up to 500 m). Finally, for P4, the steep slopes of the valley prevent sound from propagating and the AS is restricted to the bottom of the valley. In addition, the striations noticeable on P1 and P4 correspond to interference patterns due to the monochromatic calculation. Such pattern would not be visible in a broadband calculation.
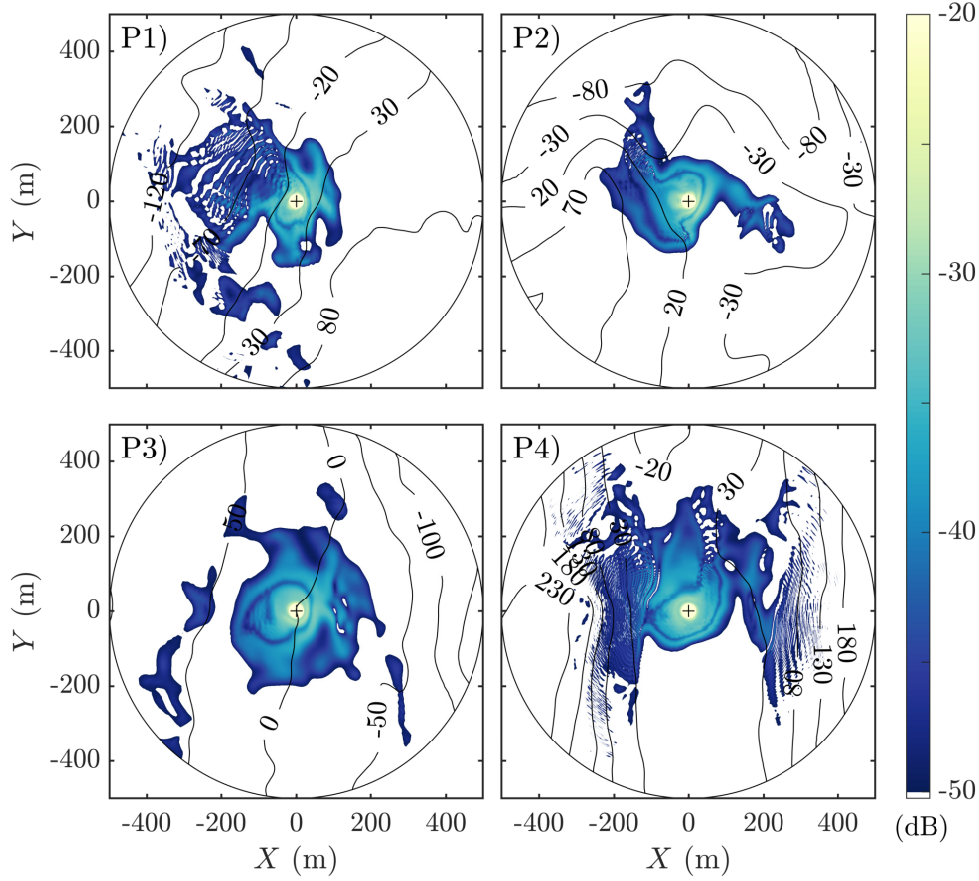
Figure 4.14 – Map of the propagation loss PL for the four positions (shown in Fig. 4.13), at 1 m height, for a 1000 Hz frequency signal, in nearly homogeneous atmospheric condition: $u_* = 0.05$ m.s^{-1}, $\theta^* = 0$ K, $z_S = 10$ m. Contour lines are drawn every 50 m in thin line.

Influence of meteorological conditions

The impact of meteorological conditions on the AS is now investigated. For that, the AS is calculated as a function of the governing parameters for the wind and temperature profiles defined in Sec. 4.3.1. For the wind, the relevant parameter is still the friction velocity u_*. However, for the temperature, the sensible heat flux Q_H is now chosen instead of θ_*, because of its simpler physical interpretation. Indeed, the sensible heat flux represents the transfer of heat to the surface from the overlying air induced by the temperature difference between the ground surface and the atmosphere. It is related to u_* and θ_* by:

$$Q_H = -\theta_* \rho_0 c_p u_*, \qquad (4.12)$$

where c_p is the specific heat at constant pressure. The sensible heat flux depends on solar radiation and cloud cover. Thus, on a clear night we have $Q_H < 0$, which leads to a positive temperature gradient and, hence, a positive sound speed gradient that favors sound propagation at long range. On the contrary, $Q_H > 0$ on a clear day, inducing a negative sound speed gradient that opposes sound propagation.

The AS is first computed for several values of the sensible heat flux Q_H and $u_* =$

Figure 4.15 − Map of the propagation loss PL for different values of Q_H, at 1 m height, for a 1000 Hz frequency signal, and at P1 (shown in figure 4.13). Reference case is b), with values $u_* = 0.3$ m.s^{-1}, $Q_H = 0$ W.m^{-2}, $z_S = 10$ m. Plots a) and c) respectively depict the influence of sensible heat flux from $Q_H = -100$ to 400 W.m^{-2}. All other parameters are the same as the reference case. Contour lines are drawn every 50 m in thin line. The red arrow depicts u_* and the wind direction.

0.3 m.s^{-1}. Corresponding MOST parameters and weather conditions are given in Tab. 4.4. The values chosen for Q_H have been taken from Ostashev & Wilson (2016), and measurement data over snow were provided in Mott et $al.$ (2013). They are assumed to be representative of the snow radiation behavior. Maps of PL for position 1 are shown in Fig. 4.15. Thus, a change from $Q_H = 400$ W.m^{-2}, corresponding to a clear daytime Fig. 4.15(c), to $Q_H = -100$ W.m^{-2} corresponding to a clear nighttime over snow Fig. 4.15(a), induces an increase in the area of 30 %.

Table 4.4 − Atmospheric conditions used in active space calculations, derived from the sensible heat flux: MOST parameters, wind speed 2 m above the ground, and celerity gradient in the wind direction Δc_{eff}^+.

Condition	Q_H (W.m^{-2})	u_* (m.s^{-1})	θ_* (K)	L_{MO} (m)	$U_{(2m)}$ (m.s^{-1})	Δc_{eff}^+ (m.s^{-1})
clear daytime	400	0.3	-1.38	-4.6	1.7	-2.1
daytime	200	0.3	-0.69	-9	1.9	-0.2
mostly cloudy	0	0.3	0	$-\infty$	2.2	3.8
nighttime	-50	0.3	0.17	36.6	2.4	7.8
clear nighttime	-100	0.3	0.36	18.3	2.6	13.1

Calculations of the AS are then performed for several values of u_* and for $Q_H = 0$ W.m^{-2}. The chosen values of u_*, which are: 0.05, 0.3, 0.7 and 1.1 m/s induce wind speed values at 2 m height of $U_{(2m)} = 0.4$, 2.2, 5.2, and 8.2 m/s respectively. These values imply a large scale of wind conditions, from very low to very strong wind, which slightly outstrips the proposed wind scale values of Ostashev & Wilson (2016). The corresponding maps of PL for position 1 are shown in Fig. 4.16. Increasing u_* tends to enlarge the shadow zone upwind and to reduce the AS accordingly. In addition, a modest
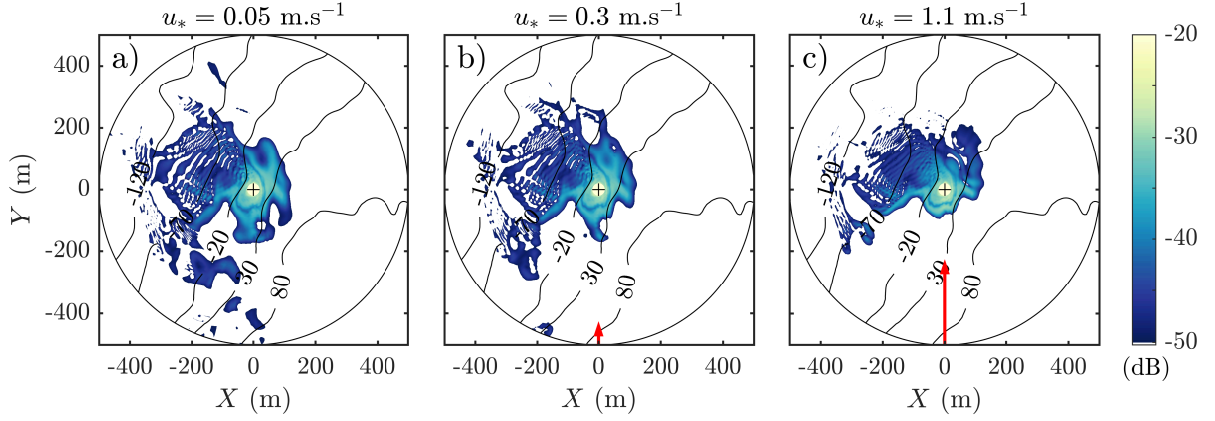
Figure 4.16 – Map of the propagation loss PL for different values of u_*, at 1 m height, for a 1000 Hz frequency signal, and at P1 (shown in figure 4.13). Reference case is b), with $u_* = 0.3$ m.s^{-1}, $Q_H = 0$ W.m^{-2}, $z_S = 10$ m. Plots a) and c) respectively depict the wind influence between $u_* = 0.05$ and 1.1 m.s^{-1}. All other parameters are the same as the reference case. Contour lines are drawn every 50 m in thin line. The red arrow depicts u_* and the wind direction.
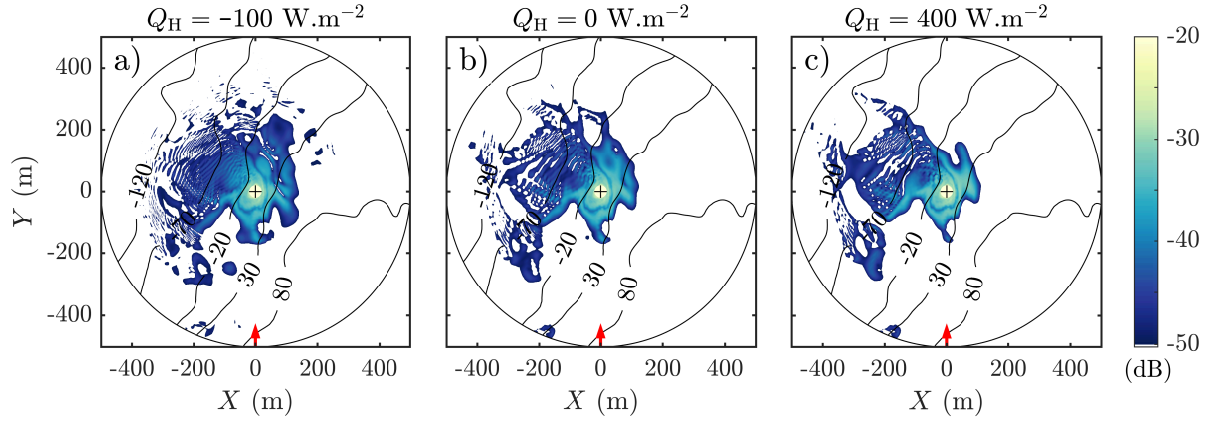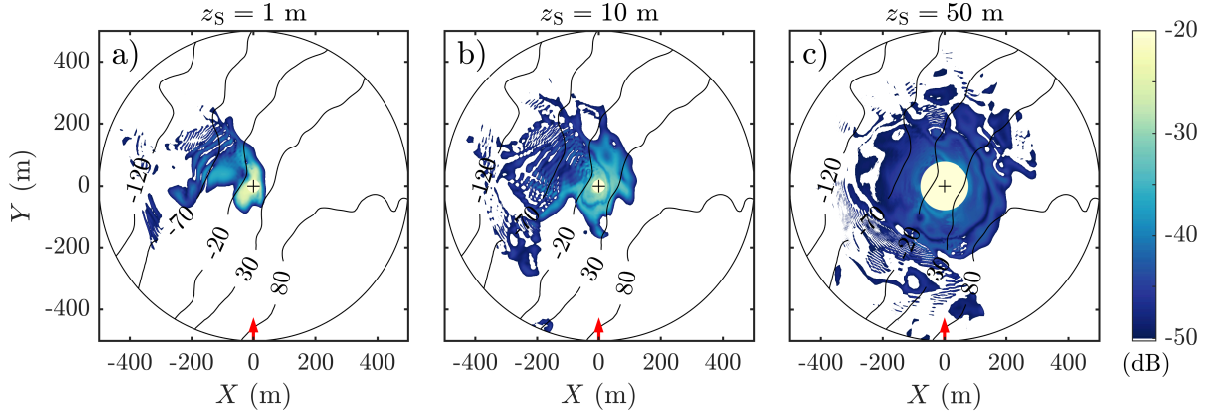

Figure 4.17 – Map of the propagation loss PL for different values of z_S, at 1 m height, for a 1000 Hz frequency signal, and at P1 (shown in figure 4.13). Reference case is b), with values are $u_* = 0.3$ m.s^{-1}, $Q_H = 0$ W.m^{-2}, $z_S = 10$ m. Plots a) and c) respectively show the influence of the source height above ground from $z_S = 1$ to 50 m. All other parameters are the same as the reference case. Contour lines are drawn every 50 m in thin line. The red arrow depicts u_* and the wind direction.

increase in the AS area is noticed downwind in the northeast direction for $u_* = 1.1$ m.s^{-1} (Fig. 4.16c). Overall, the AS area is reduced by 33 % when increasing u_* from 0.05 to 1.1 m.s^{-1}.

As previously shown for the plains habitat, nighttime provides a favorable condition for atmospheric propagation because of the temperature inversion (Larom *et al.*, 1997). The shape of the AS is also modified by wind speed and direction, but still limited by the underlying landform.

Influence of source height

Finally, the influence of the source height on the AS is estimated. Calculations are performed for $Q_H = 0$ W.m^{-2}, $u_* = 0.3$ m.s^{-1} and z_S between 1 and 50 m. The PL maps
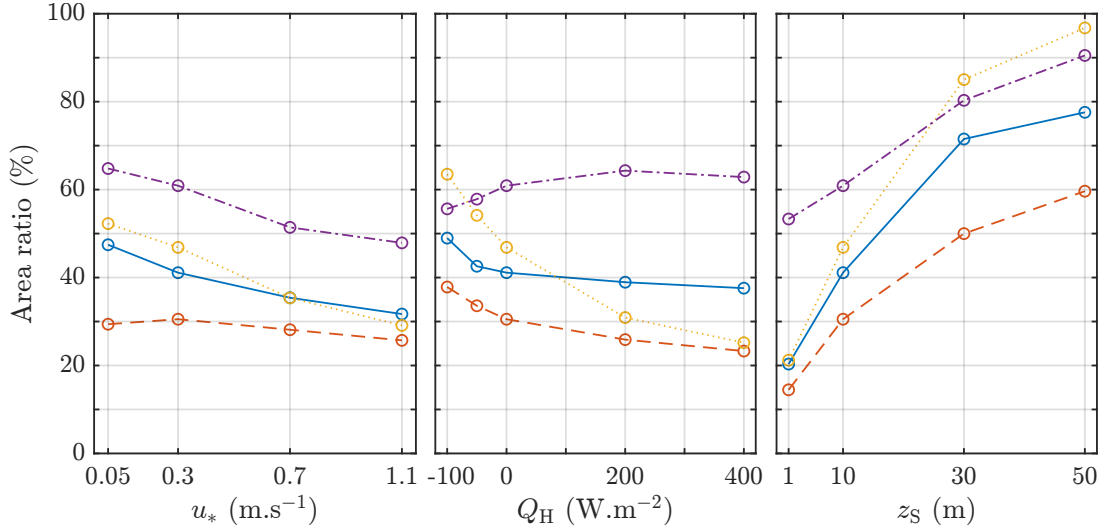
Figure 4.18 − Variations of the area ratio with the friction velocity u_*, the sensible heat flux Q_H and the source height z_S for the 4 positions shown in Fig. 4.13: 1 (——), 2 (− − −), 3 (·········), 4 (−·−·−)

are plotted in Fig. 4.17 for position 1. The source height has a considerable influence on the AS area. When the source moves up from $z_S = 1$ m (Fig. 4.17a), the area increases by 102 % for $z_S = 10$ m (Fig. 4.17b) and by $+282$ % for $z_S = 50$ m (Fig. 4.17c). Besides, the AS tends to be more circular as z_S increases, until it becomes a disk for a sufficiently high source, as seen for $z_S = 50$ m (Fig. 4.17c).

The results obtained here are consistent with previous studies. In forest environments Dabelsteen et al. (1993), Holland et al. (1998), or Mathevon et al. (2005) showed that small changes in roost height may result in a significant increase in AS. In addition, Mathevon et al. (1996) highlight the importance of the singing post to limit song degradation during propagation. The crucial role of the singing height in the AS was also noticed in open areas by Jensen et al. (2008) in hooded crow: individuals improve their signaling condition when in flight or perched compared to the ground feeding situation. Here, the increase in the AS with source height is generalized to an uneven landform.

Influence of environmental parameters on different topography

Next, the influence of environmental parameters on the AS area are discussed for the four positions on the Flaine site. For comparison purposes, the area ratio (%) is introduced as A/A_{ff}, where A_{ff} is the AS area obtained in free field for the same attenuation threshold. In free field, one has PL $= -20\log_{10}(R)$, and the parameter A_{ff} can then be simply calculated with $A_{ff} = \pi R_{ff}^2$, where R_{ff} is the maximum distance of detection in free field, which is equal to $R_{ff} = 10^{50/20} \approx 316$ m for a threshold of -50 dB.

Fig. 4.18 shows the variation of the area ratio as a function of u_*, Q_H and z_S for the four positions. The increase in the friction velocity from $u_* = 0.05$ to 1.1 m.s^{-1} induces for all positions a reduction of the area, that varies between -4 % and -23 % depending

on the topography. A similar reduction of the area in a range between -11 % and -38 % is estimated for the first three positions with the increase in Q_{H} from -100 to 400 W.m^{-2}. A slight augmentation of 7 % is however noticed for position 4. This is due to its location in a valley: upward refraction leads to increased SPLs higher up in the valley. Regarding the source height, its increase from 1 to 50 m implies in all cases a large increase in the AS area, by +37 % for position 4 in a valley, and up to +75 % for position 3 on a gentle slope.

In conclusion, the AS is dependent on the topography, the wind and temperature profiles and the source position. Both area and shape of the AS are changed by the modification of one of these conditions. We have shed light on two predominant factors: first, the topography, which constrains the spatial limits of the AS whatever the atmospheric conditions are, and second, the source height. Particularly, it can be deduced that performing a display flight while singing allows the rock ptarmigan to augment its AS, but also to overcome the constraint of the topographic heterogeneity.

4.5 Conclusion

The variability of the AS was investigated for the rock ptarmigan in mountain environment using numerical simulations. A model for atmospheric sound propagation based on the PE was proposed to calculate the AS. It accounts for the topography, the ground impedance, the wind and temperature profiles, and the atmospheric absorption. An experimental campaign was carried out in the French Alps to evaluate the model against long-range sound propagation measurements. Despite some uncertainties regarding weather conditions and snow impedance, a good agreement was obtained between calculations and measurements. The variability was also correctly reproduced by the propagation model under most conditions.

The propagation model was then applied to calculate the AS. The influence of the topography, the meteorological conditions and the source altitude on the AS was examined. It was shown that the AS is clearly asymmetric. Therefore, considering an effective distance is not relevant for such a heterogeneous environment since the AS shape is mostly driven by the underlying topography. Moreover, the source height was shown to be also a decisive parameter impacting the size and the shape of the AS. Especially, it was concluded that the display flight allows the rock ptarmigan to increase its AS and to overcome the landform heterogeneity encountered in mountain ranges. AS also depends to a lesser extent on weather conditions. The AS can be expected to change both in space, according to the movements of the birds on their territories, and in time, from day to day and even from hour to hour.

The propagation model proposed in the paper can be used to estimate AS in various habitat and weather conditions. It can be used to study communication networks and

their spatial and temporal dynamics. In addition, the ability to deduce temporal signal after its propagation is likely to provide interesting clues concerning the degradation of information carried by the vocalization (Mouterde *et al.*, 2014). However, it should be noted that the generalization and application of such a model to other species will require the knowledge of several parameters: SL, detection threshold, and background noise. An appropriate estimation of acoustic communication networks could provide insights into species behaviors, like territory defense and mating strategy. It also opens up new possibilities for automated counting techniques using audio recorders.

4.6   Additional results

4.6.1   Influence of ground impedance on active space

To assess the influence of ground type on the active space, we perform PL computations using known values of impedance. Snow impedance and alpine moor impedance are taken from previous on-site measurements (see Sec. 2.4.3). Their parameters are detailed in Table: 4.5. The rock impedance is approximated by a perfectly reflecting surface, which correspond to a zero surface admittance $\beta = 0$. The computation is performed for the position 1 in Fig. 4.13, and for a moderate wind and cloudy condition ($u_* = 0.3$ m.s^{-1}, $Q_H = 0$ W.m^{-2}), with the source height $z_S = 10$ m and the receivers heights $z_R = 1$ m.

Table 4.5 – Impedance parameters used to assess the influence of ground type on AS: effective thickness e, airflow resistivity R_s, porosity Ω, and tortuosity q^2.

Ground	e (m)	R_s (kPa.s.m^{-2})	Ω	q^2
snow	0.15	20	0.6	$1/\Omega$
alpine moor	0.006	400	0.8	$1/\Omega$
rock	0	∞	-	-

Compared to the reference case with the ground entirely covered by snow, we see differences in the PL maps when other soil types are considered (see Fig: 4.19). The PL computed over alpine moor reveals an active space area increased by 7 %, and the rocky ground implies a 51 % increase, compared to snow cover. Thus the change in ground type could significantly modify the active space.
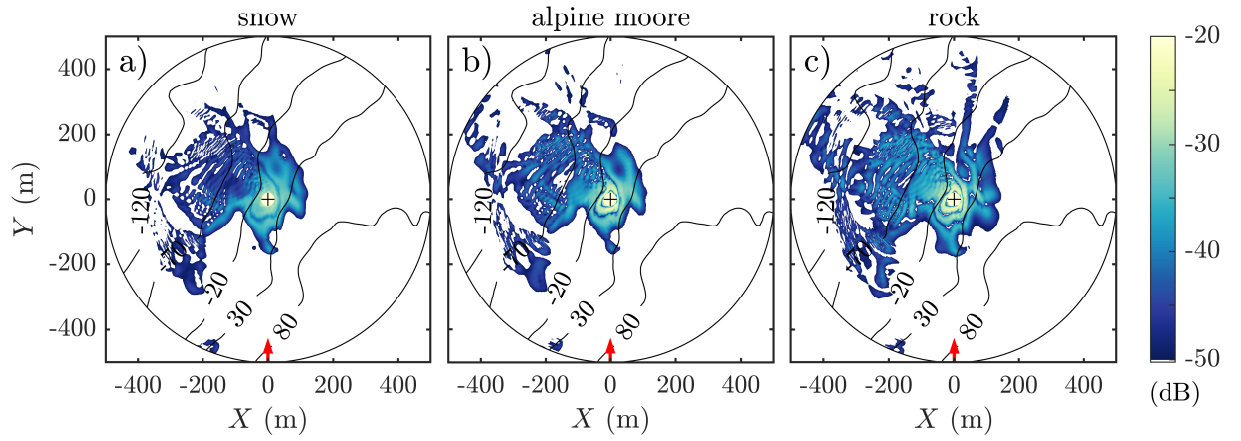
Figure 4.19 − Map of the propagation loss PL for different ground types, at 1 m height, for a 1000 Hz frequency signal, and at P1 (shown in figure 4.13). Reference case is a) with a snow cover, and values $u_* = 0.3$ m.s^{-1}, $Q_H = 0$ W.m^{-2}, $z_S = 10$ m. Plots b) and c) respectively depict the influence of alpine moor and flat rock. All other parameters are the same as the reference case. Contour lines are drawn every 50 m in thin line. The red arrow depicts u_* and the wind direction.

Chapter 5

Active spaces and territory in mountain birds: organization of acoustic network in time and space

Abstract

In the previous chapter, it was shown the importance of environmental conditions and the spatial behavior of ptarmigan in the variability of the active space. Thus, acoustic communications in the mountains are spatially constrained and the active space is determined by the position of the signalers in relation to the topography and by the variability of meteorological conditions. In the study context of a communication network in ptarmigan, the following question arises: How is the temporal and spatial organization of the communication network of rock ptarmigan affected by environmental conditions in alpine habitats? We answer in two steps, and by simulating the active spaces with the computation code previously developed. First we investigate the temporal organization of the network, questioning the reasons for the dawn chorus. Second, we construct a map of the network's spatial organization in order to evaluate the importance of display flights in territorial defense. By adopting a deterministic computation of acoustic propagation, and by taking as input spatial (topography, GPS tracking), meteorological (temperature, wind), and biological (source level, vocal activity) field data, we propose a new integrative approach for the study of acoustic communication networks. The active space model implemented this way allows us to answer with a high degree of confidence the behavioral questions raised.

Contents

5.1 Introduction

The information transmission is a key for the development of social living beings as it enables the mediation of competitive or cooperative relationships, the resource's defense, the mate choice and the avoidance of predators among others (Bradbury & Vehrencamp , 2011). This information can be either static, and not vary according to the context, or labile, and vary according to the emitter's current activity. In birds, this information is coded according to different acoustic criteria in amplitude, time and frequency dimensions (Mathevon *et al.*, 2008; Aubin *et al.*, 2014), and it carries specific and individual identity information required for recognition. The signal pass through a transmission channel between the emitter and the receiver (Weaver, 1949), and is carried by the acoustic wave. This airborne signal transmission over long distances results in a loss of information due to the alteration of the original sound wave during acoustic propagation (Wiley & Richards, 1978; Dabelsteen *et al.*, 1993; Embleton, 1996). The physical constraints on acoustic propagation depend on characteristics of the habitat, the emitter position, weather conditions and background noise (Holland *et al.*, 1998; Nemeth *et al.*, 2001; Mathevon *et al.*, 2005). These constraints determine the "active distance" below which a receiver is able to decode the signal (Marten & Marler, 1977). This spatial limitation is a key parameter insofar as it restrains communication possibilities, and influences the organization of interactions between birds (Burt & Vehrencamp, 2005).

The physical constraints have a significant impact on the transmitted information (Aubin *et al.*, 2014; Mouterde *et al.*, 2014), so they must be taken into account when studying information exchanges. To understand the phenomena affecting the active distance, many playback experiments have been used to evaluate the signal and SNR (signal-to-noise ratio) degradation from a receiver standpoint (Naguib *et al.*, 2000; Lohr *et al.*, 2003). In addition, propagation experiments conducted in different contexts provide a better understanding of the respective influences of environmental parameters (e.g. temperature, wind, soil type, habitat structure) and song post on signal transmission (Brenowitz, 1982b; Dabelsteen & Mathevon, 2002; Padgham, 2004; Balsby *et al.*, 2003; Barker *et al.*, 2009; Gall *et al.*, 2012). Finally, acoustic analysis of recordings from field transects was used to identify and quantify information loss in some species (Mouterde *et al.*, 2014, 2017). Generally, these investigations pertain to dyadic interactions, and homogeneous environments are considered.

Since Mc Gregor's work in the 90s, interactions between conspecifics have been described using the concept of communication network. That includes both the interactions between recipients and the information retrieval by eavesdropping (McGregor & Dabelsteen, 1996). Networks have been investigated either in terms of information exchange (Aubin & Jouventin, 2002; Templeton *et al.*, 2005; Mathevon *et al.*, 2008; Fernandez *et al.*, 2016; Mouterde *et al.*, 2017) or in terms of spatial organization of individuals (T'oth *et al.*, 2020; Szymkowiak, 2022). Eavesdropping in heterospecific bird communities has also been studied (Magrath *et al.*, 2015; Parejo *et al.*, 2018). Since the framework of communication networks has been established, estimating the active distance which determines communication between dyads, is no longer sufficient to model all interactions (McGregor & Peake, 2000; McGregor, 2005). Indeed, a network implies the transmission of signals between all emitters and receivers, and thus a three-dimensional view of their propagation. As acoustic propagation is constrained differently through each transmission path, which depends on the local conditions, the investigation of communication networks requires the use of the notion of active space (AS). It corresponds to the area in which any receiver can decode the signal that an emitter transmits from a given location. This consideration is even more important when the species' habitat is heterogeneous, because an emitted signal undergoes different effects of refraction, diffraction and absorption depending on direction. Few works have attempted to deal with the heterogeneous character of the habitats by using propagation models. However, they revealed the temporal and spatial variability of the active space (Larom *et al.*, 1997; Guibard *et al.*, 2022): the daily pattern of the temperature gradient and the wind condition drives the AS area, and uneven terrains induce shadow zones that result in a patchy shape of the AS, and a higher background noise level drastically reduces the area (Raynor *et al.*, 2017).

The vocal interaction modalities, like signaling over long distances, ranging, eavesdropping, alternating singing, overlapping, song matching, song switching (Todt & Naguib ,

137

2000), are intimately linked to the organization of the social network (Snijders & Naguib, 2017). The influence of sound propagation conditions on the extent of the communication network must be therefore studied. One can rightly inquire into the impact of propagation conditions at the network level. The influence of singing post, weather, and habitat structure on communication within the network is expected. To our knowledge, no physical analysis of the propagation constraints on a communication network in mountain bird has been conducted to date. Then, consequences of AS variability on the organization of communication networks remain largely unexplored.

We propose to investigate the temporal and spatial organization of communication in a heterogeneous environment. This chapter aims to bring evidences to answer the following questions:

i) Do weather conditions influence the temporal organization of communication?

ii) How is the spatial organization of communication driven by the emitter position?

For this purpose, we consider the case of a high mountain bird species, the rock ptarmigan, for which the active space estimation method is validated in Chap. 4. This species lives in high mountains, in open habitats with rugged topography, exposed to very changeable weather conditions. These conditions mean that ptarmigan must adapt to a very heterogeneous environment. During breeding season ptarmigan cocks perform courtship rituals at dawn chorus time, which are characterized by display flights with stereotyped singing (MacDonald, 1970). Display flights are a communication behavior in many species (Mikula *et al.*, 2022), fulfilling various functions such as courtship and territory defense (Slabbekoorn , 2004). These characteristics of heterogeneous environment and song in flight make the rock ptarmigan an interesting biological model to investigate our two main questions (i, ii). The framework of our study is built on the following two hypotheses:

• The first hypothesis is the so called better sound transmission at dawn. This one postulates that birds would sing at dawn to take advantage of a better transmission of their song, and thus of a more extended active space (Henwood & Fabrick, 1979; Staicer *et al.*, 1996). This schedule would decrease the cost/benefit ratio for communication within the network. The weather condition in mountain can be considered to be favorable to the propagation of the vocalizations above the snow because the vertical temperature gradient in the lower atmosphere refracts acoustic waves towards the ground, which increases the sound amplitude near the ground, and hence the active space. This hypothesis needs to be tested further for different habitats as it is still controversial (Gil & Llusia , 2020).

• The second hypothesis is the use of the singing in flight to maximize the extent of the information broadcasting area. Vocalizing during display flights rather than on the ground represents a significant advantage for communication in this type of habitat

([Guibard](#) *et al.*, 2022). It should enable the bird to cover a large part of its territory, as well as faster contact with a larger number of neighbors during the dawn chorus.

Our study is based on both field data – dawn chorus recordings, GPS tracking of birds, on-site weather data – and numerical simulations of acoustic propagation. This chapter is organized as follows: the material and methods section describes the acquisition of biological, audio and meteorological data and their processing, as well as the definition of the active space and the employed computational method. The results section first describes the temporal organization of the network, then its spatial organization. The hypothesis previously formulated are finally discussed on the basis of the results obtained in the present study.

5.2 Material and methods

5.2.1 Study site

A monitored population of rock ptarmigans lives on the Flaine ski resort (45.99N, 6.73E, 2400m a.s.l.) all year round, and especially during the breeding season ([Marin-Cudraz](#) *et al.*, 2019; [Canonne](#) *et al.*, 2020; [Novoa](#) *et al.*, 2011). The site is referred to as "Flaine". Its topography is visible on Fig. 5.8. DEM (digital elevation model) data of the bare ground with 5 m resolution was provided by the french National Geographic Institute (IGN: Institut national de l'information géographique et forestière). To avoid steep edges and to mimic the natural filling of depressions by snow cover, a low-pass filter has been applied to the DEM.

It should be noted that weather and audio data were collected on site in 2021, during a period when winter sports activities were stopped due to the human pandemic of Covid 19. Thus, the disturbance of bird activity by human presence was very limited compared to a typical spring season.

5.2.2 Subjects & GPS tracking of birds

The present study considers movement data from 5 ptarmigan cocks during the 2017 breeding season. GPS-tags (Global Positioning System Bird solar tag, e-obs GmbH, Gruenwald, Germany) provide one location with ±3 m uncertainty per minute during the dawn period from 2h40 to 4h15 UTC. The displacements are recorded in Cartesian coordinates, with X, Y representing the west-east and south-north axes respectively. Since the elevation data (on the z axis) from the GPS are not satisfactory, we subsequently refer to the underlying topography. Birds are captured one at a time, by leading them to a net previously installed above the ground ([Brenot](#) *et al.*, 2002). GPS-tags are adjusted on the back of the birds with elastics making harnesses. This equipment weights 10 g and does not exceed 2.5 % of the bird's weight. The data are downloaded by UHF

(ultra-high frequency) transmission at the end of the seven days of recording. Outliers including altitude error greater than 150 m above the ground or excessive speed greater than 54 km/h and creating a round trip with an angle less than 1° between three points were discarded (with N < 20 the number of discard points). This method of trajectory correction is adapted from Bjørneraas *et al.* (2010). The parameter N is used hereafter to indicate the number of samples in data sets. Note that some roosters not equipped with GPS tags also participated to the communication and social network.
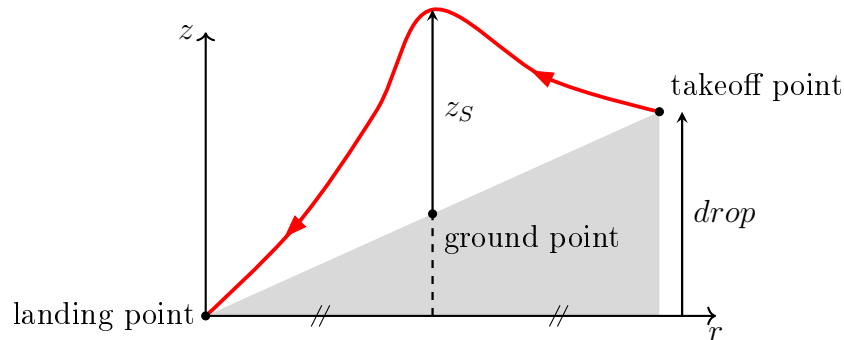
Figure 5.1 – Definition of the flight height z_S with reference to the topography along any r axis in the X,Y horizontal plane ($z_S = drop$).

Display flights are detected when the displacement is greater than 50 m in one minute. This threshold has been set after years of observations, based on the fact that ptarmigans walk slowly like other grouse. The singing positions are then considered to be located at the mean horizontal coordinates X,Y of the flight segment (i.e. in the middle position between the take off and the landing). Then the drop (i.e. the absolute difference in altitude) is calculated between these latter points (see Figure 5.1). The probability density of the absolute vertical drops indicates a median height at $z_S = 15$ m, and 95 % of cumulative probability located between 0 and 28 m (see Fig. 5.2). These drops stands for the source heights in the spatial study (Sec 5.3.2), truncated to a minimum of $z_S = 10$ m. Songs uttered during display flights are the predominant mode of communication in this species (MacDonald, 1970). Our study therefore focuses on the singing positions of the display flights. To ensure objective comparison of the singing behaviors, hypothetical songs emitted from the ground are assumed to be at the same X,Y positions as the display flights.

Each bird's territory is estimated by calculating the convex hull, called MCP (minimum convex polygon), including all the GPS positions of the 7 consecutive days. These five territories are visible on Fig. 5.8. To facilitate comparison of MCP and ASs, and to calculate their overlap rate (procedure defined in Sec 5.2.6), MCP are converted into pixel matrix of 5×5 m squares by linear interpolation. Data deduced from the GPS tracking are presented in Tab 5.1.
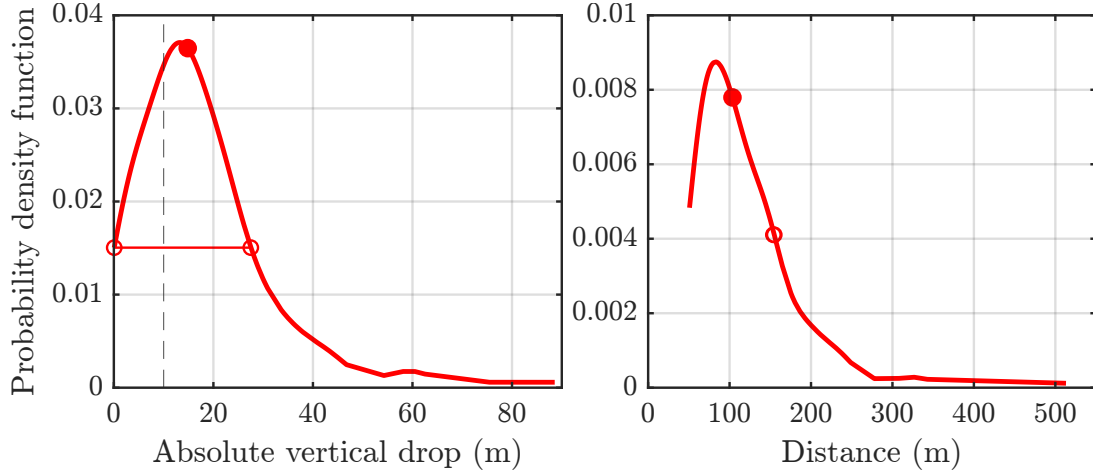
Figure 5.2 – (Left) Probability density of the height of display flights in relation to the underlying topography. These heights are calculated according to the absolute value of the difference in height between the departure and arrival of the display flights, called drop. The markers indicate the drop range for 95 % cumulative probability $(0 - 28$ m), and the filled dot indicates the median value at 15 m. The vertical dashed line at 10 m indicates the height truncation of source height for AS computations in flight. (Right) Probability density of display flights distances for the same data. The markers indicate the maximum distance for 95 % cumulative probability (156 m), and the filled dot indicates the median value at 104 m (N = 176, non parametric kernel-smoothing distribution).

5.2.3 The singing and listening of ptarmigan

Ptarmigan vocalizations are characterized by sequences of pulse trains, with a pulse rate of 21±3 ms, and the energy distributed in the frequency range [900 – 3700 Hz] (Marin-Cudraz *et al.*, 2019), the maximum amplitude being around 1000 Hz. The source level (SL, in dB ref. 20 µPa) of ptarmigan song has been deduced from on site measurements during Spring 2021. Four birds were recorded at the time of their take-off, using a hand-held sound level meter (NL52 Class 1, Rion, Tokyo, Japan). At the same time, the distance between the sound level meter and the take-off point is measured with a laser telemeter with an accuracy of ±1 m. These distances were between 6 and 20 m. Audio files have been calibrated according to the sensitivity of the sound level meter and then filtered with a band-pass filter $400 - 4000$ Hz. The maximum instantaneous level is then picked up from the first pulses sequence (see example Fig. 5.7 (A)). After subtracting the spatial decay in free field from the recorded level (RL, in dB ref. 20 µPa), following $SL = RL + 20 \log_{10}(r/r_{ref})$ with $r_{ref} = 1$ m, we obtain an estimate of the mean source level: $SL = 85 \pm 2$ dB. This SL value should be interpreted with caution, as it is derived from few measurements with no control on the directivity and inaccurate estimation of the distance.

The SL of the song may vary as a function of aggressive arousal or other factors (Perez *et al.*, 2012). In addition, it has been shown that passerine birds adapt their SL in response to a variation in background noise level (Brumm, 2004). The same phenomenon, called the Lombard effect, is observed in non-oscine birds like ptarmigan (Brumm & Zollinger, 2013). Nevertheless, for the purpose of this study, we consider the

source level as a fixed parameter. There is no data to our knowledge on the auditory masking threshold in Galliformes. The threshold for detection in noise (masked auditory threshold) is set according to a SNR (signal-to-noise ratio) of 3 dB, following the field work of Brenowitz (1982b). This threshold is considered necessary for comfortable communication in the sense of Dooling & Leek (2018).

5.2.4 Background noise & Vocal activity estimations

Automated recordings of Flaine's soundscape were made in spring 2021 with a SM4 dual-channel recorder (Wildlife Acoustics, Massachusetts, United States). Its position is depicted on Fig. 5.8. Audio samples of 10-minutes long were recorded daily between June 7th and June 12th. These recordings include each day: eight samples from 1h10 before sunrise to 20 minutes after, three samples at fixed hours 7h10, 12h10 and 15h10 UTC, and one sample at sunset time (N = 12 samples). An approximation of the vocal activity on the entire site is estimated from these audio samples.

Audio analyses of these data were performed with an in-house Python code. To ensure the best signal-to-noise ratio for the detection algorithm, only the least noisy channel (left or right) is considered. To analyze recordings in the ptarmigan frequency band, the signal of each 10-minute sample is first filtered to select the $400 - 4000$ Hz bandwidth. Then, the signal amplitude is adjusted with the SM4 microphone sensitivity previously determined by calibration in anechoic chamber. The short time sound pressure levels (SPL, in dB, ref. 20 µPa) are calculated according to non-overlapping 0.5 s windows, which gives $L_{eq,0.5s}$. Then the statistical level L_{90} defined as the pressure level exceeded 90 % of the time is computed from the $L_{eq,0.5s}$. This metric is chosen to characterize the background noise because it is not affected by short duration sound events.

Typical environmental noise contributions are wind interactions with obstacles, rain on the ground, distant busy roads, airplanes, melt water streams, distant birds and other animals, and human activities. These noise contributions are considered representative of the habitat. On the contrary, noise contributions due to the recording technique are unwanted: wind on the microphone's membrane, and rain impacting the recorder's protection.

Representative noise data were selected by listening the all audio files and analyzing their spectrogram (N =452). Removed data were those showing more than 30 % rainfall time, or a saturation appearing in more than 30 % of the sample time mostly due to gusts of wind, or constant strong wind involving noise generated at the microphone (N = 112). A wind speed threshold of 4.4 m/s at 10.4 m is set to separate recordings for which the wind-generated noise component in the microphone is dominant over the others. This threshold corresponds to a wind speed of 3 m/s at the height of the SM4 which is 1.5 m. The selection of these samples is illustrated Fig. 5.3. The use of large windscreens is not

possible due to rain and snowfalls, coupled with cold temperatures that would freeze the microphones. Minimum and maximum L_{90} values of the 340 samples that were selected are in the range of 13.3 to 33.7 dBSPL, with a median value of 19 dBSPL (see Fig. 5.4).
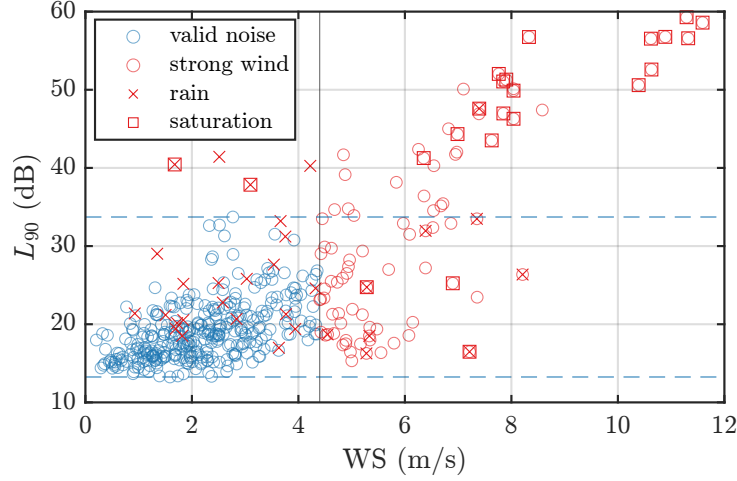
Figure 5.3 − Estimated L_{90} from SM4 audio samples (10 min samples, N = 452, from May 20 to June 28, 2021) function of wind speed measured at 10.4 m (WS). Representative noise data (valid noise, N = 330). Minimum and maximum L_{90} values considered as representative are depicted by dotted lines (Min=13.3 dBSPL, Max=33.7 dBSPL). Data excluded were those showing more than 30 % rainfall time (rain, N = 32), or saturation (saturation, N = 23), or strong wind involving noise generated at the microphone (strong wind, N = 89). Solid vertical line at 4.4 m/s represent the wind speed limit considered here, corresponding to 3 m/s at the height of the SM4 which is 1.5 m.

Song detection is performed on all selected recordings using a convolutional neural network (CNN) algorithm developed in Python language (Python, 3.9) by Jérémy Rouch (ENES team). It is composed of 4 convolution layers, 1 fully connected layer and 1 decision layer. It has been previously trained on manually annotated rock ptarmigan song data (field recordings from Norway, French Alps, and Pyrenees). These data consisted of 20630 original song samples of 0.66 s each, with an overlap of 80 %, corresponding to a total of 47 min, and 336270 negatives (non-sung) samples. Data augmentation and external data sets have been used for a 1200 epochs training process. The retained model performances on the validation data set achieved 97.4 % of precision, 94.6 % of recall, 94.3 % of balanced accuracy, and 96 % for the F1 score. The algorithm estimates the probability of having the presence of a ptarmigan song according to windows of 0.66 s with a 33 % overlap. Each time step of 0.22 s is considered as a song period if the average probability over the 3 enclosing windows is greater than 50 %. The time percentage of song is taken to be the vocal activity. Results are then presented by time periods with reference to the sunrise time. To synchronize audio and meteorological data samples (see: Sec 5.2.5), the sunrise and sunset times were calculated for each day a posteriori with a MATLAB® function[1].

---

[1]François Beauducel (2023). SUNRISE: sunrise and sunset times (https://github.com/beaudu/sunrise/releases/tag/v1.4.1), GitHub. Retrieved February 2021.

5.2.5 Meteorological data

To obtain meteorological data representative of ptarmigan habitat during the breeding season, an automated weather station (AWS) (see Fig. 5.6 AWS) has been installed in the center of the Flaine site, on a plateau area of the massif (for the location, see Fig. 5.8 AWS). This station enabled to collect temperature, humidity, atmospheric pressure, wind speed and direction data during spring 2021. Three temperature and humidity sensors (HMP155A, Vaisala, Vantaa, Finland) were placed on the weather station at the following heights: 1.1, 4.2, 9.8 m (with reference to the rock slab where the mast is anchored). To limit the sensitivity of the wind data to terrain irregularities in the vicinity of the weather station, a single wind vane (W200P-01, Vector Instruments, Saint Asaph, UK), and a single anemometer (A100LK, Vector Instruments) were mounted, at the height of 10.4 m. Finally, a pressure sensor (PTB110, Vaisala) was mounted in the acquisition box. Meteorological data were recorded (after integration or average) by a data logger (CRX-1000, Campbell Scientific, UK) over 10-minute periods.

Given the sub-zero temperatures encountered at night and the rain or snowfall that occurred during the study period, the anemometer was sometimes clogged with ice. As a precaution, samples showing wind speed less than 0.2 m/s were excluded, as this speed corresponds to the starting threshold of the anemometer rotation. The methodology for determining meteorological parameters from measurement data, as well as the calculation of temperature and wind profiles, are based on the Monin-Obukhov similarity theory (MOST) (Monin & Obukhov, 1954). Meteorological parameters were extrapolated by means of an iterative fitting procedure using the MOST and Businger–Dyer relations, as cited in Salomons (2001). The detailed procedure is described in a previous work (Guibard et $al.$, 2022). Resulting parameters are: T (K) the air temperature related to the height z_g above the ground level, T_0 (K) the air temperature near the ground, u_* (m/s) the friction velocity, and θ_* (K) the temperature scale. We also introduce the quantity $\Delta T = T(z_g = 20\text{m}) - T_0$ that indicates the temperature gradient near the ground, and $Q_{\text{H}} = -\theta_* \rho_0 c_p u_*$ the sensible heat flux (Ostashev & Wilson , 2016). Q_{H} (W.m^{-2}) represents the vertical heat flux exchanged between the atmosphere and the ground.

These meteorological parameters are used both in the computations of the temporal and the spatial studies of the acoustic communication. The weather data collected from May 20 to June 28, 2021, and the resulting parameters, synchronized with the background noise estimate from the audio samples (N = 340) are presented in Fig. 5.4. In the same way, Fig.5.5 presents the probability density function of the friction velocity u_* (m/s) and the temperature scale θ_* (K), together with the wind rose (N = 5250 samples). It details the u_* and θ_* parameter's median values used thereafter in the AS computations related to Spatial study and Temporal study with fixed meteorological conditions only. These computations performed for a fixed south wind, since most of the occurrences are from
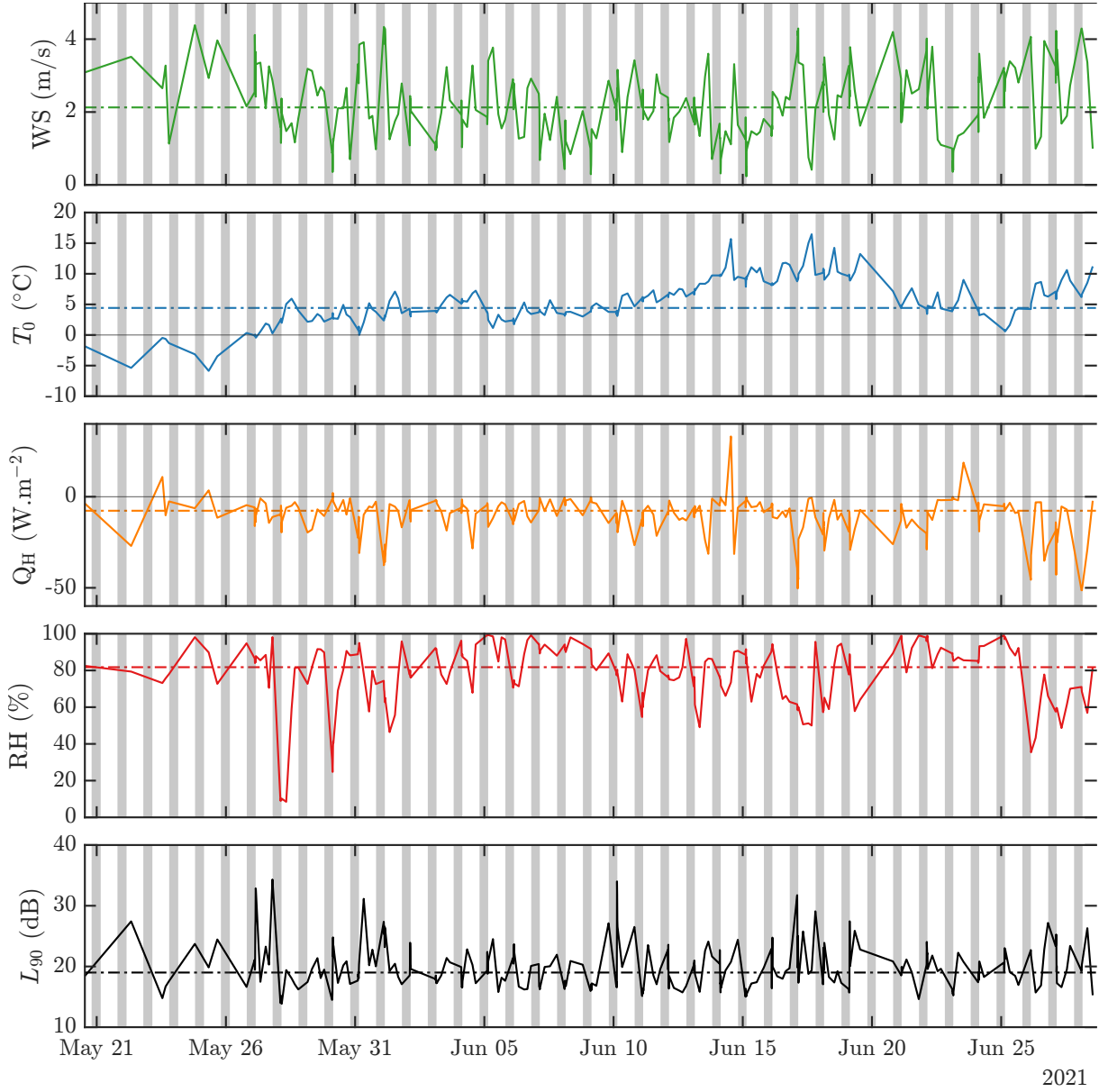
Figure 5.4 – Meteorological conditions and synchronized background noise level (10 min samples, all data corresponding to audio selected samples N = 330, from May 20 to June 28, 2021), (colored lines). Wind speed measured at 10.4 m (WS), parameters determined according to MOST: temperature deduced at ground level (T_0) and sensible heat flux at ground level (Q_H). Average relative humidity rate (RH) from the heights 1.1, 4.2, 9.8 m. Background noise L_{90} deduced from SM4 audio recordings. Median values are depicted by dashed-dotted lines, and night periods are shown with grey patches.

this direction.

5.2.6   Active space estimation

General method

We estimate the active spaces using numerical computation, and according to its four constitutive parameters introduced by Brenowitz (1982b):

(1) The SL (source level) of emitters was fixed to 85 dBSPL (sound pressure level
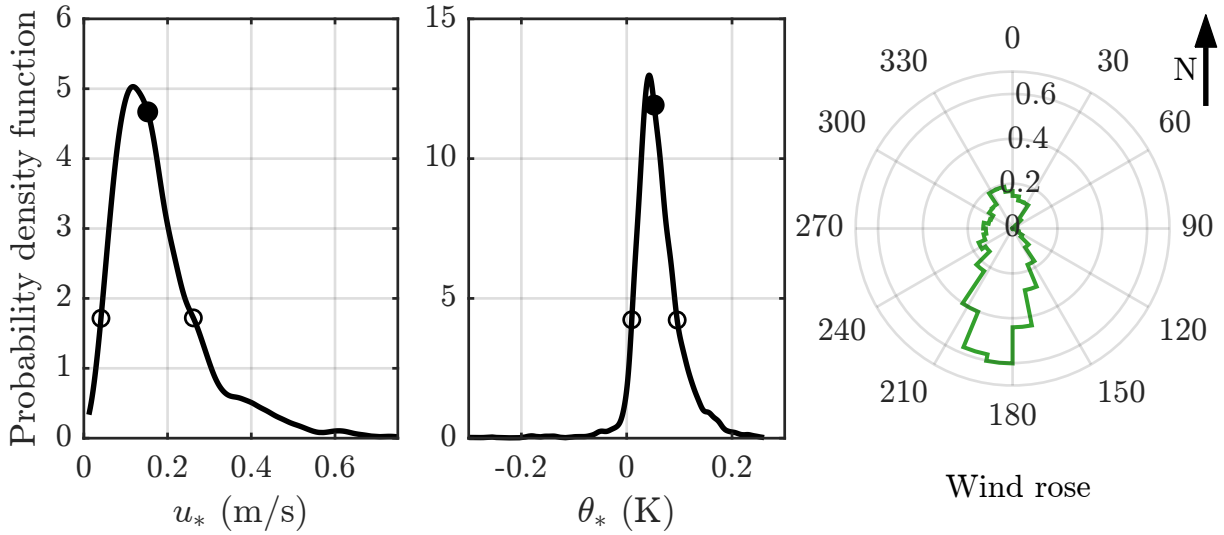
Figure 5.5 − Probability density functions of the friction velocity u_* and the temperature scale θ_*. The empty dots indicate the 95 % cumulative probability and the filled dots stands for the median values, respectively 0.15 m/s and 0.05 K. Wind rose (wind origin) measured at 10.4 m (10 min samples, all available data N = 5250, from May 20 to June 28, 2021).

(SPL) in dB relative to 20 µPa), according to previous on-site measurements on wild ptarmigans (see Sec. 5.2.3).

(2) The signal energy attenuation by transmission through the environment is called propagation loss (PL), and is a negative value. The propagation model used to compute PL is based on the WAPE (Wide Angle Parabolic Equation) method, described e.g. by Salomons (2001). It is an efficient computational method for long range sound propagation within the atmospheric boundary layer. The WAPE equation is derived from the Helmholtz equation in frequency domain by making a one way approximation. The entire PL computation method resulting in three dimensional PL is detailed in Chap. 3.

The pressure field computations are performed at 1000 Hz, within a 1 km radius around the point source. The PL value at 1000 Hz is supposed to be a reliable representation of the information loss during the propagation of the ptarmigan signal. Indeed, the parameters of the information are essentially temporal (number of pulses per sequence, duration of the sequences and silences, pulse rate and acceleration), and only two parameters are frequential (the median frequency of the first two formants) (Marin-Cudraz *et al.*, 2019). Thus, twelve of the thirteen parameters previously determined for individual recognition are effectively carried by the amplitude and phase of the wave at fundamental frequency. The source considered as acoustically omnidirectional, is placed at a height z_S with respect to each display flight, or according to a ground position with $z_S = 0.3$ m to fit with the ptarmigan height in upright position. Receptor's height is always set to $z_R = 0.3$ m.

Snow cover is assumed to extend over the entire area, as it is still largely prevalent at this time of year. The acoustic properties of the snow cover are that from a previous study on this site (see Chap. 4). Meteorological parameters are deduced from measured

temperature and wind data (see Sec. 5.2.5), using an iterative fitting procedure based on the Monin and Obukhov similarity theory (MOST). This yields a pair of parameters θ_* and u_*, respectively the temperature and wind speed scales. These inputs are used in the WAPE code, along with the average relative humidity and the wind direction, to compute the PL around the point source (see example Fig. 5.7 (C)). All these PL computations are performed with MATLAB® (MATLAB, R2017a).

(3) The background noise level (BN), is estimated using the statistical level L_{90} on the frequency band $400 - 4000$ Hz (see Sec: 5.2.4). The BN is assumed to be constant, though it varies in time and space.

(4) The detection threshold (DT) is fixed at a SNR of 3 dB following Brenowitz (1982b) (see Sec. 5.2.3).

The active space (AS) is finally defined as the aggregation of the elementary surfaces where the SPL at 1000 Hz is above the detection threshold like:

$$\text{SL} + \text{PL} \geqslant \text{DT},$$

with

$$\text{DT} = \text{BN} + \text{SNR}$$

at the receiver position.

Temporal study

To observe how the temporal variation of the atmospheric conditions influences the active space we consider a fictional display flight at a central point of the topography and close to the AWS (see "s1" point in Fig. 5.8). The source height is set to $z_S = 15$ m according to the median of the display flight heights with respect to the topography (see Fig. 5.2). Then computations are performed using the conditions related to the 340 10-minute periods defined by the vocal activity estimation procedure. We consider both the weather conditions and the background noise variations according to the measured values.

For a simplified interpretation of the results, the calculated areas are represented by their equivalent radius R_{eq}, defined with reference to an equivalent circular area as $R_{\text{eq}} = \sqrt{(A/\pi)}$, where A (m^2) is the area of the AS.

Spatial study

Positions of the sources are fixed according to averaged X, Y coordinates between takeoff and landing of each display flight (see Fig. 5.1). ASs computations are performed for each source position, at two heights: the first corresponds to the flight height (see Sec:5.2.2), and the second to the height of $z_S = 0.3$ m to mimic a bird on the ground. Meteorological conditions are fixed using median values of meteorological parameters $u_* = 0.15$ m.s^{-1},

$\theta_* = 0.05$ K.m^{-1} and wind direction 180°, i.e. from the south. Parameters deduced from 2021 meteorological data were used as inputs for the propagation computations together with birds positions recorded in spring 2017 on the same site. Indeed, these are medians over a season and stand for a representative condition.

A logical matrix of $5{\times}5$ m pixels representing the AS is obtained by linear interpolation between cylindrical coordinates of the WAPE calculation and the Cartesian coordinates (X,Y) defined by the topographic data (using MATLAB® function *ScatteredInterpolant*; boolean values are 0 inside the AS and 1 outside). The same interpolation is done for the polygons of the territories (MCP). This procedure enables to calculate the number of pixels in common and to obtain a coverage ratio of a territory by the ASs. Since multiple display flights are performed and thus multiple songs are emitted each morning, the daily AS of each bird is defined as the aggregate of all pixel matrices of its songs (i.e. according to an `or` function). The term "cumulative active space" is used to refer to the union of these areas.

5.3   Results

The following results allow us to investigate our two questions formulated in the introduction of this chapter (see Sec. 5.1). Section 5.3.1 aims to answer to the question: Are the weather conditions at dawn favorable for the propagation of vocalizations? Section 5.3.2 provides insight into the benefit of display flight behavior for acoustic communication in heterogeneous environments.

5.3.1   Temporal organization

The mean meteorological parameters on site are fairly stable during the 24 hours of the day (see Fig. 5.6). Wind speed (WS) is mostly between 1 and 6 m/s, and does not show any remarkable temporal evolution along the day. As expected, air temperature at the ground surface (T_0) shows a slight rise during the daylight with a maximum at 11:30 UTC, which is caused by the increase in solar radiation. In the same time, the vertical temperature gradient ΔT shows a slight decrease, which implies that the lower atmosphere is more homogeneous during the day than during nighttime. This observation is consistent with the variation of the determined sensible heat flux Q$_H$ which is negative during nighttime, and close to zero or even positive in some cases during daylight. The solar radiation is still weak at this time of the year. The presence of a snow cover induces a negative sensible heat flux and thus the radiation balance is directed towards the atmosphere. This means that the temperature gradient is almost always positive, which implies that the refraction of the atmosphere brings down the energy of the acoustic waves to the ground. These conditions are favorable to the acoustic propagation and increase the active space

compared to a case with homogeneous atmosphere. More precisely, the mean Q_H is equal to -22 W.m^{-2} one hour before sunrise, and increases to -1 W.m^{-2} at 09:00 UTC. Moreover, the relative humidity rate (RH) presents a clear temporal evolution, with a decrease during night and morning, and an increase in the afternoon as the snow cover melts. It reveals a temporal pattern shifted with respect to T_0, probably due to the high thermal inertia of the snow cover.

Zooming in on the sunrise period provides detailed insight into the variability of vocal activity and propagation conditions during the dawn chorus compared to other times of the day (see Fig. 5.7 (B)). Peak vocal activity is observed 50 minutes before sunrise (see 5.2.4 for computation details). During this period, vocal activity was sometimes observed at values up to 4.25 % of the time (outliers are not represented in this plot for clarity). During the day, vocal activity is close to zero, and a slight increase is recorded at sunset (15:40 from sunrise). This late activity corresponds to the dusk chorus, which is much less prominent.

In parallel, the active spaces corresponding to the conditions at recording times are computed for a representative position on the Flaine site, indicated by the s1 point close to the AWS on Fig. 5.8. These calculations are made for three configurations. First, the case named "*meteo var.*" only takes into account the variability of meteorological parameters, while the background noise (BN) is fixed at its median value $L_{90,\mathrm{med}} = 19$ dBSPL. Secondly, the case named "L_{90} *var.*" only takes into account the variability of BN, while the meteorological parameters are fixed at their median values $u_{*,\mathrm{med}} = 0.15$ m.s^{-1} and $\theta_{*,\mathrm{med}} = 0.05$ K. Thirdly, the case named "*total var.*" takes into account both weather and BN variability.

In Fig. 5.7 (D), let's consider first the case named *total var.* taking into account both meteorology and background noise variability. Considering the dispersion of the complete data set, the values of R_{eq} vary from 162 to 583 m, which corresponds to a ratio between the maximum and minimum areas of the AS equal to 13. This indicates a significant variability in the possibilities of communication. Considering the question of the temporal evolution, it appears that the median of the AS does not show any remarkable temporal variation according to the different times of the day (morning chorus, daytime, evening). The median of R_{eq} is in the interval [324, 356] m, which corresponds to a ratio between the maximum and minimum area equal to 1.2, i.e. a variation of the AS by only 20 %. This indicates that there is no advantage due to acoustic propagation in singing before dawn rather than daytime.

Now let's focus on the two sources of variability considered in this data set. It can be noticed in Fig. 5.7 (D) that the dispersion of R_{eq} induced by only the variability of the background noise (L_{90} *var.*) is [154, 422] m, whereas it is just [251, 470] m if the only variability of meteorological parameters is considered (*meteo var.*). These radius ranges correspond to a ratio between the maximum and minimum surface equal to 7.5 and 3.5
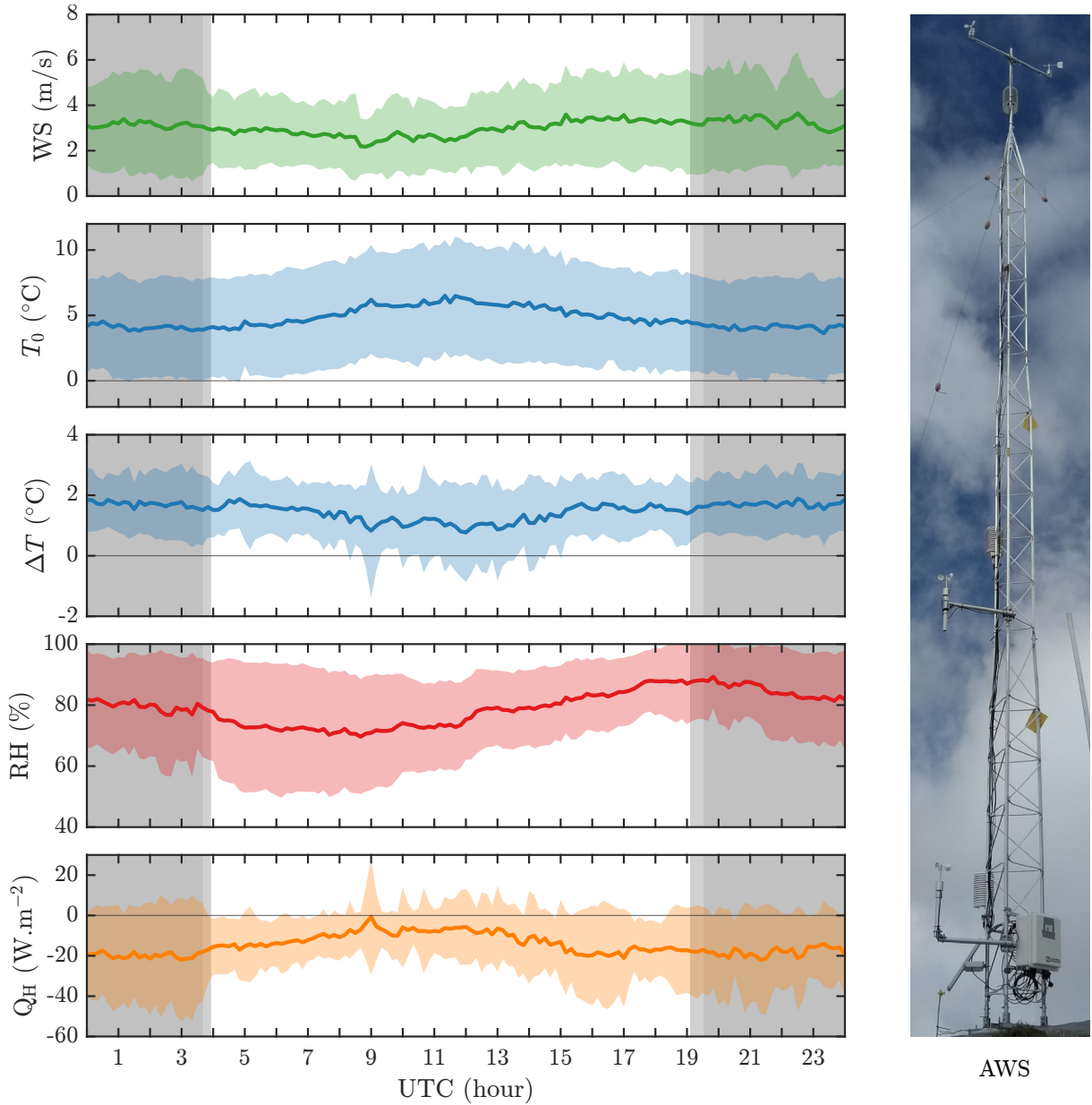
Figure 5.6 – Left: Meteorological conditions recorded every 10 min, from May 20 to June 28, 2021, mean (colored lines) and standard deviation (colored patches) according to UTC (coordinated universal time). Wind speed measured at 10.4 m (WS), average relative humidity rate (RH), and parameters determined according to MOST: air temperature calculated at ground level (T_0), temperature gradient in lower atmosphere $\Delta T = T_{(20\ m)} - T_0$, and sensible heat flux Q_H. Associated night periods (shaded region), and sunrise and sunset shifts (light shade). Right: AWS (automated weather station) used for measurements.

respectively for L_{90} *var.* and *meteo var.*. This indicates that the active space varies significantly more with the background noise than with the meteorological parameters. Indeed, the smallest AS is determined by the highest background noise level. Additional results that detail active space variations (daily and over a month) are available in Appendix B.1.

Figure 5.7 – (A): Spectrogram (color scale from −50 to 0 dB) and oscillogram of a ptarmigan song (pressure normalized to the maximum amplitude). (B): Evol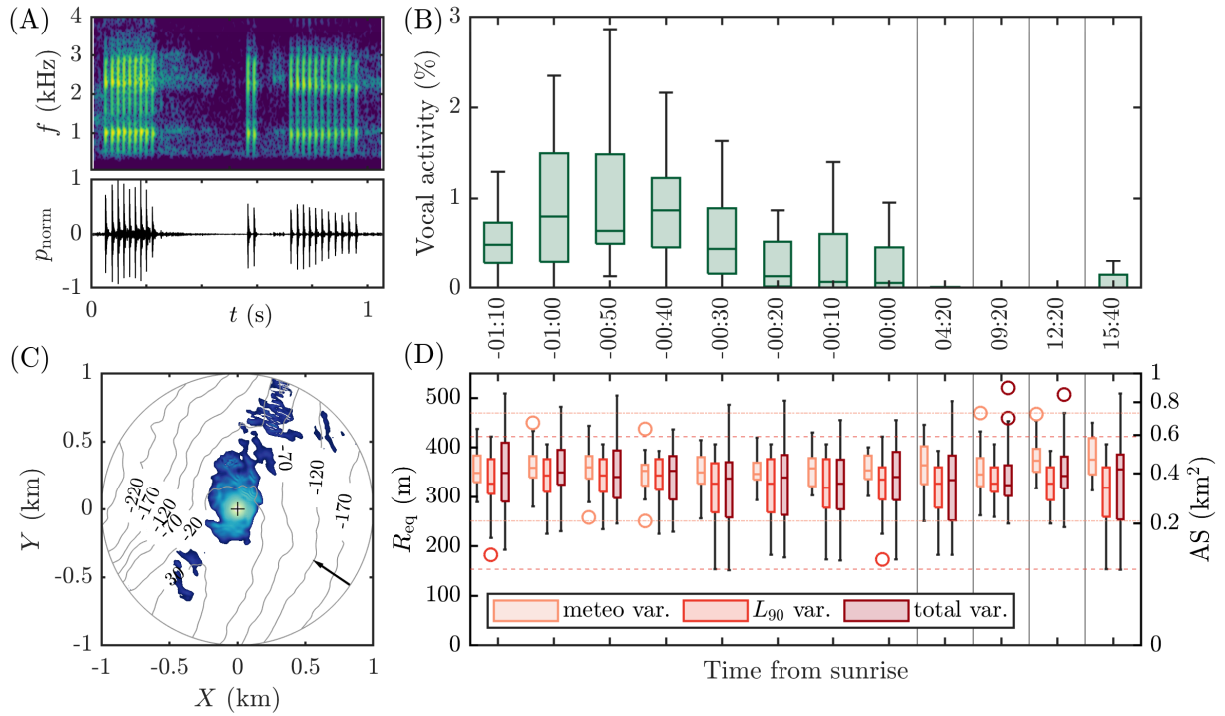ution of the estimated vocal activity during the day in % of time. (C): Map of the PL at 0.3 m above the ground, for a frequency of 1000 Hz (color scale of pressure levels relative to the SL, plotted to the threshold of the active space (-63 dB). Atmospheric conditions are equivalent to the medians of the meteorological parameters (see below), and $z_s = 15$ m. Contour lines are drawn every 50 m in thin lines, and the arrow depicts the wind direction. (D): Evolution of R_{eq} (m), the equivalent radius of the active space, during the day (time is not linearly scaled): considering the median background noise level $L_{90,med} = 19$ dBSPL and changing weather conditions (*meteo var.*), for a variable background noise level L_{90} and a fixed meteorological condition according to the median parameters $u_{*,med} = 0.15$ m/s and $\theta_{*,med} = 0.05$ K (L_{90} *var.*), and considering both meteorological and background noise variations (*total var.*). Dash dotted lines and dashed lines respectively depict the extreme values of *meteo var.* and L_{90} *var.* Box plots display the median (inner line) and first and third quartiles (lower and upper hinges, respectively), whiskers indicate 1.5 times the inter-quartile range from the hinge, and circles represent outliers.

5.3.2 Spatial organization

Five birds have been monitored during 7 days with a spatial resolution of 3 m and a recording frequency of 1 position/min. Movements, territory size (understood as the defended home range) and the position of their display flights are deduced from these data (see Tab. 5.1). It is observed that the size of the territory as well as the number of display flights are related to the reproductive status of the birds. It appears that individuals paired with a female have reduced movements and perform fewer display flights on average compared to single males.

Fig. 5.8 shows the territories of the five GPS monitored ptarmigan (determined by MCPs, defined in Sec. 5.2.2), the area occupied on June 6th in the morning (MCPs day 1), and their respective cumulative active space over that morning. The computation considers one song per display flight, so note that the more mobile birds have more source points as well (see Tab. 5.1 for details). Right side of Fig. 5.8 shows the overlap between

respective territories and the cumulative AS of birds when performing song during flights. Conversely, the left side shows this overlap if the birds were singing on the ground. This overview shows that the songs in flight, performed in a single morning, can cover almost the entire own territories, but also cover part of the neighboring territories. In detail, we see for example that the ASs of the 2 birds named *Messi* and *President* largely overlap each other, and that the AS of the bird named *Barbe bleue* covers a large part of that of its two neighbors (*Pastis* and *Ravanel*). In contrast, the left-hand plot reveals that the songs on the ground cover only a part of their own territories, and very little of the neighbor's ones.

Table 5.1 – Data from 2017 monitored birds on the Flaine site, June 6-12: number of GPS points, number of detected display flights, and area of each territory defined by the MCP.

Bird names	Mating status	GPS points (nb)	Flights (nb)	MCP area (km^2)
Barbe bleue	paired	619	27	0.148
Messi	single	644	50	0.165
Pastis	paired	638	29	0.092
President	single and then paired	567	57	0.233
Ravanel	paired	453	13	0.092
Total		2921	176	

The positions and active space data were each aggregated by day to observe the dynamics of living spaces and communication spaces. Thus, Fig. 5.9 reveals both the overlap of own territories (left plots) and the overlap of neighboring territories (right plots), by traveled areas (MCPs) and by active spaces (AS). First of all, it is shown that entire own territory coverage is obtained in six days, with an average rate of 97 % (see Fig. 5.9 top left plot). This means that the area covered by the movements occurring in the morning is much smaller than the entire territory. Secondly, the coverage of the territory by AS is calculated if the birds sing on the ground or in flight (middle left and bottom left plots). For the songs on the ground ($z_S = 0.3$ m), the average coverage is 56 % the first day, and after seven consecutive days it reaches 90 %. In contrast, the coverage obtained for the songs in flight reaches 93 % on average from the first day.

Concerning the overlap of neighboring territories by individual movements, Fig. 5.9 (top right plot) shows that it is restricted to 5 % on average, and this behavior is actually limited to unpaired birds (Messi and President: 12 % at the end of the week). It is thus shown that the interactions are for the most part remote communications. Finally, coverage of neighboring territories by ASs is calculated for ground or airborne songs (middle right and bottom right plots). At the end of the week, the overlap rate is 21 % for the songs on the ground, while it reaches 40 % if we consider the songs in flight.
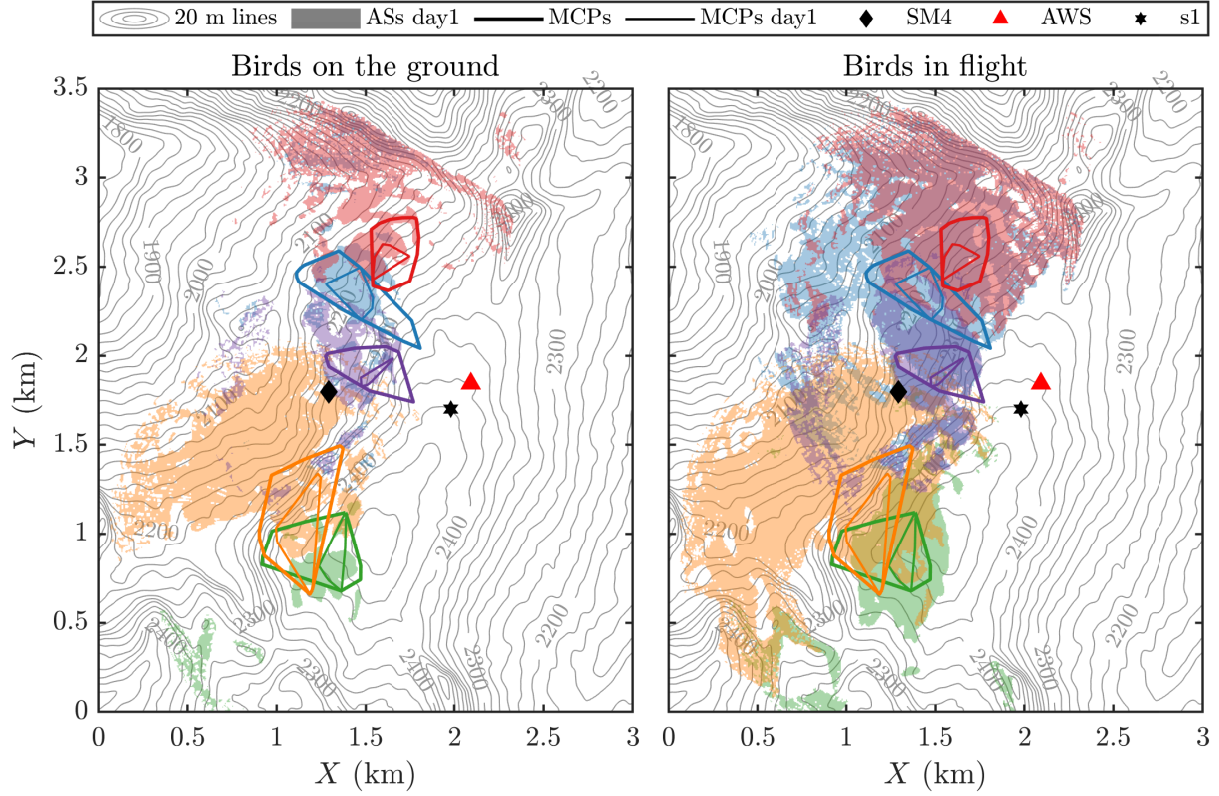
Figure 5.8 – Mapping of 5 ptarmigan territories from June 6-12, 2017 (bold polygons), occupied area during the day 1 (thin polygons), and cumulative ASs (colored areas) calculated from display flights positions of birds during the day 1: ground singing (left), and according to their flight height (right). Birds are defined by their color in Tab. 5.1 : Barbe bleue, Messi, Pastis, President, and Ravanel. Positions of the audio recorder (SM4), of the automated weather station (AWS) and of the source used for temporal variability (s1) are also represented on the topography map (20 m contour lines).

Supplementary materials detailing display flights, territories, and each day active spaces are available in Appendix B.2.

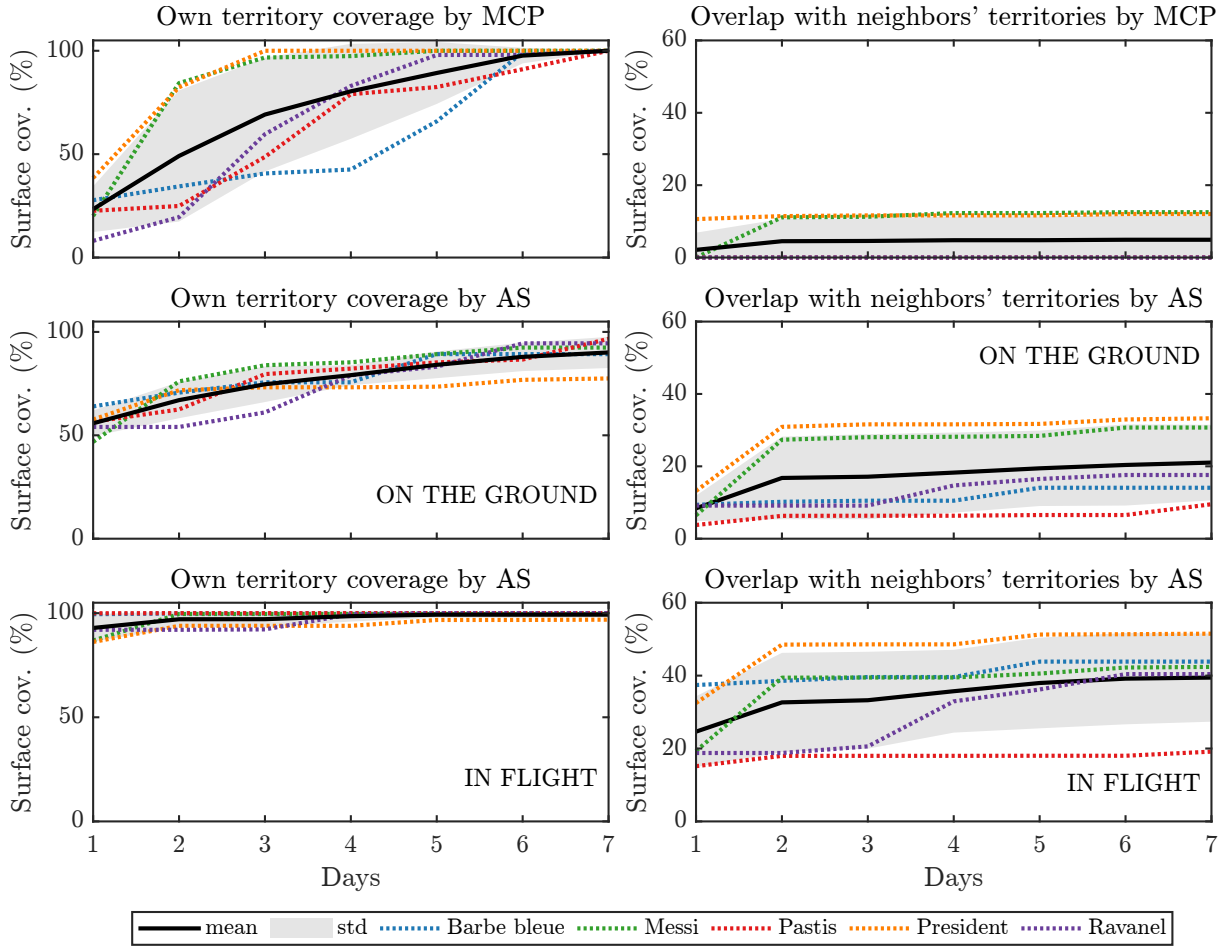Figure 5.9 – (Left) Cumulative own territory coverage of each bird: by daily MCP (top), by AS with source height fixed to $z_S = 0.3$ m (middle), and by AS with source height depending on estimated fight heights (bottom). (Right) Cumulative coverage of neighbor's territories: by daily MCP (top), by ASs with source height fixed to $z_S = 0.3$ m (middle), and by AS with source height depending on estimated fight heights (bottom).

5.4   Discussion

5.4.1   Dawn chorus can't be explained by a better sound propagation in alpine environment

The temporal dynamics of the vocalizations confirms that ptarmigan are mainly active at dawn, and thus the majority of their interactions are concentrated in this time period, as for many bird species (Staicer *et al.*, 1996). In a communication network context, we wanted to test the hypothesis of better sound transmission in the heterogeneous environment offered by the mountains. The dispersion of the observed active space values is mostly induced by the variability of the background noise, as reported for the detection spaces (Haupert *et al.*, 2022). This directly limits the detection area around a transmitter bird by setting a detection threshold. Noise conditions remain highly variable at all times the day, but the median ASs are relatively constant throughout the day. Moreover, no trend was observed indicating a lower background noise at dawn compared to the rest of the day.

Removal of audio samples for which the recording conditions were not suitable implies to significantly truncate the samples with high background noise. However, these recordings were not considered representative of the sound environment. Moreover, the probability of birds singing in the associated conditions is very low. Indeed, since the motivation for the chorus is maintained by the neighbors' responses to the songs, it is very likely that if no response can be heard, there is no more motivation and the bird stops singing. At the same time, the energy expenditure to fly increases with wind speed, which limits the motivation to perform display flights. Nevertheless, we add for information the figure representing AS temporal variability if these samples are kept (see Fig. 5.10). The major contribution of these artificial background outliers is the drastic decrease in active space, with minimum R_{eq} of 23 m. It is clear that background noise is a critical variable for the extent of the active space. This negative effect of background noise on the active space can potentially be compensated to some extent by the transmitter. According to the well-known Lombard effect, a bird can increase its emission level to compensate for a higher BN and continue to communicate with its neighbors (Brumm & Zollinger, 2013). Although this effect cannot be tested here, it is known that the background noise is not linearly compensated and the SL increase has a physiological limit (Brumm & Todt, 2002, 2004), so the consequences in terms of active space remain limited.

Other factors that determines the active space are the atmospheric conditions, modifying the acoustic propagation. In this mountain habitat, weather conditions have a dramatic effect on song spreading, implying great variability in active spaces. At this period, the snow cover still overlays most of the site. This implies that the temperature inversion, present at night, persists during the day in the atmospheric surface layer. This
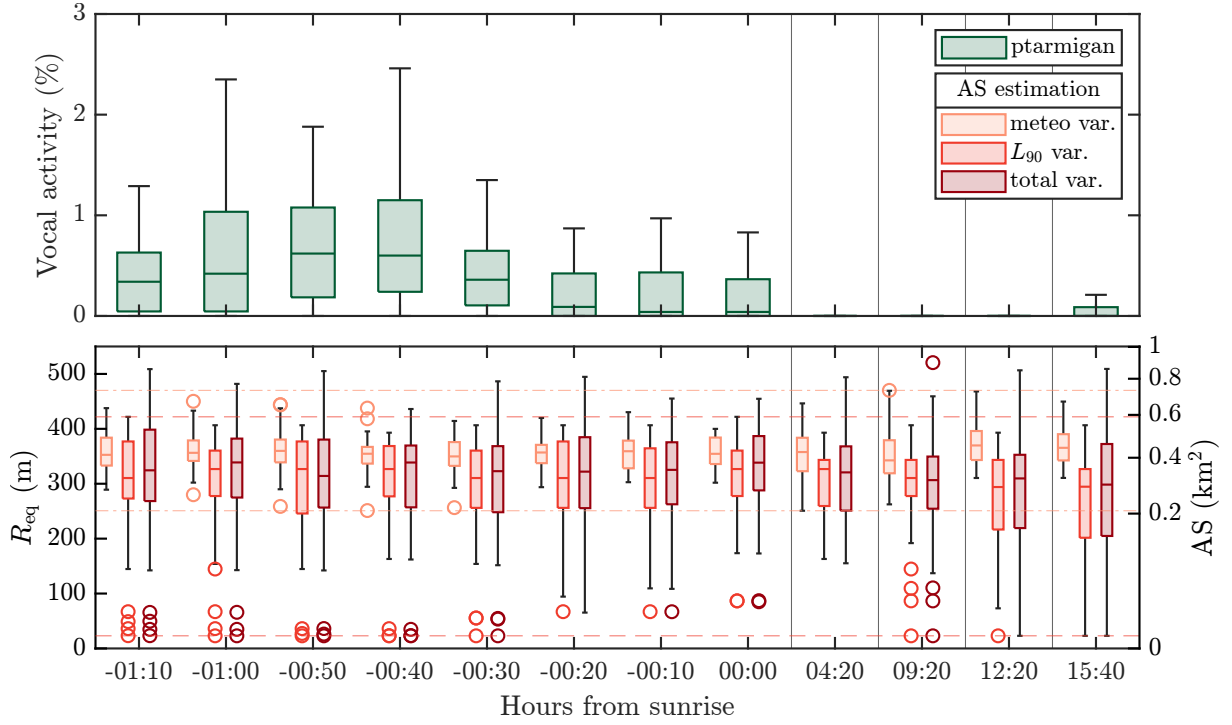
Figure 5.10 – Same figure as Fig. 5.7 (B) and (D), but with all the 452 samples (before selecting). Top: Evolution of the estimated vocal activity during the day (time percentage). Bottom: Evolution of the estimated active space during the day according to their equivalent radius R_{eq} (m): considering the median background noise level $L_{90,\text{med}} = 19$ dBSPL and changing weather conditions (meteo var.), for a variable background noise level L_{90} and a fixed meteorological condition according to the median parameters $u_{*,\text{med}} = 0.15$ m/s and $\theta_{*,\text{med}} = 0.05$ K (L_{90} var.), and considering both meteorological and background noise variations (total var.).

phenomenon is due to the radiation of the snow. Consequently, the propagation condition is essentially always favorable to the sound propagation. We observe that the difference in mean sensible heat flux observed one hour before sunrise and in the morning (9h UTC) is significant, as it increases by 21 W.m^{-2} (see Fig. 5.6). However, the change in active space area induced by this difference in condition remains minimal, with a potential change that reaches about 5 % at most (see Chap. 4). This result shows that from an acoustic propagation perspective, mountain birds have no particular interest in singing at dawn during springtime.

We conclude that the hypothesis of better transmission of the sound at dawn cannot explain in this case the temporal synchronization of the songs inducing the dawn chorus behavior. These results bear earlier studies conducted in other types of habitats, concluding thanks to propagation experiments through temperate forest that the dawn chorus cannot be explained by the better sound transmission hypothesis (Dabelsteen & Mathevon, 2002). Nevertheless, the start time of the chorus can be modified by extrinsic abiotic factors such as precipitation or ambient light (Bruni et al., 2014). The morning chorus is still the subject of multiple unresolved hypotheses, related to intrinsic functions, social functions and environmental pressures (Staicer et al., 1996). However, it is important to remember that these hypotheses must be approached differently depending on the species,

and that the chorus is certainly driven by various non-contradictory factors. Gil & Llusia (2020) identify three most probable hypotheses to date: first, dawn is a time when singing has a reduced energy cost because it does not overlap with the feeding period; second, it pays to sing early to assert territories and attract females; and third, the earlier chorus time prevents dishonest signaling by the handicap it induces. In the case of rock ptarmigan, it seems that predation pressure by raptors or foxes is a very likely hypothesis to be added, due to their prey condition in an open environment with scarce resources for carnivores. Indeed, our field observations have revealed that ptarmigan sometimes sing during the day when low clouds or fog cover the site, which hides them from predators.

5.4.2 Song in flight enable communication across territory borders in ptarmigan

Territorial male birds must be able to defend a living area for the resources it contains, as well as the female against potential floaters (Stamps, 1994), and this is achieved through the use of signaling songs. Here we show that a specific behavior of singing in flight makes it possible to cover all the own territory in one morning, even if ptarmigans roam a small area of their territory each day (see Fig. 5.9 left). This means that no matter where the bird is located in its home range, it has the ability to quickly defend its territory right up to its borders by singing on flight. This makes it particularly effective in deterring potential intruders from entering the defended territory, and asserting its borders. In contrast, songs from birds on the ground only cover a limited area, and it would take several days for a grounded bird to assert its entire territory (see Fig. 5.9 middle left). It turns out that the nature of the terrain largely constrains the propagation of songs, and increasing the source height reduces the ground effect, minimize the shadow zones and thus partly homogenize the active space around the emitter. Our results supports assumptions about the importance of the singing post (Dabelsteen *et al.*, 1993). In other environments and species, previous studies suggest that perching higher could reduce song degradation and thus increase the emitter's active space (Wilczynski *et al.*, 1989; Mathevon *et al.*, 1996, 2005; Padgham, 2004). We show that this result is also true in open habitats, and for rugged topography. The advantage of being able to cover a large area by singing in flight and to overcome the constraints of the environment seems to prevail over the additional cost of energy expenditure induced by the display flight. Other grouse species also perform display flights but no songs in flight.This behavior is putatively the result of an adaptation to the particular topography that characterizes the ptarmigan habitat.

Furthermore, we show that communication between territories is enabled by in-flight songs. Indeed, the area covered by the songs in the neighboring territories is therefore on average doubled if the songs are emitted during the display flights compared to the associated ground positions (see Fig. 5.9 right). The communication possibilities between

neighbors in adjoining territories are therefore significantly increased by the display flight behavior. Previous studies have suggested that the territorial proclamation song of male songbirds, called the broadcast song, can be detected in some species by conspecifics up to two average territory diameters away from the singer (Brenowitz, 1982b; Dabelsteen *et al.*, 1993). Our data indicate that this is not a criterion found in all territorial bird species, especially in ptarmigan. Since non-tracked males are potentially present around the tracked birds, it is thought that the overlap between AS and neighboring territories in the network should in fact be greater. However, the overlap is not 100 %, which reveals the presence of strong environmental constraints, and results in the privatization of communications to the nearest neighbors only. This means that there is no real public information in the sense of Dabelsteen (2005), because transmission occurs in most cases from one bird to another within the network. Thus, the audience is essentially made up of the competitive male and possibly the paired hen.

It has been shown previously that acoustic adaptation exists in some birds in response to the sound propagation constraints of their habitat (Ey & Fischer, 2009). We show here in the ptarmigan the behavioral adaptation of singing in flight to enable long distance communication. It appears that this behavior is of crucial importance for the organization of the communication network. In this environment, if birds would not perform display flights to sing, territorial defense would involve more physical encounters, chases and attacks within territories, leading to an unnecessary increase in energy expenditure and potential injuries.

5.5 Conclusion

We bring here a new approach of communication networks in birds, taking the example of high mountain habitats witch are still very little studied from an acoustic propagation point of view. Our numerical simulations clearly indicate that environmental constraints have a significant impact on the transmission opportunities within a bird network in such an heterogeneous open habitat. Nevertheless, we bring new elements to reject the hypothesis of the better sound transmission at dawn in high mountain environments. Despite previous observations showing a correlation between better transmission and vocal activity (Henwood & Fabrick, 1979; Staicer *et al.*, 1996), our simulations bring strong evidence that it is not valid. This hypothesis being already controversial (Gil & Llusia , 2020), our study supports that no causality exists between these two phenomena. It appears that other pressures are at work in determining the early dawn chorus in ptarmigan. First, predatory pressure from raptors and foxes makes daytime periods dangerous, as singing and flying are conspicuous (Henden *et al.*, 2017). Second, singing at dawn does not interfere with feeding activities, and represents a reduced energy cost. In addition, it pays to sing early in order to assert ownership of a territory and attract females; and it is also

a timing that prevents dishonest signalling due to the high energy expenditure it entails (Hutchinson *et al.*, 1993).

In a high mountain habitat the behavior of singing during display flights in ptarmigans turns out to be a crucial strategy for communication within this bird communication network. This result supports the benefit of singing from a greater elevation, regardless of the type of environment. Indeed, many observations of this effect have been reported for various types of forests (Mathevon *et al.*, 1996; Holland *et al.*, 1998; Mathevon *et al.*, 2005; Padgham, 2004). This behavior of singing in flight seems all the more crucial in alpine environment because there is no place to perch, and the audience is confined to the ground. This can be considered as an adaptation to the acoustic propagation constraints of the habitat. In this sense, the benefit of singing in flight gives a supporting element for AAH (acoustic adaptation hypothesis (Morton, 1975)), given its importance in maintaining long-distance communications. Although the amplitude of the songs is related to the territory size (Brenowitz, 1982b; Opaev & Shishkina, 2021), it is noteworthy that songs in flight are essential in ptarmigan for an effective signaling towards the audience.

This work could lead to the study of optimal acoustic communication strategies in birds living in complex environments. In the case of the ptarmigan, it would be very instructive to have access to the exact times of the songs, and thus to their position. This could be made possible by the miniaturization of recorders that could be coupled to GPS beacons. Thus, we might know more about the ratio of songs performed on the ground and in flight, and we might be able to evaluate the energy expenditure involved. It is likely that ptarmigan communication behaviors are based on a fine cost/benefit optimization of singing in flight or on the ground, considering both the social context of neighbors and floaters, and the environmental conditions such as weather, habitat, and even the precise configuration of the defended territory.

Chapter 6

Detection space computation based on reciprocity principle: application to passive acoustic monitoring of mountain bird

Abstract

In the previous chapter we investigated the implications of the variability of active spaces in a communication network. We are now interested in the receiver's point of view in the context of passive acoustic monitoring of birds. Again, in an integrative way, we rely on our deterministic computation of the propagation, on physical measurements, on the scheduled audio recordings, and on a detection algorithm. The aim is to evaluate the benefit of the physical estimation of detection spaces for acoustic monitoring protocols.

To do this, we first test a method based on the acoustic reciprocity principle by adapting our propagation computation code. Then we apply this method to estimate the detection spaces of the recorders deployed on the Flaine site for the population monitoring. Thus we demonstrate the validity and interest of the reciprocal computation method for the estimation of active spaces in heterogeneous environments. Moreover, we highlight the benefit of using a physical estimation of detection spaces in a network of ARUs. On the one hand, it leads to more robust metrics calculation for species census and biodiversity monitoring. On the other hand, it helps to reduce sampling biases by revealing the coverage of the studied zone and the pseudo-replication rate of the data due to the overlap of the detection spaces. These elements improve the PAM protocols by helping to pre-design the deployment of ARUs, and to standardize the studies by providing the spatial representativeness of each audio sample.

Contents

6.1 Introduction

The use of automatic census techniques has considerably expanded in the ecoacoustic research field over the past decade thanks to the technological progress of audio recording and great advances in audio analysis (Darras *et al.*, 2019; Sugai *et al.*, 2019). On the one hand, the considerable reduction in the price of audio recorders makes their large-scale deployment possible. On the other hand, the increase in computer performance and new analysis methods facilitate the processing of larger amounts of data, especially with the emergence of machine learning and deep learning. These techniques are known as PAM (passive acoustic monitoring) and gather different protocols usually customized to the particular location and target species (Laiolo, 2010; Blumstein *et al.*, 2011). PAM enables to monitor biodiversity over large areas for long term studies (Folliot *et al.*, 2022), and to assess many ecological traits (Gibb *et al.*, 2019). Deployment of autonomous recording units (ARUs) provides information at multiple scales depending on the analysis method: soundscape, species, population and individual. Various metrics are used to qualify the sound samples of geophony, anthropophony or biophony, and to quantify diversity by acoustic indices, presence or absence of target species, vocal activity, and individual counts. Among the various approaches currently in use, *acoustic diversity indices* provides a promising tool to describe soundscapes (Sueur *et al.*, 2014; Sánchez-Giraldo *et al.*, 2020). These provide a repeatable description and quantification of soundscapes including all sound sources: biophonic, geophonic and anthropophonic (Gasc *et al.*, 2013). Despite the still elusive link between these acoustic metrics and biodiversity indices (Buxton *et al.*, 2018;

Eldridge *et al.*, 2018), their use has rapidly spread throughout the ecoacoustic community (Alcocer *et al.*, 2022). It should be noted that the great variety of indices, which are often developed for a particular ecosystem soundscape (or a group of comparable ecosystems), hampers the comparison of studies. There is now a need to harmonize the description of soundscapes and to make a more objective assessment, using more robust metrics that incorporate the sampled area. At a finer scale, it is possible to measure the vocal activity (VA) of a focal species using audio analysis algorithms that identify species-specific vocalizations (Pérez-Granados *et al.*, 2019a), or to use clustering by unsupervised machine learning algorithm for example to monitor diverse species (Morales *et al.*, 2022). Then the analysis of these data on a large spatial or temporal scale provides information on the phenology of these species. It is possible to combine PAM together with an occupancy model (Wood & Peery, 2022) to estimate a threatened species distribution (Campos-Cerqueira & Aide, 2016) for example. At the population level, the enumeration of individuals, regardless of their respective rate of vocal activity, can be done using individual recognition and clustering algorithms (Peake & McGregor, 2001; Adi *et al.*, 2010; Marin-Cudraz *et al.*, 2019).

Survey protocols using ARUs present a promising prospect to complement the still widely used point count (conducted with human listeners) (Darras *et al.*, 2018). In spite of the drawbacks of hardware failure, they enable to increase temporal sampling with permanent or periodic listening at fixed time intervals. They also provide the opportunity to reduce the observer bias, to bypass the wildlife avoidance effect, to study more simply remote sites and difficult terrain, and to target rare species on a large scale (Shonfield & Bayne, 2017; Darras *et al.*, 2019; Freitas *et al.*, 2022). Besides, the use of large networks of ARUs requires a sampling plan to determine where and how many recorders should be installed, as well as their recording periods (Bradfer-Lawrence *et al.*, 2019; Pérez-Granados & Traba, 2021). Despite these challenges, PAM offer a great advance for biodiversity and population trend estimations, assessing climate change impacts on phenology and distribution, and understanding ecosystems disturbance and recovery dynamics (Ross *et al.*, 2023).

However, most of these PAM methods do not consider the sampling area associated with each ARU location and measurement period. Yet the estimation of the sampling area is essential from an ecological point of view to infer the phenology of a species or the trends of a population, and to establish for example a robust measure of abundance (the number of individuals per unit area) (Pérez-Granados & Traba, 2021). It is known that environmental conditions influence the propagation of acoustic signals, and thus constrain the active space (AS) of signaling animals (Dabelsteen *et al.*, 1993; Guibard *et al.*, 2022), and also the detection space (DS) of a recorder (Haupert *et al.*, 2022). The AS and DS are related by the four parameters defining them: the source level (SL), the sound pressure decay due to propagation called propagation loss (PL), the background

noise (BN) at the receiver, and the detection performance in noise (Knight *et al.*, 2017). These two spaces vary considerably depending on the animal studied (its position, its SL source level, its spectrum), its habitat (the topography, the vegetation, the ground type), and the environmental conditions (the local meteorology, the background noise) (Lambert & McDonald, 2014; Darras *et al.*, 2016; Guibard *et al.*, 2022). The variability of DS induces a great uncertainty in the spatial origin of the recorded information, and thus in the metrics deduced from these recordings (Pacifici *et al.*, 2008; Sánchez-Giraldo *et al.*, 2020; Toth *et al.*, 2022). Some of the potential pitfalls of species monitoring by acoustics are pseudo-replication, i.e. ambiguity about the number of independent observations specified when using a statistical inference, and the lack of consideration for the variability of sampling areas. That is why the generalization of ecoacoustic studies requires to know the detection space associated with each recording. Indeed, the DS data can be used to standardize the sampling and thus to compare the results between surveys and between sites, which is still difficult today given the variety of methods used. Moreover, the knowledge of the spatial coverage related to each ARU can provide a valuable indication of the overlap rate of the spatial coverage, and can be used to evaluate the pseudo-replication related to the spatial distribution of an ARU network. In addition, it would be possible to use a DS estimate to integrate a fine acoustic modeling into the detection probability computation (Darras *et al.*, 2016). It appears that the use of a propagation model to inform the PAM methods would yield a great advance in terms of reliability and standardization of sampling.

So far, in most ecoacoustic studies, the spatial sampling criterion used is a threshold distance. It can be evaluated according to a minimum SNR measured in propagation experiments along transects (Darras *et al.*, 2016), or by human recognition of playbacks (Yip *et al.*, 2017). In addition, the determination of recognition by human expert or algorithm as a function of distance is based on statistical models using distance sampling (Buckland *et al.*, 2004; Darras *et al.*, 2018), effective detection radius (EDR) (Sólymos *et al.*, 2013), or distance truncation (Hedley *et al.*, 2021). Other studies attempt to consider sound degradation using an attenuation model fitted by maximum likelihood method on experimental data and vegetation density, but with little reference to the underlying physics (Royle, 2018). In order to define a single parameter that describes the attenuation in different environments, a habitat attenuation coefficient was introduced by Haupert *et al.* (2022). This coefficient is used to describe a linear decay of the excess attenuation (EA, defined as the range-dependent attenuation, excluding geometric decay and atmospheric absorption) in foret habitat assumed to be homogeneous and isotropic. This habitat attenuation coefficient is described as depending on the type of environment and the frequency. This method, like the threshold distance, assumes a one-dimensional approximation of the propagation, and thus neglects the heterogeneity of the habitats, the topographical constraints and the meteorological variability. However,

it has been shown that the wind and temperature profiles have a significant influence on the propagation through the refraction effect (Wilson, 2003). In addition, the topography limits the insonified areas according to the line of sight (LOS) from the source (Blairon, 2002; Parakkal *et al.*, 2018). Under the LOS, we refer to geometric shadow zones. Finally, these phenomena are combined with the ground effect, and the type of ground is often heterogeneous in natural environments (Gauvreau *et al.*, 2002).

To achieve reliable estimates of the detection space in heterogeneous environments, we propose to use a physically explicit model based on the wide angle parabolic equation (WAPE). This model previously tested for the computation of active spaces (Guibard *et al.*, 2022), provides reliable PL computations in three dimensions and according to frequency. It takes into account any moderate topography, heterogeneous ground type and variable weather conditions, and provide sound level maps.

The purposes of this study are multiple. On the one hand, we want to adapt the computation code detailed in Chap. 3 to the problem of detection spaces. We want to test the possibility of using the acoustic reciprocity principle (Helmholtz, 1860) to perform a detection space computation from the receiver position. Indeed, a direct computation from all potential sources to a single receiver implies a considerable computational cost, as a simulation has to be run for each source. This is why a reciprocal computation from the receiver seems more efficient. The DS could be obtained from a single simulation. On the other hand, we want to explore the interest of such a model for PAM, by performing an application for a bird species that has a low density and lives in a heterogeneous environment. Based on these two lines of research, this chapter aims to answer the following questions:

• Does the WAPE method used with an N×2D computation ensure a valid application of the reciprocity principle?

• Does the detection space helps to reduce the variance of indices when monitoring a bird population in heterogeneous environments?

• Does the detection space estimation give the ability to refine the acoustic sampling spatially and temporally?

To answer these questions, we first test the reciprocity computation with the WAPE method. Direct and reciprocal comparative computations are performed first in 2D for various atmospheric conditions, and then in 3D taking the example of recorder positions on the Flaine site. Then we rely on a PAM campaign of a rock ptarmigan population conducted in the French Alps, on the Flaine site in spring 2021 to asses the detection spaces at a fine spatial and temporal scale. We use the vocal activity of the rock ptarmigan estimated by means of a in-house CNN-based (Convolutional Neural Network) detection algorithm as a proxi of an abundance index (Borker *et al.*, 2014; Pérez-Granados *et al.*, 2019a).

6.2 Reciprocity validation using 2D WAPE and N×2D mapping

6.2.1 Reciprocity method applied to the WAPE code

The computation of detection spaces requires particular precautions that we detail in this section by introducing the methods. Note that the reciprocity principle is employed thereafter using the same propagation code described in Chap. 3, which description is not repeated here. The considered parameters for the application of the detection space computation are then specified.

As the computation of acoustic propagation from multiple potential sources to a single receiver is very costly, a quick way to estimate a detection space is to perform an indirect computation from the known receiver in all directions around. This amounts to a PL computation similar to that of the active space. This analogy is valid in a homogeneous atmosphere and for any given boundaries by virtue of the reciprocity principle. Formulated by Helmholtz (1860), this principle postulates that a given source and receiver can be interchanged without changing the sound pressure obtained at the receiver. Further on, its application to a moving inhomogeneous medium, such as the atmospheric surface layer when convected by a mean wind, necessarily implies some modifications. The flow reversal theorem (FRT), elaborated on the basis of earlier contributions delimiting its domain of validity (Landau & Lifshitz, 1959; Lyamshev, 1961; Dowling, 1983) has been detailed by Howe (1975). The FRT states that the reciprocity principle remains valid for a moving medium, provided that the direction of convection is reversed, as shown Fig. 6.1. The reciprocity principle without considering mean flow has been previously checked for general 2D narrow angle PE and high order Padé approximation in underwater acoustic fields computation (Godin *et al.*, 1999; Mikhin, 2001).
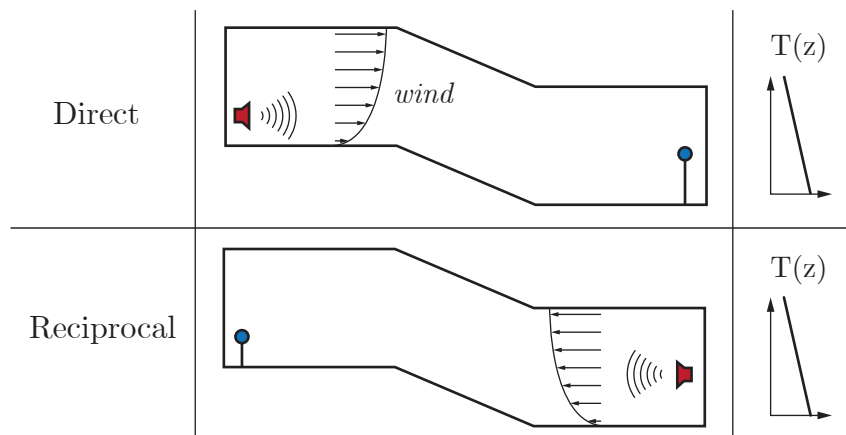

Figure 6.1 – Schematic diagram of the reciprocal computation: direct computation is done with fixed temperature and wind profiles (top), and the reciprocal computation is done with the source and the receiver exchanged (bottom). The direction of propagation is therefore reversed, and the wind profile too.

To use the FRT in a reciprocal pressure field computation with WAPE method, we take the opposite of the mean wind speed profile $\overline{V}(z)$. This leads to modify the associated c_{eff} profile (see Eq. (4.11)). We thus introduce the reciprocal effective sound speed,

$$c'_{\text{eff}}(z) = c_0(z) - \overline{V}(z)\cos\psi, \tag{6.1}$$

where ψ is the angle between the wind direction and the direction of the acoustic propagation plane, and the sound speed $c_0(z)$ is approximated by:

$$c_0(z) = \sqrt{\gamma R_{\text{GP}} T(z)}, \tag{6.2}$$

with $\gamma = 1.4$ the ratio of the specific heat in air, $R_{\text{GP}} = 287$ J.kg^{-1}.K^{-1} the specific gas constant for dry air, and $T(z)$ the temperature profile in Kelvin. The temperature profile remain the same in both computation and so does $c_0(z)$. Note that reversing both the propagation direction and the wind speed profile leads to the same c_{eff} profile used in the direct and reciprocal computations. That is why a unique c_{eff} profile is plotted in subsequent figures.

The reciprocity of the WAPE code is first tested in a 2D configuration for two types of topography, and for several wind conditions (see Sec. 6.2). These wind conditions are set downwind to upwind, by varying the friction velocity u_* from -0.5 to 0.5 m.s^{-1}, and by keeping the temperature scale to $\theta_* = 0$ K. In the following we consider two 3D configurations in order to verify the reciprocity for the application to detection spaces with our N×2D method (see Sec. 6.2.4). The impedance parameters are set as in Sec. 2.4.3 for a typical snow cover with the effective thickness $e = 0.15$ m, the airflow resistivity $R_s = 20$ kPa.s.m^{-2}, the porosity $\Omega = 0.6$, and the tortuosity $q^2 = 1.6$. We detail the settings used for the validation of the reciprocal computation in Tab. 6.1.

First we test the reciprocity principle with the 2D WAPE code between two points over a real topography. These comparisons show the agreement of the direct (from a source to a receiver) and reciprocal calculations (from the receiver to the source) for a large spectrum and under different refraction conditions. The topography of the Flaine site is used as an example.

Table 6.1 − Settings for the validation of the reciprocal computation. We use the topography of Flaine and ARU locations 1 and 2 (see Fig. 2.4).

Method	2D	N×2D
Topography	ARU 1 (two directions) 1) in direct sight 2) in shadow zone	ARU 1 and 2 (all around) Cartesian grid (10×10 m)
Source/receiver	one source, one receiver	2601 grid points reference point at the center
Distance	200 m	up to 350 m (diagonal)
Atmosphere (c_{eff})	$\theta_* = 0$ K, $u_* = [-0.5 \text{ to } 0.5]$ m/s	$\theta_* = 0.05$ K, ARU1: $u_* = 0.15$ m/s, east wind ARU2: $u_* = 0.3$ m/s, south wind
Ground impedance	snow	snow
Frequency band	$[500 - 3000]$ Hz, 50 Hz step	$[500 - 3000]$ Hz, 50 Hz step

6.2.2   Case of a direct view (in 2D)

We consider a realistic slope, extracted from the DEM of the Flaine site, with source/receiver heights respectively equal to 1.5 m and 15 m to match the typical heights of a recorder and a bird in flight. The source-receiver horizontal distance is set to 200 m. The computation domains used in the direct and reverse directions are drawn in Fig. 6.2. The domains are defined in such a way that the terrain profile matches perfectly for both computations.
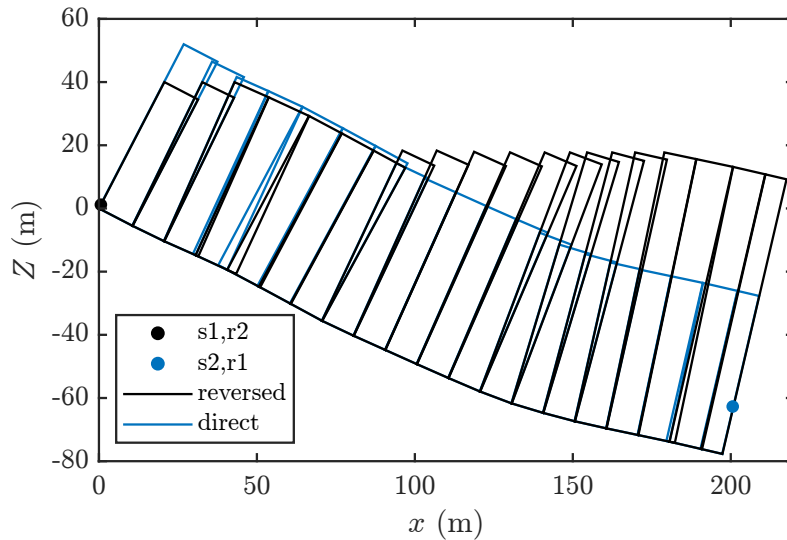
Figure 6.2 − Rectangular computation domains for reciprocal (black) and direct (blue) pressure field computation, respectively towards the right and towards the left, and reversible source/receiver positions.

The WAPE computation is first performed at 1000 Hz for a homogeneous atmosphere. The two resulting PL (propagation loss) maps are shown Fig. 6.3. The pressure field is very different between the two computations, but this is expected since the reciprocity

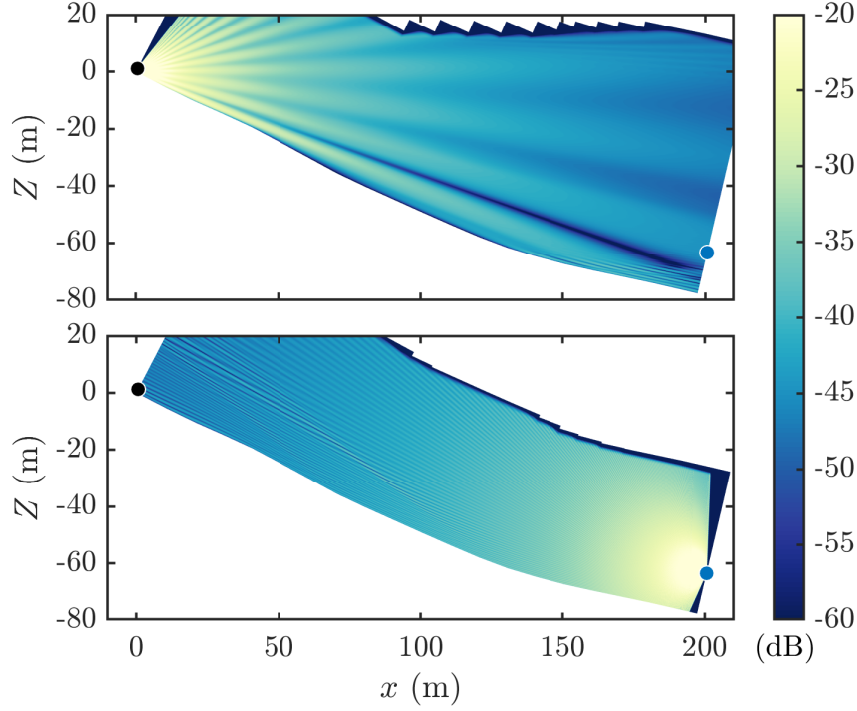principle leads to similar results only at two points.

Figure 6.3 – Maps of PL at 1000 Hz for reciprocal (top) and direct (bottom) pressure field computation, respectively towards the right and towards the left. The atmospheric condition is homogeneous with $u_* = 0$ m/s and $\theta_* = 0$ (K).

Then we perform the same computation for the frequency band [500 - 3000] Hz with a 50 Hz step, and for 5 refraction conditions. We compare in Fig. 6.4 the PL spectra at the two receivers. We see that the levels perfectly match between the direct and reciprocal computations and this on the whole frequency band [500 - 3000] Hz. Some shifts of the order of 1 to 1.5 dB are noticed at the dips locations in the spectra for $u_* = -0.5$ m/s and $u_* = -0.25$ m/s. As the interference pattern is very sensitive to the geometry, we attribute these minor errors to slightly different discretizations of the domains between the direct and reciprocal computation.

The global PL weighted according to the ptarmigan spectrum (see Fig. 2.25) are then compared (see Eq (3.43) for $\mathrm{PL_g}$ calculation). Thus we calculate the difference $\Delta\mathrm{PL}$ on the $\mathrm{PL_g}$ levels computed between the reciprocal ($\mathcal{R}$) computation from the source point (s1), and the direct ($\mathcal{D}$) computation from the s2 source point as,

$$\Delta\mathrm{PL} = \mathrm{PL_g}(\mathcal{R}) - \mathrm{PL_g}(\mathcal{D}).$$

For the five atmospheric conditions the $\Delta\mathrm{PL}$ remains between 0 dB and -0.24 dB. This shows that overall the levels are very well reproduced by a reciprocal computation for a direct view case. We will now see for a case in the shadow zone.
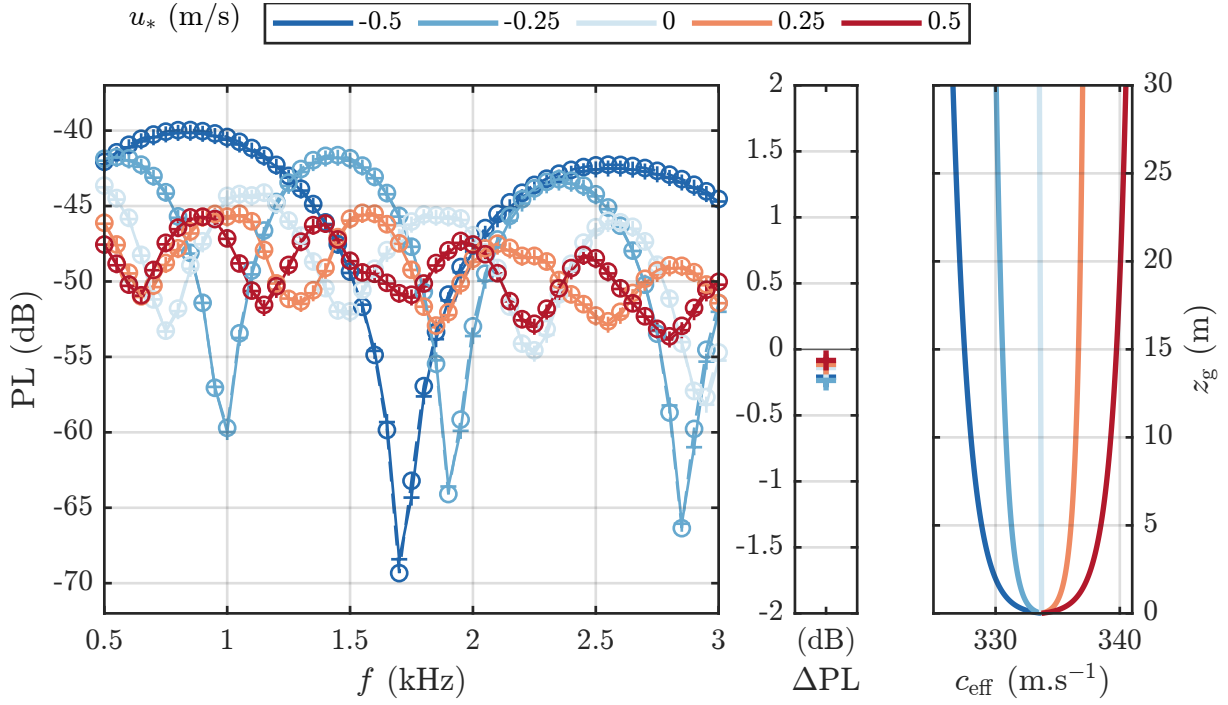
Figure 6.4 – PL spectrum in several wind conditions for reciprocal (solid line, +) and direct (dashed line, ○) pressure field computation (left), overall ΔPL weighted according to the ptarmigan spectrum (middle), and c_{eff} profiles associated (right). Refraction conditions are defined by u_* varying from -0.5 to 0.5 m/s, while $\theta_* = 0$.

6.2.3 Case of a geometrical shadow zone (in 2D)

We now consider another terrain profile, to study the case where the receiver is not directly visible from the source. As shown in Fig. 6.5, the line of sight (LOS) drawn by the green line from the source shows that the receiver is placed in the geometric shadow zone.
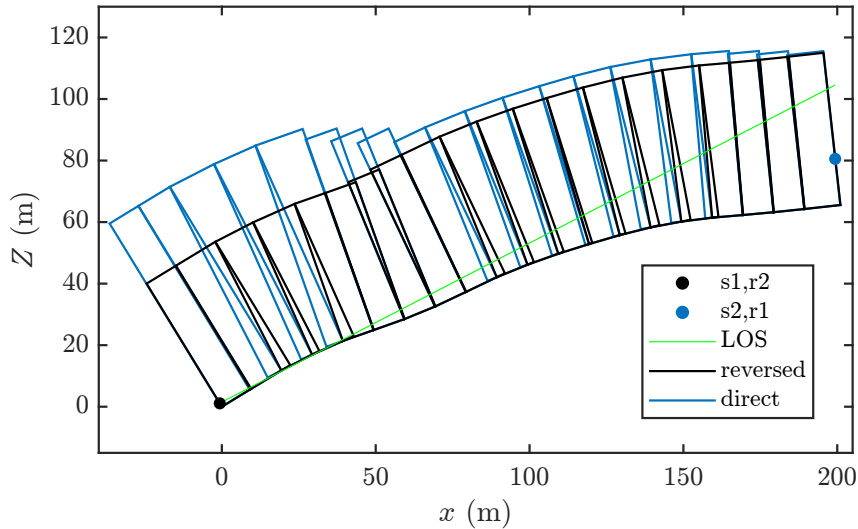
Figure 6.5 – Rectangular computation domains for reciprocal (black) and direct (blue) pressure field computation, respectively towards the right and towards the left. Reversible source/receiver positions, and LOS (line of sight) of the source.

As for the previous case, the PL maps in homogeneous condition and at 1000 Hz in
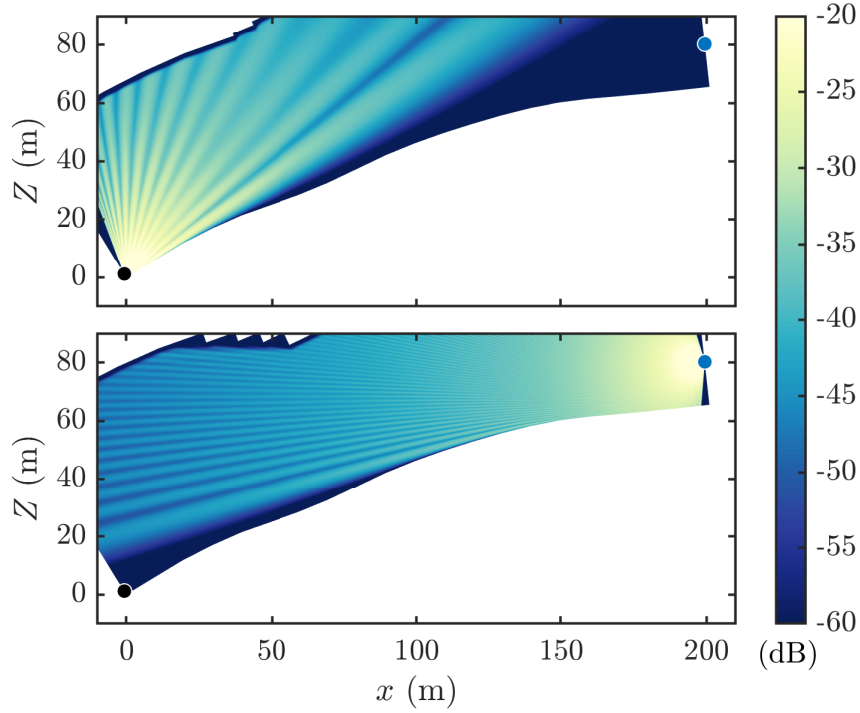
Figure 6.6 – Maps of PL at 1000 Hz for reciprocal (top) and direct (bottom) pressure field computation, respectively towards the right and towards the left. The atmospheric condition is homogeneous with $u_* = 0$ m/s and $\theta_* = 0$ K.

Fig. 6.6 shows the solution obtained for the reciprocal and direct computation. It is clear that for both directions of computation the receiver is in the shadow zone.

Then the results of the broadband computation are presented by the spectra in Fig. 6.7. For the conditions $u_* = 0$ m/s and $u_* = -0.25$ m/s, the shadow zone makes that a very small part of the energy reaches the receiver, with a PL respectively lower than -90 dB and -110 dB on the frequency band [500 - 3000] Hz. This very low energy leads to large errors with random pattern, of the order of 16 dB between the direct and reciprocal computations. These are numerical errors, which can be due to several factors. First, the discretization of the domains can lead to an incomplete convergence of the computation. Second, the phase error in the paraxial approximation is dependent on the angle to the direction of propagation (Ostashev et al., 2020). Thus, the direct and reciprocal computations may result in different phase errors in the interpolation of the computation domains. Errors could also be caused by the computation in reverse order of the diffraction on the geometry. Third, it may be related to the non-reflection conditions. The waves considered in one direction are not completely reproduced in the other direction, so the non-accounting of backscattering impacts the numerical solution. As shown by Blairon (2002), the fraction of backscattered energy is negligible for limited slopes, and frequencies of a few hundred hertz. However, it seems that in areas where the pressure field is very weak, this approximation is no longer valid.

Nevertheless, by comparing the ΔPL, it appears that the error on the global level re-

171

mains below 2 dB. In the case of a positive wind scale (0.25 and 0.5 m/s), the atmospheric refraction redirects energy towards the ground, which induces higher PL values at the receivers. The corresponding spectra, which match better between direct and reciprocal computation, also show a smaller absolute ΔPL value of about 0.19 dB.
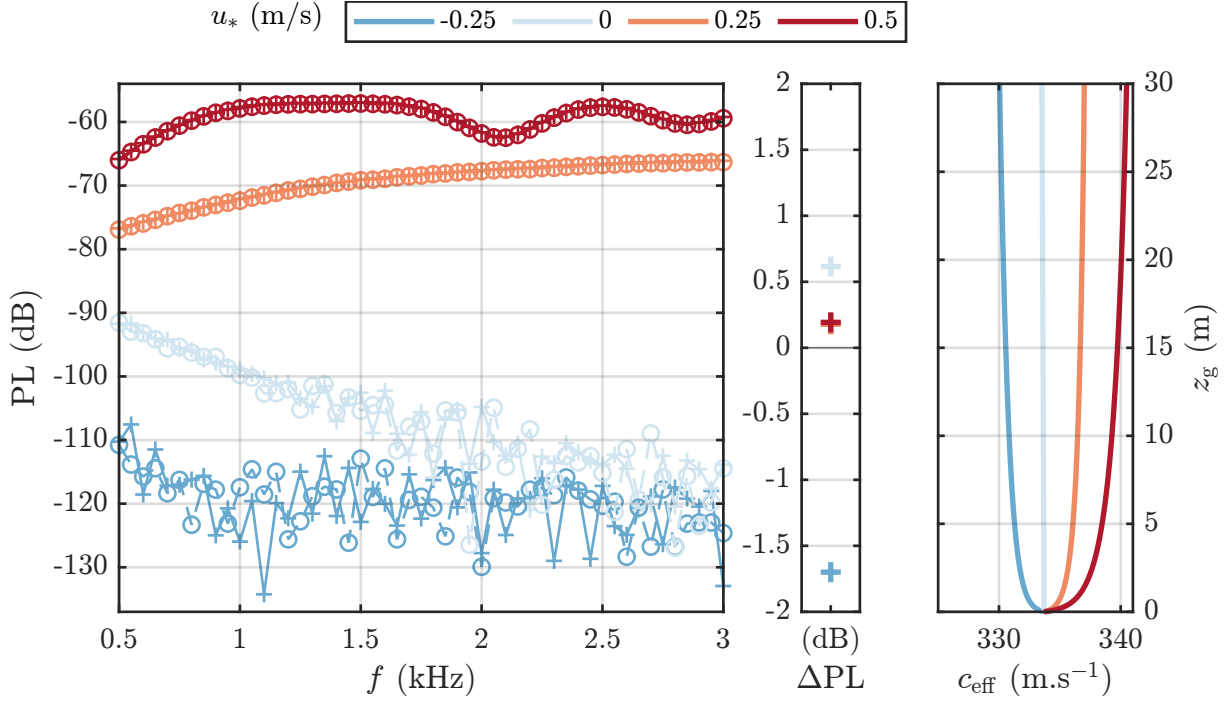

Figure 6.7 – PL spectrum in several wind conditions for reciprocal (solid line, +) and direct (dashed line, ○) pressure field computation (left), overall ΔPL weighted according to the ptarmigan spectrum (middle), and c_{eff} profiles associated (right). Refraction conditions are defined by u_* varying from -0.25 to 0.5 m/s, while $\theta_* = 0$ K.

The match between direct and reciprocal computation is therefore very satisfactory at long range, both in direct view and geometrical shadow zone cases, when the atmospheric conditions are favorable to propagation. For receivers receiving very low energy, mismatches can be noted on the spectra. However, if we consider a practical case, the pressure levels involved in these errors are so low, that they are not significant from a propagation point of view. Indeed, areas receiving such low acoustic energy are considered to be outside the detection space.

6.2.4 Reciprocity for N×2D mapping using WAPE

In this second phase of validation, we show the equivalence of the direct and reciprocal calculations for a real 3D topography. We consider the example of two ARUs on the Flaine site, with their locations detailed in Fig. 2.4 (1 and 2). The direct and reciprocal computations are performed as depicted in Fig. 6.8 for each 2601 receivers distributed on a 10 m × 10 m grid in a 500 m square. For direct computations the single receiver (the reference position simulating the ARU) is in the center of the grid, and for reciprocal

computations the single source is in the center. The height of the grid sources/receivers is set at 15 m above the ground, and the reference source/receiver at 1.5 m.
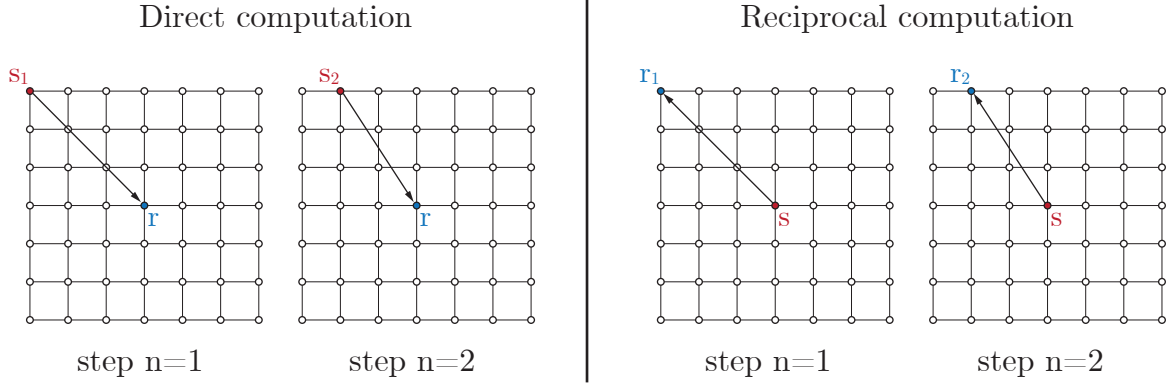

Figure 6.8 – Schematic diagram of the N×2D reciprocal computation used for validation tests.

As previously done in 2D, the differences ΔPL are then calculated for the entire grid on the PL_g levels computed between the reciprocal ($\mathcal{R}$) computation from one source point (at the ARU position towards every receivers), and the direct ($\mathcal{D}$) computation from multiple source points (each towards the ARU position). At position 1, on a moderate slope, the direct and reciprocal computations presented in Fig. 6.9 provide a quite equivalent result for the 2601 receivers.
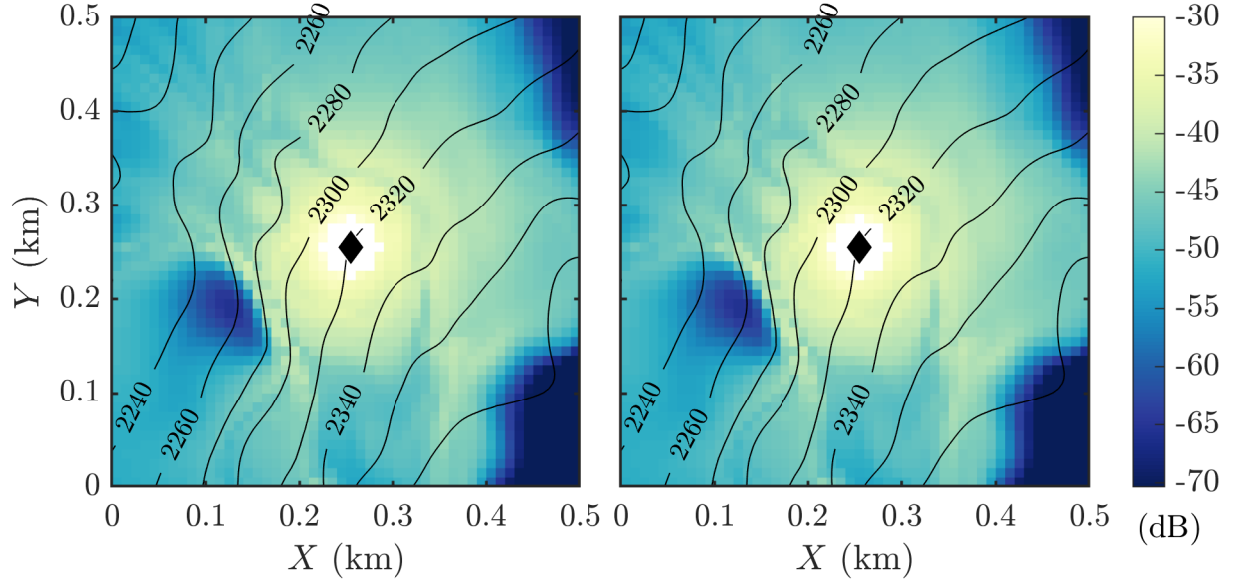
Figure 6.9 – PL for direct (left) and reciprocal (right) computation for the ARU at the position 1, with the wind coming from east, $u_* = 0.15$ m.s^{-1}, and $\theta_* = 0.05$ K. Overall PL weighted according to the ptarmigan spectrum (PL_g).

The computed ΔPL map for the ARU at position 1 is shown in Fig. 6.10, and its values are between -0.8 dB and 0.6 dB. These values appear in the first 50 m around the source. This area can be considered as part of the near field in low frequencies (the far field is defined by $k_0 R \gg 1$), and therefore present expected errors due to WAPE

paraxial approximation. Moreover, as the source of the direct calculation is located at a height of 15 m, the first reflections on the ground which are important for a close receiver, are located outside the angle of validity of the WAPE calculation. Apart from these few points, all delta values are between -0.4 and 0.4 dB, indicating that the reciprocal computation is valid for a rough mountain terrain.
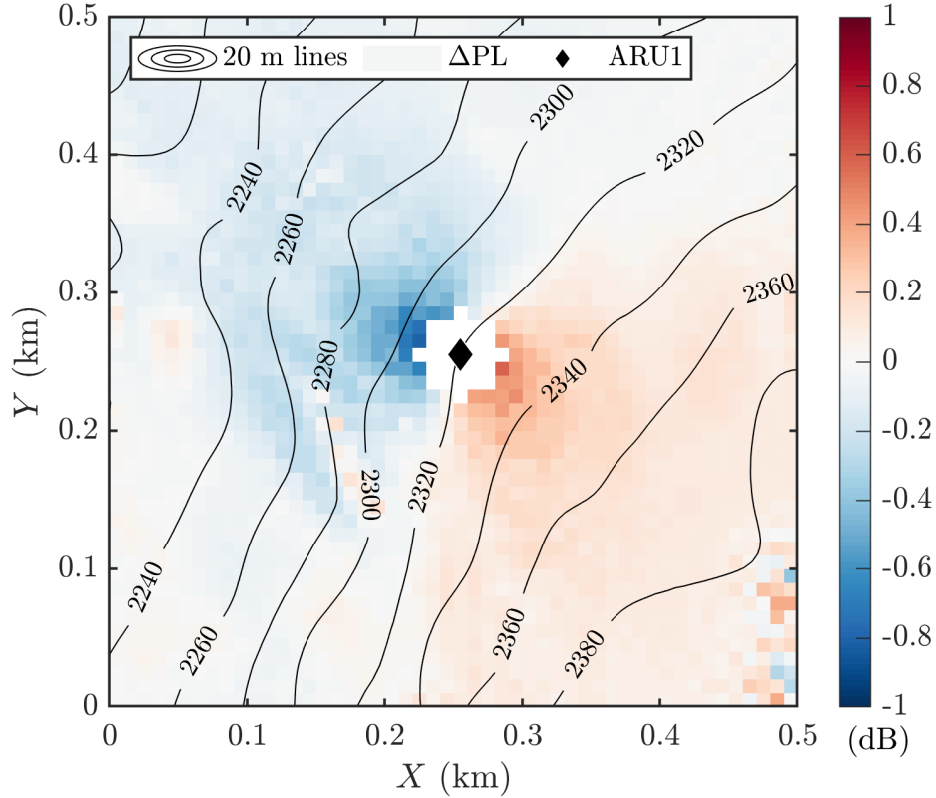

Figure 6.10 – ΔPL between reciprocal and direct computation at the ARU in position 1, calculated from overall PL weighted according to the ptarmigan spectrum (PL_g).

Another ARU position is taken as an example, this time at point 2, where the slope is steeper. The PL results of the direct and reciprocal computations are presented in Fig. 6.11. We see that a large shadow zone covers the plateau located 30 m above the recorder. The PL levels are -100 dB or lower due to the topography. These very low levels lead to significant errors, as can be seen in Fig. 6.12 which shows the ΔPL. In the south east corner that present a wide shadow zone, the variations of ΔPL are between -5.2 dB and 2.9 dB with a random error pattern. In the same way as for the 2D case in the shadow zone, we note that these disparities are not significant for the detection space, because the levels involved are far below the thresholds that are subsequently set to define the detection spaces.

Reciprocity tests in two and three dimensions for different topographies and refraction conditions show that a reciprocal computation can robustly account for propagation from a receiver to potential sources. This method brings an advantage in terms of computation cost to determine the detection space of an ARU over any topography and for various
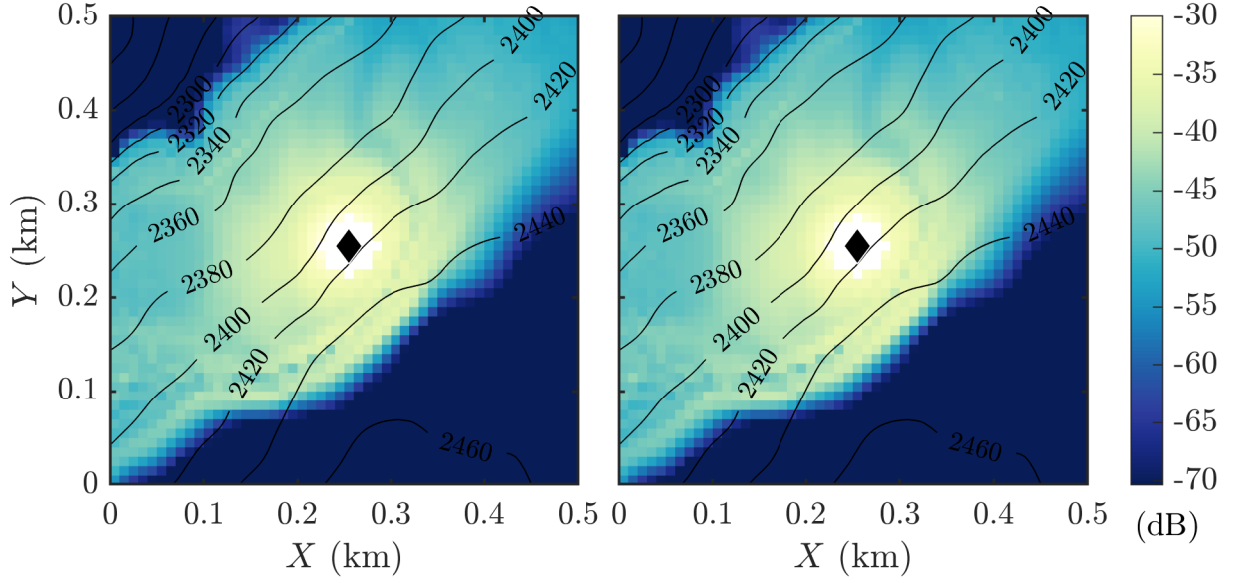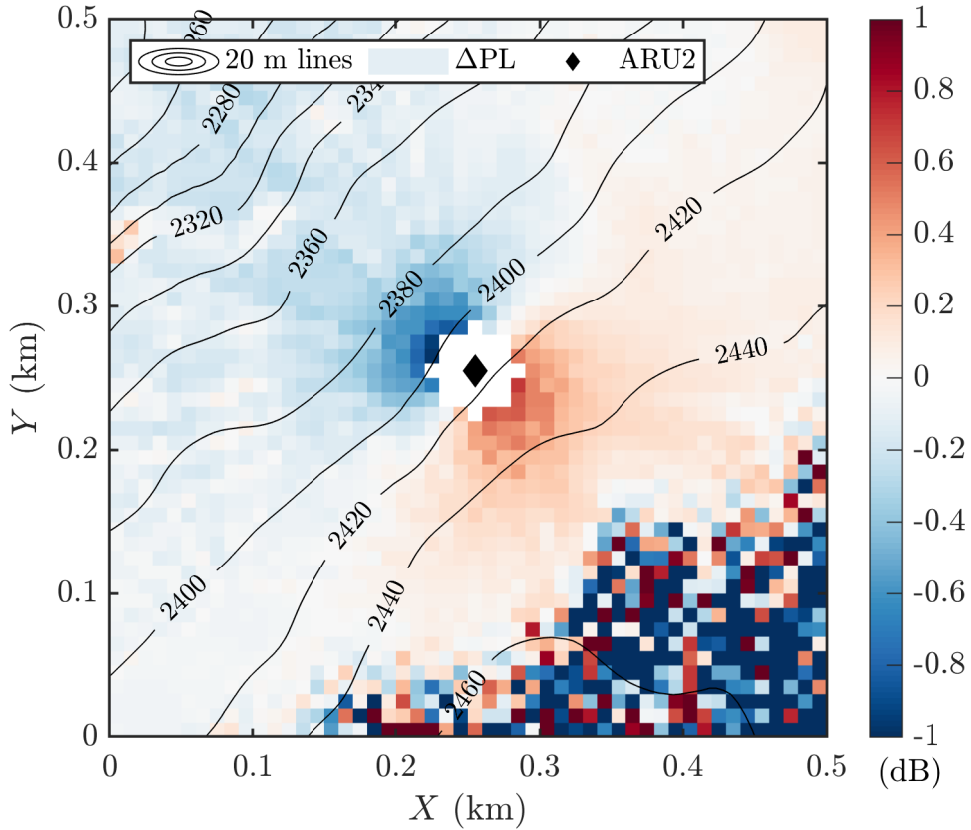
Figure 6.11 – PL for direct (left) and reciprocal (right) computation for the ARU at the position 2, with the wind coming from east, $u_* = 0.3$ m.s^{-1}, and $\theta_* = 0.05$ K. Overall PL weighted according to the ptarmigan spectrum (PL$_g$).

Figure 6.12 – ΔPL between reciprocal and direct computation at the ARU in position 2, calculated from overall PL weighted according to the ptarmigan spectrum (PL$_g$).

meteorological conditions (see comparison in Tab. 6.2).

The level disparities that were found in the very low energy areas have no impact on the determination of detection spaces. Indeed, since the PL values involved are equal

to or less than -100 dB, these zones fall outside the detection spaces according to our definition of the detection space threshold. This method is then used to finely determine the detection spaces specific to the three ARUs deployed in Flaine during the spring of 2021.

6.3 Application to detection spaces

This application aims at evaluating the PAM method applied since a few years on the Flaine site. By collecting both meteorological data and ARU audio recording on the site during the spring 2021, characterizing the sensitivity of the SM4 recorders, and evaluating the performance of the LagoNet detection algorithm, it is possible to estimate the DS of each ARU and each recording period. The detection space data can then be used to obtain a proxi of the abundance from the vocal activity.

6.3.1 Methods

We recall that the DS (detection space) is the area in which a receiver can detect an emitted call knowing its source level (SL). It is driven by the same parameters as the active space, and it is therefore possible to define its limits in the same way using SL, PL, BN (background noise) and SNR (signal-to-noise ratio) at the receiver position. A threshold of the PL is defined according to the other three parameters to fix the limit of the DS as the area where,

$$\mathrm{PL} \geqslant \mathrm{BN} + \mathrm{SNR} - \mathrm{SL}. \tag{6.3}$$

The detection threshold (DT) is defined as $\mathrm{DT} = \mathrm{BN} + \mathrm{SNR}$ at the receiver position. From the LagoNet (detection algorithm described in Sec. 2.8) performance curve, visible in Fig. 2.30, the SNR threshold is set at 0.9 dB for the detection space considering 95 % of songs detected in the background noise. The SL is set to 85 dBSPL following the estimation based on sonometer measurements on ptarmigans (see Sec. 2.7). To take into account the frequency content of ptarmigan song, the PL computation is performed for the frequencies of its two main formants, at 1100 and 2200 Hz. The global PL computed according to Eq. (3.43) is then used to determine the DSs.

Now we present the various measurements made over the period from May 21 to June 23, 2021. SM4 recorders (Wildlife acoustics) are positioned at three locations on the site referenced in Fig. 2.4. They are placed on a stake at a height of 1.5 m from the ground. They perform scheduled recordings each morning between 1h10 before and 10 minutes after sunrise. Each of these recordings is cut into 8 samples of 10 minutes, and the LagoNet algorithm is used to provide for each sample a BN value (according to L_{90}) and a vocal activity (VA) duration in seconds. The determination method of VA and BN is detailed in Sec. 2.8.

The automated weather station (AWS) installed in the central zone of the site (on the plateau) provides data of wind speed and direction, temperature, humidity and atmospheric pressure every minute (see AWS location Fig. 2.4). The sensors installed on this AWS are listed Sec. 2.5.1. These meteorological data are then averaged according to 10-minute clusters to match the audio recording periods, and then used to determine temperature and wind speed profiles $(T(z), U(z))$ based on the Monin-Obukhov similarity theory (MOST) (Monin & Obukhov, 1954) (see Sec. 2.5.2). This leads to an average sound speed profile c_{eff} for each sample, based on the average wind direction according to Eq. (4.11). The average atmospheric pressures and relative humidity are also used for the calculation of the atmospheric absorption coefficient (see Sec. 1.3.2) and snow impedance (see Sec. 2.4.2). Considering that snow covers most of the site at this time of year, the impedance parameters are set according to previous measurements with the effective thickness $e = 0.15$ m, the airflow resistivity $R_s = 20$ kPa.s.m^{-2}, the porosity $\Omega = 0.6$, and the tortuosity $q^2 = 1.6$ (see Sec. 2.4.3).

6.3.2 Results

An example of two estimated DS is shown in Fig. 6.13 for a high and low BN. It is observed that the three DSs are not circular, have a very different shape, and are constrained by the topography. For example, DS 2 has an elongated shape due to the position of ARU 2 above a steep slope. However, a very low BN makes it possible to listen to the zone below (see Fig. 6.13 right). Furthermore, we see that the DSs overlap significantly in the case of a low BN. This overlap may induce pseudo-replication of VA data between sampling areas.

The temporal evolution of the vocal activity (VA) in seconds, the BN citerion of L_{90} and the DS's estimated areas for the 3 ARUs are summarized in Fig. 6.14. The song detections are clearly more frequent for the ARU 3 than for the ARU 2, and the ARU 1 detects very few songs. This may be due to the variable presence of birds around the recorders, but also to the position of the recorders in relation to the landscape, as well as their exposure to the wind. Indeed, depending on the position, a recorder will not have the same detection area, and moreover, its exposure to the prevailing wind will determine the current levels of BN it measures. The BN can drastically reduce the SNR and therefore the sampling area. Indeed the L_{90} is significantly higher for ARU 1 on most days, which may partly explain its low detection rate of ptarmigan songs.

The DS's areas computed for each 10 min period are also plotted in km^2. The mean areas of the three ARUs over the entire period are respectively equal to 0.67, 0.80, and 1.43 km^2 (with N = 256 samples for each ARU). These statistics are summarized in Tab. 6.3. The great variability in area can be explained with the L_{90} and the meteorology variations, but also with the respective position of the ARUs on topography.
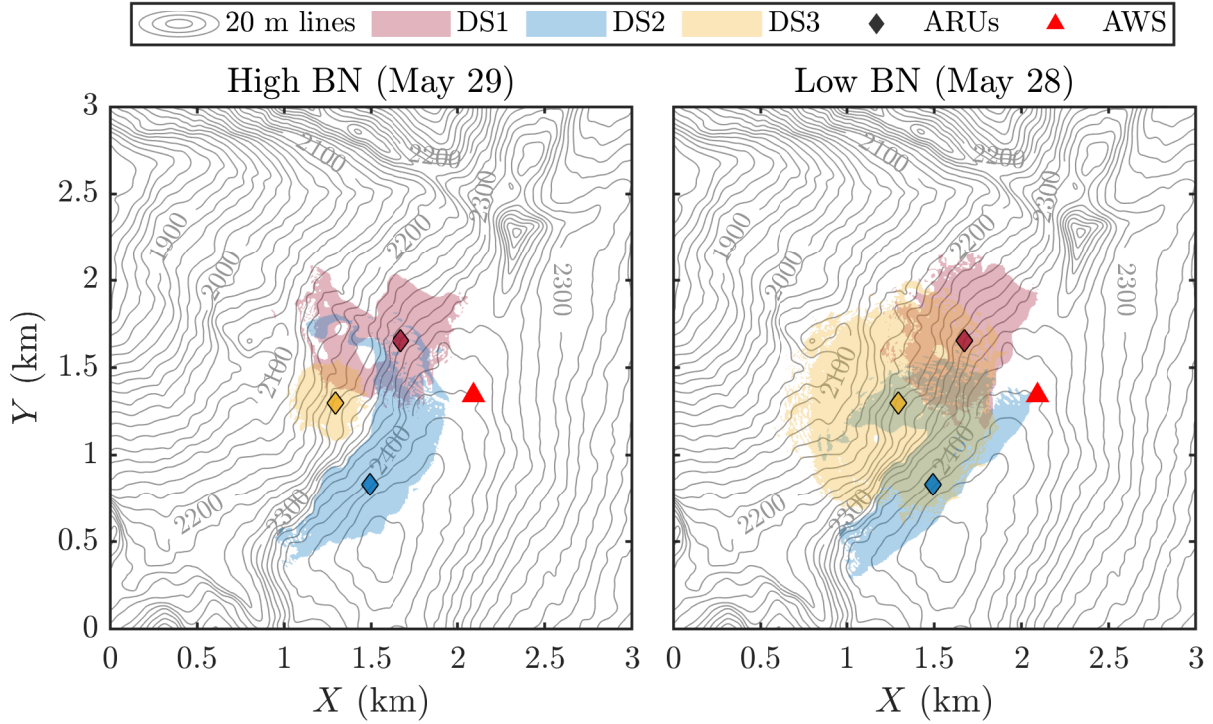
Figure 6.13 − Detection spaces of ARUs on the Flaine site for two days with high BN on May 29 (left), and with low BN on May 28 (right): BN levels at the ARU 1, 2 and 3 are respectively (29, 25 and 36 dBSPL), and (22, 13 and 14 dBSPL), and the associated overlap rates are 15 % and 41 %. Note that the weather is different between these two days.

In order to quantify the real ptarmigan activity on the site in a global way, we define a more relevant indicator than the raw VA detected. The DSs estimate is used to create this indicator, the vocal activity per unit area VA/Area (s/km^2), which leads to an activity density. Fig. 6.15 presents the respective distributions of the two indicators. As the DS areas are distributed around 1 km^2, the distributions of VA and VA/Area look similar overall, with a slight reduction on the ARU3 boxchart. VA is mainly comprised between 0 and 10 seconds per 10-minute period, with maximums around 30 seconds. This indicates that VA is relatively low in ptarmigan even during the dawn chorus, compared to the activity in passerines for example (Pérez-Granados *et al.*, 2019b). This is due to the low density of ptarmigan males induced by the size of their territory, and also to their discreet character.

To compare the robustness of these two indicators, we standardize (reduced centered variable) the two quantities, leading to *va* and *va/area* (dimensionless). Then we compare their interquartile range (*iqr*) for each ARU.

Fig. 6.16 shows that the dispersion of the area-related vocal activity (*va/area*) is narrower than that of the raw vocal activity (*va*) for all three ARUs. This second indicator therefore converges to a lower variability. We conclude that its values are more representative of the actual activity in the vicinity of each ARU.

We now focus on the interest of the DS for refining the sampling. The sampling
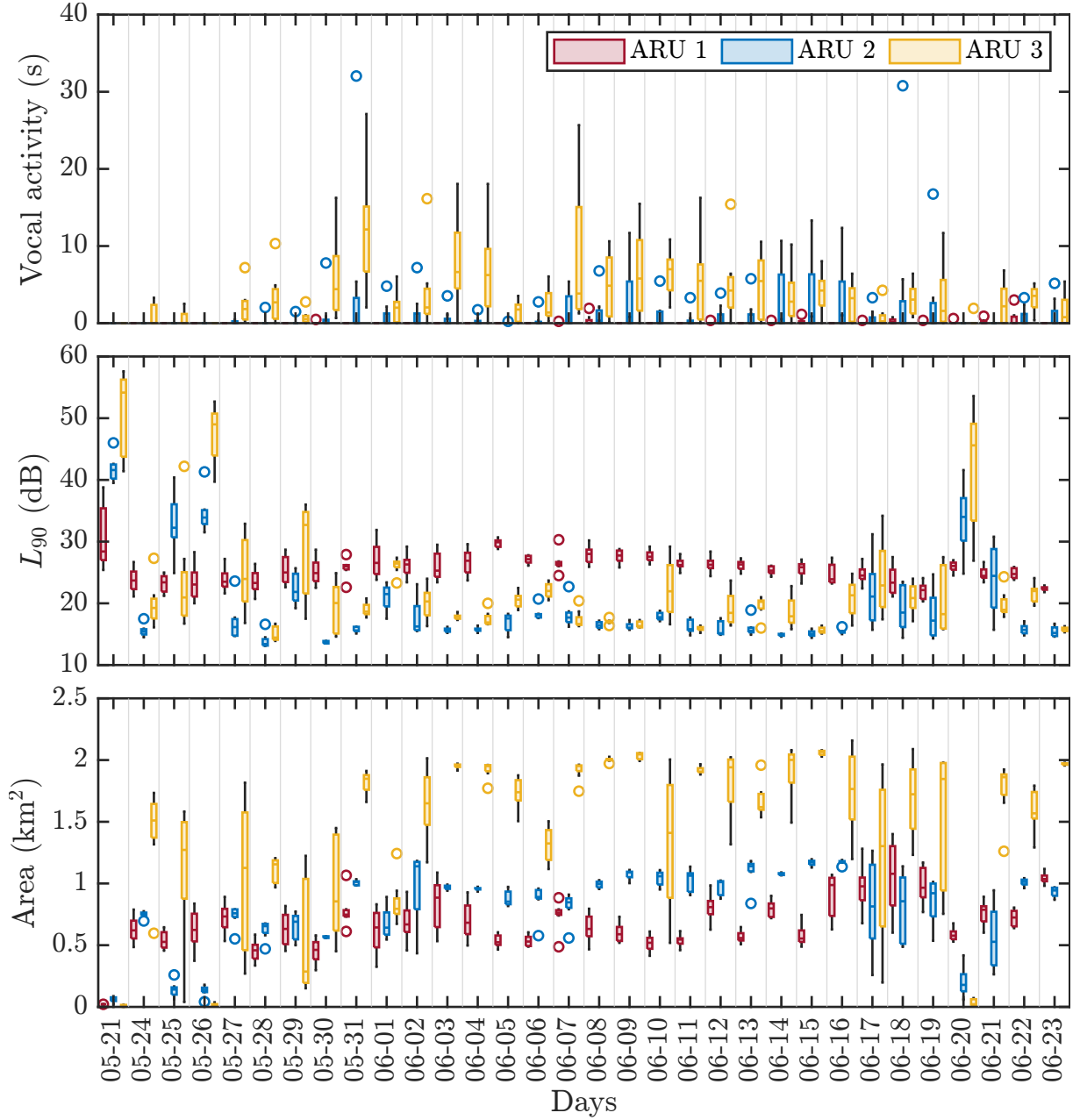
178

Figure 6.14 – Dispersion of the vocal activity (VA), the background noise L_{90}, and the estimated detection space area, during the recorded morning period (8×10 min). VA is plotted in seconds for the three ARUs according to the day (number of non-zero data: 20, 66, 194 respectively for ARUs 1, 2 and 3). Box plots display the median (inner line) and first and third quartiles (lower and upper hinges, respectively), whiskers indicate 1.5 times the inter-quartile range from the hinge, and circles represent outliers.

effort can thus be quantified spatially and temporally. The values of the entire DS areas, calculated as the union of the three DS, and overlaps per day are plotted in Fig. 6.17 in increasing order of area. Note that in supplementary material Fig. 6.19 presents the whole data set in the same way, and Fig. 6.18 presents the data by day. It can be seen that 90 % of the total area that could be sampled over the period is reached after 19 days. Given the difficulty of predicting weather conditions, and thus detection areas in real time during a census campaign, this time indication can be used to set the duration
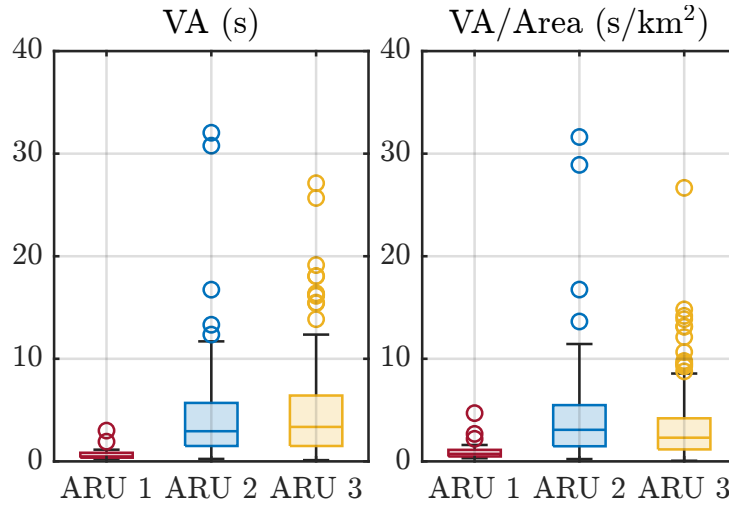
Figure 6.15 − Distribution of vocal activity indices on the Flaine site for the three ARUs locations: estimated vocal activity from CNN (VA), estimated vocal activity divided by the estimated sampled area (VA/Area). (number of non-zero data: 20, 66, 194 respectively for ARUs 1, 2 and 3)
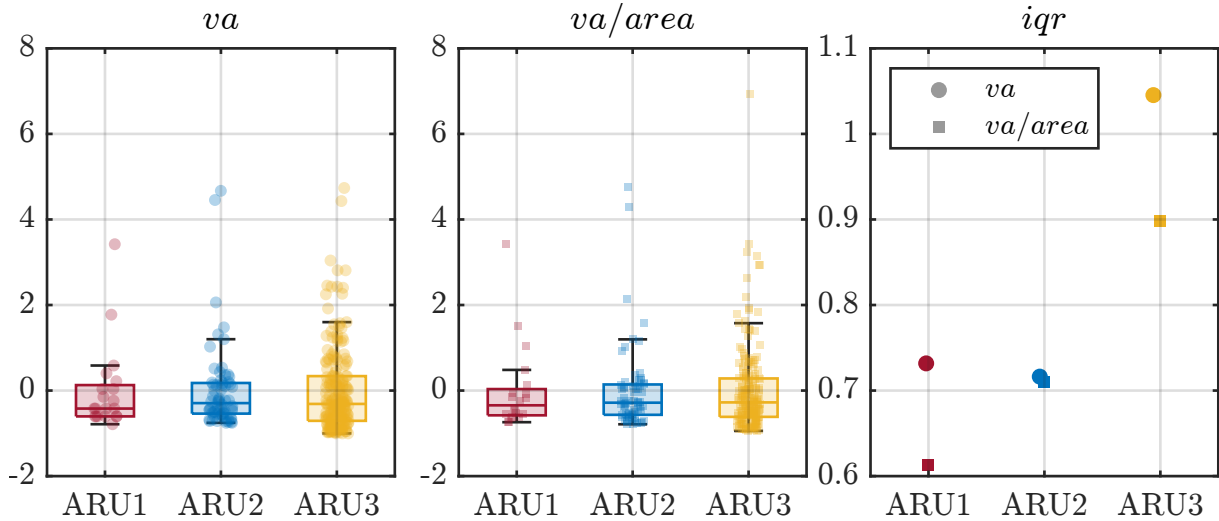

Figure 6.16 − Dispersion of the standardized abundance indexes (va, and $va/area$) according to the three ARUs locations, and associated plot of their inter-quartile range. Box plots display the median (inner line) and first and third quartiles (lower and upper hinges, respectively), whiskers indicate 1.5 times the inter-quartile range from the hinge, and markers represent data.

of an on-site measurement campaign. It is very likely that after this number of days, the gain in spatial sampling is reduced, as the sampled area reaches a plateau.

In addition, we see that the percentage of DS overlap is significant and can reach 56 % on some days. This overlap corresponds to the overlapping area of at least two of the DSs. This means that songs recorded by two or three ARUs could potentially come from the same bird if it sings in this overlapping area. This situation leads to pseudo-replication of data. Therefore, knowledge of this overlap can provide a tool to estimate the proportion of vocal activity common to several ARUs. We see that overlap areas are highly variable between ARU pairs.
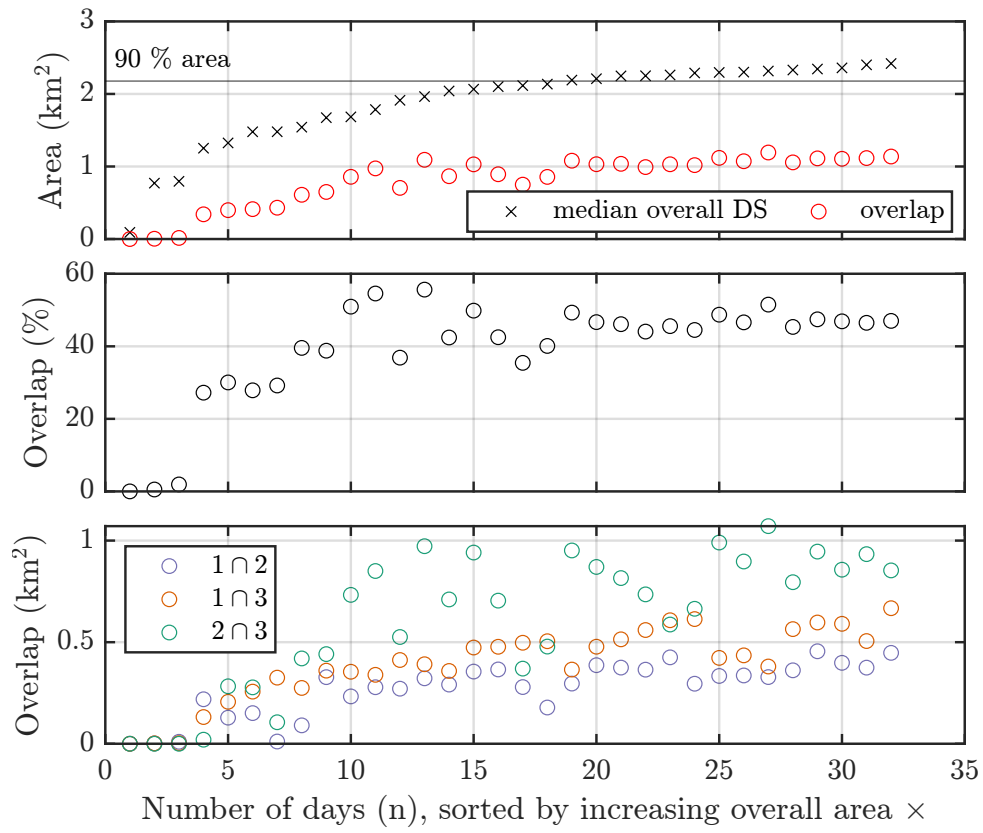
Figure 6.17 – Daily median area of the union of DSs sorted by ascending order, and overlap (top), overlap percentage of at least two DSs (middle), and overlap area between pairs of ARUs (bottom).

6.4   Discussion

In the context of passive acoustic monitoring, it is crucial to relate the acoustic metrics to a sampling area in order to standardize the protocols (Sólymos *et al.*, 2013; Darras *et al.*, 2018), according to environmental conditions of the habitat, topography, meteorology and background noise (MacLaren *et al.*, 2018; Castro *et al.*, 2019; Haupert *et al.*, 2022). Indeed, although recommendations on the temporal scheduling and placement of ARUs have been published (Aide *et al.*, 2013; Pieretti *et al.*, 2015; Shonfield & Bayne, 2017; Stowell *et al.*, 2019), it is necessary to develop a methodology to estimate the detection spaces. To generalize the detection space computation to a heterogeneous and three-dimensional environment, we use a propagation code based on the parabolic equation. We now discuss the results related to the three questions raised in the introduction of this chapter (see Sec. 6.1), and the perspectives of our approach.

Our WAPE code is based on wave physics and simulates the propagation by taking into account topography, ground type, and meteorology in an explicit way. This provides a methodological advantage compared to semi-empirical approaches implemented in "black box" codes such as SPreAD-GIS toolbox (Reed *et al.*, 2009, 2012) which is still widely used in ecoacoustic applications (Raynor *et al.*, 2017; Piña-Covarrubias *et al.*, 2019). The WAPE code enables to use the reciprocity principle to quickly compute the detection space of a receiver. We compare in Tab. 6.2 the computational costs related to a direct computation performed for a grid of sources (as depicted in Fig. 6.8), and to a reciprocal computation performed in cylindrical coordinates as described in Sec. 3.3. This comparison of methods indicates that the reciprocal computation requires on average half the time of the direct computation. The reciprocal computation is also simpler to implement because of the use of cylindrical coordinates. With an angular step of 2°, only 180 computations are required compared to 2601 for the direct method. Another advantage of the reciprocal computation is to provide a much finer mesh of receivers (potential sources) on the computation planes, and thus a more detailed DS estimation. Note that the reciprocal computation would be even more interesting in the perspective of using a full 3D code, because this would imply a prohibitive time with a direct approach.

Table 6.2 − Computational cost comparison in terms of CPU hours between direct and reciprocal DS computation on the Flaine site for ARU locations 1 and 2 (see Fig. 2.4). Results are presented for the direct and reciprocal methods that use a different coordinate system.

		Direct method	Reciprocal method
Recorder	Coordinates	Cartesian grid (10×10 m)	Cylindrical (dθ = 2°, dr = 1 m)
ARU 1		426 h	186 h
ARU 2		458 h	207 h
Mean		442 h	196 h

We showed that DS can be robustly computed using a reciprocal propagation computation from the recorder location. Indeed, the deviations of the global levels from the direct computation remain minimal for different refraction conditions in direct view with errors lower than 0.5 dB, as well as in shadow zone with errors lower than 2 dB. Larger errors of the order of -5.2 dB to 2.9 dB were found in shadow zones far from the source and for PLs below -100 dB. Since these values are outside the detection spaces for bioacoustic applications given the SL values of biological sources and outdoor BN levels, these numerical errors do not to affect the DS boundaries. These results show that the reciprocal method provides a precise image of the DS specific to each recorder and to each sampling period. With respect to our first question, we can now conclude that the WAPE method ensures a valid application of the reciprocity principle.

Regarding the second question, we now focus on the variability of DS and its importance for the calculation of abundance indices. We show that DS is not circular and that it varies with time and according to the position of the recorder, similarly to the AS (Guibard *et al.*, 2022). It is therefore crucial to take this variability into account in the sampling plans and in the data analysis, which was not done until now, as the DS was considered as circular and varying only according to the habitat, the species and the background noise (Darras *et al.*, 2018; Haupert *et al.*, 2022).

The DS variability implies that the effective sampling depends on environmental conditions that change over time, and is therefore responsible for part of the VA dispersion observed in our study. Thus, we took into account the sampling area related to each period and measurement location to calculate a vocal activity density (VA/Area). This procedure enables to reduce the variability of the metric used, especially for recorders that detect strong and constant vocal activity. The significance of this result can be nuanced, however, by the fact that density is low in this species, and there is a lot of movements during the morning chorus with display flights, and wind is highly variable even during a 10-minute measurement period. It would be of great interest to confirm our results by studying the vocal activity of other species, in different habitats, and with wider spatial sampling involving many ARUs. Overall we have shown that the detection space computation provides important information on the area associated with the acoustic indices derived from automated recordings (Sueur *et al.*, 2014; Sánchez-Giraldo *et al.*, 2020). This procedure can be used, for example, with an individual recognition algorithm (Marin-Cudraz *et al.*, 2019) to accurately determine the abundance (i.e. the number of individuals) over a given zone.

The results of our application on the Flaine site lead to a discussion of our third question concerning the refinement of acoustic sampling in PAM protocols. The knowledge of the actual area sampled at each time period provides crucial data for standardization in long-term monitoring. Indeed, it is possible to unify the sampling effort afterwards (Wood *et al.*, 2021) by selecting the measurement days that maximize the area for each

recorder. In addition, it is possible to obtain a preliminary estimate of the required effort to ensure the proper survey of a given zone. On the spatial scale, the detection spaces provide information on the overlap of the samples. The overlap calculation is used to quantify the theoretical pseudo-replication rate of the data. It can be used to weight the acoustic metrics obtained at each ARU and thus unify the spatial sampling performed by a recorder network. Overall, the detection spaces make it possible to predict a sampling plan on a spatial and temporal scale (Skalak *et al.*, 2012). Their estimates are essential to support recommendations on the timing and positioning of ARUs (Aide *et al.*, 2013; Pieretti *et al.*, 2015; Shonfield & Bayne, 2017; Stowell *et al.*, 2019). By optimizing the position of the recorders beforehand (Piña-Covarrubias *et al.*, 2019; Goetschi *et al.*, 2022) and limiting the recording time to that necessary to sample the target zones (Pieretti *et al.*, 2015), a census supervisor can refine acoustic surveys in space and time. Moreover this optimization leads to minimize the costs related to the deployment of ARUs on a physically informed basis, while maintaining sampling meaningfulness for the focal species. A numerical study prior to a measurement campaign would help to find trade-offs between financial cost, number of ARUs and size of area surveyed, and number of census days.

It has been shown that in temperate mountain habitats, a combined procedure using point count and ARUs could significantly increase the efficiency and accuracy of a counting protocol (Drake *et al.*, 2021). We argue that we develop a reliable method to identify gaps and overlaps in sampled areas, that makes possible to reduce sampling biases (Anderson, 2001; Bonar *et al.*, 2011). The detection space computed from the physical parameters of propagation condition is not subject to the biases of distance sampling methods (Van Wilgenburg *et al.*, 2017). It is therefore a robust criterion for the comparison of different acoustic monitoring campaigns. Nevertheless, it requires the acquisition of a sufficient and reliable volume of data on topography, ground type and weather. This effort, added to that of numerical modeling, can however pay off to facilitate later analysis and make conclusions more robust.

This deterministic method of DS computation can then be integrated into a broader detection probability calculation, which considers the spatial and temporal behavior of the species and its preferential habitats, to develop a robust acoustic monitoring protocol (Yoccoz *et al.*, 2001). It could include a probability distribution of the background noise levels during the sampling period and the detection algorithm performance function of SNR (Knight *et al.*, 2017; Haupert *et al.*, 2022). Moreover, it could be coupled with a occupancy prediction modeling (Rappaport *et al.*, 2020), as previously done in ptarmigan using distance sampling (Pedersen *et al.*, 2012). Such an integrated model would be a very effective tool to inform sampling plan of biodiversity survey and to assist in the management of protected areas.

6.5 Supplementary material

Tab. 6.3 is related to Fig. 6.14 and details the statistics of vocal activity, background noise and DS area for the three ARUs. It distinguishes between the values calculated for the full group of samples, and for the group excluding the samples with zero speech activity. This table is cited Sec. 6.3 and the discussed values are bold type.

Table 6.3 – Summarized statistics on vocal activity, background noise and detection space area of the three ARUs: all samples (N = 3 × 256 = 768), and excluding VA= 0 (N(ARU 1) = 20, N(ARU 2) = 66 and N(ARU 3) = 194, leading to N = 280).

	ARU	All samples			Excluding VA= 0		
		VA	L_{90}	Area	VA	L_{90}	Area
		(s)	(dBSPL)	(km^2)	(s)	(dBSPL)	(km^2)
mean	1	0.06	25.6	**0.67**	0.76	25.2	0.77
	2	1.20	19.5	**0.80**	4.66	16.5	0.98
	3	3.66	22.5	**1.43**	4.83	19.9	1.58
SD	1	0.27	2.6	0.23	0.66	1.9	0.21
	2	3.59	7.1	0.32	5.86	2.7	0.19
	3	4.59	9.3	0.65	4.71	4.3	0.49
min	1	0	20.0	0.02	0.24	20.3	0.52
	2	0	13.1	0.02	0.24	13.2	0.26
	3	0	13.9	0.00	0.12	13.9	0.07
max	1	3.00	38.8	1.40	3.00	28.0	1.26
	2	32.04	46.0	1.27	32.04	31.2	1.19
	3	27.12	57.6	2.16	27.12	35.7	2.16
median	1	0	25.7	0.64	0.48	25.6	0.71
	2	0	16.3	0.92	2.94	16.1	1.01
	3	2.04	19.6	1.66	3.36	18.9	1.76
iqr	1	0.00	3.1	0.26	0.48	2.6	0.28
	2	0.30	5.3	0.41	4.20	2.0	0.18
	3	5.16	6.7	0.80	4.92	5.4	0.65
mode	1	0	26.1	0.02	0.36	23.4	0.64
	2	0	15.7	0.56	3.30	14.8	0.57
	3	0	16.1	1.91	0.78	16.1	1.91

Fig. 6.18 is related to the data of Fig. 6.17 but displays the areas and overlap for all samples in chronological order.

Fig. 6.19 is related to the data of Fig. 6.17 but displays all samples by ascending order of the overall DS area.

We can observe on Fig. 6.20 the increase of the overlapped area according to the total
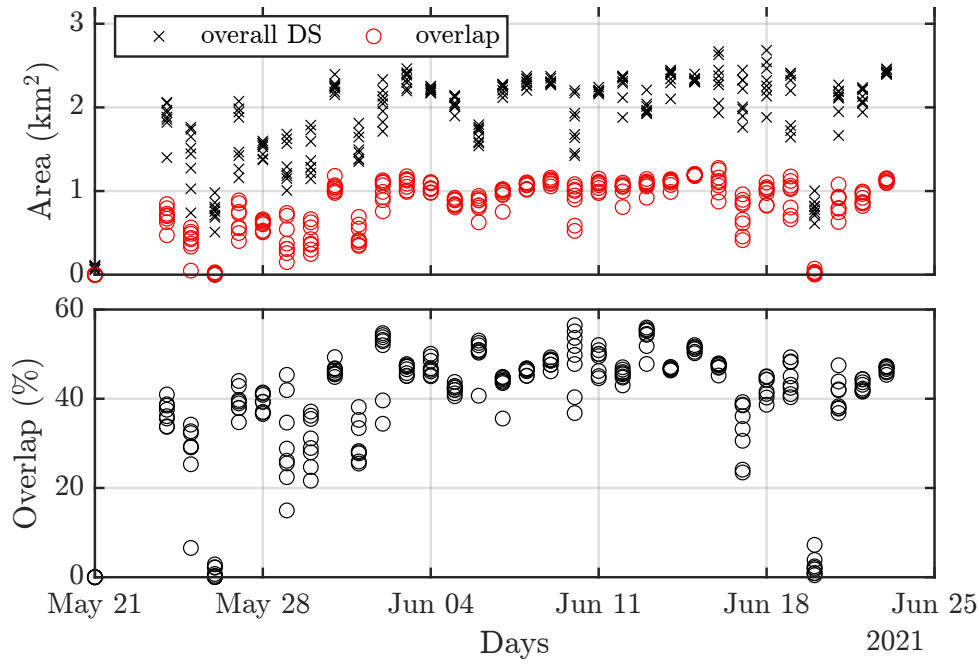
Figure 6.18 – Area of the union of DSs according to the day (top), and overlap percentage of at least two DSs (bottom).
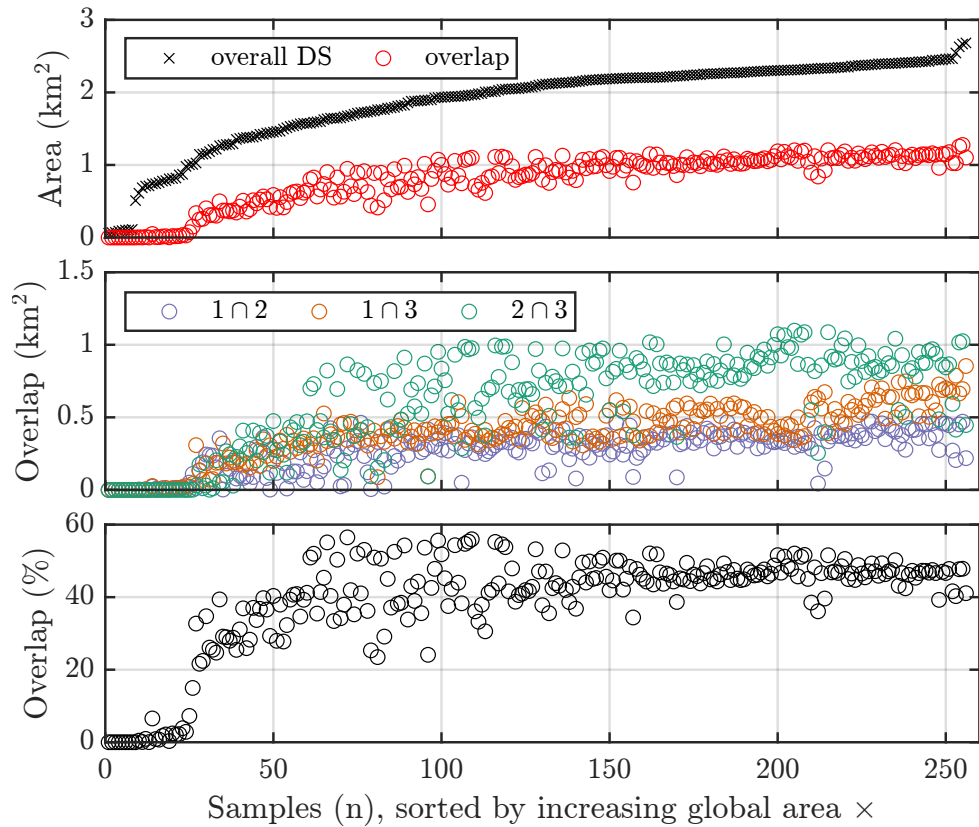
Figure 6.19 – Area of the union of DSs sorted by ascending order, and corresponding overall overlap (minimum of 2 overlapping DSs) (top); detailed overlaps between each DSs pair (middle); and overall overlap as a percentage of the overall sampled area (bottom).

area of the DS (union of the three DS). From a threshold of 1 % overlap, we can explain by a linear regression the increase of the overlap according to the total area.
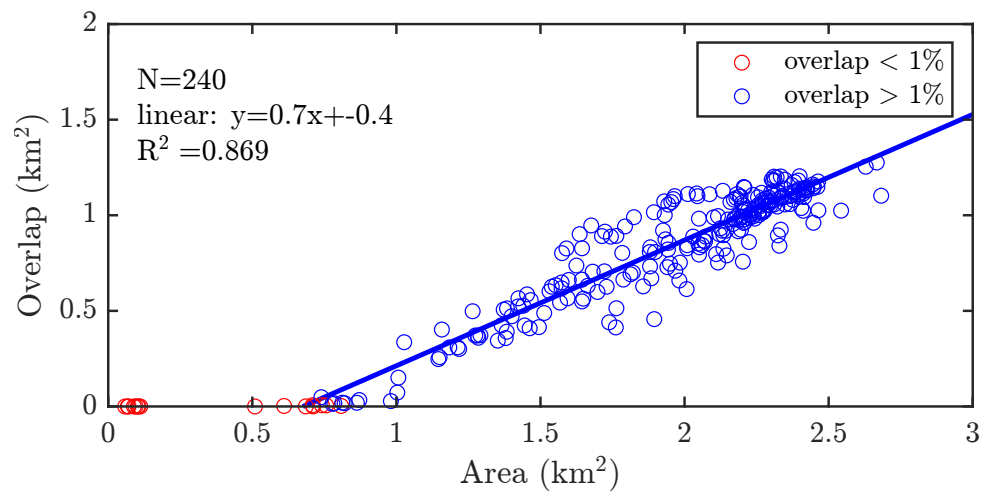
Figure 6.20 – Overall overlap according to the areas of the union of DSs sorted by ascending order, and linear regression from samples with an overlap greater than 1% (number of samples N, linear expression, and determination coefficient R^2).

Chapter 7

General discussion

Contents

The integration of the acoustic propagation phenomenon in its complexity is crucial to assess information transmission in the environment and to realistically describe acoustic networks (Marten & Marler, 1977; Wiley & Richards, 1978; Embleton, 1996). Studies of animal communication networks mostly use propagation experiments to assess the transmission of vocalizations in the environment (Hardt *et al.*, 2021), but these are only representative of a given location and a particular propagation condition (in time and space). We have therefore chosen to adopt a theoretical approach using propagation simulation to carry out parametric studies on a large number of cases related to behavior and

propagation conditions, and given a minimum of field data. Until now, the long-range propagation models used in the bioacoustic and ecoacoustic fields were mainly based on semi-empirical approaches (Henwood & Fabrick, 1979; Raynor *et al.*, 2017), which hampered the consideration for the complexity of the phenomena involved in heterogeneous habitats.

Acoustic communication & detection
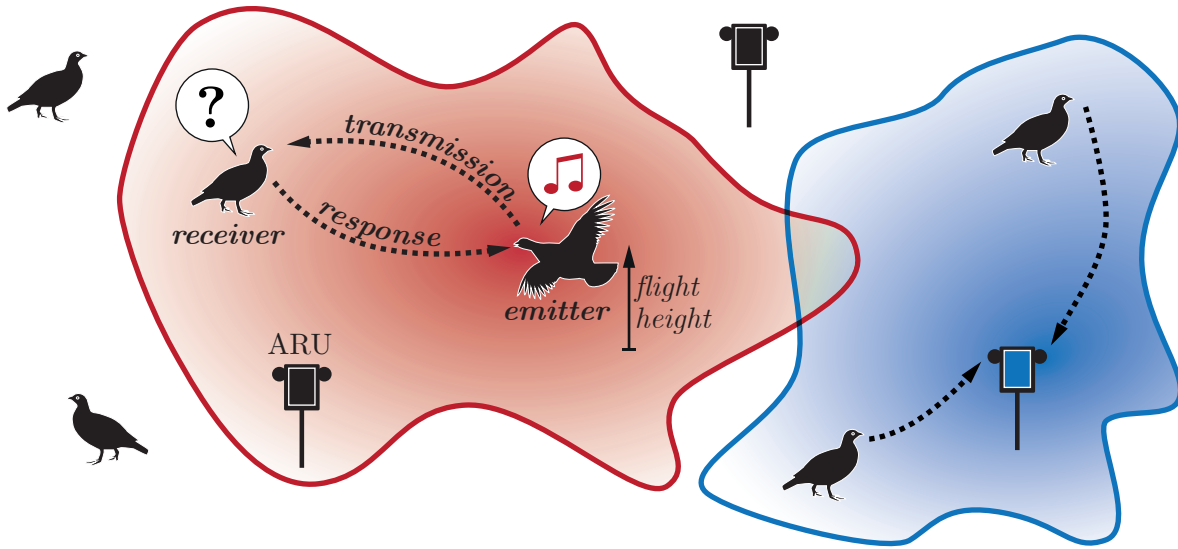
Acoustic propagation modeling   Applications
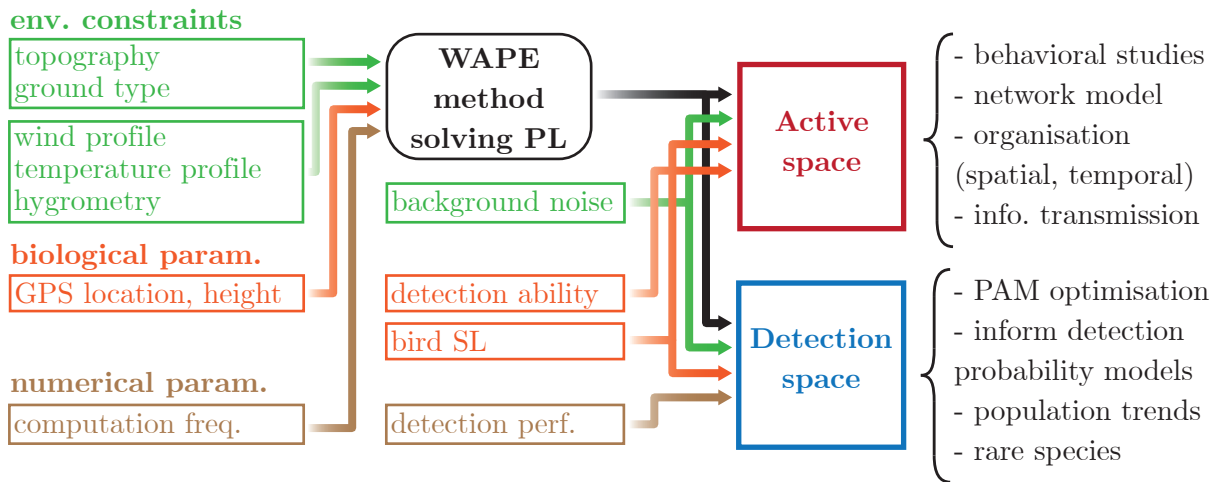
Figure 7.1 – Summary diagram of the modeling of active and detection spaces and their applications: The upper part depicts the acoustic communication that takes place in the species' habitat within the network. The chain of information transmission occurs between an emitter and a receiver within the active space of the former (▭). Conversely, the information of a song is captured by a receiver (ARU) if it occurs in its detection space (▭). The lower part describe the whole model through the data allocation (➡ data assignment), and details the applications related to the determination of active and detection spaces.

To address this challenge, we developed a propagation code based on the parabolic equation that computes 3D maps of PL (propagation loss). It takes into account the topography, the ground impedance, the wind and temperature profiles, and the atmospheric

absorption. To obtain valuable estimates of communication at the spatial scale, our comprehensive method includes computation of the PL and estimation of the source level, the background noise, and the detection threshold in noise. We summarize the modeling of active and detection spaces and their applications in Fig. 7.1. This diagram supports the discussion in the remainder of this chapter.

By taking the example of the rock ptarmigan, we have shown the contribution of propagation simulation for the analysis of acoustic communication networks, but also for the passive monitoring of populations in heterogeneous environments. In this thesis, we have laid the foundations for an integrative approach to the study of communication networks and passive acoustic monitoring methods in heterogeneous environments.

7.1 Influence of the physical parameters on the active space and detection space

The validity of our rotated WAPE propagation code has been assessed on the basis of measurements in alpine environment described in Chap. 4. In the following, we discuss the ability of the model to predict sound levels at long distances and in heterogeneous environments (see Acoustic propagation model in Fig. 7.1). In addition, we summarize the effects of propagation conditions on the active and detection spaces. We thus support the significance of taking them into account in studies of animal acoustic communication and biophony.

7.1.1 Notes on validity of the Rotated WAPE model for application to communication in ptarmigan

The results detailed in Chap. 4 show that predictions of PL using our propagation model are consistent with field measurements. Indeed, we observed that sound levels are correctly predicted up to 200 m distance and for a uneven terrain, which is true also in shadow zone (see Fig. 4.11). Moreover, the variability of the sound levels is correctly reproduced for the various downward and upward wind conditions. Even under upward propagation conditions, the sound level prediction is remarkably accurate. For the considered distance scale and frequency band the model approximations are valid, and the sound level estimates consistent. Without including the effect of tubulence in the model, the results are consistent because the atmospheric conditions are mostly stable. Buoyancy effects are minor compared to convection in our application because the temperature gradients are mostly positive above the snow (Sterk *et al.*, 2013; Mott *et al.*, 2017; Schlögl *et al.*, 2018). Moreover, the snow cover smoothes the terrain, and therefore limits the generation of potential turbulence induced by obstacles.

It turns out that the local measurements of meteorology and ground impedance provide reliable indications of conditions that may affect an entire site. Note that the expected gain in accuracy with more detailed input parameters is not guaranteed if one is unable to exhaustively characterize the medium in all three dimensions. Indeed, it is costly to measure weather conditions on site, and the exact values can obviously not be known at each point. Still, it is possible to simulate meteorological conditions on a meso scale using dedicated models (Lafore *et al.*, 1998; Xue *et al.*, 2000; Lihoreau *et al.*, 2006), or to simulate wind flow over a terrain with LES methods (Cheinet & Siebesma, 2009). However, such a computation adds significant additional effort, and the question of using representative input data still arises. Finally, if more complete and complex propagation models are possible in the future, it is at the expense of the computation cost. The latter is an important factor to consider when designing parametric studies.

In parallel, we showed in Chap. 6 the capacity of the code to perform an indirect computation according to the reciprocity principle. This method makes it possible to carry out reliable computations of the detection space of a recorder installed at any position. Comparisons between direct and reciprocal computations show a perfect agreement under various refraction conditions and for broadband spectra (see Figs. 6.4 and 6.4). The 3D comparisons reveal that the detection space carthographies are valid down to a PL of -100 dB. Nevertheless, we argue that errors occurring below this PL are not significant in the determination of the DS since the levels considered are within the limits of the PL that occur in communication applications in birds.

Despite some uncertainties regarding weather conditions, snow impedance, and snow-pack thickness, our model can reasonably be used for estimating long-range acoustic propagation in alpine habitats. The code developed on the rotating WAPE model proves to be an efficient and reliable tool for estimating both the active spaces of transmitters and the detection spaces of receivers (see Fig. 7.1). Therefore, our 3D modeling of propagation in heterogeneous media is a significant step forward in the fine-tuning of physical effects for the study of remote acoustic communication. Note also that this tool is not restricted to the habitat and species discussed in this thesis, in the sense that it is possible to modify all the input data whether it is environmental constraints (terrain, weather, background noise), biological data (source position, source level, detection thresholds), or statistics related to an audio analysis algorithm (detection performance).

7.1.2 Variability of active spaces and detection spaces induced by environmental constraints

The consequences of propagation constraints for an acoustic communication network have been described. These observations have previously led to consider the acoustic adaptation hypothesis (AAH) in animals that emit sounds (Ey & Fischer, 2009). Therefore, we

assessed the potential variability of active spaces through a parametric study in Chap. 4, observing the effects of topography and meteorology. We also observed this variability in real conditions in Chap. 5 by taking the example of communication in rock ptarmigan. Finally, we studied the effect of background noise on the detection spaces in Chap. 6. These factors modifying the active and detection spaces are reviewed here to summarize their impact.

Influence of topography

It has been shown by propagation modeling that for homogeneous atmospheric conditions, the active space is neither circular nor symmetrical on a uneven terrain (see Chap. 4). Moreover, this one is not necessarily a continuous surface, and can present a fragmented aspect. The insonified areas are mainly the gentle downward slopes, and the upward slopes in direct view. Thus a promontory is not necessarily a privileged location for a singing bird, given the steep slopes surrounding it.

Influence of local meteorology

The influence of local meteorology on active spaces has also been evaluated. The ground radiation condition, assessed by the sensible heat flux Q_{H}, determines the vertical temperature profile in low wind conditions. Our results show that for radiation conditions observable in mountainous areas ($Q_{\mathrm{H}} = [-100, 0, 400]$ W.m^{-2}), the AS variation induced between night and day can extend from $+7$ % to -38 % depending on the topography around the source (fixed at 10 m high, see Fig. 4.18). Note that sensible heat flux values encountered over meadow can be much higher and thus have a greater impact the AS variation (Ostashev & Wilson , 2016). For variable wind conditions, the expected increase in sound levels downwind and decrease is found to be closely related to the underlying topography. On uneven terrain, the wind reduces the AS in most cases. Its area can thus go down to -17 % compared to a homogeneous condition for the studied topographies (steep slope, gentle slope, promontory, and valley). The effect of temperature and humidity fluctuations have been included in our computations using the atmospheric absorption coefficient. Its impact on propagation is well documented elsewhere (see Sec.1.3.2). The considerable fluctuations in temperature and humidity encountered in mountain areas within the ASL (see Fig. 5.6) imply a significant variation of the absorption (see in Fig. 1.8 the influence of T and RH on $\overline{\alpha}$ in dB/m). These changes must be taken into account, as they have an even more significant influence at high frequencies and long propagation distances.

Influence of the ground type

We also investigate in Sec. 4.6 the influence of ground types. Computations of AS for different grounds such as snow, alpine moor and rock reveal the importance of this parameter. The variations in AS areas observed at 1000 Hz between the absorbing snow cover and the reflecting rock are of the order of 50 %. The heterogeneous nature of the ground was not included in our applied computations, as most of the communications related to territory establishment in male ptarmigan occur in early spring when a large part of their habitat is still covered by snow. However, the model can take into account a range-dependent impedance (Bérengier *et al.*, 2003). Soil type data (snow, moor, rock) could be extracted from drone photographs for example, and directly applied to the computation in the same way as the DEM.

Conclusion

We have seen the different sources of variability in AS and DS from a propagation perspective. These observations of sensitivity to environmental conditions justify the inclusion of ground and meteorological data in the code. This fine modeling technique proves to be an important advance for the use of AS and DS concepts in heterogeneous environments. In addition, the variability of AS and DS in terms of shape and area are likely to have a significant impact on acoustic communications in heterogeneous environments. Therefore, we argue that physical propagation modeling tools are essential to realistically estimate the spatial boundaries of acoustic communication. This approach provides an accurate assessment of the communication modalities between senders and receivers within the networks, and has many applications in the bioacoustic and ecoacoustic research fields.

7.1.3 Applicability of the propagation code, improvement possibilities and perspectives

One of the limitations of the model lies in the approximations made for the description of the atmosphere. First of all, the vertical and transverse winds are not considered, nor the interactions of the airflow with the topography. These 3D effects can lead to significant variations in sound levels for long propagation distances (Khodr *et al.*, 2020). For unstable atmospheric conditions, due to a strong negative vertical temperature gradient, the turbulent kinetic energy is non-negligible compared to the mean flux, and should be considered for the atmosphere description (Ostashev & Wilson , 2016). Indeed, our approximation without turbulence can lead to an underestimation of the levels in these cases of high instability, and a fortiori for the propagation of high frequencies at long distance. These instability conditions are mainly found during the day for high incidence solar radiation (close to normal) above fields for example. The generalization of our model for

applications to other types of habitat may therefore require modifications. Nevertheless, we recall here that it is possible to evaluate the effect of atmospheric turbulence with a PE approach (Chevret *et al.*, 1996; Blanc-Benon *et al.*, 2002).

Another limitation of our approach is the inability to consider potential echoes. Only the waves propagated in 2D are computed to simulate AS and DS. We know that some rock barriers are left bare after snowfall, and can act as reflectors. In addition, the melting snow uncovers grass and rock surfaces during the spring season. In fact, close echoes (to sender or receiver) could affect the information transmission to the receiver by modifying the directionality of the signal propagation. In contrast, far echoes (from sender or receiver) have a very reduced amplitude after a few hundred meters of propagation. This considerably reduces the probability of their detection, and therefore their relevance to communication. More generally, backscattering is not computed with the WAPE method, which can lead to greater errors as the slope is steeper. Beyond 40 degrees of slope, the proportion of backscattered energy is potentially greater than 1 % for frequencies of a few hundred hertz (Blairon, 2002). It has to be noticed that ptarmigan sometimes sit in rocky barriers or on rocky promontories whose snow has been blown by the wind. These particular positions imply a change in directivity, and may increase the energy fraction emitted to the receivers (due to reflection on the rock). In order to take into account both the 3D effects of reflection and convection on the topography and the effect of turbulence, we can consider solving the linearized Euler equations (Ehrhardt, 2013; Dragna *et al.*, 2014b; Van Renterghem, 2014).

Furthermore, in order to adapt our model to closed environments, it would be possible to add an absorption term that account for losses due to leaves and trunks of the vegetation (Haupert *et al.*, 2022). In addition, to finely consider the reflections due to trees, a model solving temporally the propagation of pulses in an arbitrary geometry as the FDTD or TLM can be used (Chobeau, 2014).

Finally, we have not investigated the advantages of the computation of propagated time signals. These data would provide quantitative support for the exchange of information between individuals in a network. Moreover, it would be possible to obtain maps of the amount of information relative to an acoustic signature of the species or an individual (detailed in subsequent sections). However, the computation cost of our model would have to be re-evaluated, since the required frequency step is of the order of 10 Hz for a reliable reconstruction of the signal. Note that a temporal resolution of the parabolic equation is also possible (Leissing *et al.*, 2009), and that the TLM, LEE and ray tracing methods also provide a direct temporal solution.

In spite of the different modifications applicable to the developed model and the other possible approaches discussed above, it must be retained that the gain in accuracy is to be balanced with the modeling effort required. Still, the order of magnitude of the uncertainty on the estimated sound levels must be considered in relation to the requirements of the

bioacoustic application.

7.2 Influence of physiology and behavior of birds on the active space

In a communication context between two birds, if the receiver is located within the active space of the signaler, it is assumed to receive some amount of information (see Fig. 7.1). The intermediate step of the transmission chain, the acoustic propagation, has been described in the previous section. Now we focus on the influence of the source and receiver characteristics on the active space.

7.2.1 Importance of source modeling for AS & DS

Importance of source signal, source level, and directivity

We have accurately assessed the frequency and temporal content of ptarmigan songs. This was done on the basis of field measurements at close range of the individuals (see Sec. 2.7). Two main peaks in the spectrum have been identified, and the temporal structure in series of pulses has been outlined. For the ptarmigan, which is a non-oscine bird, the question of the influence of frequency variability on AS does not arise. Indeed, its song is stereotyped and the frequency modulations are very limited. Thus, the intra-individual and inter-individual variability is not significant from a propagation point of view. Nevertheless, a more thorough study would be necessary for an application to passerines. However, for our application, we note that the frequency band considered in the PL computation changes the spatial extent of the AS (see Fig. 3.9). Precisely, when the AS is computed considering a large number of frequencies, it presents a smoother aspect than when considering a single formant. Indeed, by computing a global PL, the interferences are spatially averaged. Note also that for the same source level the single frequency computation at 1000 Hz leads to a slightly larger AS, for the same reason as above. For our applications, we have alternately used a 1000 Hz frequency, or the two main formants, or the complete discretized ptarmigan spectrum. This enabled us to adapt the computational cost. However, it must be remembered that the frequency content has an impact on the active space.

The field measurements were also used to determine the ptarmigan source level by means of a geometric decay correction. These field measurements are difficult to carry out on a wild species such as the ptarmigan, so few individuals could be recorded. Nevertheless, a first estimate of the inter-individual variability could be obtained with: SL $= 85 \pm 2$ dB. In the absence of more complete data on the variability of SL, we considered the mean SL for the AS estimation. This SL result is comparable to that of

the corncrake (*Crex crex*), which is a non-passerine bird of similar size (Ręk & Osiejuk, 2011; Aubin & Mathevon, 2020). More extensive measurements on birds from different sites could provide a distribution probability of ptarmigan SL. This distribution would be an interesting input to include in the AS calculations.

Finally, we note that ptarmigan-specific directivity has not been included in the active space model so far. The BEM modeling (see Sec. 2.7.3) gave us a rough idea of the directivity for a bird the size of the ptarmigan. However, further simulations need to be conducted to capture the complexity of the bird's acoustic radiation. From these first results, however, we know that the bird can reasonably be considered as omnidirectional in the far field in our computations at 1000 Hz. An error is potentially made at higher frequencies. Nonetheless, the importance of higher frequencies must be put into perspective at greater distances for the estimation of the active space (as their level decay is stronger with distance). To evaluate this directivity in more detail, it would be interesting to perform measurements in an anechoic chamber (Larsen & Wahlberg, 2017). It seems difficult to conduct measurements on a living bird, so a solution would be to use a stuffed bird an place a transducer in place of the beak.

Implications of singing during display flights for ptarmigan

AS simulations were performed for several typical Alpine topographies and for moderate wind by varying the source height. Our results detailed in chapter 4 reveal that the source height is a determining factor for the AS estimation. A source on the ground (at 1 m height) has an AS particularly constrained by natural barriers, which is very reduced compared to the value in free field (from 14 % to 53 % depending on the terrain). Conversely, an elevated source (i.e. 10 m high or more) obtains a more extensive AS (from 60 % to 97 % depending on the terrain), and all the more homogeneous and circular as it is high. Indeed, the elevation of the source reduces the importance of the ground effect, of the micro-topography, and also of the wind and temperature profiles. Note that many measurement campaigns carried out in various types of forests highlighted the benefit of singing from a greater elevation (Mathevon *et al.*, 1996; Holland *et al.*, 1998; Mathevon *et al.*, 2005; Padgham, 2004). Our simulations made for an alpine habitat supports these findings; we support that this effect is true regardless of the type of environment.

In our study, songs during display flights were considered to be uttered from a fixed location, at the peak of a bell-shaped trajectory. Nevertheless, two remarks can be made on this point. First, a bird uttering its song during display flight is a moving source. Considering the bird's speed in flight and time duration of the song, it is questionable to estimate its propagation from a fixed source point. If we consider a flight at an average speed of 30 km/h, and a song duration of 2 seconds, we obtain a noise source in motion over a distance of about 17 m. With respect to the effective radii of the estimated active

spaces in flight, this distance can be negligible when the background noise is low and the propagation conditions are favorable (order of 3 % of the radius), but not when the conditions are bad (up to 30 % of the radius). It appears that the active space can potentially be underestimated for cases unfavorable to propagation, if we do not consider the movement of the source. In addition, some shadow zones due to the relief, if they are close to the source, could not exist because of the change of line of sight during the flight. It is likely that a calculation of a cumulative active space in different successive points would show these effects.

Another remark concerns the moment of the song. By simplification we considered the song at the time of the apogee of the display flight. However, as the flights are performed over variable landforms, it is likely that the song is not systematically uttered at this point. Specifically, some flights may be low, just over a hump-shaped profile for example, and other flights may be effortless glides along a slope. These different trajectories lead to the consideration of songs close to takeoff or close to landing. An effective way to clarify this point would be a tracking experiment using a GPS tag with microphone attached to the bird, providing both acceleration and audio data. The precise positions and trajectories of the flights would thus be known, as well as the times of the songs. These two types of data, involving an accelerometer and a microphone, require a significant amount of energy and a large volume of onboard memory. The type of equipment used so far for monitoring is not compatible with these measurements, and other existing beacons are either too heavy to equip ptarmigan, or not autonomous in energy, or without UHF transmission modules. It would be necessary to consider another type of beacon, and the recapture of equipped birds at the end of the experiment. The stress induced on the individuals during a second capture would strongly increase the chances of death. This solution has not been considered until now because this species is already very weakened by the climate change and by the anthropic pressure in its alpine environment.

7.2.2 Importance of receiver characteristics for AS & DS

Receiver bird signal detection

As previously explained in Sec. 1.4, measurements of response to masking playback in oscine and non-oscine birds highlighted a minimum SNR of 3 dB for recognition in noise (King *et al.*, 1981; Brenowitz, 1982b; Amagai *et al.*, 1999). This threshold is evaluated from behavioral responses in different species in the field or in the laboratory. It was used in our applications to estimate the active space required for communication between birds. This threshold measure has the disadvantage of not considering the transmitted information content, which leaves uncertainty on the prioritization of communication possibilities in the active space. If the behavioral response requires at least detection, it has not been clearly examined whether this threshold corresponds to discrimination,

or recognition. Indeed, these experiments do not quantify the motivational state of the receiver, although it is known that it may modify its response. The SNRs required for different communication qualities could be evaluated from playback-based lab studies in social species, starting with individual discrimination and recognition with typical outdoor noise spectrum (Mouterde *et al.*, 2014).

In the context of bird acoustic monitoring, song detection and retrieved information quantity can be inferred by a recognition algorithm based on the information criteria. A method was proposed by Marin-Cudraz *et al.* (2019) for the recognition of individuals in ptarmigan records, and information criteria were determined. These criteria could be used in the future to evaluate the sub-spaces of the DS, and to qualify more finely the spatial sampling used for automated acoustic census campaigns. The same principle could be applied to AS, enabling to distinguish sub-spaces in the communication network, related to: the individual, the species or the dialect.

Background noise assessment for investigating communication behavior and vocal activity

Background noise is a critical parameter of sound propagation in the environment as it determines the emergence of a source signal at the position of the receivers. In our application of AS to ptarmigan communication, the background noise was estimated from the ARU recordings at the Flaine site (see Chap. 5). We estimated the background noise perceived by the ptarmigan with the statistical level L_{90}, calculated from L_{eq} (equivalent levels) over a 0.5 s sampling period. This sampling time is of the order of magnitude of the duration of a ptarmigan song, which is about 2 s. The L_{90} metric was chosen considering that ambient noise is mostly low in the mountain habitat, and that rare events such as the song of a passerine perched on the ARU, wind gusts, or the passage of an airplane are not representative of the level perceived by the birds during communication. However, the representativeness of this index in terms of time and space is questionable. Indeed, the BN is estimated by 10-minute periods, and the songs are of the order of two seconds. This is why a statistical index is preferred to an equivalent level over the time period. A finer sampling would be possible for specific applications to behavior over short periods. Spatially, it is clear that the BN is not homogeneous because it is largely due to the wind and its interaction with the heterogeneous ground and obstacles. Our evaluation is point-based from fixed ARUs, but our temporal sampling enables to smooth the observed levels by integrating the influence of wind variation over 10 minutes, and thus to obtain a reliable estimate of the BN around the ARU.

The BN measurement is inevitably impaired by the noise generated through the interaction of the wind with the microphone membrane. Note that the effect of wind on the noise generated in a microphone can be evaluated by empirical relations (see Appendix B.4). This indication can help us to sort out invalid samples on the basis of wind

speed as previously done (see Fig. 5.3). This could eventually be used to resolve this ambiguity in the BN estimation.
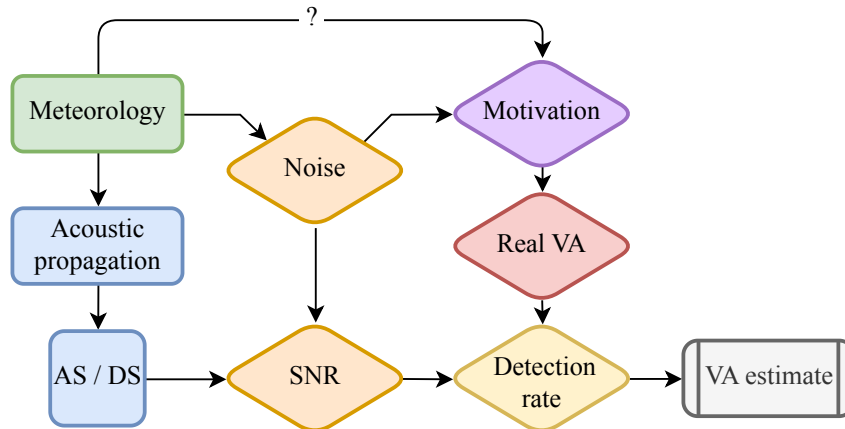
Figure 7.2 – Functional block diagram of interactions between meteorology and estimated vocal activity (VA) ($\rightarrow$ cause and effect relationship).

In the context of bioacoustic and ecoacoustic studies, BN is a confounding factor which potentially influences both the estimations of VA (vocal activity) by modifying the detection rate, and the motivation of the birds to sing (Haupert *et al.*, 2022). This problem is illustrated by the diagram in Fig. 7.2. It is well known that a positive retroaction occurs during the dawn chorus. Indeed, a bird that hears more competitors singing is more frequently encouraged to respond, and thus to sing more (Burt & Vehrencamp, 2005). Thus a higher background noise, which causes the DS spatial restriction, may induce a lower response rate. The confusion between real VA and its estimated value by a detection algorithms should be given special attention in the future, but could not be addressed in detail in this thesis. To unravel the influence of environmental conditions on behavior, acoustic monitoring of the birds using a miniaturized microphone coupled to the equipped GPS tag would provide information on the timing of songs and the actual number of vocalizations (Rutz & Troscianko, 2013; Eisenring *et al.*, 2022). This data would be sufficient to determine if ptarmigan motivation to sing is dependent on background noise and/or weather conditions. This last point was examined by observing the effect of rain on the movements of a bird (see supplementary in Appendix B.3).

7.3 Acoustic communication network in ptarmigan & prospects

Modeling of active and detection spaces gives the opportunity for network analysis of long distance communications. This type of analysis has been widely addressed in gregarious animals but little for loose networks in birds (T'oth *et al.*, 2020; Szymkowiak, 2022). If the position of the birds is known, it is possible to determine which ones have the possibility

to communicate with each other or not by performing a propagation computation (see Fig. 7.1). The spatial dimension of the network, and thus the propagation constraint, can be taken into account in the functional and organizational study of the network. Thus, numerical propagation simulation offers a deterministic approach to the network organization in space and time. We used it in this thesis to provide some answers to acoustic adaptation hypotheses (Morton, 1975; Ey & Fischer, 2009), related to singing times and singing positions.

Modeling of long-distance acoustic communication networks

In Chap. 5 we present the first study of an acoustic communication network in birds in a heterogeneous environment. We addressed the complexity of the problem by combining GPS tracking of a ptarmigan population with measurements of physical field data, passive acoustic tracking, and simulations of song propagation. The simulation of the PL was performed up to 1 km around the considered bird positions with the previously developed code. The nature of the ground was taken into account using snow impedance parameters which were evaluated by field measurements. In addition, a meteorological station was installed on the Flaine site to provide wind and temperature profiles as well as atmospheric pressure and humidity. These data were also integrated into the PL computation. In parallel, acoustic monitoring was carried out using an ARU and an estimation of the vocal activity by CNN algorithm.

The fine modeling of the active spaces associated with the positions of the birds in flight, or on the ground, gives the possibility to spatially estimate the communication for each movement of the individuals in the network. We were thus able to investigate both the temporal and spatial organization of communication in rock ptarmigan.

Sound transmission at dawn in high mountain habitat

A major question related the communication of birds is to understand why they sing at dawn. One of the hypotheses we were able to test postulates that birds would communicate at dawn because the environmental conditions for the signal propagation would be the most favorable to optimize their propagation and detection space (Henwood & Fabrick, 1979; Staicer et al., 1996). We investigated this hypothesis of better sound transmission at dawn in the alpine environment using ASs simulations. By assessing the variability of the AS during the day based on measured meteorological data, we showed that there is no link between propagation conditions and the period of high vocal activity in ptarmigan. This result brings a new contribution to the study of the acoustic adaptation hypothesis (Hardt et al., 2021) in heterogeneous environment. It appears that other intrinsic, social, or environmental pressures determine the timing of the dawn chorus in mountain birds. The reasons for singing at dawn are rather to be found in the optimization of energy,

territory defense, and sexual attractiveness in birds (Gil & Llusia , 2020), but also in the avoidance of predators.

Display flights and territory defense

We studied the importance of the emitter position for communication between neighboring males in the network. Numerical simulations were used to obtain ASs for all display flights, and these were compared to ASs obtained from a relative ground-level position. These results indicate the impossibility of effective territory defense from a ground position in this type of environment, with its topographical complexity and environmental conditions. On the contrary, the songs in flight transmit the signal to the whole territory of the emitter in a very efficient way.

Furthermore, the computation of the overlap of neighboring territories by the AS shows the importance of the airborne songs for the proper functioning of the long-range communication network. Indeed, we see that the overlap of neighboring territories by the AS is on average twice as large for the airborne songs.

In a high mountain habitat the behavior of singing during display flights turns out to be a decisive strategy for territory defense within ptarmigan communication networks. This behavior can be considered as an adaptation to the environmental constraints on sound propagation in high mountains. Given their crucial role in making long-distance communications possible, the songs performed during display flights are an argument supporting the AAH (acoustic adaptation hypothesis (Morton, 1975)).

Singing and listening posts

Precise data on ground-based singing posts could allow us to study a possible adaptation of singing males to the terrain during the breeding period. Multiple criteria have been put forward to explain the choice of territories such as the quality and abundance of food and the presence of refuges (Nice, 1941). It is obvious that certain portions of the mountainous sites present a suitable configuration for singing posts. Indeed, these positions can be very advantageous from a propagation point of view. On the other hand, these posts that maximize the active space also enable to maximize the detection space and thus to efficiently monitor competitors. These positioning behaviors thus support interactive networks including signaling and eavesdropping between more than two individuals (see networks interactions Fig. 1.1). In addition, an unobstructed view allows for broader surveillance of potential predators, and increases survival rates. Better defended territories may allow for year-to-year retention. The relocation of males the following year on the same area, observed regularly on the site of Flaine for example, corroborates this postulate.

7.4 Detection spaces and passive acoustic monitoring

7.4.1 Contribution of DS estimation for PAM protocols

In Chap. 6 we present the first study to determine the detection space of audio recorders in a heterogeneous environment. This computation is based on a propagation code validated for an alpine habitat. We adopt a reciprocal approach that considers the recorder as a source, which reduces the computational cost compared to a direct approach, and leads to a more detailed mapping of the DS (see Sec. 6.4). It has been shown that the variability of DS, similar to that of AS is induced by topography, ARU position, weather conditions, ground type, and BN. It impacts the sampling area of ARUs and thus the possibilities of detecting biological sound sources in audio recordings. Ignoring it causes uncertainty in the estimation of acoustic indices such as vocal activity for example.

We propose a method to account for the spatial variability of the sampling. By defining new audio-based indices related to the DS area, such as vocal activity per square kilometer, we obtain activity densities that are independent of the recording conditions. Errors related to the arbitrary allocation of sampling area are thus minimized (Van Wilgenburg *et al.*, 2017). This helps to improve the relevance of indices with respect to the habitat and biological context by reducing the biases of the analysis method (Yoccoz *et al.*, 2001). The contribution of the propagation computation can be crucial in the case of very changing recording conditions that lead to a highly variable DS, and even more to generalize the results. Indeed, abundance estimates are commonly extrapolated to adjacent areas or similar habitats.

In the context of a population or habitat comparison, the DS knowledge brings the possibility of standardizing long-term acoustic monitoring conducted at different locations (Sólymos *et al.*, 2013; Darras *et al.*, 2018). This is also the case for comparing old studies. Standardization by spatial sampling is achievable if sufficient field data are available regarding environmental conditions, raw audio data to assess BN, employed methodology (type of the recorders), and detection algorithm performance.

We illustrate in Chap. 6 that the computation of the DS, associated with each ARU of a network, provides information on the area not covered in the study zone, but also on the overlap rate of the sampling. It is thus possible to estimate the pseudo-replication rate of the recorded data, and to correct the evaluation of the acoustic indices accordingly. When planning an acoustic monitoring campaign, the preliminary estimation of the DS could be a very informative tool to optimize the placement of ARUs (Piña-Covarrubias *et al.*, 2019; Goetschi *et al.*, 2022) , and to schedule the recording periods (Pieretti *et al.*, 2015). Indeed, avoiding the DS overlap and quantifying the required number of days for the targeted sampling would ensure an unbiased evaluation of the abundance of a species or of biodiversity indices (Anderson, 2001; Bonar *et al.*, 2011). The quantification of the DSs gives us the zone covered for each record, and provides an a posteriori assessment of

the temporal sampling efficiency (Wood *et al.*, 2021). In addition, reducing the number of ARUs by judicious placement, and refining the recording times can lead to substantial savings (installation, measurement and analysis time), and/or to allow the extension of the survey areas.

7.4.2 Towards an integrated approach to occupancy assessment using passive acoustic monitoring

It should be noted that our study on the use of DS for PAM protocols is preliminary and needs to be consolidated with comparisons on other species and habitats. The limited number of ARUs at the study site and the very low bird density of this species make it difficult to draw definitive conclusions about the method. A reduction in variance was observed between the raw VA index and the VA density mainly for the ARU which presents a high variability in DS and records a high vocal activity rate. Thus, it would be interesting to evaluate the value of fine computation of DS at a larger scale, for an extended ARU network, and for a species with a higher population density.

After having examined the interest of the method for the evaluation of vocal activity, it would be interesting to apply the same principle for the actual counting of individuals. We know that individual information criteria contained in the ptarmigan song make it possible to discriminate each bird (Marin-Cudraz *et al.*, 2019). Thus the use of a recognition algorithm coupled with the estimation of the overall DS on a mountain site would give access via a PAM protocol to the density of birds, which is the most relevant metric for population monitoring and management of natural areas.

In the perspective of a more refined approach in detection algorithms, a DS of the information could be determined from a broadband PL computation, by convolving any source signal with the frequency response at each receiver point. This would require prior knowledge of the information criteria of the target species. This would make it possible to obtain, for each sample, the DS related to each information sought: for the number of species, the DS of the specific information; for the number of individuals, the DS of the individual information. This step would bring in the longer term the opportunity of evaluating DSs specific to each acoustic diversity index (Gasc *et al.*, 2013; Sueur *et al.*, 2014).

We have adopted a propagation viewpoint on detection spaces. Nevertheless, this deterministic DS computation step leads to a global method of detection probability computation involving biological, behavioral and environmental statistics related to the target species. A model integrating occupancy estimation and active space computation informed by the probability distributions of SL, BN, and recognition performance would provide a robust tool for population assessment at large scales. It also opens up the prospect of computing the temporal detection probability related to a given focal species

and habitat. This data is particularly sought after for the monitoring of rare species, with a low source level, or not much loquacious. These species require continuous recording to maximize the detection opportunities, and this can lead to large amounts of data to analyze. The advantage of the DS here is to know precisely the areas sampled, and thus avoid the underestimation that is common at listening points for rare and disturbance-sensitive species. The latter is a crucial advantage to reliably document biodiversity loss in threatened habitats.

Appendix A

Loudspeaker design and characterization for propagation measurements

Abstract

For the needs of outdoor experiments we have developed an autonomous loudspeaker adapted to the emission of high levels in the midrange frequency band. Measurements in an anechoic chamber showed a frequency response as well as a directivity in agreement with the needs of our experiments. This section details its characteristics, as well as its acoustic specifications.

Contents

A.1 Design of the loudspeaker

General features

Amplifier: D class Focal FDS 2.350, 2x105 Watts RMS, Focal JMlab, France
Battery: 12 V, 7 Ah
Internal volume of the enclosure: 4 L

Driver

Model: Beyma 6G40Nd (low & mid frequency transducer), Beyma, Valencia, Spain
Sensitivity: 94 dB (with reference 1 W / 1 m)
Power capacity: 170 W_{AES} (according to AES2-1984 (r2003) standard)

Bass-reflex

Bass-reflex with two vents for compactness, at the tuning frequency of 97 Hz.
Resonance frequency of the coupled vents: 4000 Hz.
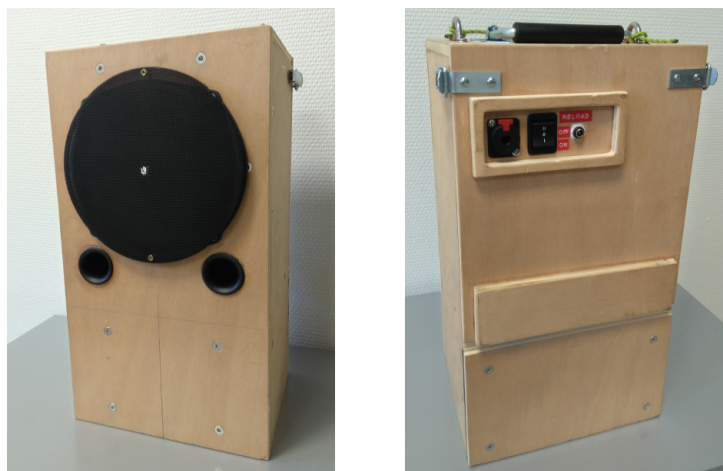
Figure A.1 – Picture of the designed autonomous loudspeaker

A.2   Acoustic characterization of the loudspeaker

This section details the frequency response and directivity measurements of the "Lago" loudspeaker designed for the various field experiments. The purpose is to measure the frequency response of the loudspeaker in the vertical and horizontal planes of a half-space and then to plot the directivity diagrams per third octave band. These measurements are used to characterize the loudspeaker before the use in propagation experiments.

Material

  – anechoic chamber, E6 building of the LMFA
  – designed autonomous speaker
  – rotating support
  – sound card Focuscrite Scarlett 2i2
  – microphone Beyerdynamic MM1

Method

A microphone is placed at a distance of 2 m from the source. A pink noise is emitted through the speaker for 30 seconds. The output signal of the sound card is recorded on one track, and the signal received by the microphone on another track. A MATLAB® code enables one to control the sound card and to synchronize the recordings. Then, the transfer function is calculated in order to characterize the frequency response of the amplifier-loudspeaker chain.
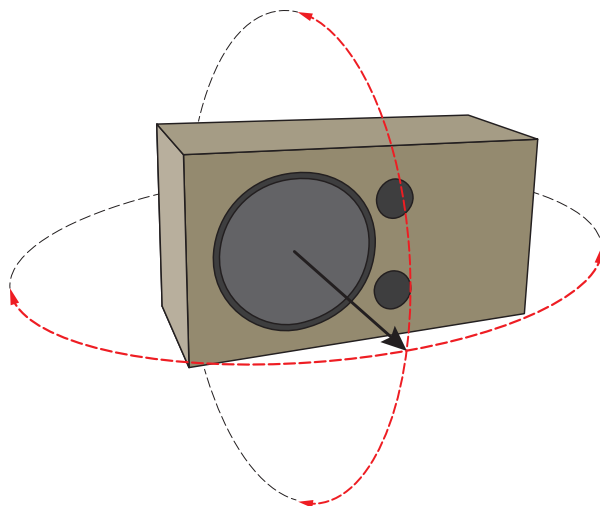
Figure A.2 − Schematic drawing of the measurement procedure. The loudspeaker is rotated along the two orthogonal planes to the ends of the red arrows.

This measurement is repeated at 180° on a vertical plane and a horizontal plane by angular steps. The reference angle 0° is marked between the source-microphone axis and the speaker axis. The angular step is chosen at 5° between −50° and 50° around the speaker axis, and at 10° beyond, up to −90° and 90°. The center of the loudspeaker membrane is aligned with the axis of rotation of the support in order to keep this distance for each step of rotation. Figure A.2 shows a schematic view of the measurement. The microphone is left at a fixed position, while the source is rotated for each measurement according to the desired angle, with the help of the goniometer graduated at 5° fixed on the support stand. The speaker is placed on the blank to allow the measurement on its vertical axis.

A.2.1 Frequency response in axis

The frequency response in the axis of the loudspeaker and at 2 m is presented in Fig. A.4. We can see that in the band of interest for impedance and propagation measurements, 100 Hz to 3000 Hz, the response is within a dynamic range of 5 dB. This enables us to properly reproduce the energy of the signals sent during the measurements.

Figure A.3 – Setup used for directivity measurement, with loudspeaker on the left and microphone on the right. (Microphones mounted on a circular stand at the top of the image are not used.)
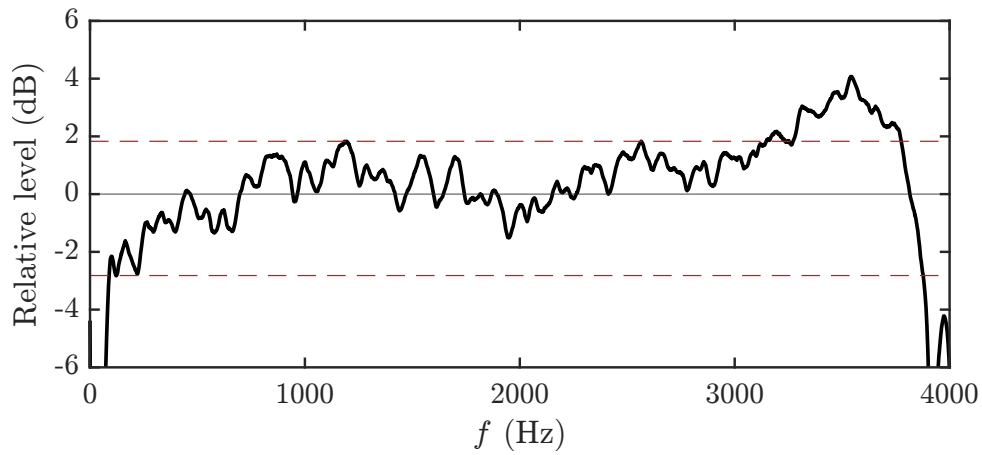
Figure A.4 – Frequency response of the loudspeaker at 2 m in the axis (solid black), and relative level limits for the 100-3000 Hz band (dotted red).

A.2.2   Directivity of the loudspeaker

The transfer functions obtained by the measurement are then divided into third octave bands. The central frequencies f_c of the considered third octave bands are detailed in Tab. A.1. An integration is performed on each band to obtain the corresponding amplitude value. Then this value is divided by the amplitude value in the orthogonal axis of the loudspeaker (0° angle). This procedure is repeated for each measurement according to its angle. The directivity diagrams are then plotted per third octave band according to the angle and level in dB with respect to the reference axis.

Table A.1 – Center frequencies of the third octave bands (directivity diagrams are plotted for frequency values marked in bold).

f_c (Hz)	50	63	80	100	125	160	200	250	315	400	500
	630	**800**	**1000**	**1250**	**1600**	**2000**	**2500**	**3150**	**4000**	5000	

Horizontal directivity

The speaker is positioned vertically, and rotated in the horizontal plane between each measurement.
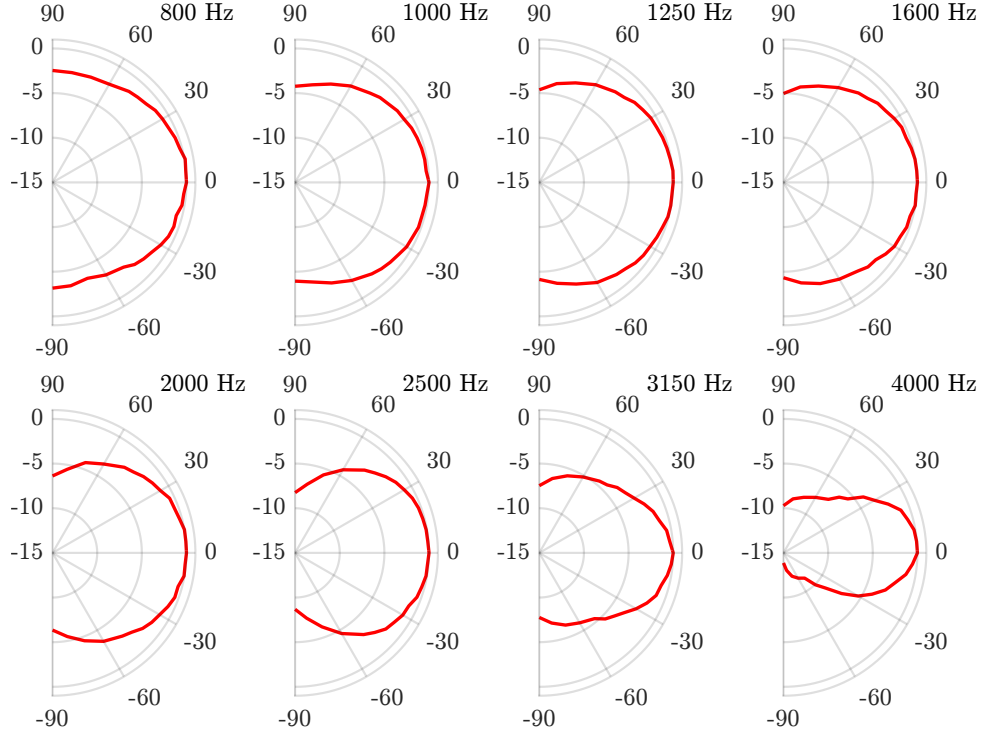
Figure A.5 − Horizontal directivity diagrams of the loudspeaker for the 1/3 octave bands from 800 Hz to 4000 Hz. Radial unit in dB relative to the reference level in axis.

Fig. A.5 shows the omnidirectional behavior of the speaker at low frequencies and the appearance of a marked directivity at high frequencies. Some directivity patterns, especially at 4000 Hz, are not symmetrical on either side of the axis. This is not expected, given the vertical symmetry of the speaker. This may be due to two factors: the uncertainty of the angular position of the speaker and the presence of echoes in the room. The use of the goniometer integrated into the tripod, should allow an uncertainty of about 1° on the angle. This factor is therefore negligible. In addition, the presence of reflective objects in the room at the time of the measurements may have increased the level received at the microphone for certain angles and certain frequencies. Metal rails as well as a jet pipe and air outlet pipes may have acted as reflectors, especially at high frequencies.

Fig. A.6 details the directivity of the loudspeaker on the horizontal plane, in narrow bands and according to the angle. This allows us to define the maximum opening angle at −3 dB depending on the frequency. In our case, the propagation measurements are made up to a frequency of 3000 Hz. We verify that for a tolerance of −3 dB at the emission, the loudspeaker presents an opening angle of 30° up to a frequency of 3200 Hz.
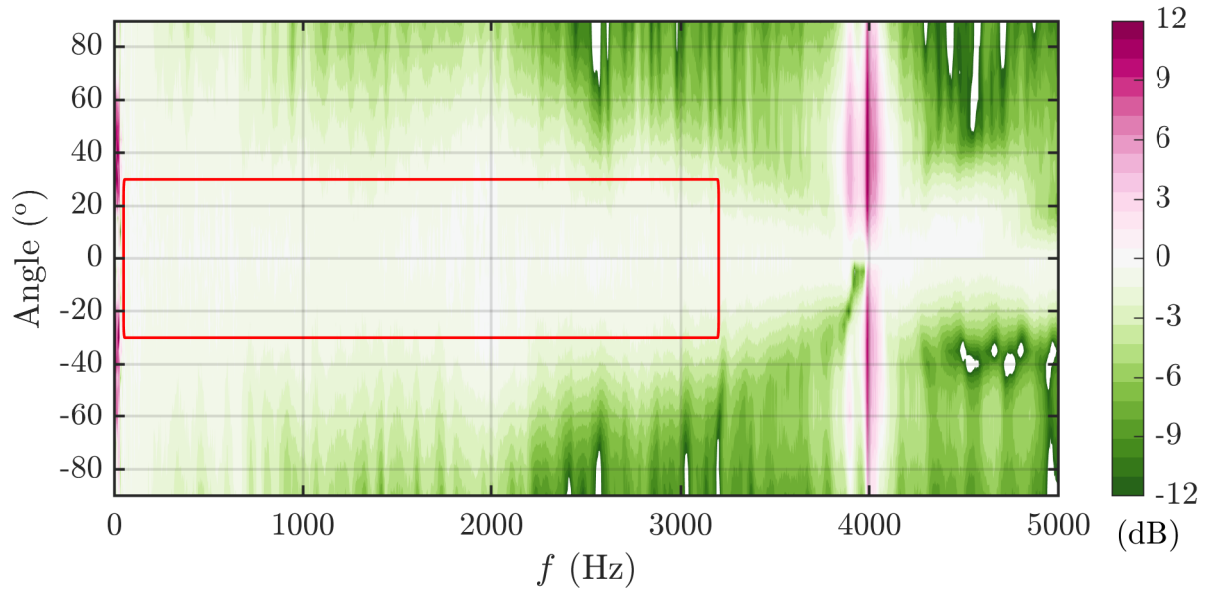
Figure A.6 – Directional pattern of the loudspeaker on the horizontal plane in narrow bands and according to the angle. The red rectangle indicates the zone (angular aperture / frequency) that is relevant for propagation measurements.

Vertical directivity

The speaker is now positioned horizontally, and rotated in the vertical plane between each measurement.
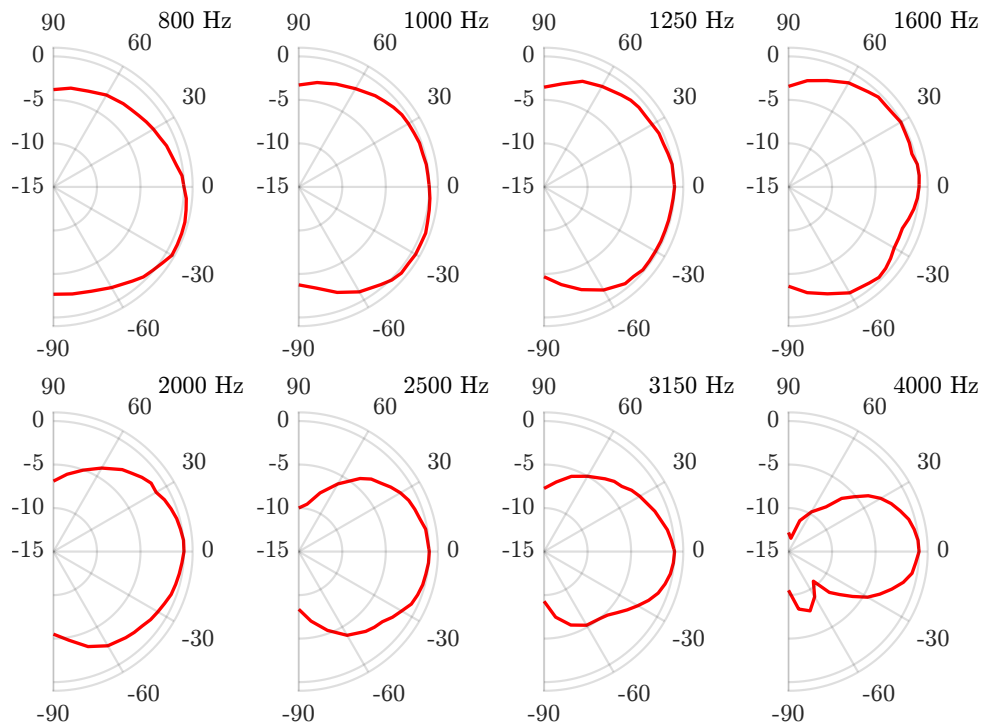
Figure A.7 – Vertical directivity diagrams of the loudspeaker for the 1/3 octave bands from 800 Hz to 4000 Hz. Radial unit in dB relative to the reference level in axis.

Fig. A.7 shows the directivity in the vertical plane of the speaker. Since the loudspeaker

is asymmetrical with respect to the top and bottom of the speaker, a slight asymmetry of the directivity patterns is expected. Indeed, we observe slightly different levels on either side of the reference axis, and this effect is marked for angles above 50°. At 4000 Hz, the effect produced by the front panel of the speaker is particularly visible, with a second lobe present on one side only.

The directivity of the loudspeaker in the vertical plane, in narrow bands and according to the angle is detailed in Fig. A.8. This allows us, as before, to define the maximum opening angle at −3 dB depending on the frequency. We verify here that for a tolerance of −3 dB at the emission, the loudspeaker presents an opening angle of 30° up to a frequency of 3200 Hz.
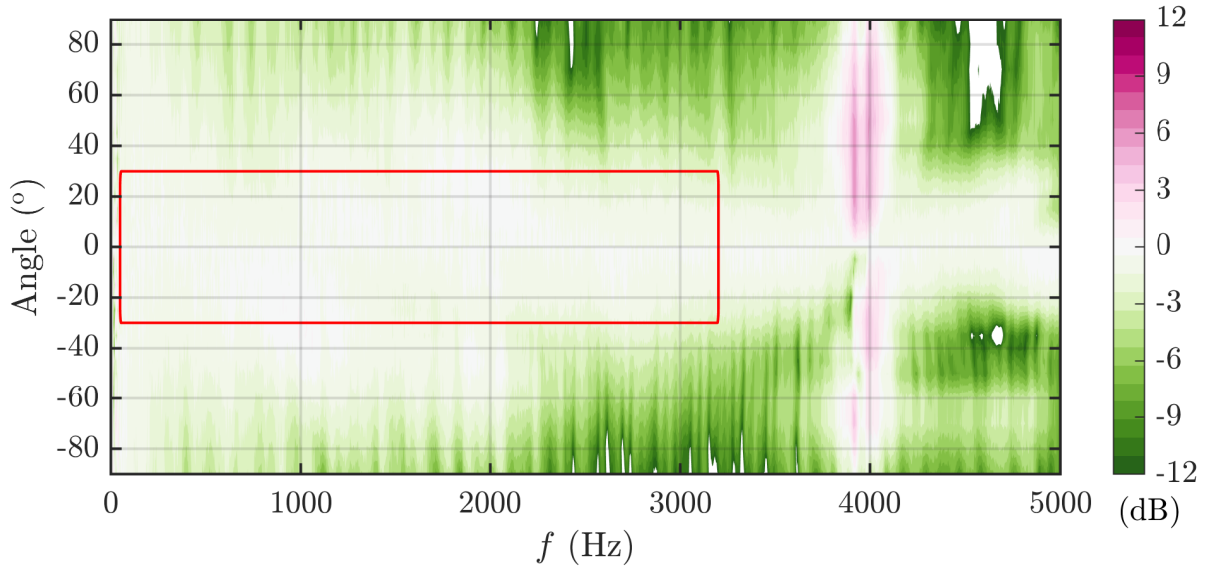
Figure A.8 − Directional pattern of the loudspeaker on the vertical plane in narrow bands and according to the angle. The red rectangle indicates the zone (angular aperture / frequency) that is relevant for propagation measurements.

A.2.3   Harmonic distortion

The harmonic distortion of the loudspeaker is measured with the free software Room Eq Wizard, in the listening room of the LMFA which is acoustically treated to offer a low reverberation time. A calibration of the measurement chain makes it possible to obtain the SPL level emitted at 1 m from the membrane and in the axis. The measurement is carried out by frequency steps by emitting a pure sine, and the level of the harmonics is then acquired. The calculation of the THD (total harmonic distortion) is carried out in relation to the level of the fundamental frequency considered, according to the ratio of the RMS values such as:

$$\text{THD} = 100 \times \frac{\sqrt{\sum_{h=2}^{H} V_{\text{RMS}}(f_h)}}{V_{\text{RMS}}(f_0)}, \tag{A.1}$$

with f_0 the fundamental frequency, f_h a harmonic frequency, H the last harmonic considered, and V_{RMS} the root mean square recorded tension.

The software enables to measure the contributions of the 2nd to the 8th harmonic, as well as the background noise level. The calculation of the sum of the contributions makes it possible to obtain the THD criterion, as well as the THD+N taking into account the noise and the non harmonic distortion. The results of these measurements can be seen in Figure A.9 and Figure A.10 respectively for the emission levels at 102 dBSPL and at 107 dBSPL. The 2nd and 3rd harmonics as well as the noise contribute for a majority to the measured distortion, the other harmonics of rank 4 and more are negligible in terms of level.

Table A.2 − THD (total harmonic distortion) and THD+N (plus noise) measured on the loudspeaker at two high source levels.

SL (dB SPL)	THD (%)	THD+N (%)
102	2.02	2.95
107	3.15	3.62

For the band 100 Hz to 5000 Hz, the calculated THD are detailed in Tab A.2. It is possible that these values are slightly exaggerated, taking into account the measurement conditions in a non-perfectly anechoic room. Moreover, the background noise of the order of 40 dB, brought by the ventilation, could have contributed to the noise measured in low frequencies. We consider these distortion values reasonable for our outdoor propagation application at high levels.
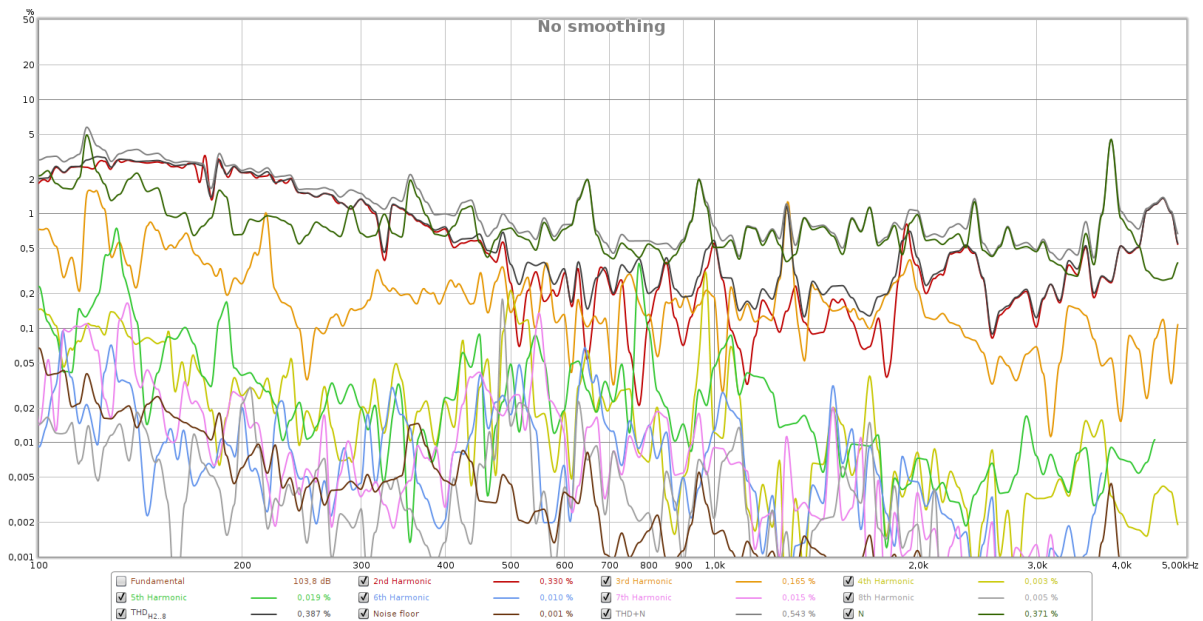
Figure A.9 − Loudspeaker THD at 102 dBSPL (black: THD, grey: THD+N)
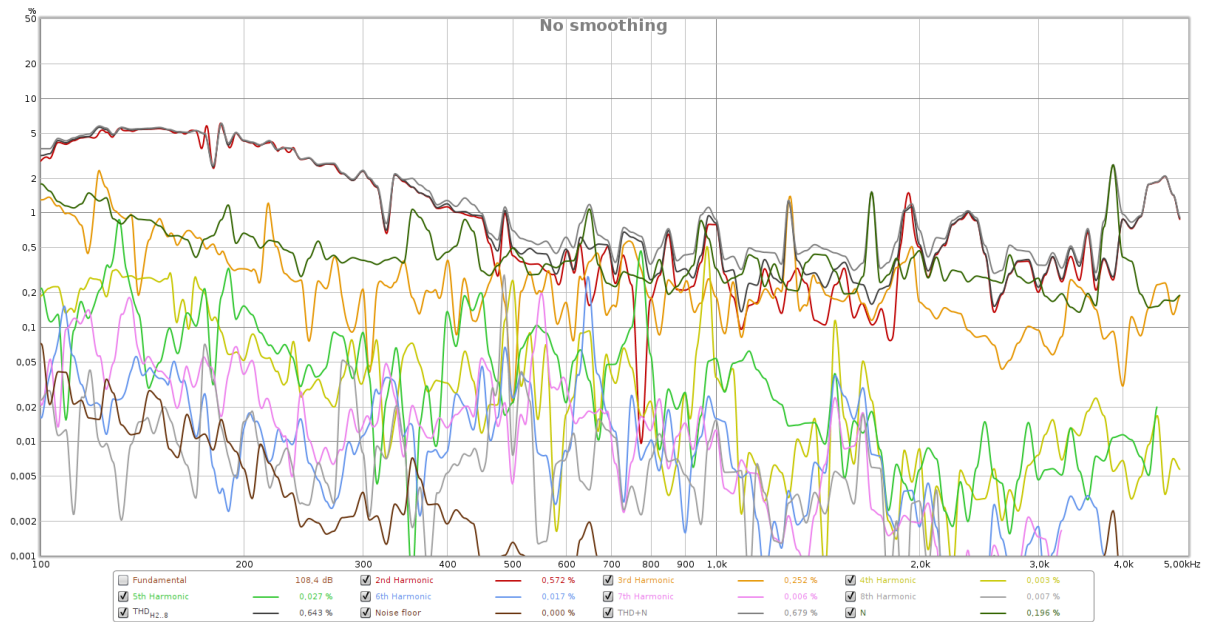
Figure A.10 – Loudspeaker THD at 107 dBSPL (black: THD, grey: THD+N)

Supplementary material of Chapter 5

Contents

B.1   Temporal variability (vocal activity and active space)

Calculation settings for active spaces computation

- Source height $z_S = 15$ m
- Receivers height $z_R = 0.3$ m

B.1.1   Over the season

No seasonal trend of the active space is observed. Note that the model does not take into account the melting of the snow cover, which modifies the surface impedance over the entire domain, uncovering patches of bare rock, lapies, or low moorland.

    The area of the active space has a limited variability (max value - min value) if we consider only the change of weather conditions, and a fixed BN: 2.3×10^5 m^2. Conversely, if the weather parameters are fixed, and the measured BN is taken into account for each sample, its variability is of 6.6×10^5 m^2. Finally, when these two variables are taken into account, the variability of the area increases to 9.9×10^5 m^2. The BN, which
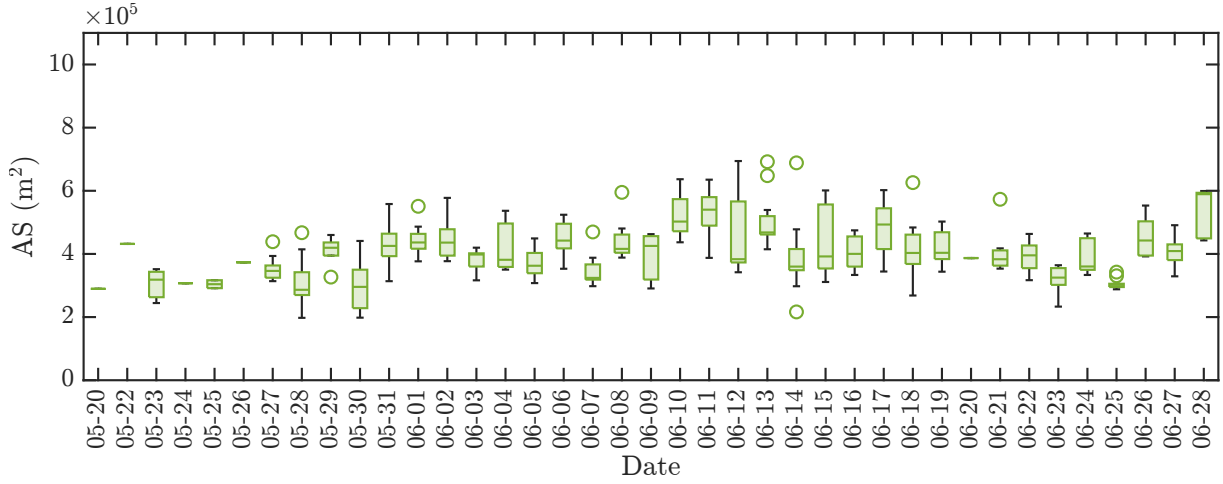
Figure B.1 − Evolution of active space over the season, considering variations in weather conditions, and a median background level $L_{90,\mathrm{med}} = 19$ dBSPL.
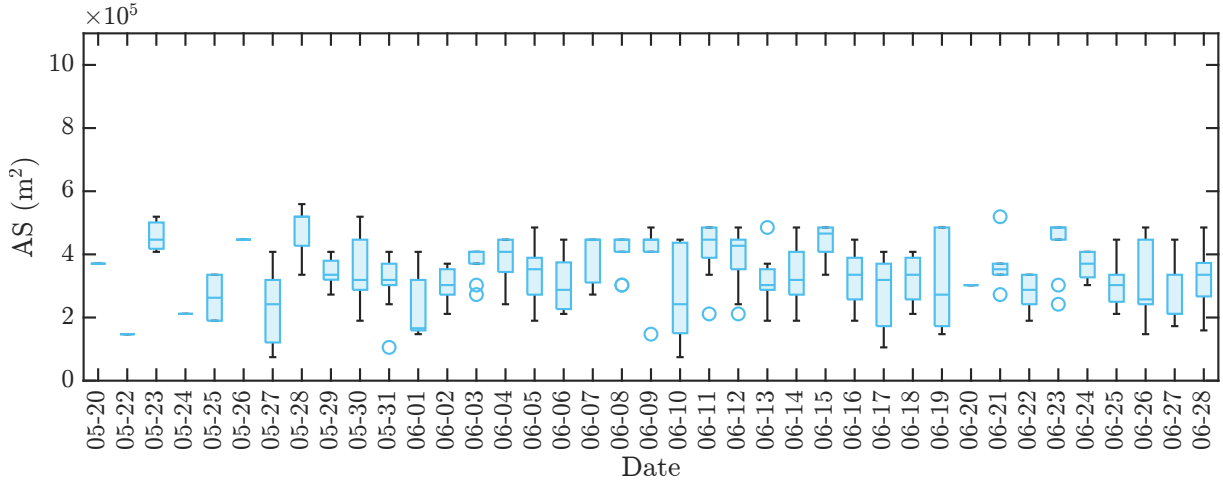
Figure B.2 − Evolution of active space over the season, considering a variable L_{90}, and a fixed meteorological condition according to median parameters $u_{*,\mathrm{med}} = 0.15$ m/s and $\theta_{*,\mathrm{med}} = 0.05$ K.
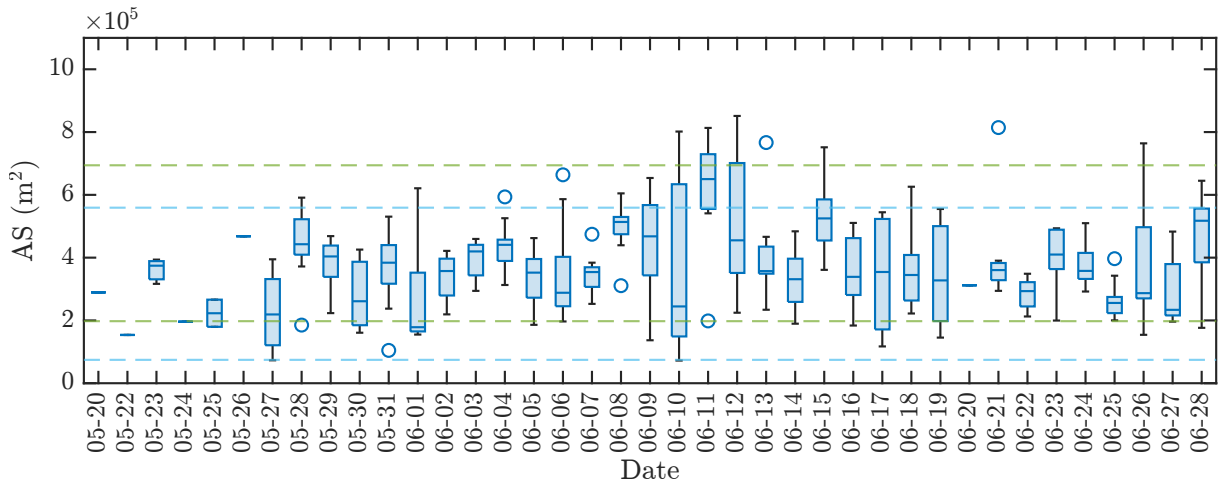
Figure B.3 − Evolution of active areas over the season, considering variation in weather and BN. The dotted lines show the min and max of the areas for the meteorological variation with median BN (green), and for the BN variation with median meteorological parameters (blue).

directly determines the decay threshold and thus the area covered by the active space, is therefore the most influential variable. But taken together the meteorological (wind and temperature profiles) and BN variations induce a variability much higher than the two phenomena observed separately. These two effects must therefore be taken into account to correctly estimate the active space.
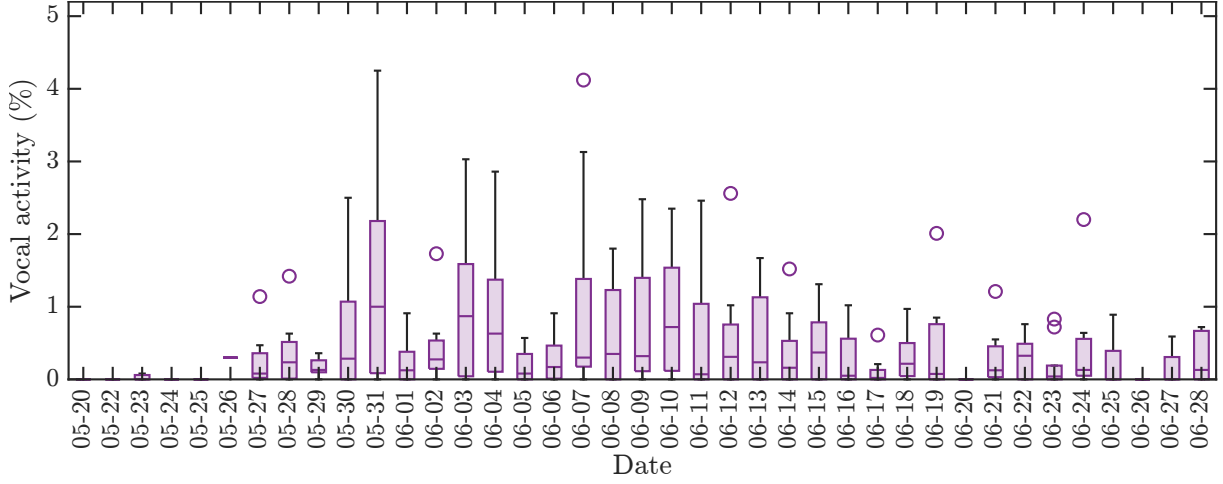
Figure B.4 − Evolution of vocal activity over the season.

B.1.2 Over the day
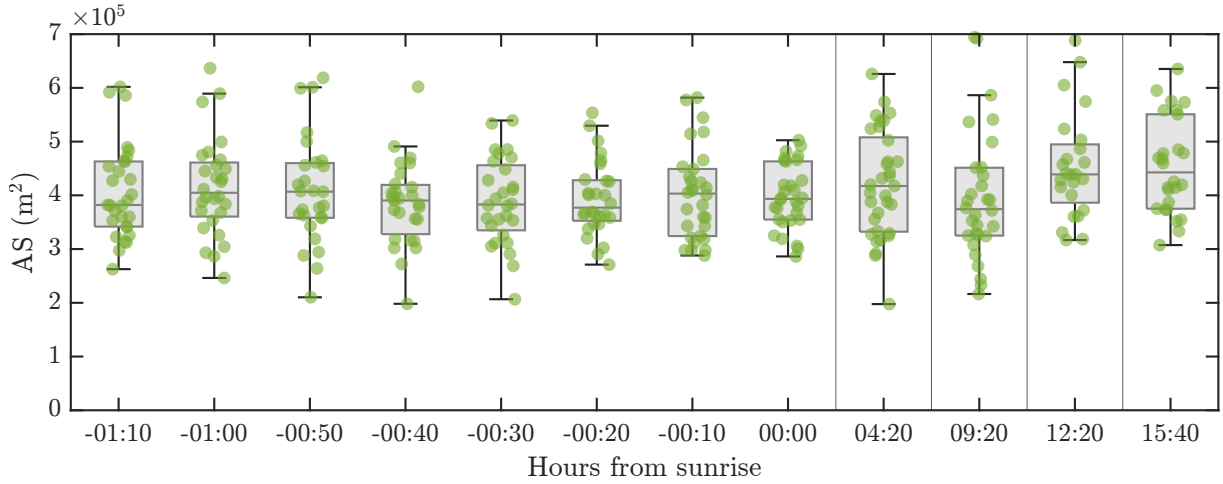
Figure B.5 − Evolution of active spaces during the day, considering the variation of weather conditions, and the median background noise level $L_{90,\text{med}} = 19$ dBSPL (time scale not respected).
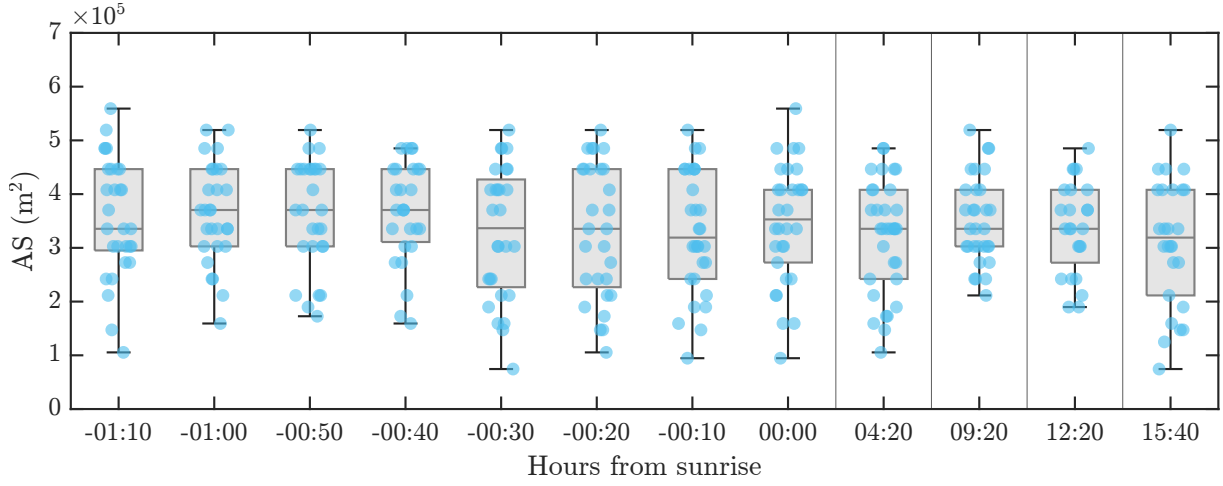
Figure B.6 − Evolution of active spaces during the day, for a variable background noise level L_{90}, and a fixed weather condition according to the median parameters $u_{*,\mathrm{med}} = 0.15$ m/s and $\theta_{*,\mathrm{med}} = 0.05$ K (time scale not respected).
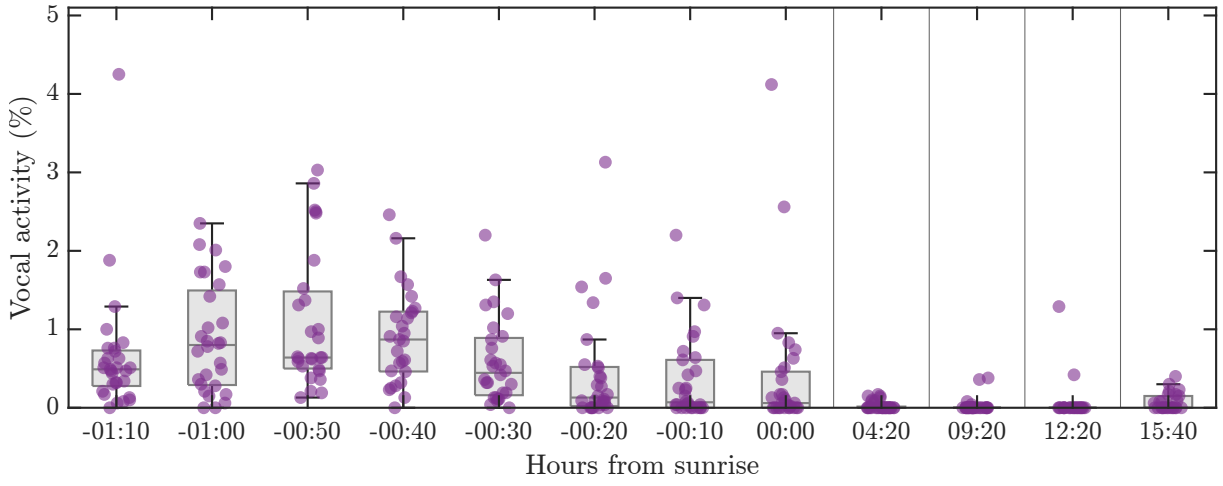
Figure B.7 − Evolution of vocal activity during the day (time scale not respected).
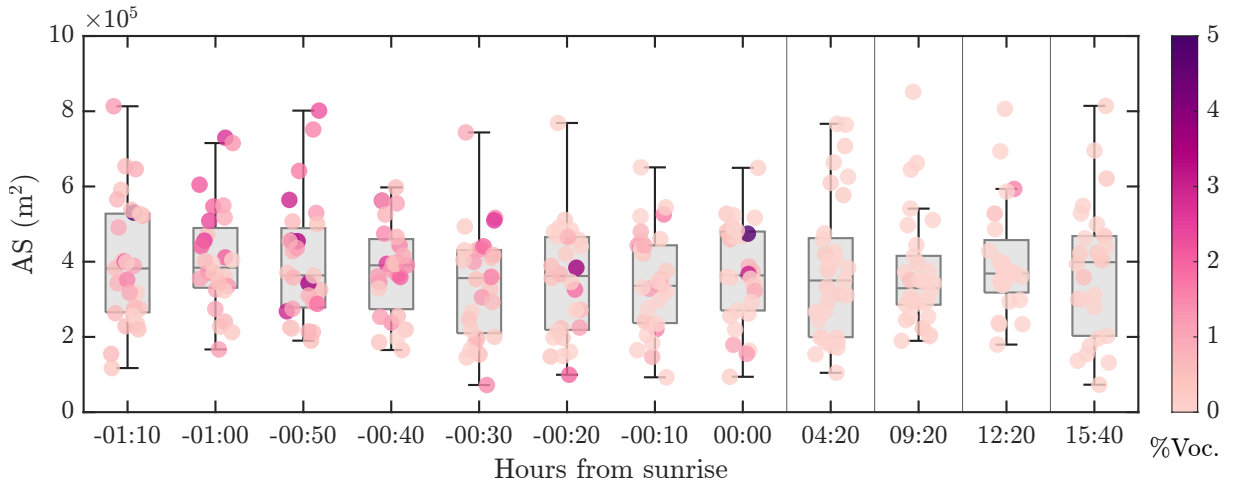
Figure B.8 − Evolution of the active spaces during the day. The color of the dots is relative to the vocal activity at the same period of time (time scale not respected).

B.1.3 Influence of background noise on AS

We plot on Fig. B.9 the AS areas computed from s1 location (see Sec. 5.2.6) estimated according to the L_{90} values (from SM4 audio samples: 10 min samples, N = 452, from May 20 to June 28, 2021 in Flaine). We show a strong correlation between the background noise and the area of the active space, with a polynomial relation of degree 3. As seen previously, the area is particularly sensitive to the detection threshold considered, and this one is directly related to the background noise. This factor is therefore of crucial importance, both for the active space and for the detection space. Moreover, its short or long term variations must be taken into account to describe the active and detection spaces. This can be of great importance for communication, but also to evaluate the sampling pressure related to an autonomous recorder.
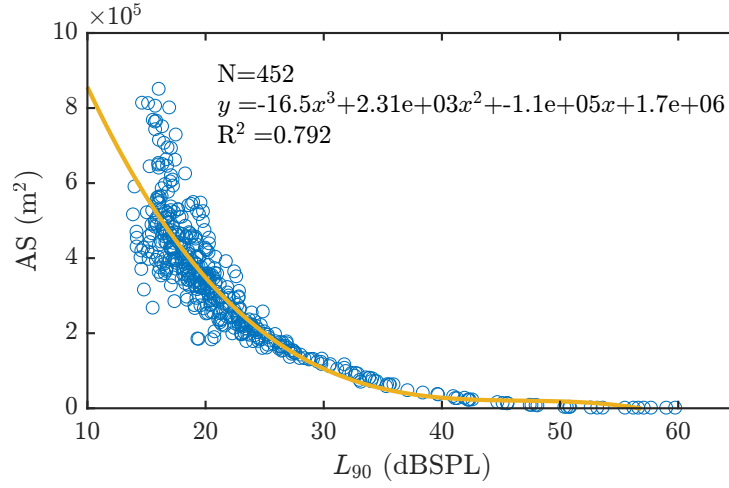
Figure B.9 − AS area function of L_{90} and polynomial regression.

B.2 Spatial variability of active spaces

Table B.1 − Data from 2017 monitored birds on the Flaine site, June 6-12: total number of display flights.

Day	1	2	3	4	5	6	7
Number of flights	27	33	37	16	31	21	11
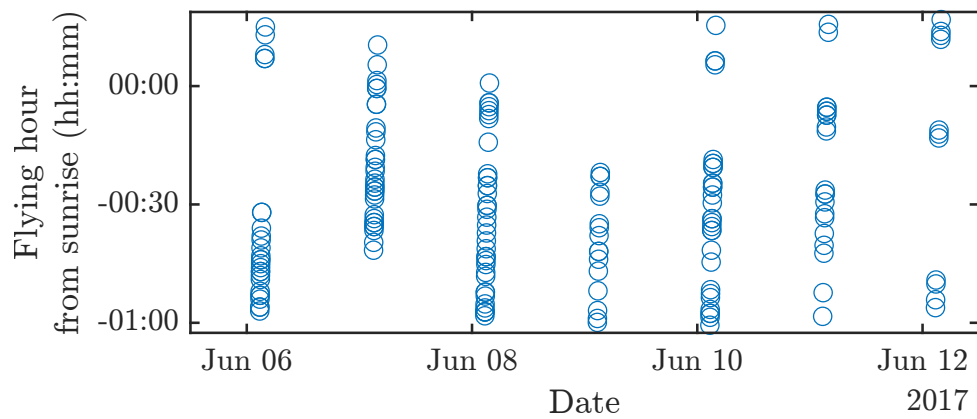
Figure B.10 – Instants of the display flights of the five tagged ptarmigan over the week June 6-12, 2017 (N=176).
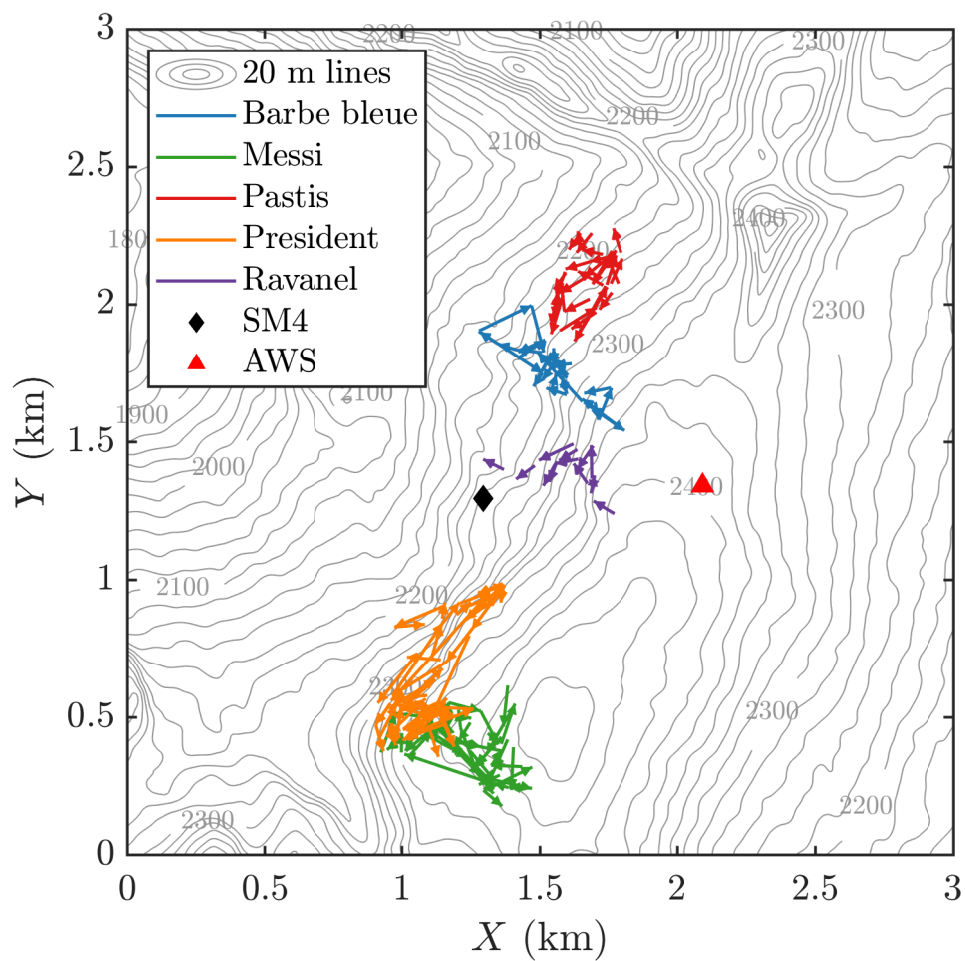
Figure B.11 – Vectors representing the display flights of the five tagged ptarmigan from June 6-12, 2017 (N=176).
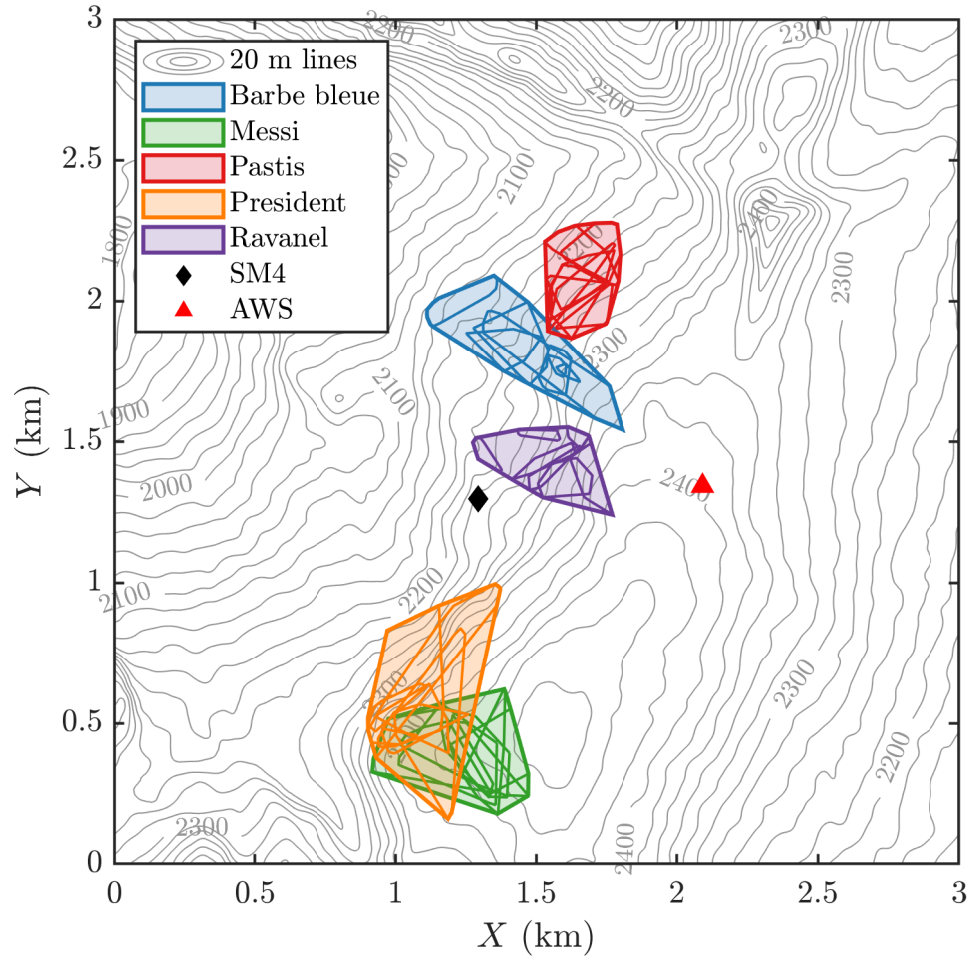
Figure B.12 − Mapping of the territories of 5 ptarmigan from 6 to 12 June 2017 determined according to the convex polygons of the GPS points on 7 days (colored areas), and occupied areas of each day (thin line polygons).
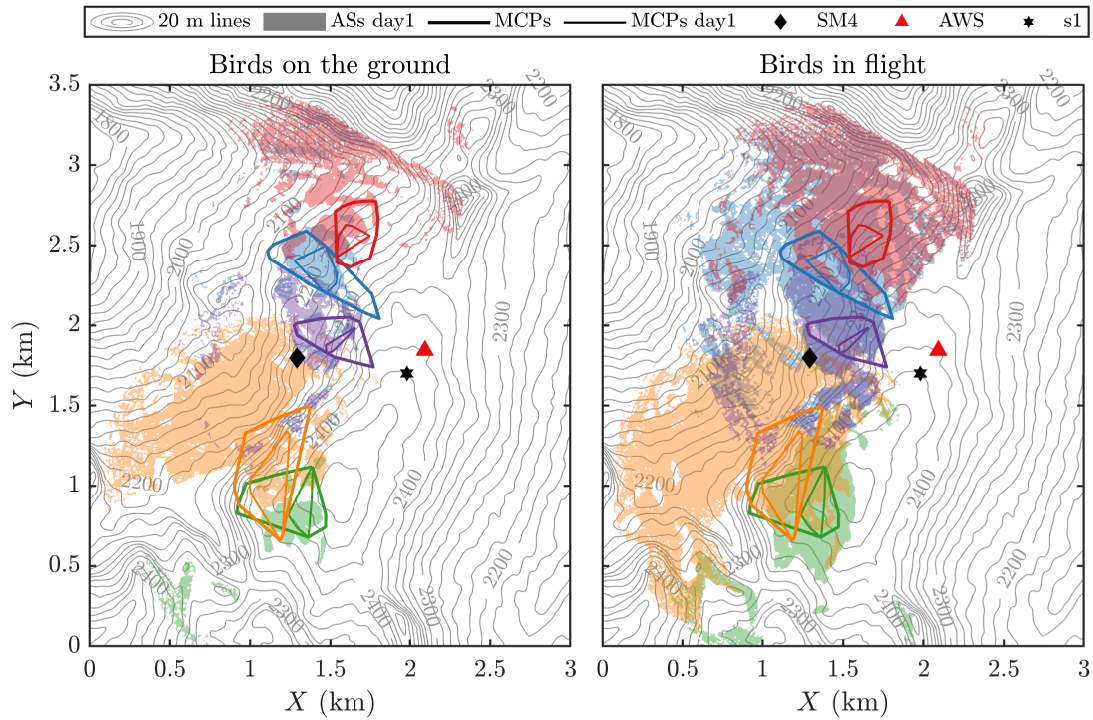
Figure B.13 − Mapping of 5 ptarmigan territories from June 6-12, 2017 (bold polygons), occupied area during the day 1 (thin polygons), and cumulative ASs (colored areas) calculated from display flights positions of birds during the day 1: ground singing (left), and according to their flight height (right). Birds are defined by their color in Tab. 5.1 : Barbe bleue, Messi, Pastis, President, and Ravanel. Positions of the audio recorder (SM4), of the automated weather station (AWS) and of the source used for temporal variability (s1) are also represented on the topography map (20 m contour lines).
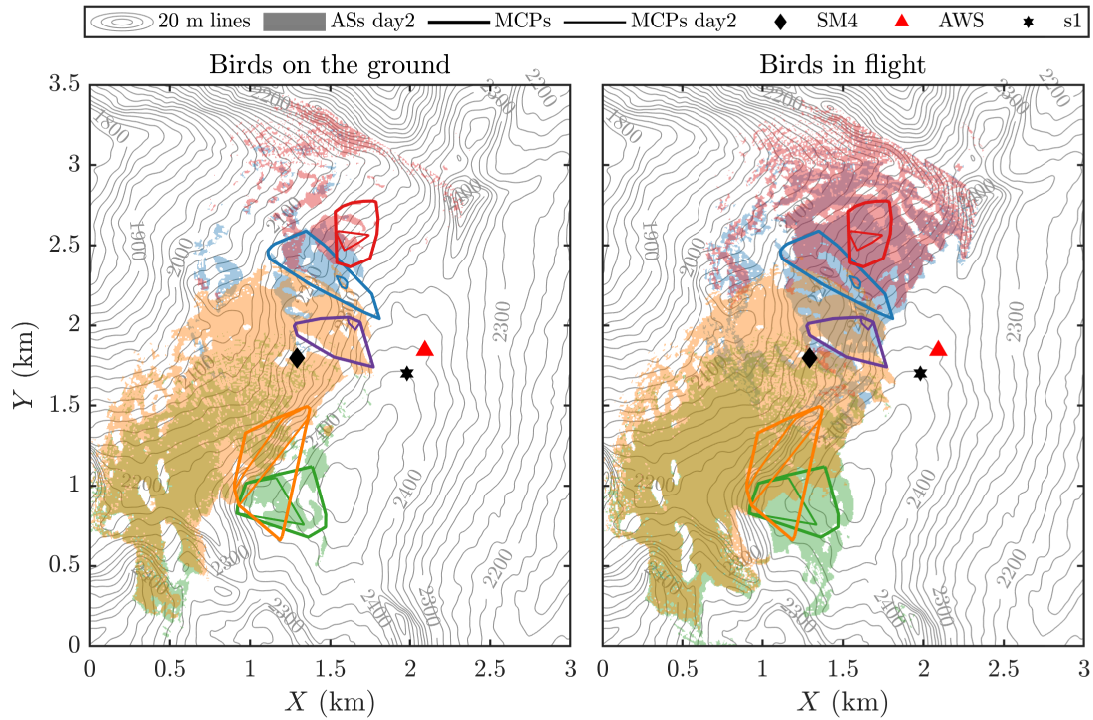
Figure B.14 − Same as Figure B.13 but for day 2.
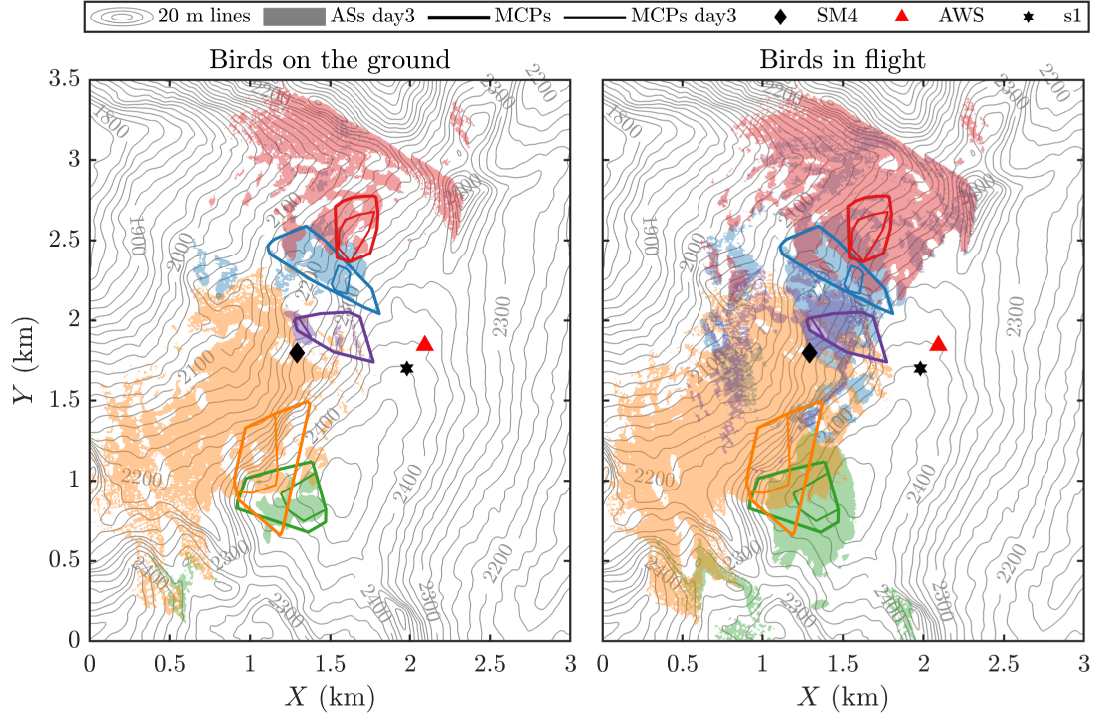
Figure B.15 – Same as Figure B.13 but for day 3.
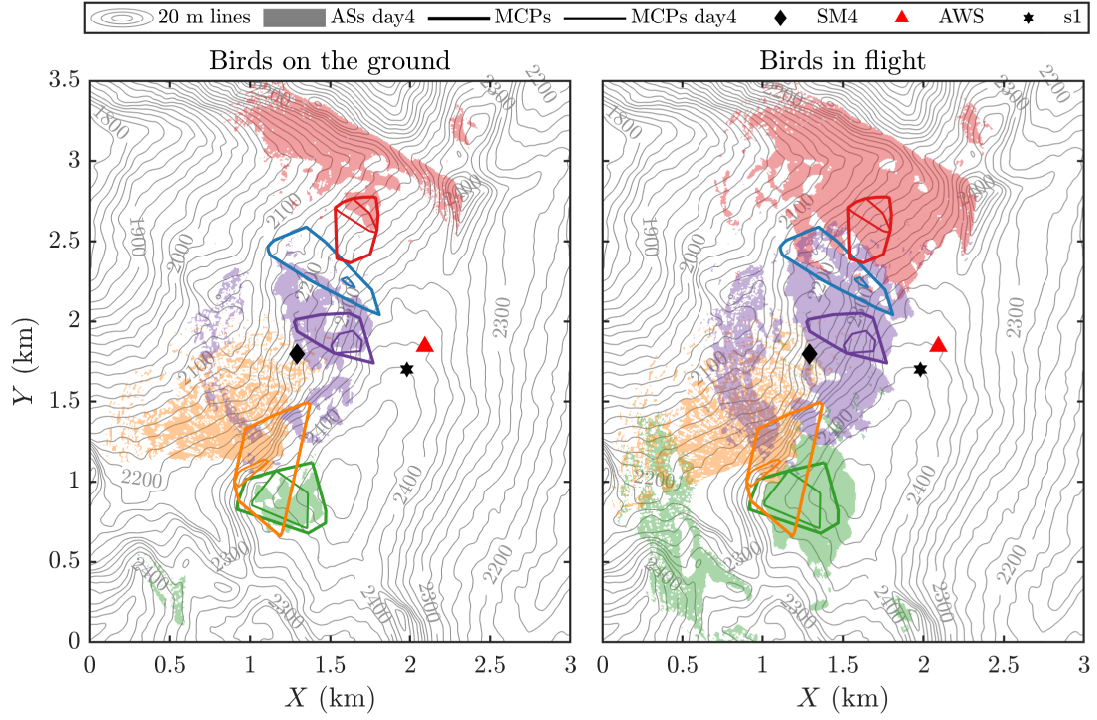
Figure B.16 – Same as Figure B.13 but for day 4.
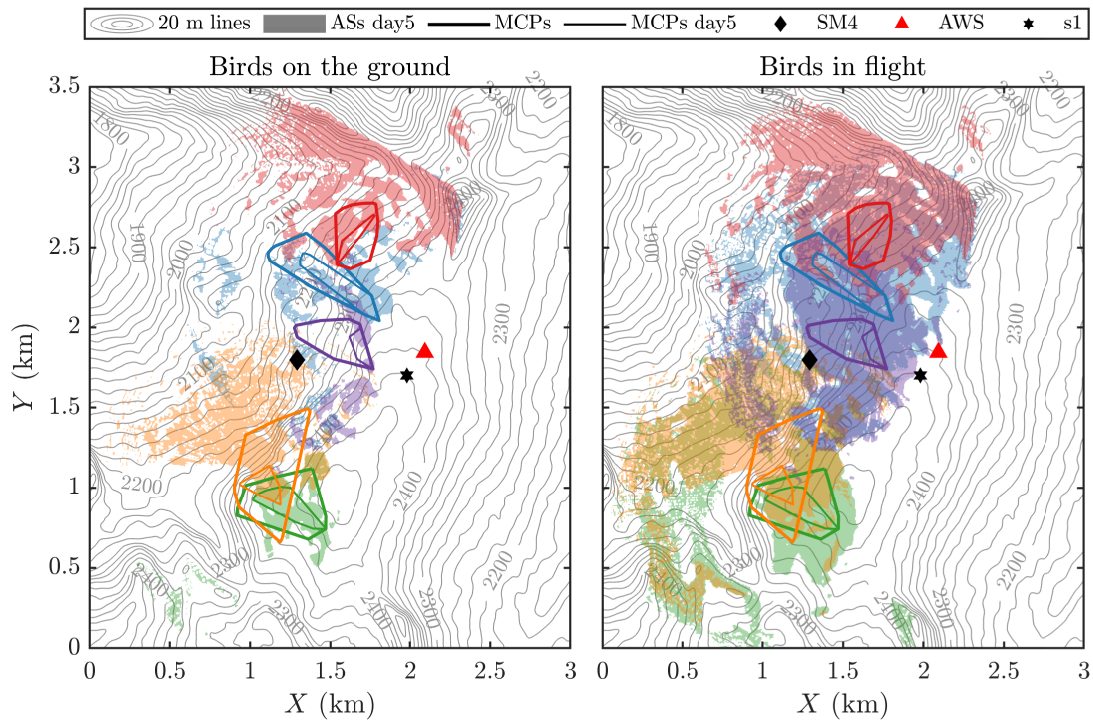
Figure B.17 – Same as Figure B.13 but for day 5.
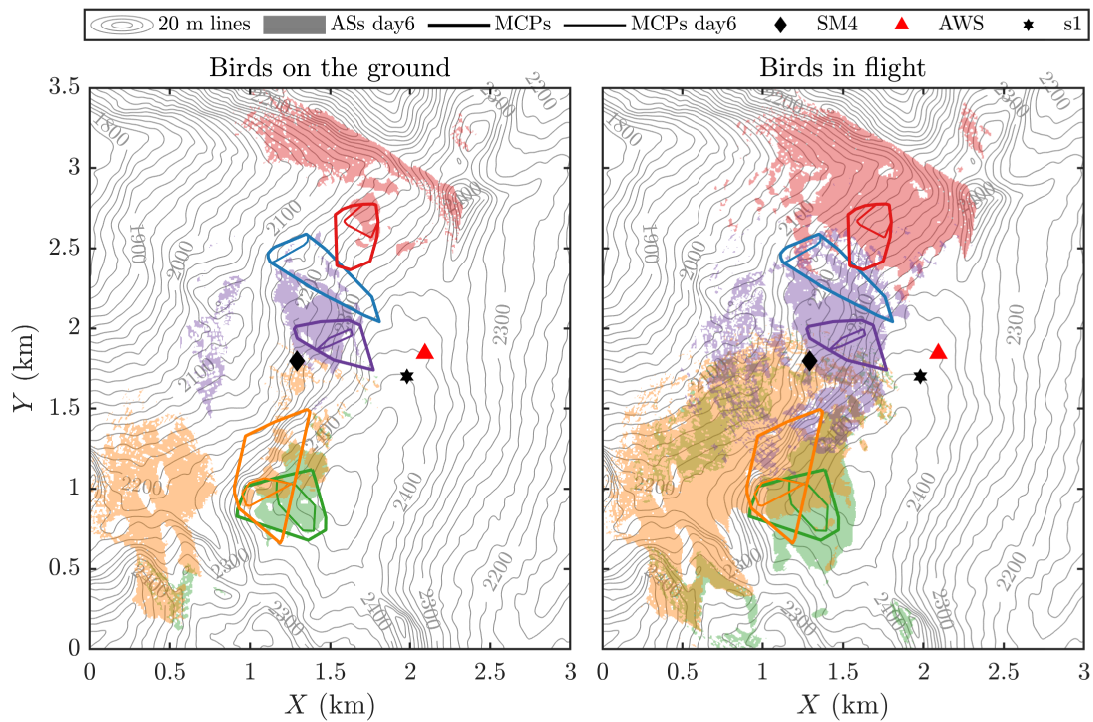
Figure B.18 – Same as Figure B.13 but for day 6.
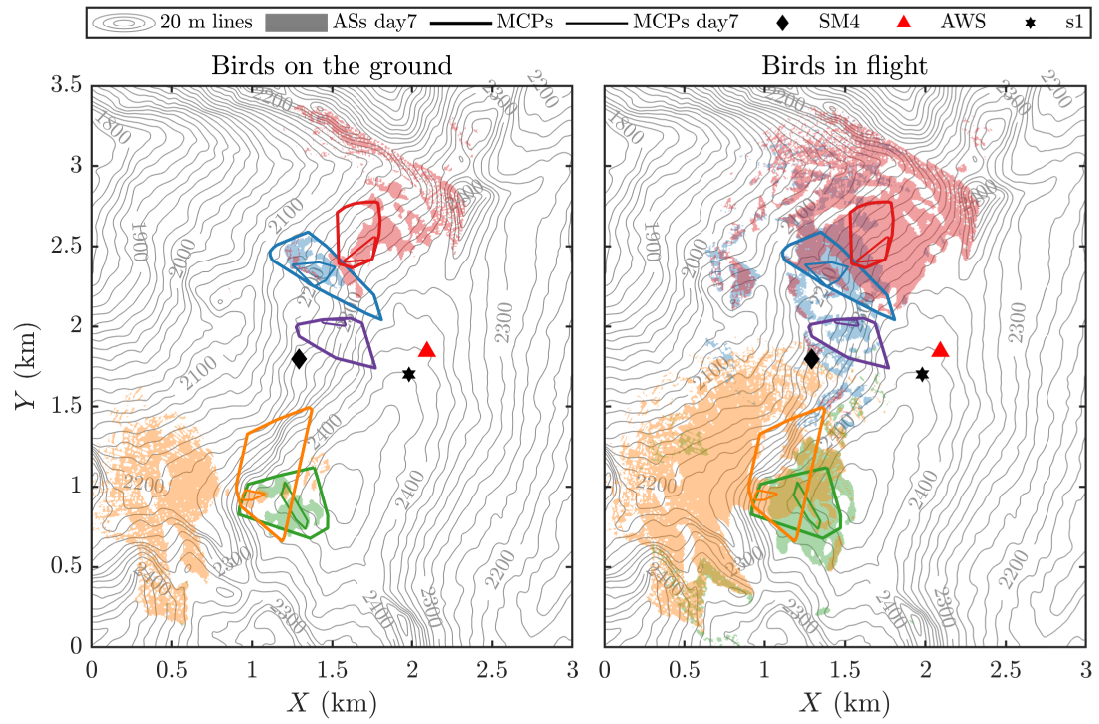
Figure B.19 – Same as Figure B.13 but for day 7.

B.3   Influence of rainfall on movements

To highlight the constraint of rain on bird movements, we use daily GPS data and data from Météo-France. The precipitation data used here comes from the Météo-France station located at the bottom of the ski resort at an altitude of 1611 m. The total distance traveled in one morning for a male ptarmigan is between 180 m and 2400 m, based on GPS tracking data of 11 ptarmigans compiled over the years 2018 to 2021 (see: Fig. B.20).

There is a significant difference between ptarmigan movements in the presence and absence of rain (T-test with paired data: t = -2.72, p-value = 0.01, N_{YES} = 11, N_{NO} = 11). In the presence of rain, there is a 39.7 % decrease in distance traveled per day, compared to days without rain.
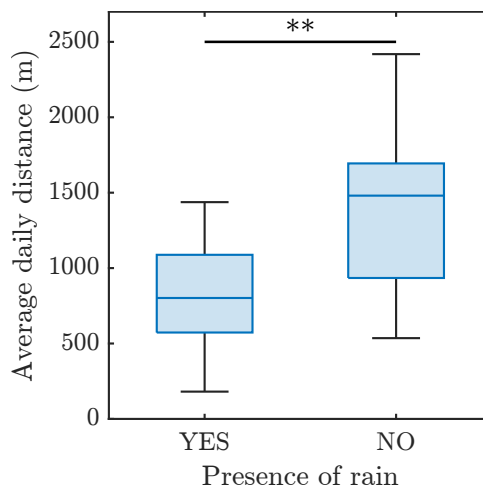
Figure B.20 − Influence of rainfall on the average daily distance traveled by ptarmigans during springtime 2018 to 2021, compared using t-test with paired data (11 monitored birds, ∗∗ means p-value < 0.01).

Thus, ptarmigans limit their movements when it rains. Several reasons can be mentioned to explain this. This behavior could be explained by the fact that rain induces a higher energy cost for the birds. They must maintain a constant body temperature, and this is to the detriment of the movements intended to protect their territory. Indeed, if the insulating layer of air trapped in the feathers is replaced by water, the birds will undergo a very important loss of heat, and they will have to compensate it by drawing from their reserves. This leads to an additional energy cost for the birds (Nye, 1964). Another reason could be the difficulty to flight with wet wings, that discourages birds to perform display flights. In addition, the increase in background noise leads to a reduction in detection space. As the detection space is reduced, neighbors are less likely to be heard, and this reduces the motivation to sing and defend the boundaries of the territory.

B.4 Effect of wind in microphones when assessing background noise

Natural background noise has been characterized in relation to wind speed by Boersma (1998). Following the relation (3) of Boersma: $L_{95} = a \log_{10}(V) + b$, with empirical coefficients a and b, and fixing $V = 3$ m/s, we found the potential background noise (BN) generated by the interaction of wind with the environment according to 1/3 octave frequency bands. It leads to $L_{95,1000\,\text{Hz}} = 20.9$ dBSPL, and $L_{95,\text{sum}} = 29.4$ dBSPL for the sum over the 1/3 octave frequency bands $500 - 3150$ Hz (to best match our analysis bandwidth strictly filtered at 400 and 4000 Hz). This last level prediction appears to be in the high range compared to our results of L_{90} between 13.3 to 33.7 dBSPL (see Fig. 5.3). Given the fact that Boersma's measurements were made on grasslands, it seems consistent that the resulting empirical relationship slightly overestimates noise levels in the case of a smooth environment such as a snowy mountain.
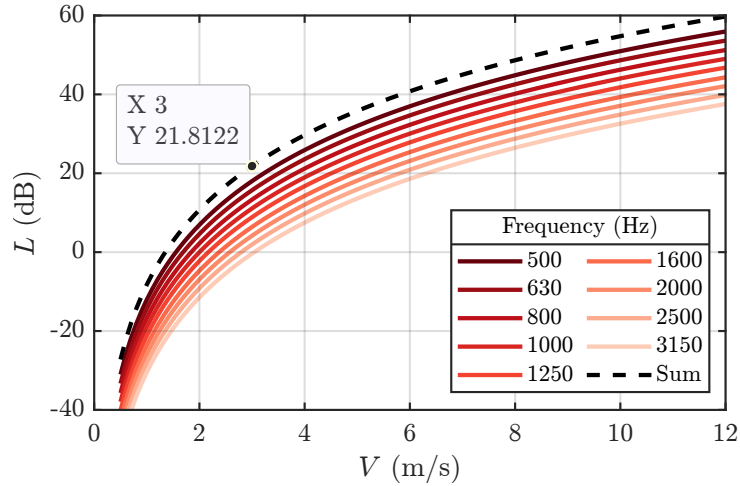
Figure B.21 – Supplementary: Estimated level of noise generated in a microphone with a 3 cm diameter windscreen, depending on the wind speed: For different $1/3$ octave band, and for the logarithmic sum over the $500 - 3150$ Hz bands.

Regarding the wind-induced noise in the microphone, we can rely on the work of van den Berg to estimate its contribution to the total noise (van den Berg, 2006). Based on a previous dimensional analysis (Strasberg, 1998), he describes the generated sound level in a 1/3 octave band as a function of wind speed and windscreen diameter as follows: $L_{1/3} = 40 \log_{10}(V/V_0) - 23 \log_{10}(f_m D/V) + 15$, with V_0 a reference velocity of 1 m/s, f_m the middle frequency of the 1/3 octave band, and D the windscreen diameter. It yields for the 3 cm windscreen mounted on the original SM4 recorder, and a wind speed of 3 m/s, $L_{1/3} = 11.1$ dBSPL at 1000 Hz, and $L_{sum} = 21.8$ dBSPL for the sum over the 1/3 octave bands $500 - 3150$ Hz, as seen in Fig. B.21. This implies that contribution of wind on the microphone to the L_{90} is significant given the samples measured below this wind speed, distributed over the range 13.3 to 33.7 dBSPL, with a median of 19 dBSPL. Finally, it

seemed reasonable to us to set this wind speed limit at 3 m/s at the microphone height and to exclude samples for which the noise induced directly in the microphone becomes predominant, i.e. 3 dB louder than the L_{90} median level.

Bibliography

Abrarov SM, Quine BM. (**2011**) "Efficient algorithmic implementation of the Voigt/complex error function based on exponential series approximation," Appl. Math. Comput., **218**(5), 1894–1902, doi: `10.1016/j.amc.2011.06.072`. (Cited page: 53).

Adi K, Johnson MT , Osiejuk TS. (**2010**) "Acoustic censusing using automatic vocalization classification and identity recognition," J. Acoust. Soc. Am., **127**(2), 874–883, doi: `10.1121/1.3273887`. (Cited page: 163).

Adrian C, Griffith SC, Naguib M, Schuett W. (**2022**) "Wild zebra finches are attracted towards acoustic cues from conspecific social groups," Behav. Ecol., **33**(3), 556–564, doi: `10.1093/beheco/arac013`. (Cited page: 7).

Akabak (demo version 3.1.7 b100 retrieve in 21.01.2023), Panzer & Partner, Software engineering and electroacoustics, Steinstr 15, D-81667 Munich, F.R. Germany. (AkAbak is the registered trademark of Panzer & Partner, J.W. Panzer, FRG) (Cited page: 74).

Aide TM, Corrada-Bravo C, Campos-Cerqueira M, Milan C, Vega G, Alvarez R. (**2013**) "Real-time bioacoustics monitoring and automated species identification," PeerJ, 1, e103, doi: `10.7717/peerj.103`. (Cited pages: 182, 184).

Albert DG. (**2001**) "Acoustic waveform inversion with application to seasonal snow covers," J. Acoust. Soc. Am., **109**(1), 91–101, doi: `10.1121/1.1328793`. (Cited pages: 117, 118).

Albert DG. (**2003**) "Observations of acoustic surface waves in outdoor sound propagation," J. Acoust. Soc. Am., **113**(5), 2495–2500, doi: `10.1121/1.1559191`. (Cited page: 53).

Alcocer I, Lima H, Sugai LSM, Llusia D. (**2022**) "Acoustic indices as proxies for biodiversity: a meta-analysis," Biol. Rev., **97**(6), 2209–2236, doi: `10.1111/brv.12890`. (Cited page: 163).

Amagai S, Dooling RJ, Shamma S, Kidd TL, Lohr B. (**1999**) "Detection of modulation in spectral envelopes and linear-rippled noises by budgerigars (*Melopsittacus undulatus*)," J. Acoust. Soc. Am., **105**(3), 2029–2035, doi: `10.1121/1.426736`. (Cited pages: 35, 198).

Anderson DR. (**2001**) "The need to get the basics right in wildlife field studies," on JSTOR, Wildlife Society Bulletin (1973-2006), **29**(4), 1294–1297. (Cited pages: 184, 203).

ANSI/ASA S1.18-2010. *Method for Determining the Acoustic Impedance of Ground Surfaces*, Accredited Standards Committee S1, Acoustics. American National Standard (revision of ANSI S1.18-1999). (Cited page: 117).

Artiss T, Martin K. (**1995**) "Male vigilance in white-tailed ptarmigan, *Lagopus leucurus*: mate guarding or predator detection?," Anim. Behav., **49**(5), 1249–1258, doi: `10.1006/anbe.1995.0157`. (Cited page: 16).

Attenborough K. (**1992**) "Ground parameter information for propagation modeling," J. Acoust. Soc. Am., **92**(1), 418–427, doi: `10.1121/1.404251`. (Cited page: 56).

Attenborough K. (**2002**) "Sound propagation close to the ground," Annu. Rev. Fluid Mech., **34**(1), 51–82, doi: `10.1146/annurev.fluid.34.081701.143541`. (Cited page: 101).

Attenborough K. (**2007**) "Sound propagation in the atmosphere," in *Handbook of Acoustics*, (Ed. TD Rossing), 113–147, Springer, New York. (Cited page: 25).

Attenborough K, Bashir I, Taherzadeh S. (**2011**) "Outdoor ground impedance models," J. Acoust. Soc. Am., **129**(5), 2806–2819, doi: `10.1121/1.3569740`. (Cited pages: 54, 56, 56, 56).

Attenborough K, van Renterghem T. (**2021**) *Predicting Outdoor Sound*, Second edition, CRC Press Taylor & Francis Group, Boca Raton, doi: `10.1201/9780429470806`. (Cited pages: 110, 118, 122).

Attenborough K, Waters-Fuller T. (**2000**) "Effective impedance of rough porous ground surfaces," J. Acoust. Soc. Am., **108**(3), 949–956, doi: `10.1121/1.1288940`. (Cited page: 101).

Aubin T, Jouventin P. (**2002**) "How to vocally identify kin in a crowd: The penguin model," Adv Stud Behav, **31**, 243–277, doi: `10.1016/S0065-3454(02)80010-9`. (Cited page: 137).

Aubin T, Mathevon N, da Silva ML, Vielliard JME, Sebe F. (**2004**) "How a simple and stereotyped acoustic signal transmits individual information: the song of the White-browed Warbler Basileuterus leucoblepharus," An. Acad. Bras. Ciênc., **76**(2), 335–344, doi: `10.1590/S0001-37652004000200022`. (Cited page: 10).

Aubin T, Mathevon N, da Silva ML. (**2014**) "Species Identity Coding by the Song of a Rainforest Warbler: An Adaptation to Long-Range Transmission?," Acta Acust. United Acust., **100**(4), 748–758, doi: `10.3813/AAA.918754`. (Cited pages: 136, 137).

Aubin T, Mathevon N. (**2020**) *Coding strategies in vertebrate acoustic communication* (Springer Nature Switzerland, Cham), doi: 10.1007/978-3-030-39200-0. (Cited pages: 107, 197).

Bailly C, Juve D. (**2000**) "Numerical solution of acoustic propagation problems using linearized Euler equations," AIAA Journal, **38**(1), 22–29, doi: 10.2514/2.949. (Cited page: 30).

Balsby T, Pedersen SB, Dabelsteen T. (**2003**) "Degradation of whitethroat vocalizations: Implications for song flight and communication network activities," Behaviour, **140**(6), 695–719, doi: 10.1163/156853903322370634. (Cited page: 137).

Baltz AP, Clark AB. (**1997**) "Extra-pair courtship behaviour of male budgerigars and the effect of an audience," Anim. Behav., **53**(5), 1017–1024, doi: 10.1006/anbe.1996.0354. (Cited page: 9).

Barker N, Dabelsteen T, Mennill D. (**2009**) "Degradation of male and female rufous-and-white wren songs in a tropical forest: effects of sex, perch height, and habitat," Behaviour, **146**(8), 1093–1122, doi: 10.1163/156853909X406446. (Cited pages: 6, 137).

Bart J, Earnst SL. (**1999**) "Relative importance of male and territory quality in pairing success of male rock ptarmigan (*Lagopus mutus*)," Behav. Ecol. Sociobiol., **45**(5), 355–359, doi: 10.1007/s002650050571. (Cited page: 16).

Bass HE, Sutherland LC, Zuckerwar AJ, Blackstock DT, Hester DM. (**1995**) "Atmospheric absorption of sound: Further developments," J. Acoust. Soc. Am., **97**(1), 680–683, doi: 10.1121/1.412989. (Cited page: 21, 21).

Bass HE, Sutherland LC, Zuckerwar AJ, Blackstock DT, Hester DM. (**1996**) "Erratum: atmospheric absorption of sound: further developments [J. Acoust. Soc. Am. **97**, 680–683 (1995)]," J. Acoust. Soc. Am., **99**(2), 1259–1259, doi: 10.1121/1.415223. (Cited page: 21).

Becker PH. (**1982**) "The coding of species-specific characteristics in bird sounds,", vol. 1 (Eds. DE Kroodsma, EM Miller, H Ouellet), 214–244, Academic Press, New York, USA. (Cited page: 10).

Bech N, Beltran S, Boissier J, Allienne JF, Resseguier J, Novoa C. (**2012**) "Bird mortality related to collisions with ski-lift cables: do we estimate just the tip of the iceberg?," Anim. Biodivers. Conserv., **35**(1), 95–98, doi: . (Cited page: 14).

Beecher MD, Stoddard PK, Loesche P. (**1985**) "Recognition of parents' voices by young cliff swallows," Auk, **102**(3), 600–605, doi: 10.1093/auk/102.3.600. (Cited page: 7).

Berenger J-P. (**1994**) "A perfectly matched layer for the absorption of electromagnetic waves," J. Comput. Phys., **114**(2), 185–200, doi: `10.1006/jcph.1994.1159`. (Cited page: 85).

Bérengier MC, Gauvreau B, Blanc-Benon P, Juvé D. (**2003**) "Outdoor sound propagation: a short review on analytical and numerical approaches," Acta Acust. United Acust., **89**(6), 980–991. (Cited pages: 25, 52, 194).

Bérengier MC, Stinson MR, Daigle GA, Hamet JF. (**1997**) "Porous road pavements: Acoustical characterization and propagation effects," J. Acoust. Soc. Am., **101**(1), 155–162, doi: `10.1121/1.417998`. (Cited pages: 54, 110).

van den Berg GP. (**2006**) "Wind-induced noise in a screened microphone," J. Acoust. Soc. Am., **119**(2), 824–833, doi: `10.1121/1.2146085`. (Cited page: 229).

Bevanger K, Brøseth H. (**2004**) "Impact of power lines on bird mortality in a subalpine area," Anim. Biodivers. Conserv., **27**(2), 67–77. (Cited page: 14).

Birkhead TR, van Balen S. (**2008**) "Bird-keeping and the development of ornithological science," Archives of Natural History, **35**(2), 281–305, doi: `10.3366/E0260954108000399`. (Cited page: 1).

Bjørneraas K, Van Moorter B, Rolandsen CM, Herfindal I. (**2010**) "Screening global positioning system location data for errors using animal movement characteristics," Journal of Wildlife Management, **74**(6):1361–1366, doi: `10.1111/j.1937-2817.2010.tb01258.x`. (Cited pages: 72, 140).

Blairon N. (**2002**) "Effets de la topographie sur la propagation des ondes acoustiques dans l'atmosphère : modélisation avec l'équation parabolique et validation sur un site extérieur,", PhD thesis, Ecole Centrale de Lyon. (Cited pages: 31, 86, 100, 165, 171, 195).

Blairon N, Blanc-Benon P, Bérengier M, Juvé D. (**2002**) "Outdoor sound propagation in complex environment: experimental validation of a PE approach," in Proceedings of the 10th International Symposium on Long Range Sound Propagation, Grenoble, France, 2002, 114–128. (Cited pages: 29, 31, 82, 109).

Blanc-Benon P, Lipkens B, Dallois L, Hamilton MF, Blackstock DT. (**2002**) "Propagation of finite amplitude sound through turbulence: Modeling with geometrical acoustics and the parabolic approximation," J. Acoust. Soc. Am., **111**(1), 487–498, doi: `10.1121/1.1404378`. (Cited pages: 29, 101, 195).

Blumstein DT, Mennill DJ, Clemins P, Girod L, Yao K, Patricelli G, Deppe JL, Krakauer AH, Clark C, Cortopassi KA, Hanser SF, McCowan B, Ali AM, Kirschel ANG. (**2011**)

"Acoustic monitoring in terrestrial environments using microphone arrays: applications, technological considerations and prospectus," J. Appl. Ecol., **48**(3), 758–767 doi: `10.1111/j.1365-2664.2011.01993.x`. (Cited page: 162).

Boersma HF. (**1998**) "Characterization of the natural ambient sound environment: Measurements in open agricultural grassland," J. Acoust. Soc. Am., **101**(4), 2104–2110, doi: `10.1121/1.418141`. (Cited page: 229).

Bonar SA, Fehmi JS, Mercado-Silva N. (**2011**) "An overview of sampling issues in species diversity and abundance surveys," in *Biological diversity: frontiers in measurement and assessment*, (Eds. AE Magurran, BJ McGill), 11–24, Oxford University Press. (Cited pages: 184, 203).

Borker AL, Mckown MW, Ackerman JT, Eagles-Smith CA, Tershy BR, Croll DA. (**2014**) "Vocal activity as a low cost and scalable index of seabird colony size," Conserv. Biol., **28**(4), 1100–1108, doi: `10.1111/cobi.12264`. (Cited page: 165).

Bossert A. (**1977**) "Bestandesaufnahmen am Alpenschneehuhn (Lagopus mutus) im Aletchgebiet," Der Ornithologische Beobachter, **74**, 95–98. (Cited page: 105).

Boucaud ICA, Perez EC, Ramos LS, Griffith SC, Vignal C. (**2017**) "Acoustic communication in zebra finches signals when mates will take turns with parental duties," Behav. Ecol., **28**(3), 645-656, doi: `10.1093/beheco/arw189`. (Cited page: 7).

Boulanger P, Waters-Fuller T, Attenborough K, Li KM. (**1998**) "Models and measurements of sound propagation from a point source over mixed impedance ground," J. Acoust. Soc. Am., **102**(3), 1432–1442, doi: `10.1121/1.420101`. (Cited page: 28).

Bradbury JW, Vehrencamp SL. (**2011**) "Principles of animal communication," 2nd edn, Sinauer Associates, Sunderland, MA. (Cited pages: 6, 136).

Bradfer-Lawrence T, Gardner N, Bunnefeld L, Bunnefeld N, Willis SG, Dent DH. (**2019**) "Guidelines for the use of acoustic indices in environmental research," Methods Ecol. Evol., **10**(10), 1796–1807, doi: `10.1111/2041-210X.13254`. (Cited page: 163).

Brackenbury JH. (**1982**) "The structural basis of voice production and its relationship to sound characteristics," in *Acoustic Communication in Birds* (Eds. DE Kroodsma, EH Miller, H Ouellet), 53–73, Academic Press, New York, USA. (Cited page: 9).

Brambilla M, Rubolini D, Appukuttan O, Calvi G, Karger DN, Kmecl P, Mihelič T, Sattler T, Seaman B, Teufelbauer N, Wahl J, Celada C. (**2022**) "Identifying climate refugia for high-elevation Alpine birds under current climate warming predictions," Global Change Biol., **28**(14), 4276–4291, doi: `10.1111/gcb.16187`. (Cited page: 15).

Brenot JF, Desmet JF, Morscheidt J. (**2002**) "Mise au point d'une méthode de capture des poules de lagopède alpine *Lagopus mutus* accompagnées de jeunes," Alauda, **70**, 190–191. (Cited pages: 71, 139).

Brenowitz EA. (**1982a**) "Long-range communication of species identity by song in the Red-winged Blackbird," Behav. Ecol. Sociobiol., **10**(1), 29–38, doi: 10.1007/BF00296393. (Cited pages: 9, 10).

Brenowitz EA. (**1982b**) "The active space of red-winged blackbird song," J. Comp. Physiol., **147**(4), 511–522, doi: 10.1007/BF00612017. (Cited pages: 35, 35, 104, 106, 137, 142, 145, 147, 158, 159, 198).

Briefer E, Rybak F, Aubin T. (**2008**) "When to be a dear enemy: flexible acoustic relationships of neighbouring skylarks, *Alauda arvensis*," Anim. Behav., **76**(4), 1319–1325, doi: 10.1016/j.anbehav.2008.06.017. (Cited page: 16).

Briefer E, Aubin T, Rybak F. (**2009**) "Response to displaced neighbours in a territorial songbird with a large repertoire," Naturwissenschaften, **96**(9), 1067–1077, doi: 10.1007/s00114-009-0567-0. (Cited page: 10).

Brodsky LM, Montgomerie RD. (**1987**) "Asymmetrical contests in defence of rock ptarmigan territories," Behav. Ecol. Sociobiol., **21**(4), 267–272, doi: 10.1007/BF00292508. (Cited page: 16).

Brodsky LM. (**1988**) "Mating tactics of male rock ptarmigan, *Lagopus mutus*: a conditional mating strategy," Anim. Behav., **36**(2), 335–342, doi: 10.1016/S0003-3472(88)80003-4. (Cited page: 16).

Brumm H. (**2004**) "The impact of environmental noise on song amplitude in a territorial bird," Journal of Animal Ecology, **73**(3), 434–440, http://www.jstor.org/stable/3505653. (Cited pages: 33, 141).

Brumm H, Schmidt R, Schrader L. (**2009**) "Noise-dependent vocal plasticity in domestic fowl," Anim. Behav., **78**(3), 741–746, doi: 10.1016/j.anbehav.2009.07.004. (Cited page: 33).

Brumm H, Todt D. (**2002**) "Noise-dependent song amplitude regulation in a territorial songbird," Anim. Behav., **63**(5), 891–897, doi: 10.1006/anbe.2001.1968. (Cited page: 155).

Brumm H, Todt D. (**2004**) "Male–male vocal interactions and the adjustment of song amplitude in a territorial bird," Anim. Behav., **67**(2), 281–286, doi: 10.1016/j.anbehav.2003.06.006. (Cited page: 155).

Brumm H, Zollinger SA. (**2013**) "Avian vocal production in noise," in *Animal communication and noise* (Ed. H Brumm), 187–227, Berlin, Heidelberg, Springer Berlin Heidelberg, doi: 10.1007/978-3-642-41494-7_7. (Cited pages: 34, 141, 155).

Bruni A, Mennill DJ, Foote JR. (**2014**) "Dawn chorus start time variation in a temperate bird community: relationships with seasonality, weather, and ambient light," J. Ornithol., **155**(4), 877–890, doi: 10.1007/s10336-014-1071-7. (Cited page: 156).

Buckland ST, Anderson DR, Burnham KP, Laake JL, Borchers DL, Thomas L. (Eds.) (**2004**) *Advanced distance sampling: estimating abundance of biological populations*, OUP Oxford. (Cited page: 164).

Buffet N, Dumont-Dayot E. (**2013**) "Bird collisions with overhead ski-cables: a reducible source of mortality," in *The Impacts of Skiing and Related Winter Recreational Activities on Mountain Environments*, (Eds. C Rixen, A Rolando), 123-136, Bentham Science Publishers, doi: 10.2174/97816080548861130101. (Cited page: 14).

Burt JM, Vehrencamp SL. (**2005**) "Dawn chorus as an interactive communication network," in *Animal communication networks* (Ed. P McGregor), 320–343, New York, Cambridge University Press, doi: 10.1017/CBO9780511610363.019. (Cited pages: 8, 136, 200).

Buxton RT, McKenna MF, Clapp M, Meyer E, Stabenau E, Angeloni LM, Crooks K, Wittemyer G. (**2018**) "Efficacy of extracting indices from large-scale acoustic recordings to monitor biodiversity," Conserv. Biol., **32**(5), 1174–1184, doi: 10.1111/cobi.13119. (Cited page: 162).

Buxton VL, Enos JK, Sperry JH, Ward MP. (**2020**) "A review of conspecific attraction for habitat selection across taxa," Ecol. Evol., **10**(23), 12690–12699, doi: 10.1002/ece3.6922. (Cited page: 15).

Caizergues A, Bernard-Laurent A, Brenot J-F, Ellison L, Rasplus JY. (**2003**) "Population genetic structure of rock ptarmigan *Lagopus mutus* in Northern and Western Europe," Mol. Ecol., **12**(8), 2267–2274, doi: 10.1046/j.1365-294X.2003.01889.x. (Cited page: 15).

Campos-Cerqueira M, Aide TM. (**2016**) "Improving distribution data of threatened species by combining acoustic monitoring and occupancy modeling," Methods Ecol. Evol., **7**(11), 1340–1348, doi: 10.1111/2041-210X.12599. (Cited page: 163).

Candel SM. (**1977**) "Numerical solution of conservation equations arising in linear wave theory: application to aeroacoustics," J. Fluid Mech., **83**(3), 465–493, doi: 10.1017/S0022112077001293. (Cited page: 28).

Candel SM. (**1979**) "Numerical solution of wave scattering problems in the parabolic approximation," J. Fluid Mech., **90**(3), 465–507, doi: `10.1017/S0022112079002354`. (Cited page: 28).

Canonne C, Novoa C, Muffat-Joly B, Resseguier J, Desmet J-F, Casadesus JB, Arvin-Berod M, Besnard A. (**2020**) "Life on the edge: common slow pace of life but contrasted trajectories of alpine rock ptarmigan populations at their southern margin," Wildl. Biol., **2020**(2), 1–11, doi: `10.2981/wlb.00628`. (Cited pages: 11, 125, 139).

Castro I, De Rosa A, Priyadarshani N, Bradbury L, Marsland S. (**2019**) "Experimental test of birdcall detection by autonomous recorder units and by human observers using broadcast," Ecol. Evol., **9**(5), 2376–2397, doi: `10.1002/ece3.4775`. (Cited page: 182).

Catchpole C, Slater PJB. (**2008**) *Bird song: biological themes and variations* Second edition, Cambridge University Press, Cambridge, UK. (Cited pages: 6, 7).

Chandler-Wilde SN, Hothersall DC. (**1985**) "Sound propagation above an inhomogeneous impedance plane," J. Sound Vib., **98**(4), 475–491, doi: `10.1016/0022-460X(85)90257-3`. (Cited page: 28).

Cheinet S, Siebesma AP. (**2009**) "Variability of local structure parameters in the convective boundary layer," J. Atmos. Sci., **66**(4), 1002–1017, doi: `10.1175/2008JAS2790.1`. (Cited pages: 24, 192).

Cheinet S, Cumin P. (**2011**) "Local structure parameters of temperature and humidity in the entrainment-drying convective boundary layer: a Large-Eddy Simulation analysis," J. Appl. Meteorol. Climatol., **50**(2), 472–481, doi: `10.1175/2010JAMC2426.1`. (Cited page: 24).

Cheinet S, Ehrhardt L, Juvé D, Blanc-Benon P. (**2012**) "Unified modeling of turbulence effects on sound propagation," J. Acoust. Soc. Am., **132**(4), 2198–2209, doi: `10.1121/1.4748584`.

Chevin L-M, Hoffmann AA. (**2017**) "Evolution of phenotypic plasticity in extreme environments," Phil. Trans. R. Soc. B, **372**, 20160138, doi: `10.1098/rstb.2016.0138`. (Cited page: 15).

Chevret P, Blanc-Benon Ph, Juvé D. (**1996**) "A numerical model for sound propagation through a turbulent atmosphere near the ground," J. Acoust. Soc. Am., **100**(6), 3587–3599, doi: `10.1121/1.417224`. (Cited pages: 24, 24, 24, 29, 101, 195).

Chien CF, Soroka WW. (**1975**) "Sound propagation along an impedance plane," J. Sound Vib., **43**(1), 9–20, doi: `10.1016/0022-460X(75)90200-X`. (Cited page: 51).

Chobeau P. (**2014**) *Modeling of sound propagation in forests using the Transmisson Line Matrix method*, PhD thesis, Université du Maine, Le Mans, France. (Cited pages: 29, 195).

Collins MD. (**1993**) "A split-step Padé solution for the parabolic equation method," J. Acoust. Soc. Am., **93**(4), 1736–1742, doi: 10.1121/1.406739. (Cited page: 84).

Collino F. (**1997**) "Perfectly matched absorbing layers for the paraxial equations," Journal of Computational Physics **131**(1), 164–180, doi: 10.1006/jcph.1996.5594. (Cited pages: 85, 110).

Cotté B. (**2008**) *Propagation acoustique en milieu extérieur complexe : Problèmes spécifiques au ferroviaire dans le contexte des trains à grande vitesse*, PhD thesis, Ecole Centrale de Lyon. (Cited page: 68).

Cotté B, Blanc-Benon P, Bogey C, Poisson F. (**2009**) "Time-domain impedance boundary conditions for simulations of outdoor sound propagation," AIAA journal, **47**(10), 2391-2403, doi: 10.2514/1.41252. (Cited page: 30).

Dabelsteen T, Larsen ON, Pedersen SB. (**1993**) "Habitat-induced degradation of sound signals: Quantifying the effects of communication sounds and bird location on blur ratio, excess attenuation, and signal-to-noise ratio in blackbird song," J. Acoust. Soc. Am., **93**(4), 2206–2220, doi: 10.1121/1.406682. (Cited pages: 27, 36, 104, 105, 130, 136, 157, 158, 163).

Dabelsteen T. (**2005**) "3. Public, private or anonymous? Facilitating and countering eavesdropping," In *Animal communication networks* (Ed. P McGregor), 38–62, New York, Cambridge University Press, doi: 10.1017/CBO9780511610363.005. (Cited page: 158).

Dabelsteen T, Mathevon N. (**2002**) "Why do songbirds sing intensively at dawn? A test of the acoustic transmission hypothesis," Acta ethologica, **4**(2), 65–72, doi: 10.1007/s10211-001-0056-8. (Cited pages: 36, 105, 137, 156).

Dallois L. (**2000**) *Propagation des ondes acoustiques dans les milieux en mouvement : extension grand angle de l'approximation parabolique*, PhD thesis, Ecole Centrale de Lyon. (Cited pages: 88, 89).

Darden SK, Pedersen SB, Larsen ON, Dabelsteen T. (**2008**) "Sound transmission at ground level in a short-grass prairie habitat and its implications for long-range communication in the swift fox *Vulpes velox*," J. Acoust. Soc. Am., **124**(2), 758–766, doi: 10.1121/1.2946704. (Cited page: 105).

Darras K, Batáry P, Furnas BJ, Grass I, Mulyani YA, Tscharntke T. (**2019**) "Autonomous sound recording outperforms human observation for sampling birds: a systematic map and user guide," Ecol. Appl., **29**(6), e01954, doi: `10.1002/eap.1954`. (Cited pages: 162, 163).

Darras K, Batáry P, Furnas B, Celis-Murillo A, Van Wilgenburg SL, Mulyani YA, Tscharntke T. (**2018**) "Comparing the sampling performance of sound recorders versus point counts in bird surveys: A meta-analysis," J. Appl. Ecol., **55**(6), 2575–2586, doi: `10.1111/1365-2664.13229`. (Cited page: 163).

Darras K, Furnas B, Fitriawan I, Mulyani Y, Tscharntke T. (**2018**) "Estimating bird detection distances in sound recordings for standardizing detection ranges and distance sampling," Methods Ecol. Evol., **9**(9), 1928–1938, doi: `10.1111/2041-210X.13031`. (Cited pages: 164, 182, 183, 203).

Darras K, Pütz P, Fahrurrozi, Rembold K, Tscharntke T. (**2016**) "Measuring sound detection spaces for acoustic animal sampling and monitoring," Biol. Conserv., **201**, 29–37, doi: `10.1016/j.biocon.2016.06.021`. (Cited page: 164, 164, 164).

Datt P, Kapil JC, Kumar A, Srivastava PK. (**2016**) "Experimental measurements of acoustical properties of snow and inverse characterization of its geometrical parameters," Appl. Acoust., **101**, 15–23, doi: `10.1016/j.apacoust.2015.07.015`. (Cited pages: 56, 56, 117, 118, 125).

Desmet JF. (**1988**) "Rock ptarmigan (Lagopus mutus helveticus, Thieneman 1829) population densities during the breeding season period in the Haut-Giffre valley (Haute-Savoie, France)," Gibier Faune Sauvage, **5**, 447–458.

Dooling RJ, Blumenrath SH. (**2013**) "Avian sound perception in noise," in *Animal Communication and Noise*, Animal signals and communication **2**, (Ed. H Brumm), Springer, Berlin, Heidelberg, 229–250, doi: `10.1007/978-3-642-41494-7_8`. (Cited page: 35).

Dooling RJ, Leek MR. (**2018**) "Communication Masking by Man-Made Noise," in *Effects of Anthropogenic Noise on Animals* (Eds. H Slabbekoorn, RJ Dooling, AN Popper, RR Fay), 23–46, Springer handbook of auditory research, **66**, Springer, New York, doi: `10.1007/978-1-4939-8574-6_2`. (Cited pages: 107, 142).

Dowling AP. (**1983**) "Flow-acoustic interaction near a flexible wall," J. Fluid Mech., **128**, 181–198, doi: `10.1017/S0022112083000439`. (Cited page: 166).

Drake A, de Zwaan DR, Altamirano TA, Wilson S, Hick K, Bravo C, Ibarra JT, Martin K. (**2021**) "Combining point counts and autonomous recording units improves avian survey efficacy across elevational gradients on two continents," Ecol. Evol., **11**(13), 8654–8682, doi: `10.1002/ece3.7678`. (Cited page: 184).

Dragna D, Blanc-Benon P, Poisson F. (**2013**) "Time-domain solver in curvilinear coordinates for outdoor sound propagation over complex terrain," J. Acoust. Soc. Am., **133**(6), 3751–3763, doi: 10.1121/1.4803863. (Cited page: 30).

Dragna D, Blanc-Benon P, Poisson F. (**2014**) "Impulse propagation over a complex site: A comparison of experimental results and numerical predictions," J. Acoust. Soc. Am., **135**(3), 1096–1105, doi: 10.1121/1.4864286. (Cited page: 118).

Dragna D, Blanc-Benon P. (**2014**). "Towards realistic simulations of sound radiation by moving sources in outdoor environments," Int. J. Aeroacoust., **13**(5-6), 405–426, doi: 10.1260/1475-472X.13.5-6.405. (Cited page: 195).

Duhamel D. (**1996**) "Efficient calculation of the three-dimensional sound pressure field around a noise barrier," J. Sound Vib., **197**(5), 547–571, doi: 10.1006/jsvi.1996.0548. (Cited page: 28).

Dutilleux G, Sandercock BK, Kålås JA. (**2023**) "Chasing the bird: 3D acoustic tracking of aerial flight displays with a minimal planar microphone array," Bioacoustics, doi: 10.1080/09524622.2023.2241420 (Cited page: 73).

Ehrhardt L. (**2013**) *Modélisation en domaine temporel de la propagation acoustique*, PhD thesis, Ecole Centrale de Lyon. (Cited page: 195).

Eisenring E, Eens M, Pradervand J-N, Jacot A, Baert J, Ulenaers E, ...Evens R. (**2022**) "Quantifying song behavior in a free-living, light-weight, mobile bird using accelerometers," Ecol. Evol., **12**(1), e8446, doi: 10.1002/ece3.8446. (Cited page: 200).

Eldridge A, Guyot P, Moscoso P, Johnston A, Eyre-Walker Y, Peck M. (**2018**) "Sounding out ecoacoustic metrics: Avian species richness is predicted by acoustic indices in temperate but not tropical habitats," Ecol. Indic., **95**(1), 939–952, doi: 10.1016/j.ecolind.2018.06.012. (Cited page: 163).

Embleton TFW. (**1996**) "Tutorial on sound propagation outdoors," J. Acoust. Soc. Am., **100**(1), 31–48,doi: 10.1121/1.415879. (Cited pages: 2, 10, 18, 104, 136, 189).

Erbe C, Thomas JA. (**2022**) "Exploring Animal Behavior Through Sound: Volume 1 : Methods," Springer Nature, doi: 10.1007/978-3-030-97540-1. (Cited page: 1).

Ey E, Fischer J. (**2009**) "The "acoustic adaptation hypothesis" – a review of the evidence from birds, anurans and mammals," Bioacoustics **19**(1-2), 21–48, doi: 10.1080/09524622.2009.9753613. (Cited pages: 36, 158, 192, 201).

Fang CF, Ling DL. (**2003**) "Investigation of the noise reduction provided by tree belts," Landscape Urban Plann., **63**(4), 187–195, doi: 10.1016/S0169-2046(02)00190-1. (Cited page: 27).

Farina A, James P. (**2016**) "The acoustic communities: Definition, description and ecological role," Biosystems, **147**, 11–20, doi: `10.1016/j.biosystems.2016.05.011`. (Cited page: 8).

Faure O. (**2014**) *Analyse numérique et expérimentale de la propagation acoustique extérieur : effets de sol en présence d'irrégularités de surface et méthodes temporelles*, PhD thesis, Ecole Centrale de Lyon. (Cited pages: 29, 101).

Fernandez MSA, Soula HA, Mariette MM, Vignal C. (**2016**) "A New Semi-automated Method for Assessing Avian Acoustic Networks Reveals that Juvenile and Adult Zebra Finches Have Separate Calling Networks," Front. Psychol., **7**(1816), 56–73, doi: `10.3389/fpsyg.2016.01816`. (Cited pages: 8, 137).

Fernando HJS, Mann J, Palma JM, Lundquist JK, Barthelmie RJ, Belo-Pereira M, ...Wang Y. (**2019**) "The Perdigão: peering into microscale details of mountain winds," Bull. Am. Meteorol. Soc., **100**(5), 799–819, doi: `10.1175/BAMS-D-17-0227.1`. (Cited page: 100).

Fok VA. (**1965**) *Electromagnetic diffraction and propagation problems (Vol. 1)* Pergamon Press. (Cited page: 82).

Foken T. (**2017**) *Micrometeorology*, Springer, Berlin Heidelberg, doi: `10.1007/978-3-642-25440-6`. (Cited page: 67).

Folliot A, Haupert S, Ducrettet M, Sèbe F, Sueur J. (**2022**) "Using acoustics and artificial intelligence to monitor pollination by insects and tree use by woodpeckers," Sci. Total Environ., 838, 155883, doi: `10.1016/j.scitotenv.2022.155883`. (Cited page: 162).

Forrest TG. (**1994**) "From sender to receiver: Propagation and environmental effects on acoustic signals," American Zoologist, **34**(6), 644–654, doi: `10.1093/icb/34.6.644`. (Cited page: 104).

Freitas B, Bas Y, Robert A, Doutrelant C, Melo M. (**2022**) "Passive Acoustic Monitoring in difficult terrains: the case of the Principe Scops-Owl," OSF Preprints, doi: `10.31219/osf.io/mfubj`. (Cited page: 163).

Furrer R, Schaub M, Bossert A, Isler R, Jenny H, Jonas T., Marti C, Jenni L. (**2016**) "Variable decline of Alpine Rock Ptarmigan (*Lagopus muta helvetica*) in Switzerland between regions and sites," J. Ornithol., **157**(3), 787–796, doi: `10.1007/s10336-016-1324-8`. (Cited page: 14).

Gabillet Y, Schroeder H, Daigle GA, L'Espérance A. (**1993**). "Application of the Gaussian beam approach to sound propagation in the atmosphere: theory and experiments," J. Acoust. Soc. Am., **93**(6), 3105–3116, doi: `10.1121/1.405722`. (Cited page: 28).

Gabrielson TB. (**2006**) "Refraction of Sound in the Atmosphere," Acoustics today, **2**(7), 7–16, doi: `10.1121/1.2961136`. (Cited page: 22).

Gall MD, Ronald KL, Bestrom ES, Lucas JR. (**2012**) "Effects of habitat and urbanization on the active space of brown-headed cowbird song," J. Acoust. Soc. Am., **132**(6), 40–53, doi: `10.1121/1.4764512`. (Cited page: 137).

Gasc A, Sueur J, Pavoine S, Pellens R, Grandcolas P. (**2013**) "Biodiversity sampling using a global acoustic approach: contrasting sites with microendemics in New Caledonia," PLoS One, **8**(5), e65311, doi: `10.1371/journal.pone.0065311`. (Cited pages: 162, 204).

Gauvreau B, Bérengier M, Blanc-Benon P, Depollier C. (**2002**) "Traffic noise prediction with the parabolic equation method: Validation of a split-step Padé approach in complex environments," J. Acoust. Soc. Am., **112**(6), 2680–2687, doi: `10.1121/1.1509074`. (Cited page: 165).

Gibb R, Browning E, Glover-Kapfer P, Jones KE. (**2019**) "Emerging opportunities and challenges for passive acoustics in ecological assessment and monitoring," Methods Ecol. Evol., **10**(2), 169–185, doi: `10.1111/2041-210X.13101`. (Cited page: 162).

Gil D, Gahr M. (**2002**) "The honesty of bird song: multiple constraints for multiple traits," Trends Ecol. Evol., **17**(3), 133–141, doi: `10.1016/S0169-5347(02)02410-2`. (Cited page: 7).

Gil D, Llusia D. (**2020**) "The bird dawn chorus revisited," in *Coding strategies in vertebrate acoustic communication* (Eds. T Aubin, N Mathevon), 45–90, Springer Nature, Switzerland, doi: `10.1007/978-3-030-39200-0_3`. (Cited pages: 1, 138, 157, 158, 202).

Gilbert KE, Raspet R, Di X. (**1990**) "Calculation of turbulence effects in an upward-refracting atmosphere," J. Acoust. Soc. Am., **87**(6), 2428–2437, doi: `10.1121/1.399088`. (Cited page: 24).

Gilbert KE, White MJ. (**1989**) "Application of the parabolic equation to sound propagation in a refracting atmosphere," J. Acoust. Soc. Am., **85**(2), 630–637, doi: `10.1121/1.397587`. (Cited pages: 28, 82).

Gill SA, Bierema AM-K. (**2013**) "On the meaning of alarm calls: a review of functional reference in avian alarm calling," Ethology, **119**(6), 449–461, doi: `10.1111/eth.12097`. (Cited page: 7).

Godin OA. (**1999**) "Reciprocity and energy conservation within the parabolic approximation," Wave Motion, **29**(2), 175–194, doi: `10.1016/S0165-2125(98)00025-0` (Cited page: 166).

Goetschi D, Martin V, Baltensperger R, Vonlanthen M, Roziers DB, Carrino F, Carrino F. (**2022**) "Optimization of sensor placement for birds acoustic detection in complex fields," in Proceedings of the 11th International Conference on Pattern Recognition Applications and Methods - ICPRAM, SciTePress, 550–559, doi: `10.5220/0010819000003122`. (Cited pages: 184, 203).

Goestchel Q, Guillaume G, Ecotière D, Gauvreau B. (**2022**) "Analysis of the numerical properties of the transmission line matrix model for outdoor sound propagation," J. Sound Vib., doi: `10.1016/j.jsv.2022.116974`. (Cited page: 29).

Grinfeder E, Lorenzi C, Haupert S, Sueur J. (**2022**) "What do we mean by soundscape? A functional description," Front. Ecol. Evol. **10**, 894232, doi: `10.3389/fevo.2022.894232`. (Cited page: 34).

Guan X, Rao X, Song G, Wang D. (**2022**) "The evolution of courtship displays in Galliformes," Avian Res., **13**, 100008, doi: `10.1016/j.avrs.2022.100008`. (Cited page: 16).

Guibard A, Sèbe F, Dragna D, Ollivier S. (**2022**) "Influence of meteorological conditions and topography on the active space of mountain birds assessed by a wave-based sound propagation model," J. Acoust. Soc. Am., **151**(6), 3703–3718, doi: `10.1121/10.0011545`. (Cited pages: 38, 103, 137, 139, 144, 163, 164, 165, 183).

Guillaume G, Picaut J, Dutilleux G, Gauvreau B. (**2011**) "Time-domain impedance formulation for transmission line matrix modelling of outdoor sound propagation," J. Sound Vib., **330**(26), 6467–6481, doi: `10.1016/j.jsv.2011.08.004`. (Cited page: 29).

Guillaume G, Faure O, Gauvreau B, Junker F, Bérengier M, L'Hermite P. (**2015**) "Estimation of impedance model input parameters from *in situ* measurements," Appl. Acoust., **95**, 27–36, doi: `10.1016/j.apacoust.2015.01.024`. (Cited pages: 57, 117, 118).

Guyomarc'h G, Bellot H, Vionnet V, Naaim-Bouvet F, Déliot Y, Fontaine F, Puglièse P, Nishimura K, Durand Y, Naaim M. (**2019**) "A meteorological and blowing snow data set (2000–2016) from a high-elevation alpine site (Col du Lac Blanc, France, 2720 m a.s.l.)," Earth System Science Data **11**(1), 57–69, doi: `10.5194/essd-11-57-2019`. (Cited pages: 44, 45, 112).

Hardt B, Benedict L. (**2021**) "Can you hear me now? A review of signal transmission and experimental evidence for the acoustic adaptation hypothesis," Bioacoustics, **30**(6), 716–742, doi: `10.1080/09524622.2020.1858448`. (Cited pages: 2, 36, 189, 201).

Hart PJ, Ibanez T, Paxton K, Tredinnick G, Sebastián-González E, Tanimoto-Johnson A. (**2021**) "Timing is everything: Acoustic niche partitioning in two tropical wet forest bird communities," Front. Ecol. Evol., **9**(753363), 1–10, doi: `10.3389/fevo.2021.753363`.

Harris CM. (**1966**) "Absorption of Sound in Air versus Humidity and Temperature," J. Acoust. Soc. Am., **40**(1), 148–159, doi: `10.1121/1.1910031`. (Cited page: 22).

Haupert S, Sèbe F, Sueur J. (**2022**) "Physics-based model to predict the acoustic detection distance of terrestrial autonomous recording units over the diel cycle and across seasons: Insights from an Alpine and a Neotropical forest," Methods Ecol. Evol., **00**, 1–17, doi: `10.1111/2041-210X.14020`. (Cited pages: 27, 34, 155, 163, 164, 182, 183, 184, 195, 200).

Hedley RW, Wilson SJ, Yip DA, Li K, Bayne EM. (**2021**) "Distance truncation via sound level for bioacoustic surveys in patchy habitat," Bioacoustics, **30**(3), 303–323, doi: `10.1080/09524622.2020.1730240`. (Cited page: 164).

Heimann D, Gross G. (**1999**) "Coupled simulation of meteorological parameters and sound level in a narrow valley," Appl. Acoust., **56**(2), 73–100, doi: `10.1016/S0003-682X(98)00018-8`. (Cited pages: 28, 63).

Helmholtz H. (**1860**) "Theorie der Luftschwingungen in Röhren mit offenen Enden," De Gruyter, 1860(57), 1–72, doi: `10.1515/crll.1860.57.1`. (Cited pages: 165, 166).

Henden J-A, Ims RA, Fuglei E, Pedersen ÅØ. (**2017**) "Changed Arctic-alpine food web interactions under rapid climate warming: implication for ptarmigan research," Wildl. Biol., **2017**(SP1), 1–11, doi: `10.2981/wlb.00240`. (Cited page: 158).

Henwood K, Fabrick A. (**1979**) "A quantitative analysis of the dawn chorus: Temporal selection for communicatory optimization," Am. Nat., **114**(2), 260–274, doi: `10.1086/283473`. (Cited pages: 2, 27, 36, 102, 105, 105, 138, 158, 190, 201).

Hill EM, Koay G, Heffner RS, Heffner HE. (**2014**) "Audiogram of the chicken (gallus gallus domesticus) from 2 Hz to 9 kHz," J. Comp. Physiol., **200**(10), 863–870, doi: `10.1007/s00359-014-0929-8`. (Cited page: 35).

Hinze JO. (**1959**) *Turbulence*, McGraw and Hill, New York. (Cited page: 24).

Hofmann J, Heutschi K. (**2007**) "Simulation of outdoor sound propagation with a transmission line matrix method," Appl. Acoust., **68**(2), 158–172, doi: `10.1016/j.apacoust.2005.10.006`. (Cited page: 29).

Holder K, Montgomerie R. (**1993**) "Context and consequences of comb displays by male rock ptarmigan," Anim. Behav., **45**(3), 457–470, doi: `10.1006/anbe.1993.1057`. (Cited page: 12).

Holland J, Dabelsteen T, Pedersen SB, Larsen ON. (**1998**) "Degradation of wren *Troglodytes troglodytes* song: Implications for information transfer and ranging," J. Acoust. Soc. Am., **103**(4), 2154–2166, doi: 10.1121/1.421361. (Cited pages: 105, 130, 136, 159, 197).

Hopp SL, Morton ES. (**1998**) "Sound playback studies," in *Animal acoustic communication*, (Eds. SL Hopp, MJ Owren, CS Evans), 323–352, Springer, Berlin/Heidelberg, doi: 10.1007/978-3-642-76220-8_10. (Cited page: 1).

Hovick TJ, Elmore RD, Dahlgren DK, Fuhlendorf SD, Engle DM. (**2014**) "REVIEW: Evidence of negative effects of anthropogenic structures on wildlife: a review of grouse survival and behaviour," J. Appl. Ecol., **51**(6), 1680–1689, doi: 10.1111/1365-2664.12331. (Cited page: 14).

Howe MS. (**1975**) "The generation of sound by aerodynamic sources in an inhomogeneous steady flow," J. Fluid Mech. **67**(3), 597–610, doi: 10.1017/S0022112075000493. (Cited page: 166).

del Hoyo J, Elliott A, Sargatal J. (**1994**) "Handbook of the Birds of the World - Volume 2," Lynx Edicions, Spain, ISBN 978-84-87334-15-3. (Cited pages: 12, 13, 17).

Hutchinson JMC, McNamara JM, Cuthill IC. (**1993**) "Song, sexual selection, starvation and strategic handicaps," Anim. Behav., **45**(6), 1153–1177, doi: 10.1006/anbe.1993.1139. (Cited page: 159).

Imperio S, Bionda R, Viterbi R, Provenzale A. (**2013**) "Climate change and human disturbance can lead to local extinction of alpine rock ptarmigan: new insight from the western Italian Alps," PLoS One, **8**(11), e81598, 1–11, doi: 10.1371/journal.pone.0081598. (Cited page: 15).

ISO (**1993**) ISO 9613-1:1993(E), *Acoustics - Attenuation of sound during propagation outdoors - Part 1: Calculation of the absorption of sound by the atmosphere* (International Organization for Standardization, Geneva, Switzerland). (Cited pages: 21, 91, 111).

Jameson A, Baker T. (**1983**) "Solution of the Euler equations for complex configurations," 6th Computational Fluid Dynamics Conference (AIAA), Danvers, 293–302, doi: 10.2514/6.1983-1929.. (Cited page: 30).

Jensen KK, Larsen ON, Attenborough K. (**2008**) "Measurements and predictions of hooded crow (*Corvus corone cornix*) call propagation over open field habitats," J. Acoust. Soc. Am., **123**(1), 507–518, doi: 10.1121/1.2817363. (Cited pages: 105, 130).

Jobling JA. (**1991**) *Dictionary of scientific bird names* Oxford University Press. (Cited page: 12).

Johns PB, Beurle RL. (**1971**) "Numerical solution of 2-dimensional scattering problems using a transmission-line matrix," Proc. Inst. Electr. Eng., **118**(9), 1203–1208, doi: `10.1049/piee.1971.0217`. (Cited page: 29).

Johnsgard PA. (**2008**) "14 rock ptarmigan," in *Grouse and Quails of North America*, University of Nebraska, 225–239. (Cited page: 106, 106).

Kagawa Y, Tsuchiya T, Fujii B, Fujioka K. (**1998**) "Discrete Huygen's model approach to sound wave propagation," J. Sound Vib., **218**(3), 419–444, doi: `10.1006/jsvi.1998.1861`. (Cited page: 29).

Kazemi A, Kesba M, Provini P. (**2023**) "Realistic three-dimensional avian vocal tract model demonstrates how shape affects sound filtering (Passer domesticus)," J. R. Soc. Interface, **20**(198), 20220728, doi: `10.1098/rsif.2022.0728`. (Cited page: 9).

Khodr C, Azarpeyvand M, Green DN. (**2020**) "An iterative three-dimensional parabolic equation solver for propagation above irregular boundaries," J. Acoust. Soc. Am., **148**(2), 1089–1100, doi: `10.1121/10.0001766`. (Cited pages: 29, 100, 109, 194).

King AP, West MJ, Eastzer DH, Staddon JER. (**1981**) "An experimental investigation of the bioacoustics of cowbird song," Behav. Ecol. Sociobiol., **9**(3), 211–217, doi: `10.1007/BF00302940`. (Cited pages: 35, 198).

Kirkup S. (**2019**) "The Boundary Element Method in Acoustics: A Survey," Appl. Sci., **9**(8), 1642, doi: `10.3390/app9081642`. (Cited page: 28).

Knight E, Hannah K, Foley G, Scott C, Brigham R, Bayne E. (**2017**) "Recommendations for acoustic recognizer performance assessment with application to five common automated signal recognition programs," Avian Conserv. Ecol., **12**(2), doi: `10.5751/ACE-01114-120214`. (Cited pages: 164, 184).

Kroodsma DE, Miller EH, Ouellet H. (Eds.) (**1982**) "Acoustic communication in birds: Song learning and its consequences,", vol. 2, Academic Press, New York, USA. (Cited page: 17).

Kroodsma DE. (**1982**) "Song repertoire: Problems in their definition and use," in *Acoustic communication in birds*, vol. 2, (Eds. DE Kroodsma, EM Miller), 125–146, Academic Press, New York, USA. (Cited page: 6).

Kroodsma DE. (**2004**) "The diversity and plasticity of birdsong," in *Nature's music: the science of birdsong*, (Eds. P Marler, H Slabbekoorn), 108-131, Academic Press. (Cited page: 7).

Laiolo P. (**2010**) "The emerging significance of bioacoustics in animal species conservation," Biol. Conserv., **143**(7), 1635–1645, doi: 10.1016/j.biocon.2010.03.025. (Cited page: 162).

Lafore JP, Stein J, Asencio N, Bougeault P, Ducrocq V, Duron J, Fischer C, Héreil P, Mascart P, Masson V, Pinty JP, Redelsperger JL, Richard E, Vilà-Guerau de Arellano J. (**1998**) "The Meso-NH atmospheric simulation system. Part I: adiabatic formulation and control simulations," Ann. Geophys., **16**(1), 90–109, doi: 10.1007/s00585-997-0090-6. (Cited page: 192).

Lamancusa JS, Daroux PA. (**1998**) "Ray tracing in a moving medium with two-dimensional sound-speed variation and application to sound propagation over terrain discontinuities," J. Acoust. Soc. Am., **93**(4), 1716–1726, doi: 10.1121/1.406737. (Cited page: 28).

Lambert KTA, McDonald PG. (**2014**) "A low-cost, yet simple and highly repeatable system for acoustically surveying cryptic species," Austral Ecology, **39**(7), 779–785, doi: 10.1111/aec.12143. (Cited page: 164).

Landau LD, Lifshitz EM. (**1959**) *Course of Theoretical Physics*, vol. 6, Fluid mechanics, Pergamon. (Cited page: 166).

Larom D, Garstang M, Payne K, Raspet R, Lindeque M. (**1997**) "The influence of surface atmospheric conditions on the range and area reached by animal vocalizations," Journal of Experimental Biology, **200**(3), 421–431, doi: 10.1242/jeb.200.3.421. (Cited pages: 2, 102, 105, 129, 137).

Larsen ON, Dabelsteen T. (**1990**) "Directionality of blackbird vocalization. Implications for vocal communication and its further study," Ornis Scandinavica, **21**(1), 37–45, doi: 10.2307/3676376. (Cited page: 76).

Larsen ON, Goller F. (**2002**) "Direct observation of syringeal muscle function in songbirds and a parrot," J. Exp. Biol., **205**(1), 25–35, doi: 10.1242/jeb.205.1.25. (Cited page: 9).

Larsen ON, Wahlberg M. (**2017**) "Sound and sound sources," in *Comparative bioacoustics: An overview*, (Eds. C Brown, T. Riede), 3–61, Bentham Science Publishers, doi: 10.2174/9781681083179117010004. (Cited page: 197).

Larsen ON. (**2020**) "To shout or to whisper? Strategies for encoding public and private information in sound signals," in *Coding strategies in vertebrate acoustic communication*, (Eds. T Aubin, N Mathevon), 11–44, Springer Nature, Switzerland, doi: 10.1007/978-3-030-39200-0_2. (Cited pages: 9, 10, 32, 32).

Larsson C. (**1997**) "Atmospheric absorption conditions for horizontal sound propagation," Appl. Acoust., **50**(3), 231–245, doi: `10.1016/S0003-682X(96)00068-0`. (Cited page: 22).

Lee D, Pierce AD, Shang E-C. (**2000**) "Parabolic equation development in the twentieth century," J. Comput. Acoust., **8**(04), 527–637, doi: `10.1142/S0218396X00000388`. (Cited page: 82).

Leissing T, Jean P, Defrance J, Soize C. (**2009**) "Nonlinear parabolic equation model for finite-amplitude sound propagation over porous ground layers," J. Acoust. Soc. Am., **126**(2), 572–581, doi: `10.1121/1.3158937`. (Cited page: 195).

Lengagne, T., and Slater, P. J. B. (**2002**) "The effects of rain on acoustic communication: tawny owls have good reason for calling less in wet weather," Proc. R. Soc. Lond. B, **269**(1505), 2121–2125, doi: `10.1098/rspb.2002.2115`. (Cited page: 105).

Li KM, Taherzadeh S, Attenborough K. (**1998a**) "An improved ray-tracing algorithm for predicting sound propagation outdoors," J. Acoust. Soc. Am., **104**(4), 2077–2083, doi: `10.1121/1.423721`. (Cited page: 28).

Li, K. M., Waters-Fuller, T., and Attenborough, K. (**1998b**). "Sound propagation from a point source over extended-reaction ground," J. Acoust. Soc. Am., **104**(2), 679–685, doi: `10.1121/1.423307`. (Cited pages: 54, 54, 57, 110).

Lihoreau, B., Gauvreau, B., Bérengier, M., Blanc-Benon, P., and Calmet, I. (**2006**) "Outdoor sound propagation modeling in realistic environments: Application of coupled parabolic and atmospheric models," J. Acoust. Soc. Am., **120**(1), 110–119,doi: `10.1121/1.2204455`. (Cited pages: 29, 82, 109, 192).

Lin YT, Newhall AE, Miller JH, Potty GR, Vigness-Raposa KJ. (**2019**) "A three-dimensional underwater sound propagation model for offshore wind farm noise prediction," J. Acoust. Soc. Am., **145**(5), EL335–EL340, doi: `10.1121/1.5099560`. (Cited page: 93).

Little CJ, Rizzuto M, Luhring TM, Monk JD, Nowicki RJ, Paseka RE, Stegen JC, Symons CC, Taub FB, Yen JDL. (**2022**) "Movement with meaning: integrating information into meta-ecology," Oikos, **2022**(8), e08892, doi: `10.1111/oik.08892`. (Cited page: 9).

Lohr B, Wright TF, Dooling RJ. (**2003**) "Detection and discrimination of natural calls in masking noise by birds: estimating the active space of a signal," Anim. Behav., **65**(4), 763–777, doi: `10.1006/anbe.2003.2093`. (Cited pages: 105, 137).

Loning H, Griffith SC, Naguib M. (**2021**) "Zebra finch song is a very short-range signal in the wild: evidence from an integrated approach," Behav. Ecol., **33**(37–46), doi: `10.1093/beheco/arab107`. (Cited page: 105).

López-Moreno JI, Vicente-Serrano SM. (**2007**) "Atmospheric circulation influence on the interannual variability of snow pack in the Spanish Pyrenees during the second half of the 20th century," Hydrol. Res., **38**(1), 33–44, doi: `10.2166/nh.2007.030`. (Cited page: 14).

Lyamshev LM. (**1961**) "On certain integral relations in the acoustics of a moving medium," in Doklady Akademii Nauk, vol. 138, 575–578, Russian Academy of Sciences. (Cited page: 166).

MacDonald S. (**1970**) "The breeding behavior of the rock ptarmigan," Living Bird **9**, 195–238. (Cited pages: 16, 17, 106, 138, 140).

MacLaren AR, Crump PS, Royle JA, Forstner MRJ. (**2018**) "Observer-free experimental evaluation of habitat and distance effects on the detection of anuran and bird vocalizations," Ecol. Evol., **8**(24), 12991–13003, doi: `10.1002/ece3.4752`. (Cited page: 182).

Magrath RD, Pitcher BJ, Gardner JL. (**2009**) "An avian eavesdropping network: alarm signal reliability and heterospecific response," Behav. Ecol., **20**(4), 745–752, doi: `10.1093/beheco/arp055`.

Magrath RD, Haff TM, Fallow PM, Radford AN. (**2015**) "Eavesdropping on heterospecific alarm calls: from mechanisms to consequences," Biol. Rev., **90**(2), 560–586, doi: `10.1111/brv.12122`. (Cited page: 137).

Malavasi R, Farina A. (**2013**) "Neighbours' talk: interspecific choruses among songbirds," Bioacoustics, **22**(1), 33-48, doi: `10.1080/09524622.2012.710395`. (Cited page: 6).

Marler P, Dufty A, Pickert R. (**1986**) "Vocal communication in the domestic chicken: II. Is a sender sensitive to the presence and nature of a receiver?," Anim. Behav., **34**, 194–198, doi: `10.1016/0003-3472(86)90023-0`. (Cited page: 9).

Marler P. (**2004**) "Bird calls: a cornucopia for communication," in *Nature's music: the science of birdsong*, (Eds. P Marler, H Slabbekoorn), 132–177, Academic Press. (Cited page: 6).

Marin-Cudraz T, Muffat-Joly B, Novoa C, Aubry P, Desmet J-F, Mahamoud-Issa M, Nicolè F, Van Niekerk MH, Mathevon N, Sèbe F. (**2019**) "Acoustic monitoring of rock ptarmigan: A multi-year comparison with point-count protocol," Ecological Indicators **101**, 710–719, doi: `10.1016/j.ecolind.2019.01.071`. (Cited pages: 18, 107, 125, 139, 141, 146, 163, 183, 199, 204).

Marin-Cudraz T. (**2019**) *Potentialité de la bioacoustique comme outil de dénombrement d'espèces difficile d'accès : cas du Lagopède alpin (Lagopus muta)*, PhD thesis, Université Lyon/Saint-Étienne. (Cited page: 45).

Marques TA, Thomas L, Martin SW, Mellinger DK, Ward JA, Moretti DJ, Harris D, Tyack PL. (**2013**) "Estimating animal population density using passive acoustics," Biol. Rev., **88**(2), 287–309, doi: `10.1111/brv.12001`.

Marten K, Marler P. (**1977**) "Sound transmission and its significance for animal vocalization," Behavioral Ecology and Sociobiology **2**, 271–290, doi: `10.1007/BF00299740`. (Cited pages: 104, 136, 189).

Martin K, Altamirano TA, de Zwaan DR, Hick KG, Vanderpas A, Wilson S. (**2021**) "Avian ecology and community structure across elevation gradients: The importance of high latitude temperate mountain habitats for conserving biodiversity in the Americas," Global Ecol. Conserv., **30**, e01799, doi: `10.1016/j.gecco.2021.e01799`. (Cited page: 15).

Martinoli A, Preatoni DG, Bisi F, Gagliardi A, Martinoli A. (**2017**) "Where is the pulse to have the finger on? A retrospective analysis of two decades of Alpine Galliforms census and game bag data in Italy," Eur. J. Wildl. Res., **63**(4), 1–12, doi: `10.1007/s10344-017-1122-5`. (Cited page: 14).

Mathevon N, Aubin T, Dabelsteen T. (**1996**) "Song degradation during propagation: Importance of song post for the wren troglodytes troglodytes," Ethology **102**(3), 397–412, doi: `10.1111/j.1439-0310.1996.tb01135.x`. (Cited pages: 36, 130, 157, 159, 197).

Mathevon N, Aubin T, Vielliard J, da Silva ML, Sebe F, Boscolo D. (**2008**) "Singing in the rain forest: How a tropical bird song transfers information?," PLoS ONE, **3**(2), e1580, 1–6, doi: `10.1371/journal.pone.0001580`. (Cited pages: 105, 136, 137).

Mathevon N, Charrier I, Jouventin P. (**2003**) "Potential for individual recognition in acoustic signals: a comparative study of two gulls with different nesting patterns," C. R. Biol., **326**(3), 329-337, doi: `10.1016/S1631-0691(03)00072-6`. (Cited page: 7).

Mathevon N, Dabelsteen T, Blumenrath SH. (**2005**) "Are high perches in the blackcap *Sylvia atricapilla* song or listening posts? A sound transmission study," J. Acoust. Soc. Am., **117**(1), 442–449, doi: `10.1121/1.1828805`. (Cited pages: 36, 105, 130, 136, 157, 159, 197).

Mattiussi C. (**2000**) "The finite volume, finite element, and finite difference methods as numerical methods for physical field problems," Adv. Imaging Electron Phys., **121**, 143–279, doi: `10.1016/S1076-5670(00)80012-9`. (Cited page: 30).

Mathworks, Inc., Natick, Massachusetts, United States, *MATLAB version 9.2.0.538062 (R2017a)*, 2017. (Cited page: 147).

Maysenhölder W, Heggli M, Zhou X, Zhang T, Frei E, Schneebeli M. (**2012**) "Microstructure and sound absorption of snow," Cold Reg. Sci. Technol., **83-84**, 3–12, doi: `10.1016/j.coldregions.2012.05.001`. (Cited page: 56, 56).

Mcgregor PK. (1991) "The singer and the song: on the receiving end of bird song," Biol. Rev., **66**(1), 57–81. doi: `10.1111/j.1469-185X.1991.tb01135.x`. (Cited page: 1).

McGregor PK. (**2005**) *Animal communication networks* (Cambridge University Press, Cambridge), doi: `10.1017/CBO9780511610363`. (Cited pages: 1, 7, 104, 137).

McGregor PK, Dabelsteen T. (**1996**) "Communication networks," in *Ecology and evolution of acoustic communication in birds*, (Eds. DE Kroodsma, EH Miller), 409–425, Cornell University Press, Ithaca. (Cited pages: 104, 137).

McGregor PK, Horn AG. (**2014**) "Communication and social networks," in *Animal social networks* (Eds. J Krause, R James, DW Franks, DP Croft), 409–425, Oxford University Press. (Cited page: 1).

McGregor PK, Peake TM. (**2000**) "Communication networks: social environments for receiving and signalling behaviour," Acta Ethol., **2**(2), 71–81, doi: `10.1007/s102110000015`. (Cited page: 137).

Michelsen A, Larsen ON. (**1983**) "Strategies for acoustic communication in complex environments," in *Neuroethology and Behavioral Physiology: Roots and Growing Points*, (Eds. F Huber, H Markl), 321–331, Springer Berlin Heidelberg, doi: `10.1007/978-3-642-69271-0_23`. (Cited page: 2).

Mikhin D. (**2001**) "Energy-conserving and reciprocal solutions for higher-order parabolic equations," J. Comput. Acoust., **09**(01), 183–203, doi: `10.1142/S0218396X01000450`. (Cited page: 166).

Mikula P, Toszogyova A, Albrecht T. (**2022**) "A global analysis of aerial displays in passerines revealed an effect of habitat, mating system and migratory traits," Proc. R. Soc. Lond. B, **289**(1973), 20220370, doi: `10.1098/rspb.2022.0370`. (Cited pages: 16, 138).

Monin AS, Obukhov AM. (**1954**) "Basic laws of turbulent mixing in the surface layer of the atmosphere," Contrib. Geophys. Inst. Acad. Sci. USSR. **151** 163–187. (Cited pages: 63, 114, 144, 177).

Moore HM, Attenborough K, Rogers J, Lee S. (**1991**) "In-situ acoustical investigations of deep snow," Appl. Acoust., **33**, 281–301, doi: `10.1016/0003-682X(91)90018-A`. (Cited pages: 56, 56, 56, 117, 118).

Morales G, Vargas V, Espejo D, Poblete V, Tomasevic JA, Otondo F, Navedo JG. (**2022**) "Method for passive acoustic monitoring of bird communities using UMAP and a deep neural network," Ecol. Inf., **72**, 101909, doi: `10.1016/j.ecoinf.2022.101909`. (Cited page: 163).

Morton ES. (**1975**) "Ecological sources of selection on avian sounds," Am. Nat., **109**(965), 17–34, doi: `10.1086/282971`. (Cited pages: 159, 201, 202).

Mott R, Gromke C, Grünewald T, Lehning M. (**2013**) "Relative importance of advective heat transport and boundary layer decoupling in the melt dynamics of a patchy snow cover," Adv. Water Resour., **55**, 88–97, doi: `10.1016/j.advwatres.2012.03.001`. (Cited page: 128).

Mott R, Schlögl S, Dirks L, Lehning M. (**2017**) "Impact of extreme land surface heterogeneity on micrometeorology over spring snow cover," J. Hydrometeorol., **18**(10), 2705–2722, doi: `10.1175/JHM-D-17-0074.1`. (Cited pages: 70, 191).

Mourer-Chauvire C. (**1975**) "Faunes d'oiseaux du pléistocène de France: Systématique, évolution et adaptation, interprétation paléoclimatique," Geobios, **8**(5), 333–352, doi: `10.1016/S0016-6995(75)80048-9`. (Cited page: 13).

Mouterde SC, Theunissen FE, Elie JE, Vignal C, Mathevon N. (**2014**) "Acoustic communication and sound degradation: How do the individual signatures of male and female zebra finch calls transmit over distance?," PLoS ONE, **9**(7), e102842, doi: `10.1371/journal.pone.0102842`. (Cited pages: 132, 137, 137, 199).

Mouterde SC, Elie JE, Mathevon N, Theunissen FE. (**2017**) "Single neurons in the avian auditory cortex encode individual identity and propagation distance in naturally degraded communication calls," J. Neurosci., **37**(13), 3491–3510, doi: `10.1523/JNEUROSCI.2220-16.2017`. (Cited page: 137, 137).

Naguib M, Klump GM, Hillmann E, Grießmann B, Teige T. (**2000**) "Assessment of auditory distance in a territorial songbird: accurate feat or rule of thumb?," Anim. Behav., **59**(4), 715–721, doi: `10.1006/anbe.1999.1354`. (Cited page: 137).

Nemeth E, Winkler H, Dabelsteen T. (**2001**) "Differential degradation of antbird songs in a neotropical rainforest: adaptation to perch height?," J. Acoust. Soc. Am., **110**(6), 3263–3274, doi: `10.1121/1.1420385`. (Cited page: 136).

Nice MM. (**1941**) "The role of territory in bird life," Am. Midl. Nat., **26**(3), 441–487. (Cited pages: 1, 8, 202).

NORDTEST, Method NT ACOU 104:1999. Ground surfaces: determination of the acoustic impedance, November 1999. ISSN 0283-7145, Proj. 1365-97. (Cited page: 117).

Novoa C, Desmet J-F, Brenot J-F, Muffat-Joly B, Arvin-Bérod M, Resseguier J, Tran B. (**2011**) "Demographic traits of two alpine populations of rock ptarmigan," in *Ecology, Conservation, and Management of Grouse*, (Eds. BK Sandercock, K Martin, G Segelbacher), 267–280, University of California Press, Berkeley, California, [Sandercock K (Series Editor): Studies in Avian Biology, vol 39], doi: `10.1525/9780520950573-022`. (Cited pages: 11, 125, 139).

Nye PA. (**1964**) "Heat loss in wet ducklings ans chicks,", Ibis, **106**(2), 189–197, doi: `10.1111/j.1474-919X.1964.tb03695.x`. (Cited page: 228).

Ochi GM, Swearingen ME. (**2022**) "Parabolic equation comparisons with Galerkin discretization and boundary fitted grid for modeling infrasound propagation: 2D versus 3D," Proceedings of Meetings on Acoustics, **45**(1), 022002, doi: `10.1121/2.0001551`. (Cited page: 100).

Okanoya K, Dooling R.J. (**1987**) "Hearing in passerine and psittacine birds: A comparative study of absolute and masked auditory thresholds," J. Comp. Psychol., **101**(1), 7–15, doi: `10.1037/0735-7036.101.1.7`. (Cited page: 35).

Opaev AS, Shishkina EM. (**2021**) "Song amplitude and population density in two sympatric warblers, *Phylloscopus schwarzi* and *P. fuscatus*," Bioacoustics, **30**(3), 272–283, doi: `10.1080/09524622.2020.1720816`. (Cited page: 159).

Ostashev VE, Juvé D, Blanc-Benon P. (**1997**) "Derivation of a wide-angle parabolic equation for sound waves in inhomogeneous moving media," Acta Acustica **83**, 455-460. (Cited pages: 84, 110).

Ostashev VE, Wilson DK. (**2016**) *Acoustics in moving inhomogeneous media* CRC Press Taylor & Francis Group, London, doi: `10.1201/b18922`. (Cited pages: 24, 70, 70, 115, 128, 128, 144, 193, 194).

Ostashev VE, Wilson DK, Liu L, Aldridge DF, Symons NP, Marlin D. (**2005**) "Equations for finite-difference, time-domain simulation of sound propagation in moving inhomogeneous media and numerical implementation," J. Acoust. Soc. Am., **117**(2), 503–517, doi: `10.1121/1.1841531`. (Cited page: 30).

Ostashev VE, Muhlestein MB, Wilson DK. (**2019**) "Extra-wide-angle parabolic equations in motionless and moving media," J. Acoust. Soc. Am., **145**(2), 1031–1047, doi: 10.1121/1.5091011. (Cited page: 29).

Ostashev VE, Wilson DK, Muhlestein MB. (**2020**) "Wave and extra-wide-angle parabolic equations for sound propagation in a moving atmosphere," J. Acoust. Soc. Am., **147**(6), 3969–3984, doi: 10.1121/10.0001397. (Cited pages: 109, 171).

Pacifici K, Simons TR, Pollock KH. (**2008**) "Effects of vegetation and background noise on the detection process in auditory avian point-count surveys," Auk, **125**(3), 600–607, doi: 10.1525/auk.2008.07078. (Cited page: 164).

Padgham M. 2004 "Reverberation and frequency attenuation in forests - implications for acoustic communication in animals," J. Acoust. Soc. Am., doi: 10.1121/1.1629304. (Cited pages: 137, 157, 159, 197).

Parakkal S, Gilbert KE, Di X, Bass HE. (**2010**) "A generalized polar coordinate method for sound propagation over large-scale irregular terrain," J. Acoust. Soc. Am., **128**(5), 2573–2580, doi: 10.1121/1.3495941. (Cited page: 165).

Parejo D, Avilés JM, Expósito-Granados M. (**2018**) "Receivers matter: the meaning of alarm calls and competition for nest sites in a bird community," Oecologia, **187**(3), 707–717, doi: 10.1007/s00442-018-4139-x. (Cited page: 137).

Pandit MM, Bridge ES, Ross JD. (**2022**) "Environmental conditions lead to shifts in individual communication, which can cause cascading effects on soundscape composition," Ecol. Evol., **12**(10), e9359, doi: 10.1002/ece3.9359.

Parris KM. (**2002**) "More bang for your buck: the effect of caller position, habitat and chorus noise on the efficiency of calling in the spring peeper," Ecol. Model., **156**(2-3), 213–224, doi: 10.1016/S0304-3800(02)00170-9. (Cited page: 105).

Paszke A, Gross S, Massa F, Lerer A, Bradbury J, Chanan G, Killeen T, Lin Z, Gimelshein N, Antiga L,... Chintala S. (**2019**) "PyTorch: An imperative style, high-performance deep learning library," in *Advances in Neural Information Processing Systems*, **32**, 8024–8035, Curran Associates, Inc. Retrieved from: http://papers.neurips.cc/paper/9015-pytorch-an-imperative-style-high-performance-deep-learning-library.pdf. (Cited page: 78).

Peake TM, McGregor PK. (**2001**) "Corncrake Crex crex census estimates: a conservation application of vocal individuality," Animal Biodiv. and Cons., **24**(1), 81–90. (Cited page: 163).

Pedersen ÅØ, Bårdsen B-J, Yoccoz NG, Lecomte N, Fuglei E. (**2012**) "Monitoring Svalbard rock ptarmigan: Distance sampling and occupancy modeling," J. Wildl. Manage., **76**(2), 308–316, doi: `10.1002/jwmg.276`. (Cited page: 184).

Perez EC, Elie JE, Soulage CO, Soula HA, Mathevon N, Vignal C. (**2012**) "The acoustic expression of stress in a songbird: Does corticosterone drive isolation-induced modifications of zebra finch calls?," Horm. Behav., **61**(4), 573–581, doi: `10.1016/j.yhbeh.2012.02.004`. (Cited pages: 9, 141).

Pérez-Granados C, Bota G, Giralt D, Barrero A, Gómez-Catasús J, Bustillo-De La Rosa D, Traba J. (**2019**) "Vocal activity rate index: a useful method to infer terrestrial bird abundance with acoustic monitoring," Ibis, **161**(4), 901–907, doi: `10.1111/ibi.12728`. (Cited pages: 163, 165).

Pérez-Granados C, Gómez-Catasús J, Bustillo-de la Rosa D, Barrero A, Reverter M, Traba J. (**2019**) "Effort needed to accurately estimate Vocal Activity Rate index using acoustic monitoring: A case study with a dawn-time singing passerine," Ecol. Indic., **107**, 105608, doi: `10.1016/j.ecolind.2019.105608`. (Cited page: 178).

Pérez-Granados C, Traba J. (**2021**) "Estimating bird density using passive acoustic monitoring: a review of methods and suggestions for further research," Ibis, **163**(3), 765–783, doi: `10.1111/ibi.12944`. (Cited page: 163, 163).

Pierce AD. (**2019**) *Acoustics: an introduction to its physical principles and applications*, Third Edition, Springer International Publishing, Switzerland, doi: `10.1007/978-3-030-11214-1`. (Cited page: 28).

Pieretti N, Duarte MHL, Sousa-Lima RS, Rodrigues M, Young RJ, Farina A. (**2015**) "Determining temporal sampling schemes for passive acoustic studies in different tropical ecosystems," Trop. Conserv. Sci., **8**(1), 215–234 doi: `10.1177/194008291500800117`. (Cited pages: 182, 184, 184, 203).

Pijanowski BC, Farina A, Gage SH, Dumyahn SL, Krause BL. (**2011**) "What is soundscape ecology? An introduction and overview of an emerging new science," Landscape Ecol, **26**(9), 1213–1232, doi: `10.1007/s10980-011-9600-8`. (Cited page: 34, 34).

Piña-Covarrubias E, Hill AP, Prince P, Snaddon JL, Rogers A, Doncaster CP. (**2019**) "Optimization of sensor deployment for acoustic detection and localization in terrestrial environments," Remote Sens. Ecol. Conserv., **5**(2), 180–192, doi: `10.1002/rse2.97`. (Cited pages: 182, 184, 203).

Podos J, Warren PS. (**2007**) "The Evolution of Geographic Variation in Birdsong," in *Adv. Study. Behav.* **37**, 403–458, Academic Press, doi: `10.1016/S0065-3454(07)37009-5`. (Cited page: 7).

Potapov RL, Sale R. (**2014**) "Grouse of the World,", New Holland. (Cited pages: 11, 13).

Premat E, Gabillet Y. (**2000**) "A new boundary-element method for predicting outdoor sound propagation and application to the case of a sound barrier in the presence of downward refraction," J. Acoust. Soc. Am., **108**(6), 2775–2783, doi: `10.1121/1.1290512`. (Cited page: 28).

Python Software Foundation. Python Language Reference, version **3.9** with PyTorch 1.7 package. Available at `http://www.python.org`. (Cited pages: 78, 143).

R Core Team (**2021**). R: A language and environment for statistical computing. R Foundation for Statistical Computing, Vienna, Austria, `https://www.R-project.org/`. (Cited page: 72).

Rappaport DI, Royle JA, Morton DC. (**2020**) "Acoustic space occupancy: Combining ecoacoustics and lidar to model biodiversity variation and detection bias across heterogeneous landscapes," Ecol. Indic., **113**, 106172, doi: `10.1016/j.ecolind.2020.106172`. (Cited page: 184).

Raynor EJ, Whalen CE, Bomberger Brown M, Powell LA. (**2017**) "Location matters: evaluating Greater Prairie-Chicken (Tympanuchus cupido) boom chorus propagation," Avian Conserv. Ecol. **12**(2):17, 1–11, doi: `10.5751/ACE-01126-120217`. (Cited pages: 27, 105, 137, 182, 190).

Recio MR, Mathieu R, Denys P, Sirguey P, Seddon PJ. (**2011**) "Lightweight GPS-tags, one giant leap for wildlife tracking? An assessment approach," PLoS One, **6**(12), e28225, doi: `10.1371/journal.pone.0028225`. (Cited page: 1).

Reed SE, Boggs JL, Mann JP. (**2009**) "SPreAD-GIS: an ArcGIS toolbox for modeling the propagation of engine noise in a wildland setting,", Version 1.2, Wilderness Society, San Francisco, California, USA. (Cited pages: 27, 182).

Reed SE, Boggs JL, Mann JP. (**2012**) "A GIS tool for modeling anthropogenic noise propagation in natural ecosystems," Environ. Model. Software, **37**, 1–5, doi: `10.1016/j.envsoft.2012.04.012`. (Cited pages: 27, 102, 182).

Reichert MS, Enriquez MS, Carlson NV. (**2021**) "New dimensions for animal communication networks: Space and time," Integr. Comp. Biol., **61**(3), 814–824, doi: `10.1093/icb/icab013`. (Cited page: 104).

Reiners WA, Driese KL. (**2001**) "The propagation of ecological influences through heterogeneous environmental space," BioScience, **51**(11), 939–950, doi: `10.1641/0006-3568(2001)051[0939:TPOEIT]2.0.CO;2`. (Cited page: 105).

Reithmaier LM, Göckede M, Markkanen T, Knohl A, Churkina G, Rebmann C, Buchmann N, Foken T. (**2006**) "Use of remotely sensed land use classification for a better evaluation of micrometeorological flux measurement sites," Theor. Appl. Climatol., **84**(4), 219–233, doi: `10.1007/s00704-005-0168-6`. (Cited page: 67).

Ręk P, Osiejuk TS. (**2011**) "Nonpasserine bird produces soft calls and pays retaliation cost," Behav. Ecol., **22**(3), 657–662, doi: `10.1093/beheco/arr027`. (Cited pages: 107, 197).

Revermann R, Schmid H, Zbinden N, Spaar R, Schröder B. (**2012**) "Habitat at the mountain tops: how long can Rock Ptarmigan (*Lagopus muta helvetica*) survive rapid climate change in the Swiss Alps? A multi-scale approach," J. Ornithol., **153**(3), 891–905, doi: `10.1007/s10336-012-0819-1`. (Cited page: 15).

Ross SRP, O'Connell DP, Deichmann JL, Desjonquères C, Gasc A, Phillips JN, Sethi SS, Wood CM, Burivalova Z. (**2023**) "Passive Acoustic Monitoring provides a fresh perspective on fundamental ecological questions," Funct. Ecol., doi: `10.1111/1365-2435.14275`. (Cited page: 163).

Royle JA. (**2018**) "Modelling sound attenuation in heterogeneous environments for improved bioacoustic sampling of wildlife populations," Methods Ecol. Evol., **9**(9), 1939–1947, doi: `10.1111/2041-210X.13040`. (Cited pages: 27, 164).

Van Renterghem T. (**2014**) "Efficient outdoor sound propagation modeling with the Finite-Difference Time-Domain (FDTD) method: a review," Int. J. Aeroacoust., **13**(5-6), 385–404, doi: `10.1260/1475-472X.13.5-6.385`. (Cited pages: 30, 195).

Ruff ZJ, Lesmeister DB, Appel CL, Sullivan CM. (**2021**) "Workflow and convolutional neural network for automated identification of animal sounds," Ecol. Indic., **124**, 107419, doi: `10.1016/j.ecolind.2021.107419`. (Cited page: 78).

Rutz C, Troscianko J. (**2013**) "Programmable, miniature video-loggers for deployment on wild birds and other wildlife," Methods Ecol. Evol., **4**(2), 114–122, doi: `10.1111/2041-210x.12003`. (Cited page: 200).

Sack RA, West M. (**1995**)"A parabolic equation for sound propagation in two dimensions over any smooth terrain profile: The generalized terrain parabolic equation (GT-PE)," Appl. Acoust., **45**(2), 113–129, doi: `10.1016/0003-682X(94)00039-X`. (Cited pages: 29, 82).

Saleh AHM, Blanchfield P. (**1990**) "Analysis of acoustic radiation patterns of array transducers using the TLM method," Int. J. Numer. Model. Electron. Networks Devices Fields, **3**(1), 39–56, doi: `10.1002/jnm.1660030106`. (Cited page: 29).

Salomons EM. (**1998**) "Improved Green's function parabolic equation method for atmospheric sound propagation," J. Acoust. Soc. Am., **104**(1), 100–111, doi: 10.1121/1.423260. (Cited page: 28).

Salomons EM. (**2001**) *Computational Atmospheric Acoustics* Springer Netherlands, Dordrecht, doi: 10.1007/978-94-010-0660-6. (Cited pages: 21, 52, 53, 63, 64, 90, 108, 109, 115, 144, 146).

Sánchez-Giraldo C, Bedoya CL, Morán-Vásquez RA, Isaza CV, Daza JM. (**2020**) "Ecoacoustics in the rain: understanding acoustic indices under the most common geophonic source in tropical rainforests," Remote Sens. Ecol. Conserv., **6**(3), 248–261, doi: 10.1002/rse2.162. (Cited pages: 162, 164, 183).

Saunders JC, Denny RM, Bock GR. (**1978**) "Critical bands in the parakeet (*Melopsittacus undulatus*)," J. Comp. Physiol., **125**(4), 359–365, doi: 10.1007/BF00656871. (Cited page: 35, 35).

Schlögl S, Lehning M, Mott R. (**2018**) "How are turbulent sensible heat fluxes and snow melt rates affected by a changing snow cover fraction?," Front. Earth Sci., **6**(154), 1–13, doi: 10.3389/feart.2018.00154. (Cited pages: 70, 191).

Scridel D, Brambilla M, de Zwaan DR, Froese N, Wilson S, Pedrini P, Martin K. (**2021**) "A genus at risk: Predicted current and future distribution of all three Lagopus species reveal sensitivity to climate change and efficacy of protected areas," Divers. Distrib., **27**(9), 1759–1774, doi: 10.1111/ddi.13366. (Cited page: 15).

Searcy WA, Andersson M. (**1986**) "Sexual Selection and the Evolution of Song," Annu. Rev. Ecol. Syst., **17**, 507–533. (Cited page: 7).

Searcy WA, Nowicki S. (**2008**) "Bird Song and the Problem of Honest Communication: How is the honesty of animal signals maintained when exaggeration and bluff are so tempting?," Am. Sci., **96**(2), 114–121. (Cited page: 7).

Searcy WA, Nowicki S. (**2005**) "The evolution of animal communication: Reliability and deception in signaling systems," Princeton University Press. (Cited page: 7).

Shonfield J, Bayne E. (**2017**) "Autonomous recording units in avian ecological research: current use and future applications," Avian Conserv. Ecol., **12**(1), doi: 10.5751/ACE-00974-120114. (Cited pages: 163, 182, 184).

Skalak SL, Sherwin RE, Brigham RM. (**2012**) "Sampling period, size and duration influence measures of bat species richness from acoustic surveys," Methods Ecol. Evol., **3**(3), 490–502, doi: 10.1111/j.2041-210X.2011.00177.x. (Cited page: 184).

Slabbekoorn H. (**2004**) "Singing in the wild: the ecology of birdsong," in *Nature's Music The Science of Birdsong*, (Eds. P Marler, H Slabbekoorn), 178–205, Academic Press/Elsevier, San Diego, doi: 10.1016/B978-012473070-0/50009-8. (Cited page: 138).

Snijders L, Naguib M. (**2017**) "Communication in Animal Social Networks: A Missing Link?," in *Adv. Study. Behav.* **49**, 297–359, Academic Press, San Diego, doi: 10.1016/bs.asb.2017.02.004. (Cited page: 138).

Sólymos P, Matsuoka SM, Bayne EM, Lele SR, Fontaine P, Cumming SG, Stralberg D, Schmiegelow FKA, Song SJ. (**2013**) "Calibrating indices of avian density from non-standardized survey data: making the most of a messy situation," Methods Ecol. Evol., **4**(11), 1047–1058, doi: 10.1111/2041-210X.12106. (Cited pages: 164, 182, 203).

Staicer CA, Spector DA, Horn AG. (**1996**) "The dawn chorus and other diel patterns in acoustic signaling," in *Ecology and Evolution of Acoustic Communication in Birds*, (Eds. DE Kroodsma, EH Miller), 426–453, Ithaca, Cornell University Press, New-York, doi: 10.7591/9781501736957-033. (Cited pages: 36, 138, 155, 156, 158, 201).

Stamps J. (**1994**) "Territorial Behavior: Testing the Assumptions," In *Adv. Study. Behav.*, (Eds. PJB Slater, JS Rosenblatt, CT Snowdon, M Milinski), 173–232, Academic Press, San Diego. (Cited pages: 16, 157).

Sterk HAM, Steeneveld GJ, Holtslag AAM. (**2013**) "The role of snow-surface coupling, radiation, and turbulent mixing in modeling a stable boundary layer over Arctic sea ice," J. Geophys. Res. Atmos., **118**(3), 1199–1217, doi: 10.1002/jgrd.50158. (Cited pages: 70, 191).

Storch I. (**2000**) "Grouse : status survey and conservation action plan 2000-2004," IUCN, Gland, Switzerland and Cambridge. (Cited page: 14, 14).

Stowell D, Wood MD, Pamuła H, Stylianou Y, Glotin H. (**2019**) "Automatic acoustic detection of birds through deep learning: The first bird audio detection challenge," Methods Ecol. Evol., **10**(3), 368–380, doi: 10.1111/2041-210X.13103. (Cited pages: 182, 184).

Strasberg M. (**1998**) "Dimensional analysis of windscreen noise," J. Acoust. Soc. Am., **83**(2), 544–548, doi: 10.1121/1.396148. (Cited page: 229).

Strawn SN, Hill EM. (**2020**) "Japanese quail (coturnix japonica) audiogram from 16 Hz to 8 kHz," J. Comp. Physiol., **206**(5), 665–670, doi: 10.1007/s00359-020-01428-4. (Cited page: 35).

Striedter GF, Freibott L, Hile AG, Burley NT. (**2003**) "For whom the male calls: an effect of audience on contact call rate and repertoire in budgerigars, *Melopsittacus undulatus*," Anim. Behav., **65**(5), 875–882, doi: `10.1006/anbe.2003.2135`. (Cited page: 9).

Stull RB. (**1988**) "An introduction to boundary layer meteorology,", Kluwer Academic Publishers. (Cited pages: 63, 66).

Sueur J, Farina A, Gasc A, Pieretti N, Pavoine S. (**2014**) "Acoustic indices for biodiversity assessment and landscape investigation," Acta Acust United Acust., **100**(4), 772–781. (Cited pages: 162, 183, 204).

Sugai LSM, Silva TSF, Ribeiro Jr JW, Llusia D. (**2019**) "Terrestrial passive acoustic monitoring: review and perspectives," BioScience, **69**(1), 15–25, doi: `10.1093/biosci/biy147`. (Cited page: 162).

Suthers R. (**2004**) "How birds sing and why it matters," in *Nature's Music: The Science of Birdsong*, (Eds. P Marler, H Slabbekoorn), 272–295, Elsevier Academic Press, New York. (Cited page: 9).

Szymkowiak J. (**2022**) "Eavesdropping on conspecific alarm calls links birds across territory borders into a population-wide information network," Anim. Behav., **192**(8), 85–93, doi: `10.1016/j.anbehav.2022.07.012`. (Cited pages: 7, 137, 200).

Tam CK. (**2012**) "Computational aeroacoustics: A wave number approach," Cambridge University Press. (Cited page: 30).

Tappert FD. (**1977**) "The parabolic equation approximation method," in *Wave Propagation and Underwater Acoustics*, (Eds. JB Keller, JS Papadakis), Lecture Notes in Physics, **70**, Springer-Verlag, Heidelberg. (Cited page: 82).

Tayor PA, Lee RJ. (**1984**) "Simple guidelines of estimating wind speed variation due to small scale topographic features," Climatological Bull., Canada, **18**(22), 3–32. (Cited page: 63).

Templeton CN, Carlson NV. (**2019**) "Communication Networks,", in *Encyclopedia of animal behavior*, (Ed. JC Choe), 568-580, Elsevier Academic Press. (Cited page: 7).

Templeton CN, Greene E. (**2007**) "Nuthatches eavesdrop on variations in heterospecific chickadee mobbing alarm calls," Proc. Natl. Acad. Sci., U.S.A., **104**(13), 5479–5482, doi: `10.1073/pnas.0605183104`. (Cited page: 8).

Templeton CN, Greene E, Davis K. (**2005**) "Allometry of alarm calls: Black-Capped Chickadees encode information about predator size," Science, **308**(5730), 1934–1937, doi: `10.1126/science.1108841`. (Cited pages: 7, 137).

Tobias JA, Planqué R, Cram DL, Seddon N. (**2014**) "Species interactions and the structure of complex communication networks," Proc. Natl. Acad. Sci. U.S.A., **111**(3), 1020–1025, doi: 10.1073/pnas.1314337111. (Cited page: 8).

Todt D, Naguib M (**2000**) "Vocal Interactions in Birds: The Use of Song as a Model in Communication," in *Adv. Study. Behav.*, 247–296, Academic Press, Cambridge, MA, USA, doi: 10.1016/S0065-3454(08)60107-2. (Cited page: 137).

Tóth Z, Jaloveczki B, Tarján G. (**2020**) "Diffusion of social information in non-grouping animals,", Front. Ecol. Evol., **8**, 586058, doi: 10.3389/fevo.2020.586058. (Cited pages: 137, 200).

Toth CA, Pauli BP, McClure CJW, Francis CD, Newman P, Barber JR, Fristrup K. (**2022**) "A stochastic simulation model for assessing the masking effects of road noise for wildlife, outdoor recreation, and bioacoustic monitoring," Oecologia, **199**(1), 217–228, doi: 10.1007/s00442-022-05171-2. (Cited page: 164).

UICN France, MNHN, LPO, SEOF, ONCFS. (**2016**) "La Liste rouge des espèces menacées en France - Chapitre Oiseaux de France métropolitaine," Paris, France. (Cited page: 14).

Van Wilgenburg S, Sólymos P, Kardynal K, Frey M. (**2017**) "Paired sampling standardizes point count data from humans and acoustic recorders," Avian Conserv. Ecol., **12**(1), doi: 10.5751/ACE-00975-120113. (Cited pages: 184, 203).

Vecherin SN, Wilson DK, Ostashev VE. (**2011**) "Incorporating source directionality into outdoor sound propagation calculations," J. Acoust. Soc. Am., **130**(6), 3608–3622, doi: 10.1121/1.3655881. (Cited page: 76).

Vehrencamp SL, Bradbury JW, Gibson RM. (**1989**) "The energetic cost of display in male sage grouse," Anim. Behav., **38**(5), 885–896, doi: 10.1016/S0003-3472(89)80120-4. (Cited page: 15).

Vehrencamp SL. (**2000**) "Handicap, index, and signal elements of bird song," in *Animal signals*, (Eds. Y Espmark, T Amundsen, G Rosenqvist), 277–300, Tapir Academic Press, Trondheim, Norway. (Cited page: 7).

Vignal C, Mathevon N, Mottin S. (**2004**) "Audience drives male songbird response to partner's voice," Nature, **430**, 448–451, doi: 10.1038/nature02645. (Cited page: 9).

Voskamp A, Hof C, Biber MF, Böhning-Gaese K, Hickler T, Niamir A, Willis SG, Fritz SA. (**2022**) "Projected climate change impacts on the phylogenetic diversity of the world's terrestrial birds: more than species numbers," Proc. R. Soc. B., **289**, 20212184, doi: 10.1098/rspb.2021.2184. (Cited page: 15).

Wang H, Cosnefroy M, Hornikx M. (**2021**) "An arbitrary high-order discontinuous Galerkin method with local time-stepping for linear acoustic wave propagation," J. Acoust. Soc. Am., **149**(1), 569–580, doi: `10.1121/10.0003340`. (Cited page: 30).

Warren PS. (**2003**) "Winter dialects in the bronzed cowbird and their relationship to breeding-season dialects," Anim. Behav., **65**(6), 1169–1178, doi: `10.1006/anbe.2003.2156`. (Cited page: 7).

Watson A. (**1972**) "The behaviour of ptarmigan.," Br. Birds, **65**(1), 6–26. (Cited page: 105).

Weaver W. (**1949**) "Recent contributions to the mathematical theory of communication," in *The mathematical theory of communication*, (Eds. CE Shannon, W Weaver), 1–28, University of Illinois Press, Urbana. (Cited pages: 9, 136).

Whitehead H. (**2008**) *Analyzing animal societies: quantitative methods for vertebrate social analysis*, University of Chicago Press. (Cited page: 1).

Wilczynski W, Ryan MJ, Brenowitz EA. (**1989**) "The Display of the Blue-black Grassquit: The Acoustic Advantage of Getting High," Ethology, **80**(1-4), 218–222, doi: `10.1111/j.1439-0310.1989.tb00741.x`. (Cited pages: 36, 157).

Wiley RH, Richards DG. (**1978**) "Physical constraints on acoustic communication in the atmosphere: Implications for the evolution of animal vocalizations," Behav. Ecol. Sociobiol., **3**(1), 69–94, doi: `10.1007/BF00300047`. (Cited pages: 2, 105, 136, 189).

Wilson DK. (**1993**). "Relaxation-matched modeling of propagation through porous media, including fractal pore structure," J. Acoust. Soc. Am., **94**(2), 1136–1145, doi: `10.1121/1.406961`. (Cited page: 110).

Wilson DK, Wyngaard JC, Havelock DI. (**1998**) "The effect of turbulent intermittency on scattering into an acoustic shadow zone," J. Acoust. Soc. Am., **99**(6), 3393–3400, doi: `10.1121/1.414984`. (Cited page: 24).

Wilson DK. (**2003**) "The sound-speed gradient and refraction in the near-ground atmosphere," J. Acoust. Soc. Am., **113**(2), 750–757, doi: `10.1121/1.1532028`. (Cited pages: 22, 63, 165).

Wood CM, Kahl S, Chaon P, Peery MZ, Klinck H. (**2021**) "Survey coverage, recording duration and community composition affect observed species richness in passive acoustic surveys," Methods Ecol. Evol., **12**(5), 885–896, doi: `10.1111/2041-210X.13571`. (Cited pages: 183, 204).

Wood CM, Peery MZ. (**2022**) "What does 'occupancy' mean in passive acoustic surveys?," Ibis, **164**(4), 1295–1300, doi: `10.1111/ibi.13092`. (Cited page: 163).

Xue M, Droegemeier KK, Wong V. (**2000**) "The Advanced Regional Prediction System (ARPS) – A multi-scale nonhydrostatic atmospheric simulation and prediction model. Part I: Model dynamics and verification," Meteorol. Atmos. Phys., **75**(3), 161–193, doi: 10.1007/s007030070003. (Cited page: 192).

Ydenberg RC, Giraldeau LA, Falls JB. (**1988**) "Neighbours, strangers, and the asymmetric war of attrition," Anim. Behav., **36**(2), 343–347, doi: 10.1016/S0003-3472(88)80004-6. (Cited page: 16).

Yee K. (**1966**) "Numerical solution of initial boundary value problems involving Maxwell's equations in isotropic media," IEEE Trans. Antennas Propag., 14(3), 302–307, doi: 10.1109/tap.1966.1138693. (Cited page: 30).

Yip D, Leston L, Bayne E, Sólymos P, Grover A. (**2017**) "Experimentally derived detection distances from audio recordings and human observers enable integrated analysis of point count data," Avian Conserv. Ecol, **12**(1), doi: 10.5751/ACE-00997-120111. (Cited page: 164).

Yoccoz NG, Nichols JD, Boulinier T. (**2001**) "Monitoring of biological diversity in space and time," Trends Ecol. Evol., **16**(8), 446–453, doi: 10.1016/S0169-5347(01)02205-4. (Cited pages: 184, 203).

Yuldashev PV, Karzova MM, Khokhlova VA, Blanc-Benon Ph. (**2021**) "Numerical Simulation of a Nonlinear Parabolic Equation for Analyzing The Perceived Loudness Statistics of Sonic Boom Wave after Propagation Through Atmospheric Turbulent Layer," Acoust. Phys., **67**(1), 26–37, doi: 10.1134/S1063771021010061. (Cited page: 29).

Zollinger SA, Goller F, Brumm H. (**2011**) "Metabolic and respiratory costs of increasing song amplitude in zebra finches," PLoS One, **6**(9), e23198, doi: 10.1371/journal.pone.0023198. (Cited page: 34).